

Anatomical localisation and functional coupling of the nociceptin receptor in dog brain

Emma E. Johnson

Nociceptin (NOP), the endogenous ligand for the nociceptin receptor, NOP, has many actions, including analgesia, potentially via both endogenous and exogenous modulation. This study aims to determine the anatomical localisation of NOP receptors in the dog brain and to determine if NOP receptors are functionally coupled to NOP.

Anatomical localisation and functional coupling of the nociceptin receptor in dog brain

Emma E. Johnson

Department of Cancer Studies and Molecular Medicine
Division of Anaesthesia, Critical Care and Pain Management

Thesis submitted for the degree of Doctor of Philosophy
November 2003



**University of
Leicester**

UMI Number: U179524

All rights reserved

INFORMATION TO ALL USERS

The quality of this reproduction is dependent upon the quality of the copy submitted.

In the unlikely event that the author did not send a complete manuscript and there are missing pages, these will be noted. Also, if material had to be removed, a note will indicate the deletion.



UMI U179524

Published by ProQuest LLC 2013. Copyright in the Dissertation held by the Author.
Microform Edition © ProQuest LLC.

All rights reserved. This work is protected against
unauthorized copying under Title 17, United States Code.



ProQuest LLC
789 East Eisenhower Parkway
P.O. Box 1346
Ann Arbor, MI 48106-1346

Anatomical localisation and functional coupling of the nociceptin receptor in dog brain

Emma E. Johnson

Nociceptin (N/OFQ), the endogenous ligand for the nociceptin receptor, NOP, has many physiological roles, particularly in pain and cardiovascular modulation. There is an abundance of research for this system in humans and small laboratory species though none yet in dog.

Radioligand binding showed significantly lower density of NOP (B_{\max} $28.7 \pm 2.8 \text{ fmol mg}^{-1}$ protein) in dog brain membranes compared to rat (B_{\max} 137.0 ± 12.9). However the binding of various NOP and opioid ligands were similar indicating a pharmacologically identical receptor. Interestingly, there is a 3 fold higher density of total opioid receptors in dog compared to NOP although the significance of this is not fully understood.

Functional studies show that NOP couples to G proteins and that N/OFQ stimulated $\text{GTP}\gamma^{35}\text{S}$ binding in dog (E_{\max} 1.17 ± 0.01 , pEC_{50} 8.21 ± 0.17), which could be antagonised by the selective NOP antagonist, J-113397 with a pK_B value of 8.58.

Antibodies raised against full sequence N/OFQ showed no cross reactivity towards homologous opioid peptides and had an antibody titre of 1/3600. These antibodies were used in immunohistochemistry to localise N/OFQ in whole dog brain sections. N/OFQ's distribution was found to correlate with that reported for other species and for its precursor, preproN/OFQ.

[leucyl- ^3H]N/OFQ autoradiography showed extensive distribution for dog NOP *in situ* which was co-localised with N/OFQ. Highest binding was observed in the neocortex, piriform cortex, hippocampus, caudate nuclei and putamen. Dog piriform cortex showed approximately 5 fold less specific binding compared to that observed in rat.

This thesis describes a functional low density NOP in dog brain. Moreover peptide and receptor co-localise in areas of the brain involved in, for example, pain and cardiovascular modulation. Further *in vivo* studies of the role of N/OFQ in the dog are clearly warranted.

For Stevie,

Keep duckin' n divin', webbin' n weavin'.

Love you, Little Sis

Acknowledgements

I have achieved a dream. The last three years have been a learning experience but also a life one; three years full of exciting research, travelling, dancing, Leicester, coffee, Ramsgate, Mario's chippery, shopping and gossips, made infinitely memorable because of the friendships cemented...

I am indebted to so many; Helen Jenkins for French lessons and guidance with the beloved β -imager, Nick Clarke for autoradiographical methodology, Emma Levett for histological staining, John MacDonald for help with western blotting, Johannes Zanzinger, Peter Widdowson and Mark Hawthorn for useful discussions, Mike Martin-Short and Marianne Taylor for assistance during my time at Pfizer Ltd, Mike Walters from Imaging Research for invaluable advice with MCID, Giro, Remo and all at the University of Ferrara for friendship, support and peptide synthesis and many thanks to John Lees & Dave Bassford for patience with autoradiographical imaging and help with image format and analysis.

A special mention to Simon Westbrook (a VB on you this time!) without whom I would not have been here in the first place and to Mira Tomanovic, for much inspiration and friendship.

Here's to Paul, Trisha, John, Chris, Ed, Tim, Jim and the rest of our department... so much fun, picnics, roadkill, ski-ing and erm, slap 'er! I feel privileged to have worked with such people. Also Steeeeve and Andy for Brighton Beach, T in the Park, twister and endless laughs. I WANNA!

Much love to Mum, Dad and Stevie for believing in me and being there, to dearest Anne and Peter as second parents for enduring me again and again, to beautiful Theo, my soul mate and amaretto partner who kept me typing, living and laughing across the miles, and to Adam Nice, chief scanner and tracer, for all the best TLC in the world, hugs and tissues. I am forever beholden to you all.

Finally, and most importantly, my supervisors! Thanks to Bev, who has offered so much time, support, financial assistance and encouragement despite the distance and a million thousand thanks to Dave... he is one of a kind whose enthusiasm and inspiration knows no boundaries, a solid rock of endless support, guidance, jokes and Friday frighteners; someone special whom I respect immensely and whom I aspire to be like one day...

And as is Pfizer tradition, a toast to the man himself... To Charles Pfizer!

Contents

LIST OF ABBREVIATIONS	I
LIST OF TABLES	IV
LIST OF FIGURES	VI
1 PAIN AND NOCICEPTION	1
1.1 ANATOMY OF THE CANINE BRAIN	1
1.1.1 <i>Structures of the brain</i>	3
1.1.2 <i>Cranial nerves</i>	4
1.2 ANATOMY OF THE CANINE SPINAL CORD	4
1.3 GENERAL CELLULAR STRUCTURE OF THE CNS	6
1.3.1 <i>Neurones</i>	7
1.3.2 <i>Synapses</i>	8
1.4 ELECTRICAL SIGNALLING IN NEURONES	11
1.4.1 <i>Action potentials</i>	11
1.4.2 <i>Propagation of impulses</i>	12
1.5 PAIN PERCEPTION	13
1.5.1 <i>Nociceptors</i>	14
1.5.2 <i>Ascending pathways</i>	15
1.5.3 <i>Descending pathways</i>	17
1.5.4 <i>Gate control theory of pain</i>	18
1.6 MEDIATORS AT NOCICEPTORS	20
1.6.1 <i>Kinins</i>	21
1.6.2 <i>Capsaicin</i>	21
1.6.3 <i>Nerve growth factor</i>	22
1.6.4 <i>5-Hydroxytryptamine</i>	22
1.6.5 <i>Protons</i>	23
1.7 CENTRAL MEDIATORS	23
1.7.1 <i>Tachykinins</i>	24
1.7.2 <i>Calcitonin gene-related peptide</i>	25
1.7.3 <i>Glutamate</i>	25
1.7.4 <i>γAminobutyric acid</i>	27
1.8 OPIOID PHARMACOLOGY	27
1.8.1 <i>Endogenous opioids</i>	27
1.8.2 <i>Receptor subtypes</i>	29
1.8.3 <i>Expression and localisation</i>	34
1.8.4 <i>Effects of opioids</i>	35
1.9 NOCICEPTIN PHARMACOLOGY	37
1.9.1 <i>Nociceptin receptors</i>	37
1.9.2 <i>Endogenous nociceptin</i>	39
1.9.3 <i>Expression and localisation</i>	41
1.9.4 <i>Effects of N/OFQ</i>	44
1.10 CURRENT RESEARCH LIGANDS	45

1.11	CLINICAL ANALGESICS	46
1.12	AGE-RELATED DISEASES IN DOGS	49
1.13	THESIS AIMS	50
2	MATERIALS AND METHODS	52
2.1	SOURCES OF MATERIALS	52
2.2	BUFFERS, MEDIA AND REAGENTS.....	54
2.3	PEPTIDE SYNTHESIS	55
2.4	SYNTHESIS OF NOVEL RADIOLIGAND [³ H]N/OFQ(1-13)NH ₂	56
2.5	ANIMAL CARE AND ETHICS	56
2.6	BRAIN MEMBRANE PREPARATION	57
2.7	CELL CULTURE	57
2.8	CELL MEMBRANE PREPARATION	58
2.9	WHOLE CELL PREPARATION.....	59
2.10	PROTEIN ASSAY	59
2.11	THEORY OF RADIOLIGAND BINDING	60
2.11.1	<i>Radioactive decay</i>	60
2.11.2	<i>Efficiency of detecting radioactivity</i>	61
2.11.3	<i>Law of mass action</i>	62
2.11.4	<i>Non-specific binding</i>	63
2.11.5	<i>Calculating radioactive concentration</i>	64
2.12	ASSAY CONDITIONS	65
2.13	TIME COURSE ASSAYS.....	65
2.14	SATURATION BINDING	66
2.15	COMPETITION BINDING	68
2.16	NaCl/GTPγS SHIFT EXPERIMENTS	69
2.17	GTPγ ³⁵ S BINDING.....	69
2.18	FORSKOLIN STIMULATED CAMP FORMATION.....	71
2.19	LIGANDS INVESTIGATED	72
2.20	TISSUE SECTIONING	74
2.21	AUTORADIOGRAPHY	75
2.22	IMMUNOLOGICAL TECHNIQUES.....	75
2.23	DATA ANALYSIS AND STATISTICAL TESTS.....	75
3	RESULTS: RADIOLIGAND BINDING.....	76
3.1	INTRODUCTION	76
3.2	TIME COURSE OF [LEUCYL- ³ H]N/OFQ	77
3.3	SATURATION BINDING OF [LEUCYL- ³ H]N/OFQ, [³ H]N/OFQ13 AND [³ H]DPN	78
3.4	COMPETITION BINDING OF [LEUCYL- ³ H]N/OFQ	85
3.5	COMPETITION BINDING OF [³ H]DPN.....	88
3.6	DISCUSSION	94
4	RESULTS: FUNCTIONAL BINDING.....	97
4.1	INTRODUCTION	97
4.2	NaCl/GTPγS SHIFT.....	98
4.3	AGONIST STIMULATED GTPγ ³⁵ S BINDING	100
4.4	ANTAGONISM OF GTPγ ³⁵ S STIMULATION	103
4.5	DISCUSSION	106

5	RESULTS: IN VITRO CHARACTERISATION OF CJ-X	110
5.1	INTRODUCTION	110
5.2	COMPETITION OF [LEUCYL- ³ H]N/OFQ AND [³ H]DPN IN DOG AND RAT	111
5.3	COMPETITION OF [LEUCYL- ³ H]N/OFQ AND [³ H]DPN IN CHO MEMBRANES	113
5.4	GTPγ ³⁵ S BINDING IN CHO _{HNOP} MEMBRANES	115
5.5	CJ-X EFFECTS ON CAMP FORMATION	118
5.6	DISCUSSION	119
6	TISSUE SECTIONING AND STAINING	124
6.1	MICROTOME SECTIONING	124
6.2	REMOVAL OF SECTIONS FROM TAPE	125
6.3	ADHESIVE COATING OF GLASS SLIDES	126
6.3.1	<i>Poly-L-lysine</i>	126
6.3.2	<i>Gelatin</i>	126
6.3.3	<i>VectabondTM</i>	126
6.4	CRYOSECTIONING	127
6.5	COMPARING ADHESIVE COATINGS	128
6.6	OPTIMISED CYROSECTIONING	129
6.7	HISTOLOGICAL STAINING	131
6.7.1	<i>Haematoxylin and Eosin</i>	131
6.7.2	<i>Cresyl Fast Violet</i>	132
6.8	STAINING RESULTS	132
6.8.1	<i>Haematoxylin and Eosin</i>	132
6.8.2	<i>Cresyl Fast Violet</i>	133
6.9	DISCUSSION	134
7	AUTORADIOGRAPHY	136
7.1	[LEUCYL- ³ H]N/OFQ LABELLING <i>IN SITU</i>	136
7.2	[¹²⁵ I](TYR ¹⁴)N/OFQ LABELLING <i>IN SITU</i>	139
7.3	RESULTS	140
7.3.1	[¹²⁵ I](Tyr ¹⁴)N/OFQ autoradiograms	140
7.3.2	[leucyl- ³ H]N/OFQ autoradiograms	143
7.3.3	<i>Errors in quantitative autoradiography</i>	157
7.4	DISCUSSION	158
8	IMMUNOLOGICAL TECHNIQUES	163
8.1	ANTIBODY PRODUCTION	163
8.1.1	<i>Conjugation of hapten to carrier</i>	164
8.1.2	<i>Emulsification of immunogen</i>	167
8.1.3	<i>Immunisation of animals</i>	168
8.2	ELISA	169
8.2.1	<i>Results</i>	171
8.3	ANTIBODY PURIFICATION	176
8.4	WESTERN BLOTTING	180
8.4.1	<i>SDS PAGE</i>	181
8.4.2	<i>Immunoblotting</i>	183
8.4.3	<i>Results</i>	185
8.5	IMMUNOHISTOCHEMISTRY	190

8.5.1	Results.....	191
8.6	DISCUSSION.....	201
9	GENERAL DISCUSSION.....	204
9.1	SUMMARY OF FINDINGS.....	204
9.2	LOW EXPRESSION OF NOP.....	205
9.3	LIGAND AFFINITY FOR NOP.....	207
9.4	FUNCTIONAL NOP.....	208
9.5	ANTIBODY PRODUCTION.....	208
9.6	LOCALISATION OF NOP AND ITS LIGAND N/OFQ.....	209
9.7	FURTHER WORK.....	211
10	REFERENCES.....	213
11	PUBLICATIONS ARISING FROM THIS THESIS.....	225
12	APPENDIX.....	226
12.1	SINGLE LETTER AMINO ACID CODE.....	226
12.2	EXAMPLE PROTOCOL FOR PREPARATION OF AN IMMUNOGEN.....	226
12.3	PREPARATION OF EMULSION FROM TITREMAX® 'RESEARCH ADJUVANTS' INSTRUCTIONS.....	227
12.4	USAGE OF DOG WHOLE BRAIN SECTIONS.....	228
12.5	MCID CALIBRATION CURVE FOR [LEUCYL- ³ H]N/OFQ AUTORADIOGRAPHY.....	231
12.6	EXAMPLE OF MCID DATA ANALYSIS FOR SLIDE 111 AFTER [LEUCYL- ³ H]N/OFQ AUTORADIOGRAPHY.....	231
CTD	Acetylcholine receptor	
CTOP	D-Phe-Cys-Tyr-D-Tyr-Ome-Tic-Phe-Tic-NH ₂	
CV	cerebellar vermis	
CW	cerebellar white matter	
CWM	cerebellar white matter	
DA	diazepam A	
DAB	3,3'-diaminobenzidine-HCl	
DADLE	[D-Ala ² , D-Leu ⁵] enkephalin	
DAMGO	[Tyr-D-Ala-Gly-Phe ³ -Gly ⁴] enkephalin	
DOP	δ or OP ₁ opioid receptor	
DPDPE	[D-Pen ¹ , D-Pen ⁵] enkephalin	
dpm	disintegrations per minute	
GHDPN	glycyl-L-histidine	
DSLET	[D-Ser ² , Leu ⁵] enkephalin-Arg ⁶	
EDTA	ethylenediamine tetraacetic acid	
EGTA	ethyleneglycol-bis(2-aminoethyl)triethanol-N,N,N',N'-tetraacetic acid	
ELISA	enzyme-linked immunosorbent assay	
ET	enkephalin	
[FG]	[Phe ¹ , Orn ² , NH ₂ -NH ₂ Gly ³]N/OFQ (1-13NH ₂)	
FM	formaldehyde fixation	
GABA	γ-aminobutyric acid	
GDP	guanosine diphosphate	

List of Abbreviations

5-HT	5-hydroxytryptamine or serotonin
ACTH	adrenocorticotrophic hormone
ALOH	[Arg ¹⁴ ,Lys ¹⁵]N/OFQ(1-17)OH
AMPA	(±)- α -amino-3-hydroxy-5-methylisoxazole-4-propionic acid
Amy	amygdala
ANOVA	analysis of variance
AP	alkaline phosphatase
APS	ammonium persulphate
ASIC	acid-sensing ion channels
ATP	adenosine triphosphate
BCIP/TNBT	5-bromo-4-chloro-3-indolylphosphate/nitro blue tetrazolium
BK	bradykinin
BSA	bovine serum albumin
cAMP	cyclic adenosine monophosphate
CaC	caudal colliculus
cc	corpus callosum
CC	crus cerebri
CGRP	calcitonin gene related peptide
CH	cerebellar hemisphere
CHO	Chinese hamster ovary
Cl	claustrum
CLIP	corticotropic-like intermediary peptide
CN	caudate nucleus
CNo	cerebellar nodulus
CNS	central nervous system
CP	cerebellar peduncles
CTD	AcRYRWK-NH ₂
CTOP	D-Phe-Cys-Tyr-D-Trp-Orn-Thr-Pen-Thr-NH ₂
CV	cerebellar vermis
CW	cerebellar white matter
CWM	cerebral white matter
D _a	dynorphin A
DAB	3,3'-diaminobenzidine-HCl
DADLE	[D-Ala ² , D-Leu ⁵] enkephalin
DAMGO	Tyr-D-Ala-Gly-MePhe-Gly(ol)-enkephalin
DOP	δ or OP ₁ opioid receptor
DPDPE	[D-Pen ² ,D-Pen ⁵]-enkephalin
dpm	disintegrations per minute
[³ H]DPN	diprenorphine
DSLET	[D-Ser ² ,Leu ⁵]enkephalin-Thr ⁶
EDTA	ethylenediamine-tetraacetic acid
EGTA	ethyleneglycol-bis(β -aminoethyl ether)N,N,N',N'-tetraacetic acid
ELISA	enzyme linked immunosorbent assay
ET	epithalamus
[F/G]	[Phe ¹ ψ (CH ₂ -NH)Gly ²]N/OFQ(1-13)NH ₂
FM	mamillothalamic bundle
GABA	γ -aminobutyric acid
GDP	guanosine diphosphate

G protein	guanine-nucleotide binding protein
GPCR	G protein coupled receptor
GTP	guanosine triphosphate
GTP γ S	guanosine 5'-O-(3-thiotriphosphate)
HEPES	N-2-hydroxyethylpiperazine-N'-2-ethanesulphonic acid
Hip	hippocampus
HPLC	high pressure liquid chromatography
HRP	horseradish peroxidase
Hypo	hypothalamus
[¹²⁵ I](Tyr ¹⁴)N/OFQ	[¹²⁵ I](Tyr ¹⁴)N/OFQ(1-17)OH
IAd	interthalamic adhesion
IC	internal capsule
IMS	industrial methylated spirits
IN	interpeduncular nucleus
JTC-801	N-(4-amino-2-methylquinolin-6-yl)-2-(4-ethylphenoxyethyl)benzamide monohydrochloride
KLH	keyhole limpet haemocyanin
KOP	κ or OP ₂ opioid receptor
LC	locus coeruleus
[leucyl- ³ H]N/OFQ	[leucyl- ³ H]N/OFQ(1-17)OH
Leu-E	leu-enkephalin
LGN	lateral geniculate nucleus
LPH	lipotropin
LV	lateral ventricles
MA	mesencephalic aqueduct
MCP	middle cerebellar peduncle
MCP detector	microchannel plate detector
Met-E	met-enkephalin
MGN	medial geniculate nucleus
MOP	μ or OP ₃ opioid receptor
MPBST	non-fat dry milk in PBS with Tween-20
MSH	melanocyte stimulating hormone
MTN	medial thalamic nuclei
NalBzOH	naloxone benzoylhydrazone
Neo	neocortex
NEP	neutral endopeptidase
NGF	nerve growth factor
NK	neurokinin
NMDA	N-methyl-D-aspartate
NO	nitric oxide
Noc	nocistatin
cysNoc	CAEPVADEADEVEQKQLQ-NH ₂
N/OFQ	nociceptin, N/OFQ(1-17)OH
cysN/OFQ	CFGGFTGARKSARKLANQ-NH ₂
N/OFQ-NH ₂	N/OFQ(1-17)NH ₂
N/OFQ5	N/OFQ(1-5)NH ₂
N/OFQ9	N/OFQ(1-9)NH ₂
N/OFQ11	N/OFQ(1-11)NH ₂
N/OFQ12	N/OFQ(1-12)NH ₂
N/OFQ12-17	N/OFQ(12-17)OH
N/OFQ13	N/OFQ(1-13)NH ₂

NOP	nociceptin receptor, ORL1 or OP ₄
NOP epitope	GVQPGSETAVAILR-NH ₂
cysNOP epitope	CGVQPGSETAVAILR-NH ₂
<i>nor</i> BNI	<i>nor</i> -binaltorphimine
[Nphe ¹]	[Nphe ¹]N/OFQ(1-13)NH ₂
NSB	non-specific binding
OC	optic chiasm
OS	olfactory stria
P	putamen
PAG	periaqueductal grey
PAGE	polyacrylamide gel electrophoresis
Pal	pallidum
PBS	phosphate buffer saline
PBST	PBS with Tween-20
PEI	polyethylenimine
[(<i>p</i> F)Phe ⁴]	[(<i>p</i> F)Phe ⁴]N/OFQ(1-13)NH ₂
PG	prostaglandin
Piri	piriform cortex
PL	phospholipase
POMC	proopiomelanocortin
PTx	pertussis toxin
RC	rostral colliculus
RCP	rostral cerebellar peduncle
RN	red nucleus
Ro64-6198	(1 <i>S</i> ,3 <i>aS</i>)-8-(2,3,3 <i>a</i> ,4,5,6-hexahydro-1 <i>H</i> -phenalen-1-yl)-1-phenyl-1,3,8-triazaspiro[4.5]decan-4-one
SA	specific activity
SDS	sodium dodecyl sulphate
Sep	septum
SN	substantia nigra
SP	substance P
Sulfo-MBS	<i>m</i> -Maleimidobenzoyl- <i>N</i> -hydroxysulfosuccinimide ester
T	thalamus
TBS	tris buffered saline
TBST	TBS with Tween-20
TEMED	<i>N,N,N',N'</i> -tetramethyl-1,2-diaminoethane
TFA	trifluoroacetic acid
TN	trigeminal nerve
TRPV	transient receptor potential vanilloid receptor
UFP-101	[Nphe ¹ ,Arg ¹⁴ ,Lys ¹⁵]N/OFQ-NH ₂
VN	vestibular nucleus
VP	ventral pons
VSCC	voltage-sensitive calcium channels

List of Tables

TABLE 1.1 The 12 cranial nerves of the CNS.....	4
TABLE 1.2 Summary of neurotransmitters in ascending and descending non-nociceptive and nociceptive pathways of the nervous system.....	20
TABLE 1.3 Mediators act on afferent nociceptors to control neuromodulator release	21
TABLE 1.4 Structure of endogenous bioactive mammalian opioid ligands from specific opioid precursors (sequence homology shown in bold) and their specificity at opioid receptor subtypes	29
TABLE 1.5 Recent IUPHAR classification systems for the opioid receptors	30
TABLE 1.6 Initial reports of the cloning of NOP (Mogil et al., 2001).....	38
TABLE 1.7 Summary of research tools and clinical drugs for opioid and nociceptin receptor classes	47
TABLE 1.8 The ageing process of dogs.....	49
TABLE 2.1 Ligands used in this study. Red shows important modifications.....	72
TABLE 3.1 B_{\max} (fmol mg^{-1} protein) and pK_d values obtained in saturation binding experiments with [<i>leucyl</i> - ^3H]N/OFQ, [^3H]N/OFQ13 and [^3H]DPN. Data are mean \pm s.e.m ($n=3-5$)	84
TABLE 3.2 pK_i values obtained in competition binding of [<i>leucyl</i> - ^3H]N/OFQ by a range of ligands with activity at NOP and classical opioid receptors in dog and rat brain membranes. Data are mean \pm s.e.m ($n=3-15$)	85
TABLE 3.3 pK_i values for one and two site competition of [^3H]DPN with selective opioid ligands in dog and rat brain membranes. Data are mean \pm s.e.m ($n=3-10$). For Fraction _{HIGH} values see Table 3.4	90
TABLE 3.4 Relative proportions (% of total for MOP, DOP and KOP) in dog and rat brain membranes. The values shown in italics represent the proportions expressed as fmol mg^{-1} protein, when B_{\max} values for dog and rat are 77.7 ± 5.3 and 79.1 ± 18.2 , respectively. Data are mean \pm s.e.m ($n=3-10$)	92
TABLE 4.1 One and two site analysis of [<i>leucyl</i> - ^3H]N/OFQ competition curves in the absence and presence of NaCl/GTP γ S (H represents high and L low affinity sites). Data are mean \pm s.e.m ($n=3$)	100
TABLE 4.2 Comparison of estimated N/OFQ potency and efficacy at native NOP expressed in dog brain and CHO _{hNOP} cells. Data are mean \pm s.e.m ($n=3-12$)	102
TABLE 4.3 Effects of a range of N/OFQ ligands at single concentrations on GTP γ ^{35}S binding to dog brain membranes. Data are stimulation factor at $10\mu\text{M}$ (except N/OFQ, $1\mu\text{M}$) presented as mean \pm s.e.m ($n=3-12$)	102
TABLE 4.4 J-113397 (100nM), [<i>Nphe</i> 1] and [F/G] (both at $1\mu\text{M}$) competitively antagonised N/OFQ stimulated GTP γ ^{35}S binding to dog brain membranes. Comparative data with J-113397 in CHO _{hNOP} membranes are also shown. Data are mean \pm s.e.m from paired experiments ($n=3-5$).....	104
TABLE 4.5 N/OFQ ($1\mu\text{M}$) stimulated GTP γ ^{35}S binding to $G_{\alpha i 1-3}$ subunits. Differences in total dpm bound represent the different mass of tissue used, lower GDP ($5\mu\text{M}$) and higher magnesium ions (5mM). Data are mean \pm s.e.m ($n=3$) and is presented here with kind permission of John McDonald	109
TABLE 5.1 Interaction of CJ-X with NOP and classical opioid receptors in [<i>leucyl</i> - ^3H]N/OFQ and [^3H]DPN competition binding with dog and rat brain membranes. Data are mean \pm s.e.m ($n=3-5$).....	111

TABLE 5.2 Interaction of CJ-X with NOP and classical opioid receptors in [<i>leucyl</i> - ³ H]N/OFQ and [³ H]DPN competition binding assays using membranes prepared from CHO cells expressing recombinant receptors. Data are mean±s.e.m (<i>n</i> =3-6)	113
TABLE 5.3 pEC ₅₀ and E _{max} values for CJ-X and N/OFQ stimulated GTPγ ³⁵ S binding to CHO _{hNOP} membranes and inhibition of forskolin stimulated cAMP formation in whole CHO _{hNOP} cells. Data are mean±s.e.m (<i>n</i> =3-6).....	115
TABLE 5.4 CJ-X and N/OFQ (10μM) stimulated GTPγ ³⁵ S binding and inhibition of forskolin stimulated cAMP formation in CHO _{hNOP} cells is PTx sensitive. Data are mean±s.e.m (<i>n</i> =3).....	118
TABLE 5.5 Comparison of the activity of CJ-X and a range of currently available non-peptide NOP agonists at recombinant receptor systems.....	121
TABLE 6.1 Sectioning pattern for dog brain	130
TABLE 7.1 Images of [¹²⁵ I](Tyr ¹⁴)N/OFQ autoradiography in whole dog brain sections exposed against film for 48hr. Numbers refers to slide number (Appendix section 12.4) and are in order from anterior to posterior	142
TABLE 7.2 [<i>leucyl</i> - ³ H]N/OFQ autoradiograms of whole dog brain depicting NOP binding sites in situ	145
TABLE 7.3 Expression of NOP receptors (quoted as specific intensity in nCi mg ⁻¹) in various brain areas as determined in [<i>leucyl</i> - ³ H]N/OFQ autoradiography. Note blanks in table denote area not tested (<i>n</i> =3)	153
TABLE 8.1 Timetable for immunisation of animal	168
TABLE 8.2 Summary of titres for all antibodies. For comparison to anti-N/OFQ, the titre of Abcam was estimated to be 1/529.....	173
TABLE 8.3 Composition of different percentage running gels (total volume 10.01ml) ..	181
TABLE 8.4 Composition of 4.5% stacking gel (total volume 10.01ml).....	182
TABLE 8.5 Molecular weight (M _r) of SeeBlue markers used in SDS PAGE. N/OFQ and NOP are included for comparative purposes.....	183
TABLE 9.1 Comparison of NOP receptor expression in brain membrane preparations from various species with different radioligands	206

List of Figures

FIGURE 1.1 Medial view of canine brain showing five major brain areas (from Brain Gross Anatomy http://vanat.cvm.umn.edu/grossbrain/ , accessed November 2003).....	2
FIGURE 1.2 Canine cranial nerves are associated with particular functions (from Veterinary Neurobiology at http://vanat.cvm.umn.edu/neurolab/Lab4/L4index.html , accessed November 2003).....	5
FIGURE 1.3 Physiology of transverse section through the spinal cord (Martin, 2002)	5
FIGURE 1.4 Canine vertebrae column, which surrounds and protects the spinal nerves. There are 8 cervical, 13 thoracic, 7 lumbar, 3 sacral plus 5 caudal vertebrae (from Veterinary Neurobiology at http://vanat.cvm.umn.edu/neurolab/Lab4/L4index.html , accessed November 2003).....	6
FIGURE 1.5 Key features of a neuronal cell (Despopoulos et al., 1986)	7
FIGURE 1.6 Synaptic junctions (Greenstein et al., 2000)	9
FIGURE 1.7 Key features of a synapse (Strange, 1996).....	10
FIGURE 1.8 Conductance of sodium and potassium giving rise to an action potential (Despopoulos et al., 1986).....	12
FIGURE 1.9 Conduction velocity is directly related to fibre diameter, which accounts for the first ‘fast’ and then the second ‘slow’ pain.....	15
FIGURE 1.10 Afferent nociceptive input to spinal cord and ascending pathways (Greenstein et al., 2000)	16
FIGURE 1.11 The human spinothalamic pain-temperature pathway crosses over the cord almost immediately and ascends to the thalamus and the somatosensory cortex. The inset shows the plane of these regions within the brain (Bear et al., 2001)	17
FIGURE 1.12 Descending human pain pathways. A variety of brain structures, many of which are affected by behavioural state, can influence activity within the PAG of the midbrain. The PAG can influence the raphe nuclei of the medulla, which in turn modulates the flow of nociceptive information through the dorsal horns of the spinal cord (Bear et al., 2001).....	18
FIGURE 1.13 Melzack and Wall’s gate theory of pain (Bear et al., 2001)	19
FIGURE 1.14 Proopiomelanocortin (POMC) system (Greenstein et al., 2000).....	28
FIGURE 1.15 Proposed transmembrane topography of rat DOP subtype (Fukuda et al., 1995). Note closed circles show homology with MOP and open circles represent non-identical amino acids.....	31
FIGURE 1.16 Schematic representation of signal transduction events resulting from opioid agonist interaction with either classical or NOP receptors (R in diagram) in neurones. Receptor (R) activation leads to G-protein interaction and eventual α -subunit dissociation. $G_i\alpha$ can then inhibit adenylyl cyclase to decrease cAMP formation, activate voltage-sensitive potassium channels to produce hyperpolarisation or close voltage-sensitive calcium channels decreasing intracellular calcium. The net effect is decreased neuronal activity	33
FIGURE 1.17 Schematic representation of the production and primary sites of metabolism of N/OFQ. The 17 amino acid peptide is drawn showing the message/address domains responsible for functional activity and binding affinity, respectively. Also noted in the message domain are the two pharmacophores, Phe ¹ and Phe ⁴	42
FIGURE 2.1 Specimen protein standard curve	60
FIGURE 3.1 Typical one phase exponential association time course for [<i>leucyl</i> - ³ H]N/OFQ binding in dog and rat membranes illustrates a saturable stable receptor system.....	78
FIGURE 3.2 Typical saturation isotherms for [<i>leucyl</i> - ³ H]N/OFQ binding in dog (A) and rat (B) brain membranes	80

FIGURE 3.3 Typical sigmoidal transformation of specific binding data for [<i>leucyl</i> - ³ H]N/OFQ binding in dog and rat brain membranes.....	81
FIGURE 3.4 Typical saturation binding isotherms for [³ H]N/OFQ13 in the dog (A) and rat (B). Sigmoidal transformations of specific binding data are depicted in C	82
FIGURE 3.5 Specimen saturation binding isotherms for [³ H]DPN in the dog (A) and rat (B). Sigmoidal transformations of specific binding data are depicted in C	83
FIGURE 3.6 Competition curves of [<i>leucyl</i> - ³ H]N/OFQ for a range of unlabelled ligands in dog brain membranes. Data are mean±s.e.m (n=3-15)	86
FIGURE 3.7 Competition curves of [<i>leucyl</i> - ³ H]N/OFQ for a range of unlabelled ligands in rat brain membranes. Data are mean±s.e.m (n=3-15)	87
FIGURE 3.8 Positive correlation between pK _i values in dog and rat	88
FIGURE 3.9 One site competition curves of [³ H]DPN for a range of opioid ligands in dog (A) and rat (B) brain membranes. Data are mean±s.e.m (n=3-8)	91
FIGURE 3.10 Two site competition of [³ H]DPN by cyprodime (A), naltrindole (B) and norBNI (C) in dog and rat brain membranes. Data are mean±s.e.m (n=3-4)	93
FIGURE 4.1 Specimen curves of [<i>leucyl</i> - ³ H]N/OFQ competition in dog brain membranes modelled to one and two sites. The area under the curve denoted in red illustrates the high affinity proportion of the two site curve	99
FIGURE 4.2 Allosteric regulation of NOP by non-hydrolysable GTPγS indicates that NOP exists as two different affinity states, high (H), when N/OFQ-NOP couples to the trimeric G protein and low (L), when, in the presence of the GTPγS, the G protein is activated and dissociates from the ternary complex	99
FIGURE 4.3 Stimulation of GTPγ ³⁵ S binding to dog (A) and CHO _{hNOP} cell (B) membranes. Data are mean±s.e.m (n=4-6)	101
FIGURE 4.4 N/OFQ stimulated GTPγ ³⁵ S binding to dog (n=5) membranes is competitively antagonized by the selective NOP antagonist J-113397 (100nM). Data are mean±s.e.m (n=4).....	103
FIGURE 4.5 N/OFQ stimulated GTPγ ³⁵ S binding to dog membranes is competitively antagonized by 1μM [Nphe ¹] (A) and 1μM [F/G] (B). Data are mean±s.e.m (n=4) 105	105
FIGURE 5.1 Competition curves of [<i>leucyl</i> - ³ H]N/OFQ and [³ H]DPN for CJ-X in dog (A and B) and rat (C and D) membranes. N/OFQ and naloxone are included as reference ligands. Data are mean±s.e.m (n=6-15)	112
FIGURE 5.2 Competition curves of [<i>leucyl</i> - ³ H]N/OFQ and [³ H]DPN for CJ-X in CHO _{mDOP} (A), CHO _{rMOP} (B), CHO _{rKOP} (C) and CHO _{hNOP} (D) membranes. N/OFQ, cyprodime, naltrindole and norBNI are included as reference ligands. Data are mean±s.e.m (n=3-6)	114
FIGURE 5.3 Effects of CJ-X and N/OFQ on the binding of GTPγ ³⁵ S to membranes prepared from CHO _{hNOP} (A) and CHO _{INDhNOP} (B) cells (included with kind permission of John McDonald). Data are mean±s.e.m (n=3-6).....	116
FIGURE 5.4 CJ-X stimulation of GTPγ ³⁵ S binding to membranes prepared from CHO _{hNOP} cells is competitively antagonized by the selective NOP antagonist J-113397. Inset shows Schild analysis yielding a pA ₂ of 8.57, CR is concentration ratio(section 2.17). Data are mean±s.e.m (n=5)	117
FIGURE 5.5 Effects of CJ-X and N/OFQ on forskolin stimulated cAMP formation in whole CHO _{hNOP} cells. Data are mean±s.e.m (n=5).....	118
FIGURE 5.6 Saturation steps in the stimulus-response mechanisms of receptor systems obscure the ability to observe differences in efficacy. (Panel A) The stimulus to three hypothetical agonists of relative efficacy Agonist 3=1, Agonist 2=0.6, and Agonist 1=0.2 (as measured by maximal stimulation of GDP-GTP exchange) is shown. (Panel	

B) The stimulus produced in panel A is processed through a hyperbolic saturable stimulus-response function of output = input/(input+3). (Panel C) The output of Panel B is further processed through another saturable stimulus-response function output = input/(input+0.03) (Kenakin, 2002).....	122
FIGURE 6.1 A microtome is used for whole brain sectioning. 3M tape is pressed along the top of the block, over the mounted sample, so collecting the section as it is cut	125
FIGURE 6.2 A cryostat used to section small tissue samples.....	127
FIGURE 6.3 A dog brain matrix	129
FIGURE 6.4 Slides showing a typical haematoxylin and eosin stain. The sections are in order from anterior to posterior and the number refers to slide number (Appendix section 12.4).....	133
FIGURE 6.5 Cresyl Fast Violet staining showing neuronal distribution in whole dog brain sections. The sections are in order from anterior to posterior and the number refers to slide number (Appendix section 12.4).....	135
FIGURE 7.1 Schematic diagram of microchannel plate detector. Slides are placed in the sample holder and imaged under vacuum	138
FIGURE 7.2 [¹²⁵ I](Tyr ¹⁴)N/OFQ autoradiograms of NSB slides 166, 191 and 211. Numbers refer to slide number (Appendix section 12.4) and are in order from anterior to posterior.....	141
FIGURE 7.3 Images of [<i>leucyl</i> - ³ H]N/OFQ labelled NSB slides. Palette is pale blue through to black with black being most intense, i.e. most radioligand bound. Numbers refers to slide number (Appendix section 12.4) and are in order from anterior to posterior...	144
FIGURE 7.4 Autoradiogram A and B (actual field of view of MCP detector) show [<i>leucyl</i> - ³ H]N/OFQ binding in dog vas deferens (1; 10 sections), dog skeletal muscle (2), rat mid-coronal brain section (3) and dog mid-coronal brain section (B; total binding). Total binding (T) and NSB are as indicated. Palette is pale blue through to black with black being most intense, i.e. most radioligand bound.....	156
FIGURE 7.5 Total [<i>leucyl</i> - ³ H]N/OFQ binding in rat cortex is significantly higher than binding in dog cortex and dog vas deferens. No [<i>leucyl</i> - ³ H]N/OFQ binding was observed in dog skeletal muscle (n=3-5)	157
FIGURE 7.6 Overlay of [<i>leucyl</i> - ³ H]N/OFQ autoradiograms and [¹²⁵ I](Tyr ¹⁴)N/OFQ autoradiograms	159
FIGURE 7.7 Significantly higher binding of [<i>leucyl</i> - ³ H]N/OFQ is observed in rat cortex (A) compared to dog cortex (B). Autoradiograms are not to scale and the intensity varies from black through to bright orange with orange being the most intense	161
FIGURE 8.1 Chemical structure of Sulfo-MBS.....	165
FIGURE 8.2 Reaction scheme of Sulfo-MBS with a sulfhydryl containing peptide.....	165
FIGURE 8.3 Graph showing the elution of maleimide-activated KLH complex from PD10 column	166
FIGURE 8.4 Immunogen (peptide conjugated to KLH via Sulfo-MBS crosslinker)	167
FIGURE 8.5 Basic principles of indirect ELISA. Note as there are two F _c binding sites on the primary antibody (1°Ab) then two or more secondary antibodies (2°Ab) can bind	169
FIGURE 8.6 Sample graph of antibody titre – X dilution value corresponding to half the maximal absorbance is quoted as antibody titre (from Antibodies: From Design to Assay www.2.perkin-elmer.com/pa/3409/html/toc.html , accessed December 2000)	171
FIGURE 8.7 Increasing titres were observed with booster immunisations for anti-N/OFQ (A) antibodies tested in ELISAs using 2µg ml ⁻¹ N/OFQ as antigen. B shows the titre graph for Abcam antibodies. Data are mean±s.e.m (n=3-5).....	174

FIGURE 8.8 Increasing titres were observed with booster immunisations for anti-Noc (A) and anti-NOP (B) antibodies tested in ELISAs with $2\mu\text{g ml}^{-1}$ cysNoc or the NOP epitope. Data are mean \pm s.e.m ($n=3-5$)..... 175

FIGURE 8.9 Cross reactivity of anti-N/OFQ (A), Abcam (B) anti-Noc (C) antibodies with a serial dilution of various antigens (Ag) 177

FIGURE 8.10. Sample trace showing the loading of anti-Noc antibodies to XK16 Protein G column and washing with buffer. A very similar trace was obtained on elution of the antibodies with glycine 178

FIGURE 8.11 Protein concentration of eluted fractions from affinity chromatography of anti-Noc antiserum 179

FIGURE 8.12 Antibody titre against cysNoc (blue) of anti-Noc antibodies increased slightly after affinity purification. Low affinity is observed for Noc (black) with no improvement after purification..... 180

FIGURE 8.13 A Western blot sandwich 183

FIGURE 8.14 A 8% running gel did not separate the bands of the molecular markers sufficiently as only 6 bands (shown by arrows) are visible. Lanes 1 – 4 contain 20, 15, 10 and $5\mu\text{l}$ of markers, respectively 185

FIGURE 8.15 Picture of 15% gel (A) loaded with markers in four lanes and membrane (B) illustrating transfer of proteins. Lanes 1 – 4 contain 20, 15, 10 and $5\mu\text{l}$ of markers, respectively..... 186

FIGURE 8.16 Dot blotting showing binding of anti-NOP (A-C) and anti-N/OFQ antibodies (D-F). Primary antibody was 1/2000 and AP-conjugated secondary antibody was varied from 1/10000, 1/20000 and 1/50000 (from left to right). Red circles denote CHO_{hNOP} membrane preparation, green denotes cysNOP epitope and black N/OFQ at the concentrations (μg) noted 188

FIGURE 8.17 Example of Western blotting in which membranes were labelled with 1/2000 anti-N/OFQ (A) and anti-NOP (B) antibodies, followed by 1/50000 HRP conjugated secondary antibody, then exposed to film for 1min. Antigens were at $7.5\mu\text{g}$ with $20\mu\text{l}$ per well..... 189

FIGURE 8.18 Various dilutions of primary anti-N/OFQ and Abcam antibodies exhibit staining in IHC corresponding to N/OFQ. A - C anti-N/OFQ at dilutions of 1/500, 1/1000 and 1/2000, respectively; D, Abcam at 1/2000; E, control (no primary antibody) and F, brain atlas on a haematoxylin/eosin stained section showing main areas of interest..... 192

FIGURE 8.19 Immunostaining in the presence of $10\mu\text{M}$ N/OFQ (B) reduces binding of anti-N/OFQ antibodies at 1/10000 (A). C is control (no primary antibody) and D, brain atlas on a haematoxylin/eosin stained section showing main areas of interest 193

FIGURE 8.20 Various incubation times (A 5, B 7 and C 9min) for DAB substrate produced positive staining. D shows control (no primary antibody) and E shows brain atlas on a haematoxylin/eosin stained section with main areas of interest..... 194

FIGURE 8.21 IHC staining showing distribution of N/OFQ in whole dog brain sections. The sections are in order from anterior to posterior and the number refers to slide number (Appendix section 12.4) 200

FIGURE 8.22 Slide 187 (A) depict N/OFQ (brown stain) localisation in dog brain sections and atlas B (slide 185) shows haematoxylin and eosin staining. N/OFQ is therefore distributed in brain areas associated with pain perception, cardiovascular function and learning and memory 202

FIGURE 9.1 N/OFQ (A) and NOP (B) are localised in situ in dog brain in functionally important area 210

1 Pain and nociception

Opium, extracted from the poppy plant *Papaver somniferum*, has been used medicinally and recreationally for thousands of years. Galen described its use as an analgesic, as a cough suppressant and to calm asthmatics. The active component responsible for analgesia identified by Friedrich Sertürner in 1806, is the crystalline alkaloid named morphine, after Morpheus the Greek god of dreams. Its actions led to speculation regarding the existence of specific opioid receptors, of which three subtypes were later identified (Harrison *et al.*, 2000).

Recently an intriguing receptor system has been discovered which is believed to be intricately linked to this opioid system. The nociceptin receptor, NOP, was isolated in various species and its ligand has since been identified as the heptadecapeptide, nociceptin (N/OFQ) that shows sequence and structural homology to dynorphin (D_a) (Meunier *et al.*, 2000).

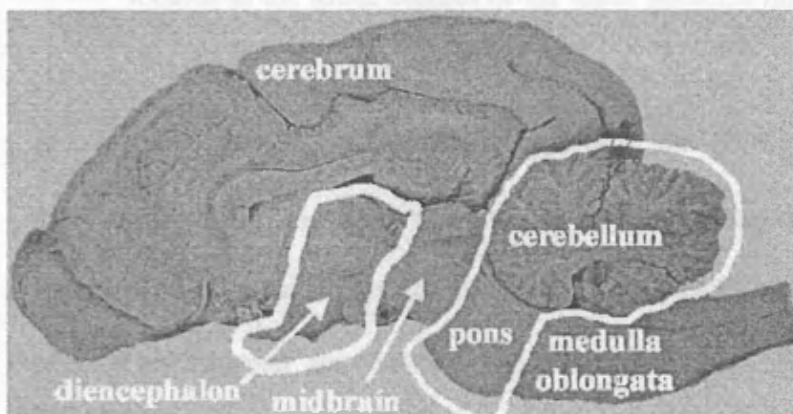
This thesis aims to characterise N/OFQ and its receptor in the dog, a species in which this peptide system has not yet been investigated. Since N/OFQ is an important neuromodulator with various physiological roles, particularly in pain (Mogil *et al.*, 2001), then this introduction presents basic canine brain anatomy, information about neuronal signalling and mediators of pain perception, and an overview of recent N/OFQ pharmacology. As there is considerable homology between the N/OFQ peptide system and that of the opioid peptides (Meunier, 1997), then opioid pharmacology is also discussed, along with current research ligands and clinical analgesic drugs.

1.1 Anatomy of the canine brain

The dog, *Canis familiaris*, is believed to be the oldest of domesticated animals and the Beagle is well described in terms of characteristics, physiology and temperament

(Andersen, 1970). Its central nervous system (CNS), as for other animals, consists of the brain and spinal cord.

The telencephalon forms the cerebrum, which is separated from the brain stem and cerebellum by the transverse fissure. It has an external grey cortical layer of pyramidal cells (neuronal cell bodies) and white (myelinated nerve axons) matter. It is enveloped in three layers of protective membranes, the meninges, or specifically the arachnoid, dura mater and pia mater. Viewed externally, it has two hemispheres with bilateral symmetry, and characteristic infoldings. It is an assembly of interconnecting smaller structures, which can be subgrouped according to their association with a particular function (Meyer, 1993). During early development, the three vesicles, formed from the rostral cephalic portion of the neural tube, are divided into five main areas (Fox, 1970; Figure 1.1).



- Telencephalon (cerebrum)
- Diencephalon
- Mesencephalon (midbrain)
- Metencephalon (pons and cerebellum)
- Myelencephalon (medulla oblongata)

FIGURE 1.1 Medial view of canine brain showing five major brain areas (from *Brain Gross Anatomy* <http://vanat.cvm.umn.edu/grossbrain/>, accessed November 2003)

These divide further to form the cerebrum, brain stem (this connects the cerebrum with the spinal cord and cerebellum) and cerebellum. The remainder of the neural tube becomes the spinal cord and the lumen of the spinal canal, which fills with cerebrospinal fluid.

1.1.1 Structures of the brain

The *telencephalon* forms the cerebrum, which is separated from the brain stem and cerebellum by the transverse fissure. It has an external grey cortical layer of intricate species-specific elevations and convulsions (gyri and sulci, respectively) with an underlying layer of white matter. Each cerebral hemisphere has four lobes and a fluid filled lateral ventricle (Fox, 1970). The white matter of the cerebrum has two fibre systems:

- *Corticocortical fibres* originate and terminate in the cortex and can be divided further into association (connect areas in the same cerebral hemisphere) and commissural (cross the neuraxis to opposite sides of cerebrum) fibres. The commissural fibres form the corpus callosum, which is the nerve tract linking the two cerebral hemispheres.
- *Projection fibres* either begin or terminate in the cortex with their other ends located in the lower centres of the basal nuclei, spinal cord or brain stem.

The lobes of the cerebral cortex, named after the adjacent bones of the skull – frontal, parietal, occipital and temporal, can be further subdivided to establish subdivisions of functional relevance. Areas not associated with particular functions and hence assumed to process information, are known as the association areas. These are not highly developed in dog compared with man (Fox, 1970).

The most rostral part of the brain stem is the *diencephalon*, which encompasses the thalamus and the hypothalamus. Posterior to the diencephalon is the *mesencephalon* or midbrain. Further back between this and the myelencephalon is the *metencephalon*. The ventral part of the metencephalon belongs to the brain stem whereas the dorsal region develops into the cerebellum. The *myelencephalon*, also known as the medulla oblongata, is the caudal most portion of the brain extending into the spinal cord (Evans, 1993).

1.1.2 Cranial nerves

There are 12 pairs of motor and sensory cranial nerves for dog and humans that arise in the brain (Table 1.1). These are roughly apportioned equally between the three brain stem segments, I-IV in midbrain, V-VIII in pons and IX-XII in the medulla and have various functions (Figure 1.2).

TABLE 1.1 The 12 cranial nerves of the CNS

NERVE	NAME	FUNCTION
I	Olfactory	Smell
II	Optic	Visual fields, ability to see
III	Oculomotor	Eye movements, eyelid opening
IV	Trochlear	Eye movements
V	Trigeminal	Facial sensation
VI	Abducens	Eye movement
VII	Facial	Eyelid closing, facial expression, taste sensation
VIII	Vestibulocochlear	Hearing, balance
IX	Glossopharyngeal	Taste sensation, swallowing
X	Vagus	Swallowing, taste sensation
XI	Accessory	Controls neck and shoulder muscles
XII	Hypoglossal	Tongue movement

1.2 Anatomy of the canine spinal cord

The spinal cord is the portion of the CNS, which is enclosed in the vertebral column and can be divided into segments. Like the brain, it consists of central grey and peripheral white matter (Martin, 2002; Figure 1.3). The grey matter is composed of the soma of efferent (to the periphery) pathways (mainly motoneurons) in the ventral horn and those of the interneurons in the dorsal horn. The soma for the afferent (to the brain) neurons can be found in the spinal ganglia (outside of the spinal cord). The white matter is composed generally of axons from the ascending and descending pathways. The central canal is continuous with the brain ventricles and is filled with circulating cerebrospinal fluid.

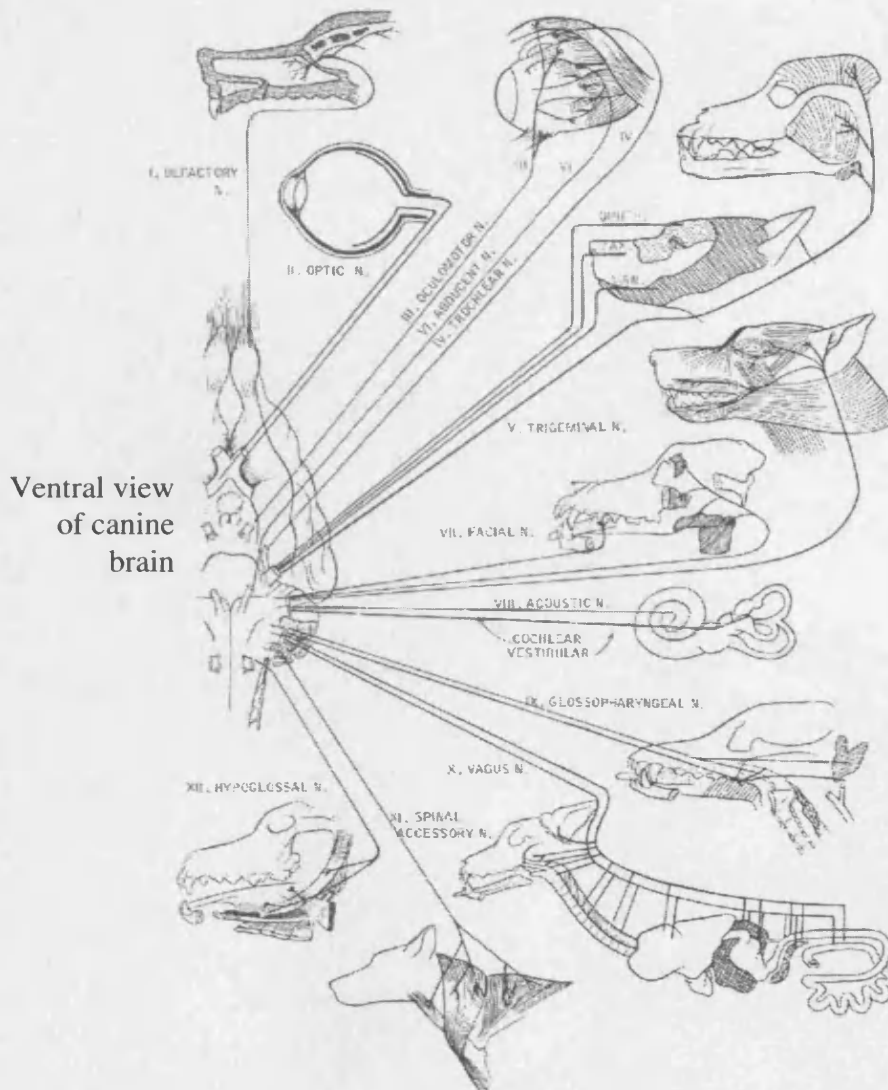


FIGURE 1.2 Canine cranial nerves are associated with particular functions (from *Veterinary Neurobiology* at <http://vanat.cvm.umn.edu/neurolab/Lab4/L4index.html>, accessed November 2003)

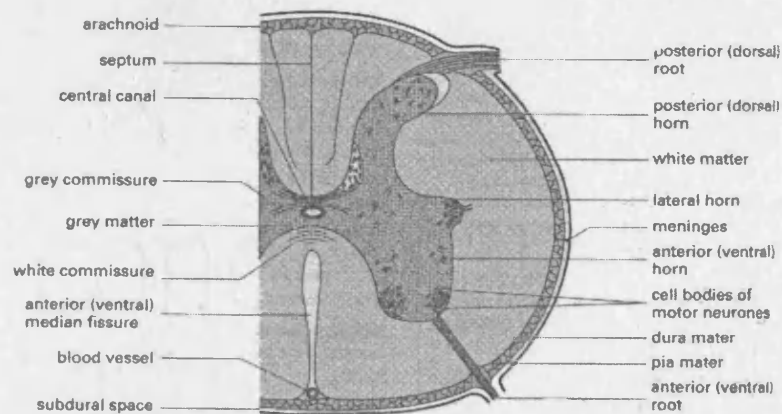


FIGURE 1.3 Physiology of transverse section through the spinal cord (Martin, 2002)

The spinal cord extends from the medulla oblongata to the lumbosacral region (Figure 1.4). Nerve fibres leave the central grey matter continuously at the appropriate vertebral level and form regular bundles of afferent and efferent fibres. These are known as the spinal nerves of which there are 36 pairs (8 cervical, 13 thoracic, 7 lumbar, 3 sacral and 5 coccygeal) in dog (compared with 31 pairs in humans).

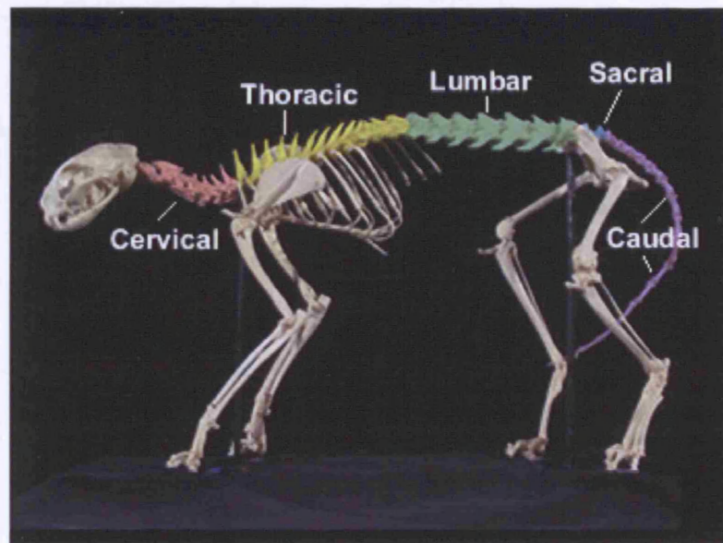
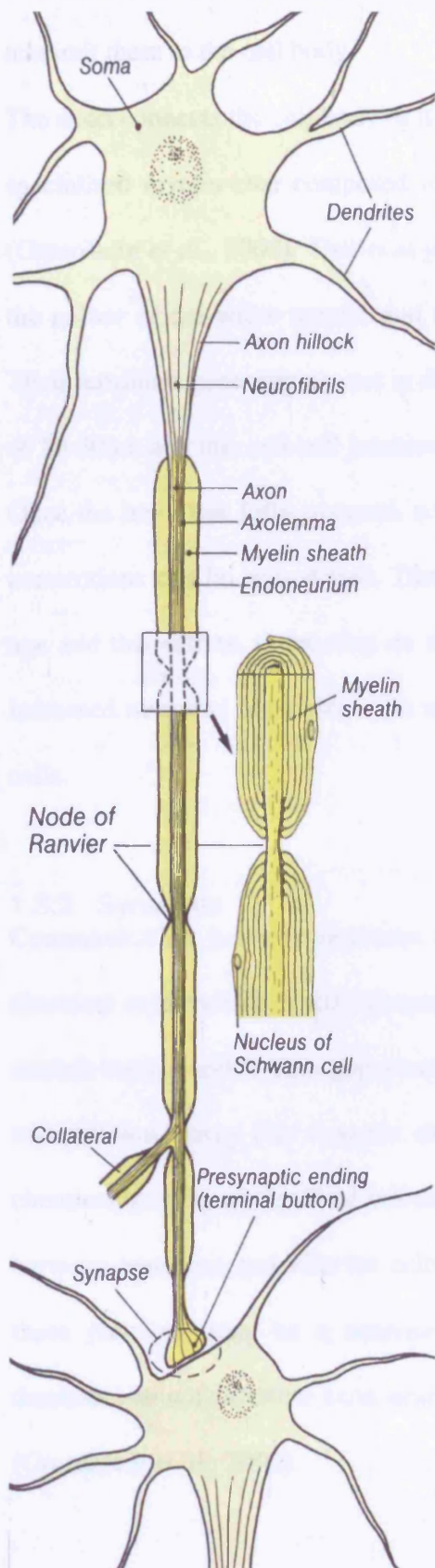


FIGURE 1.4 Canine vertebrae column, which surrounds and protects the spinal nerves. There are 8 cervical, 13 thoracic, 7 lumbar, 3 sacral plus 5 caudal vertebrae (from Veterinary Neurobiology at <http://vanat.cvm.umn.edu/neurolab/Lab4/L4index.html>, accessed November 2003)

1.3 General cellular structure of the CNS

Information is passed between various regions of the brain and overall behavioural function depends on several regions co-operating. Different aspects are processed in parallel and converge as a single output. These regions are composed of cells of which there are two major types in the brain:

- Neurones
- Neuroglial cells (provide nourishment, protection and support to neurones, not considered further)
 - Astrocytes
 - Oligodendrocytes
 - Ependymal



1.3.1 Neurones

Neuronal cells have major roles in transporting information within the brain and around the body. Within the cortex there are more than a million neurones, which are highly specialised cells with several key features as illustrated in Figure 1.5.

The shape and specialised function of the neurone depends on its cytoskeleton. This is a fibrous protein network, which provides an assembly scaffold for the axon and specificity in localising particular components. The internal cytoskeleton consists of microtubules, neurofilaments and shorter actin filaments. Cross linkages provide the supporting structure. The cytoskeleton close to the axonal membrane is mainly composed of actin filaments linked via fine filaments to the internal microtubules and the plasma membrane (Greenstein *et al.*, 2000).

FIGURE 1.5 Key features of a neuronal cell (Despopoulos *et al.*, 1986)

The soma or cell body of the neuronal cell is approximately 20µm in diameter and contains typical organelles e.g. nucleus, mitochondria, endoplasmic reticulum and Golgi body, which are

essential for normal cell function. The dendrites are projections, which receive signals and transmit them to the cell body.

The axon connects the cell body to its nerve terminal. In myelinated nerves, the axon has a specialised myelin coat composed of Schwann cells, interspaced with Nodes of Ranvier (Greenstein *et al.*, 2000). This coat gives the cell a characteristic white appearance, hence the colour of the white matter, and the ability to conduct impulses faster (section 1.5.1). Their terminals generally are not in direct contact with the adjacent neurones; there is a gap of 20-30nm and this cell-cell junction is known as a synapse.

Once the brain has fully matured, no further neuronal growth occurs though the dendritic connections can be remodelled. There is also continual considerable neuronal death with age and this differs, depending on the brain region and individual. Some neurones show increased neuronal branching with ageing perhaps to compensate for the death of nearby cells.

1.3.2 Synapses

Communication between neurones is through synaptic transmission that may be either electrical or chemical. Electrical synapses occur in nervous tissue, and between cardiac and smooth muscle cells. This gap junction relies on ionic currents through ion channels for transmission across this synaptic cleft. Chemical synapses are specialised to enable the chemical transfer of electrical information and occur generally between neurones, but also between neurones and effector cells (muscles, glands and sensory organs). In the brain these junctions may be a neurone with: a cell body (axo-somatic), a dendrite (axo-dendritic) or with another axon near the terminus (axo-axonic) as illustrated in Figure 1.6 (Greenstein *et al.*, 2000).

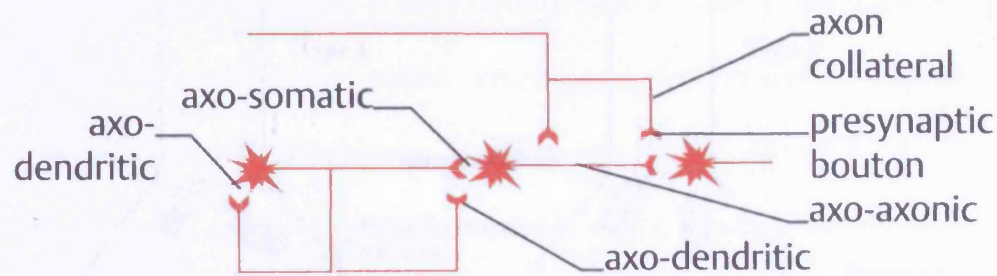


FIGURE 1.6 Synaptic junctions (Greenstein et al., 2000)

On certain cells in the CNS, a single dendritic spine may form several synapses with an incoming axon. Synapses are further classified depending on synaptic cleft width and density distribution (Figure 1.7):

- *Type I* characterised by wide synaptic cleft (30nm), dense region of post-synaptic thickening and a large active zone. Occur on spines projecting from apical or basal dendrites and are generally excitatory (glutamnergic i.e. glutamate is the primary neurotransmitter)
- *Type II* characterised by a smaller active zone, thinner clefts (~20nm), flattened vesicles and a less dense post-synaptic membrane. Occur on the soma of the pyramidal cells in the cerebral cortex and are inhibitory (GABAergic i.e. γ -aminobutyric acid (GABA) is the primary neurotransmitter)

Neurotransmitters are stored in synaptic vesicles in the nerve terminals. The conduction of an electrical impulse to the pre-synaptic membrane causes the voltage-sensitive calcium channel's (VSCC) pore to open, allowing calcium to enter the nerve terminal. This influx triggers the vesicles to fuse by exocytosis with the membrane and the neurotransmitter is secreted from the pre-synaptic membrane into the synaptic cleft.

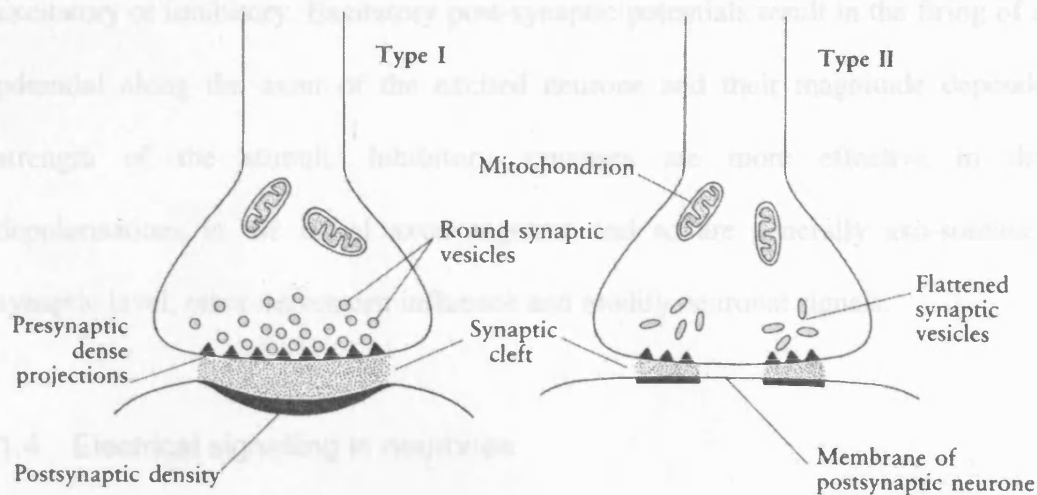


FIGURE 1.7 Key features of a synapse (Strange, 1996)

On release into the cleft, the neurotransmitter travels to the post-synaptic membrane where it is recognised by specific receptors. Depending on the receptor type, the electric excitability of the cell (via voltage-sensitive ion channels) or intracellular signal transduction (e.g. guanine nucleotide binding protein (G protein) coupled receptors (GPCR)) is then altered. Effects are generally delayed for ~0.5ms after the arrival of the action potential in the pre-synaptic nerve due to the slow diffusion of the transmitter across the cleft.

The effects of the neurotransmitter may be either inhibitory e.g. glycine, or excitatory e.g. acetylcholine. Inhibitory synapses in general induce increases in potassium efflux, which cause membrane hyperpolarisation. In contrast, excitatory effects mediated through ion channels generally cause rapid influx of sodium through voltage-sensitive sodium channels, which produce a large depolarising synaptic potential. These channels are critical for neuronal excitability and hence are a key feature of neuronal cells.

The electrical effects, i.e. the inhibitory efflux and excitatory sodium influx, occur simultaneously and summate to produce an overall post-synaptic potential, either

excitatory or inhibitory. Excitatory post-synaptic potentials result in the firing of an action potential along the axon of the excited neurone and their magnitude depends on the strength of the stimuli. Inhibitory synapses are more effective in dampening depolarisations in the initial axon segment and so are generally axo-somatic. At the synaptic level, other nerves can influence and modify neuronal signals.

1.4 Electrical signalling in neurones

All living cells are able to maintain membrane potential but only nerve and muscle cells are able to show electrical excitability.

1.4.1 Action potentials

Action potentials are similar in muscle and nerve cells though the cardiac action potential has particular unique features. Action potentials are generated by alterations in ion movement across the plasma membrane on excitation of the cell by a sufficiently strong stimulus (Figure 1.8). The resting potential (approximately -60mV) becomes less negative and the membrane is described as being depolarised. Once the threshold potential has been reached, generating an action potential is an 'all or nothing' event, irrespective of the magnitude of the stimulation. The voltage-sensitive sodium channels then open resulting in a rapid sodium influx. Inactivation occurs after <0.1ms with a slow increase in potassium movement. This efflux decreases the membrane potential and can lead to a few seconds of hyperpolarisation (when potential is more negative than at rest). This brief absolute refractory period, in which the nerve cannot be stimulated by any stimuli, is followed by a relative refractory period during which an action potential of lower amplitude can be generated. The sodium/potassium exchange pump is continually acting to restore the resting potential (Despopoulos *et al.*, 1986).

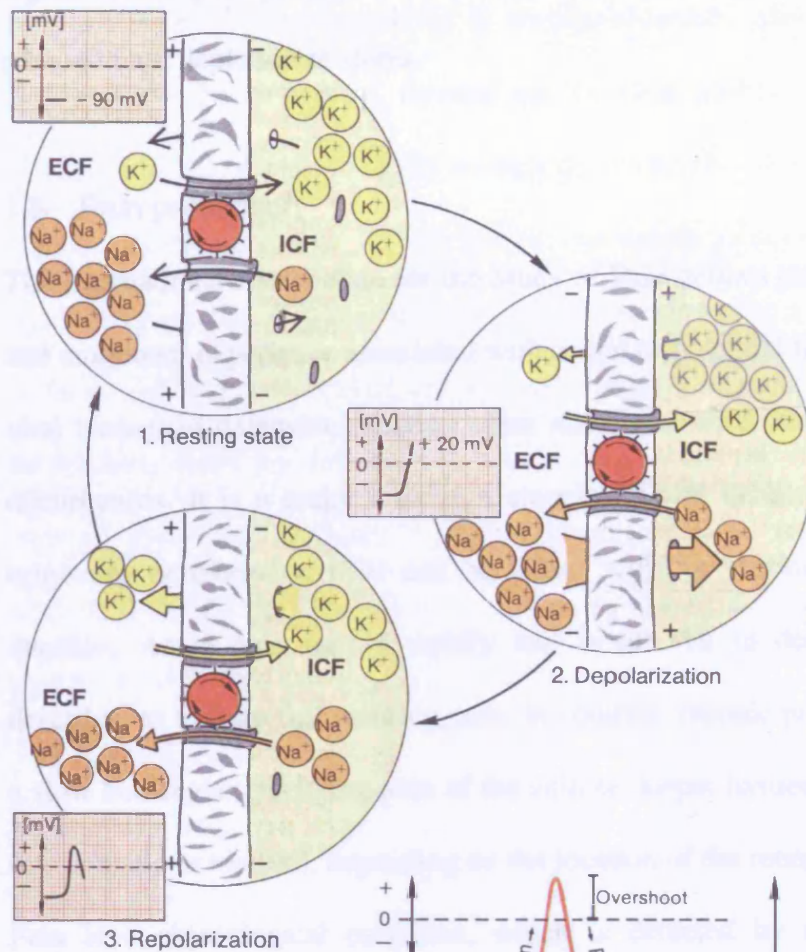
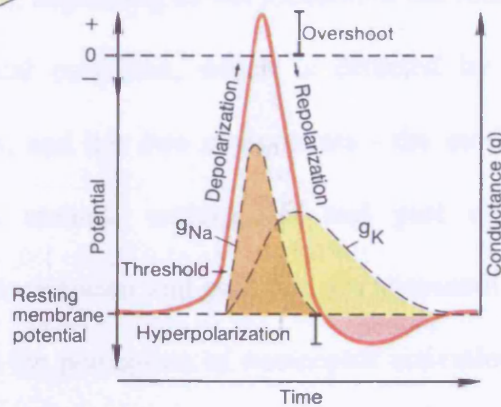


FIGURE 1.8
Conductance of sodium and potassium giving rise to an action potential (Despopoulos et al., 1986)

A. Depolarization and repolarization



1.4.2 Propagation of impulses

Generating an action potential in one area of the nerve results in a flow of current carrying the 'signal' along the axon. The speed of propagation is dependent on myelination and fibre diameter (section 1.5.1). On reaching a nerve terminal the action potential then stimulates the pre-synaptic membrane to release neurotransmitters as described above. The

higher the frequency of generated action potential, then more neurotransmitter will be released until depletion of stores.

1.5 Pain perception

The International Association for the Study of Pain defines pain as “an unpleasant sensory and emotional experience associated with actual or potential tissue damage”. Pain serves a vital biological defensive function often associated with other psychological and central disturbances. It is a major condition associated with debilitating diseases and generally originates peripherally. Pain can be either acute or chronic, depending on cause and duration. Acute pain occurs rapidly and is not felt in deeper tissues. It is generally described as a sharp fast pricking pain. In contrast, chronic pain increases with time and is a slow burning excruciating pain of the skin or deeper tissues. Pain can be further divided into somatic or visceral, depending on the location of the receptors stimulated.

Pain is a physiological condition, which is detected by refined receptors within the damaged body tissues, and has two components - the motivational-affective (emotional) component, such as anxiety, anticipation and past experiences, and the sensory-discriminative part. Nociception and pain are not necessarily analogous since nociception is the term applied to the perception of nociceptor activation by noxious stimuli, whereas pain refers to the subjective response to this particular input to the brain. One pain classification describes: physiological, inflammatory (from tissue damage) and neuropathic pain (from changes in damaged nerves). During and after injury, neurotransmission within the periphery and CNS undergoes profound changes, some of which may be permanent so altering the brain's future perspective of pain. The three key stages in the perception of pain are pain sensitivity, transmission of signals from periphery to dorsal horn of the spinal cord, and finally signals to and from the higher brain centres.

1.5.1 Nociceptors

Pain is detected by sensory endings in peripheral tissues, which are classified according to their response to mechanical, thermal and chemical stimuli. Those activated by noxious stimuli, noxious being potentially damaging, are known as nociceptors. These bare nerve endings, found in the skin, muscle tissues, and deeper viscera, detect physical or chemical changes as a result of injury and have cellular receptors for a variety of mediators on their surface, which usually lie dormant until stimulated (Tortora *et al.*, 1990).

In the skin, there are two types of nociceptors – A- and C-fibres. In general, A-fibres respond to intense mechanical or thermal stimuli and polymodal C-fibres respond to noxious stimuli from mechanical, thermal and chemical input (Messlinger, 1997). Others may respond to only one type of stimulus.

The A and C types of sensory skin afferent fibres have been distinguished depending on their ability to induce ‘sharp’ or less localised pain (Figure 1.9), and the speed of impulse transmission:

- A α /A β large diameter fibres are myelinated and faster conducting ($\sim 120\text{m s}^{-1}$) than A δ fibres. These are not usually involved in the processing of nociceptive inputs to the spinal cord, the exception being in the case of mechanical allodynia.
- A δ medium fibres of 2-7 μm diameter, are myelinated allowing impulses to travel at $\sim 15\text{m s}^{-1}$ by saltatory conduction to produce the ‘first’ sharp, intense pain. Two classes of these fibres are distinguished by their responses to intense mechanical stimuli or tissue injury.
- Unmyelinated C small fibres of 1-5 μm diameter transmit impulses at a slower speed of $\sim 1\text{m s}^{-1}$ to induce less localised ‘second’ pain, which can be described as a dull and throbbing ache.

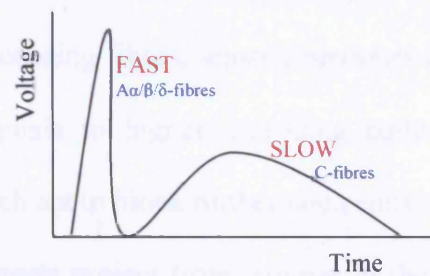


FIGURE 1.9 Conduction velocity is directly related to fibre diameter, which accounts for the first 'fast' and then the second 'slow' pain

Nociceptors of the deep tissues and viscera are categorised depending on their mechanosensitivity. Noxious mechanical stimuli specifically activate the high-threshold afferents in somatic and visceral tissues whereas many visceral afferents are affected by peristaltic contractions. Visceral pain is unique; there is no sharp pain followed by a more prolonged ache, only a poorly localised deep ache. A special class of nociceptors known as silent afferents has also been identified and these are only mechanosensitive after long periods of noxious stimulation, e.g. during inflammation or tissue injury.

1.5.2 Ascending pathways

Three main sensory pathways ascend the spinal cord: pain-temperature, proprioception-stereognosis and light touch. Afferent fibres travel into the spinal cord via the dorsal root where they synapse with specific post-ganglionic ascending collaterals, also known as nociresponsive neurones. The grey matter of the cord (section 1.2) is segmented into laminae and generally A δ - and C-fibres terminate in the dorsal horn in laminae I and V, and I and II, respectively. Some fibres ascend several segments in Lissauer's Tract before entering the grey matter to synapse in a particular layer. Many interneurones link these two layers and release mainly enkephalins to modulate afferent transmission.

Three pathways exist for processing nociceptive input from the dorsal horn; afferents can synapse directly with ascending fibres, sensory neurones may synapse with interneurons, which then transmit signals to higher ascending pathways, or afferents may link to inhibitory neurones, which act to block further nociceptive transmission.

Ascending nociceptive tracts project from laminae in the spinal cord to the brain (Figure 1.10); spinothalamic tract (from laminae I, V-VIII to the thalamus), spinoreticular tract (laminae VII and VIII to the thalamus or reticular formation), spinomesencephalic tract (laminae I and V to the periaqueductal grey (PAG) matter and other midbrain areas) and spinocervicothalamic tract (laminae III and IV to thalamus and gracile nuclei) (Greenstein *et al.*, 2000).

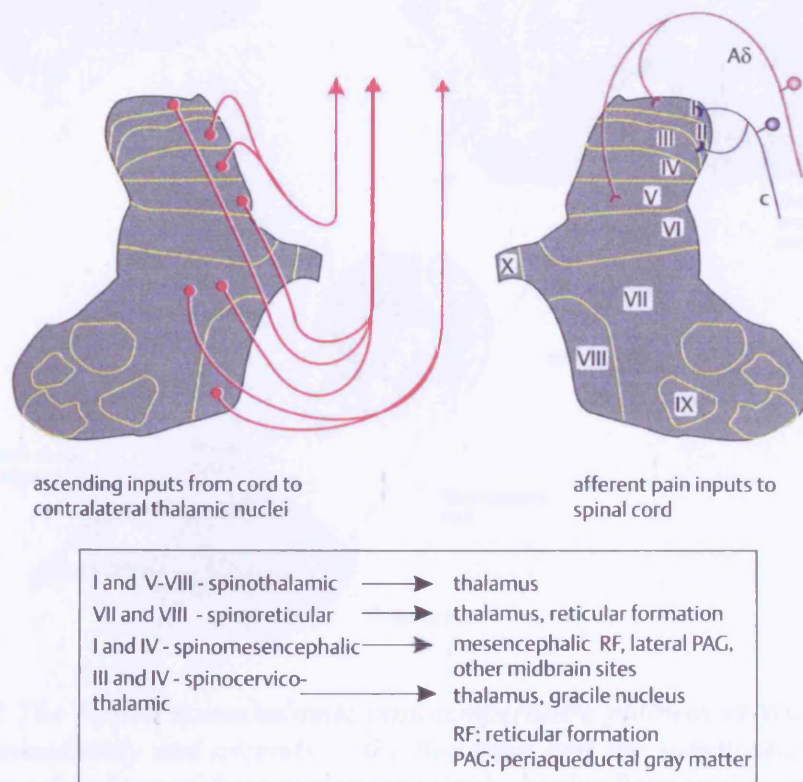


FIGURE 1.10 Afferent nociceptive input to spinal cord and ascending pathways (Greenstein *et al.*, 2000)

The pain-temperature pathway from the body follows the spinothalamic pathway. This crosses over the spinal cord almost immediately (within one or two vertebrae) after

entering and ascends through the medulla, pons and midbrain without synapsing until it reaches the thalamus. The tract then continues to the cerebral cortex (Figure 1.11).

The trigeminal pain pathway which carries information about pain in the face or head is analogous to the spinothalamic route; sensory fibres initially synapse on second order neurones in the spinal trigeminal nucleus and then cross and ascend to the thalamus in the trigeminal lemniscus (Bear *et al.*, 2001).

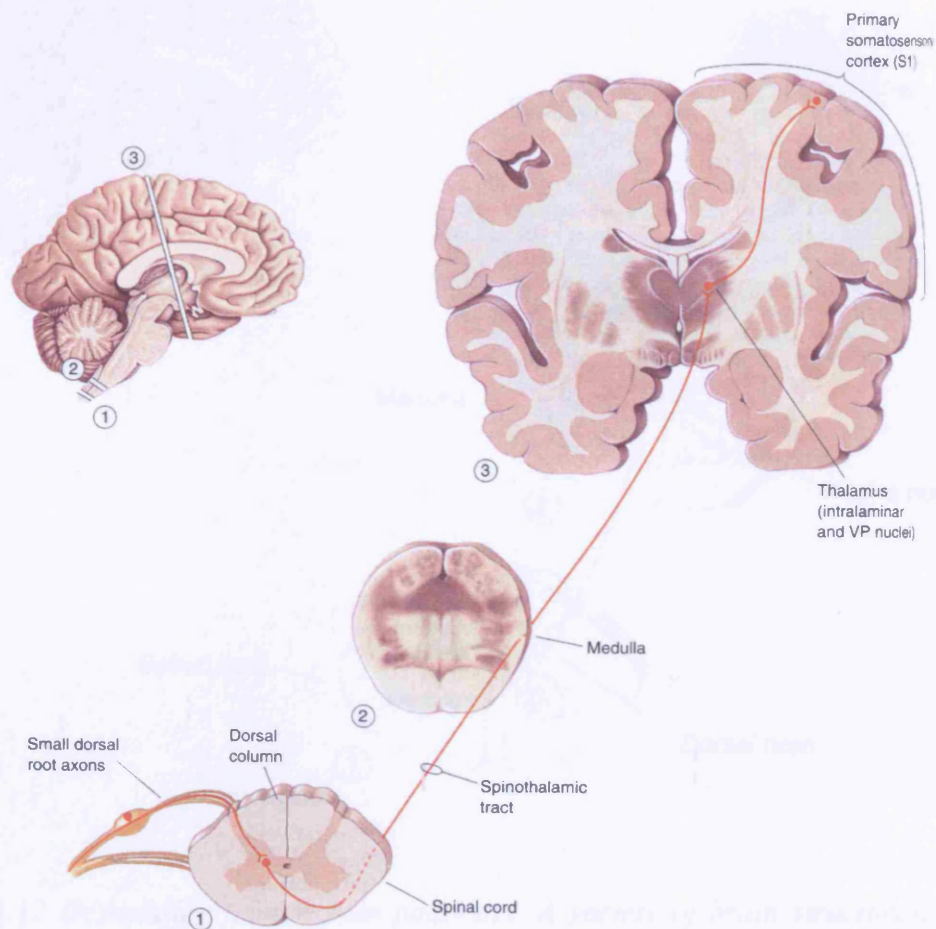


FIGURE 1.11 The human spinothalamic pain-temperature pathway crosses over the cord almost immediately and ascends to the thalamus and the somatosensory cortex. The inset shows the plane of these regions within the brain (Bear *et al.*, 2001)
 VP, ventral posterior

1.5.3 Descending pathways

Nociceptive information reaching the brain is processed and controlled by modulatory circuits within higher brain centres and through descending efferents, originating mainly

from the prefrontal and somatosensory cortex, periventricular nucleus of the hypothalamus, thalamus, midbrain PAG, and the raphe nucleus magnus in the medulla (Figure 1.12). Some neurones of the raphespinal tract from the raphe nuclei terminate in laminae II and III of the dorsal horn where they regulate interneurons.

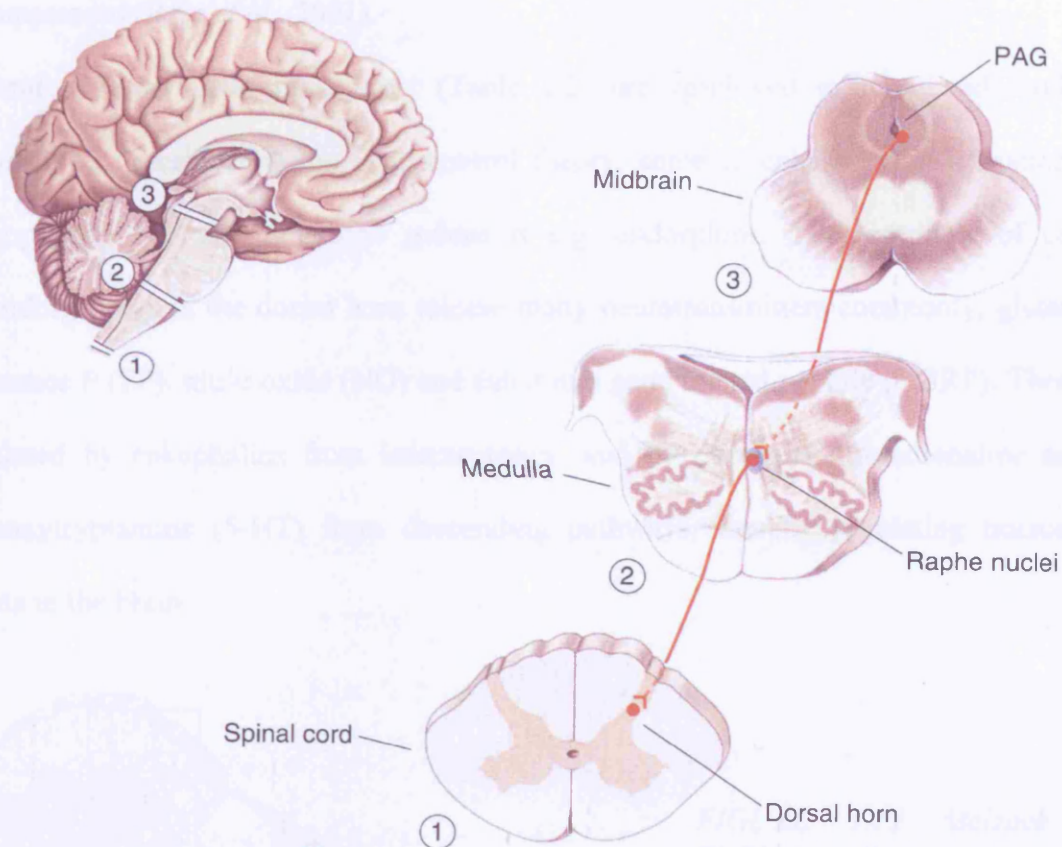


FIGURE 1.12 Descending human pain pathways. A variety of brain structures, many of which are affected by behavioural state, can influence activity within the PAG of the midbrain. The PAG can influence the raphe nuclei of the medulla, which in turn modulates the flow of nociceptive information through the dorsal horns of the spinal cord (Bear et al., 2001)

1.5.4 Gate control theory of pain

The regulation of the pain pathways by both intrinsic neurones, and those originating in the brain, led to the hypothesis of the ‘Gate control theory’. Originally proposed in 1965 by Wall and Melzack, this theory describes the transmission from one group of fibres

regulating signals in other groups as illustrated in Figure 1.13. Here, the ascending projection neurone can be directly excited by both A- and C-fibres. It can also be inhibited by the interneurone, which is both inhibited by the large C-fibre and excited by the pain A axon. Activity in the A axon is usually sufficient to trigger ascending nociceptive signals but, if the C-fibre fires concurrently so activating the interneurone, then these signals will be suppressed (Bear *et al.*, 2001).

Several different neurotransmitters (Table 1.2) are employed to relay and modulate impulses as described by the Gate control theory, some to enhance pain sensation e.g. neuropeptide FF, and others to reduce it e.g. endorphins. The terminals of central ascending fibres in the dorsal horn release many neurotransmitters commonly, glutamate, substance P (SP), nitric oxide (NO) and calcitonin gene related peptide (CGRP). These are regulated by enkephalins from interneurons, and by dopamine, noradrenaline and 5-hydroxytryptamine (5-HT) from descending pathways, thereby regulating nociceptive inputs to the brain.

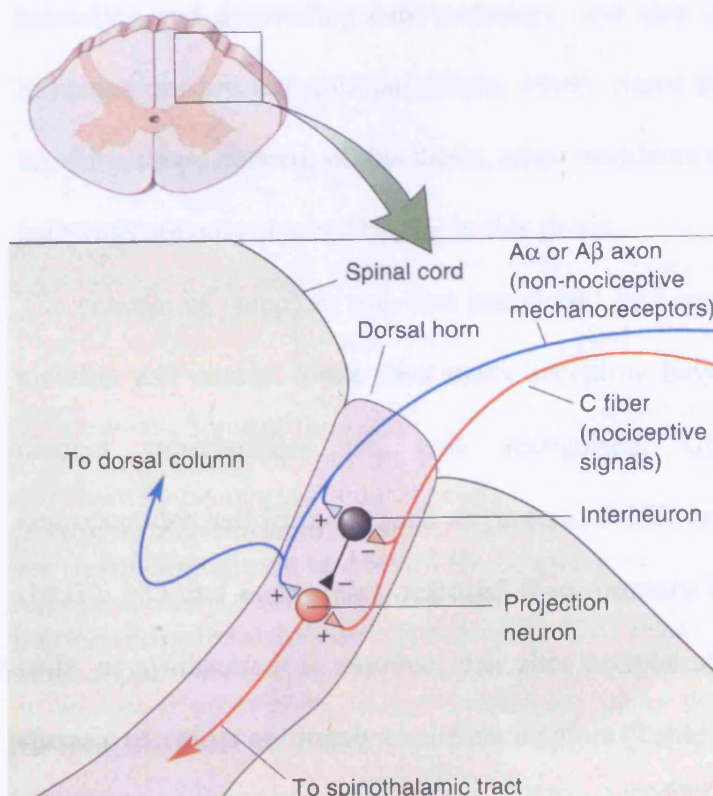


FIGURE 1.13 Melzack and Wall's gate theory of pain (Bear *et al.*, 2001)

TABLE 1.2 Summary of neurotransmitters in ascending and descending non-nociceptive and nociceptive pathways of the nervous system

Pathway	Effect of transmitter	Neurotransmitter	Localisation	
			Spinal cord	Supraspinal
Ascending	Excitatory	Glutamate	Sensory afferents to dorsal horn neurones	Efferents from cortex & cerebellum (descending)
	Inhibitory	Tachykinins	Sensory afferents to dorsal horn neurones	
		GABA	Interneurones & motorneurones	Cerebellum, neocortex, thalamus & hypothalamus
Descending	Excitatory	5-HT (also inhibitory)	Motorneurones	Raphe nuclei
		Acetylcholine	Synapses	Synapses in brain stem
	Inhibitory	Noradrenaline	Synapses	Locus coeruleus, neocortex, thalamus & cerebellum
		Opioids	Spinal cord	Thalamus & hypothalamus
		Nociceptin	Spinal cord	Thalamus & hypothalamus

1.6 Mediators at nociceptors

Opioid peptides and N/OFQ have an important role in modulating signals in both the ascending and descending pain pathways, and also can act at peripheral nociceptors to influence onward transmission (Ueda, 1999). Since these peptides (sections 1.8 and 1.9) are the primary concern of this thesis, other mediators acting at nociceptors and within pain pathways are only covered briefly in this thesis.

The concept of receptors was first introduced by Langley in 1905 in studies investigating nicotine and curare. Since then many receptors have been identified and indeed many distinct superfamilies are now recognised. Chemical inflammatory mediators, neuropeptides and irritants, such as protons, 5-HT, bradykinin (BK), nerve growth factor (NGF), NO and nucleotides, released from primary sensory terminals and non-neuronal cells, or synthesised as required, can alter peripheral nociceptor sensitivity by acting at specific receptors or directly excite nociceptors (Table 1.3).

TABLE 1.3 Mediators act on afferent nociceptors to control neuromodulator release

	Mediator	Receptor	Neuromodulator
Metabotropic	BK NGF	B2 TrkA	SP CGRP Glutamate CCK Somatostatin
Iontropic	Capsaicin Protons Heat ATP 5-HT	TRPV1 TRPV1/ASIC TRPV1/ TRPV4 P2X ₃ 5-HT ₃	

ASIC, acid sensitive ion channel; ATP, adenosine triphosphate; BK, bradykinin; CCK, cholecystokinin; CGRP, calcitonin gene related peptide; 5-HT, 5-hydroxytryptamine; NGF, nerve growth factor; P2X₃, ATP receptor; SP, Substance P; TrkA, NGF receptor; TRPV, transient receptor potential vanilloid receptor

1.6.1 Kinins

When tissue is damaged, BK and kallidin are produced from a plasma protein precursor, kininogen. BK induces pain-causing actions via GPCRs, B1 and B2, and its effects are directly enhanced by the release of prostaglandins (PG). B2 receptors are the predominant subtype found on nociceptor endings. PG do not directly cause pain but enhance the effects of other mediators, particularly 5-HT and BK via G_s proteins. This is achieved through inhibition of potassium channels and indirect effects on other similar channels. Interestingly BK may cause PG release so exerting a 'self-sensitising' effect. Other eicosanoids and prostacyclins may be important though evidence for these so far is limited.

1.6.2 Capsaicin

Capsaicin (8-methyl-N-vanillyl-6-noneamide) is the active ingredient in *Capsicum* chilli peppers, responsible for the hot burning sensation. It acts specifically through a ligand-gated ion channel, a member of the transient receptor potential vanilloid (TRPV) superfamily.

TRPV1 receptors are expressed on un-myelinated C-fibres and small A δ -fibres in the dorsal root, and have high permeability to calcium. They are activated by capsaicin, acidification (generated by tissue ischemia and inflammation) and temperatures above

43°C (Caterina *et al.*, 1997). Inflammatory mediators, such as BK or NGF, potentiate sensitivity to capsaicin and heat by activation of phospholipase (PL) C γ that relieves phosphatidylinositol-4,5-bisphosphate inhibition on the receptor. TRPV2 receptors have also been identified, which are activated by noxious heat with a threshold of 52°C and *in vivo*, by translocation to the plasma membrane in the presence of growth factors (Montell *et al.*, 2002). A vanilloid-like receptor (TRPV4) has also been proposed to exist on nociceptors. Other TRPV family members, TRPV5 and TRPV6 have recently been cloned which are highly selective for calcium and are constitutively active, resembling calcium transporter proteins (Gunthorpe *et al.*, 2002).

1.6.3 Nerve growth factor

NGF, a known mediator of persistent pain, particularly of inflammatory pain binds to its TrkA receptor. This is a member of the tyrosine kinase receptor superfamily, which on activation stimulates the inositol signalling pathway or other transduction events. Polymodal C-fibre neurones can be simply classified depending on their need for neurotrophic mediators since NGF-dependent nerves require NGF for increased synthesis of SP or CGRP. These nerves are known as TrkA-positive neurones, since they express TrkA. Other fibres such as glial cell line-derived neurotrophic factor neurones (c-Ret-positive neurones) do not express SP or TrkA.

1.6.4 5-Hydroxytryptamine

5-HT, a catecholamine found in brain cells, platelets, enterochromaffin and mast cells, is stored in the vesicles of nerve endings and released on nerve injury, inducing hyperalgesia. Several GPCRs or ligand-gated receptors have been identified for 5-HT; 5-HT₁ to 5-HT₇ and these can be further characterised. The effects of 5-HT can be either excitatory (5-HT₂) or inhibitory (5-HT₁). The major subtypes expressed in the rat dorsal horn are 5-HT_{2A} and

5-HT₃, which are responsible for 5-HT mediated nociception, particularly hyperalgesia. The 5-HT_{2A} receptor subtype is found in ~10% of dorsal root ganglia, the majority of which are C- and A δ -fibres, and its mRNA is co-localised with that for CGRP (Okamoto *et al.*, 2002). This indicates that these 5-HT neurones belong to the TrkA NGF-dependent group of neurones and are important in modulating inflammatory pain.

N/OFQ modulates 5-HT and noradrenaline release from synapses, particularly those in the cerebral cortex. In rat cortical synaptosomes, N/OFQ via activation of NOP was found to pre-synaptically inhibit 5-HT release, having a greater inhibitory effect than that observed on activation of opioid receptors (Marti *et al.*, 2003; Sbrenna *et al.*, 2000).

1.6.5 Protons

Tissue acidification occurs with inflammation, infection or ischemia. Low pH in damaged areas can open acid sensing ion channels (ASIC), leading to stimulation of nociceptors. Five subtypes of ASICs have been identified so far, each with specific kinetics, pH dependence and localisation. Four of these are located in C sensory afferents, indicating a role in proton-dependent nociception. ASIC α is distributed widely, particularly in sensory ganglia on C-fibres and appears to be co-localised with P2X ATP receptors (Caterina *et al.*, 1999).

Protons are also important modulators of TRPV1 receptors (section 1.6.2). They cannot directly activate these receptors but potentiate the effects of capsaicin (Caterina *et al.*, 1997).

1.7 Central mediators

Several neuromodulators are released in the dorsal horn from ascending afferents and descending tracts to regulate transmission to the periphery and higher brain centres. The roles of some of the known mediators are covered briefly here.

1.7.1 Tachykinins

SP (where P stands for pain), the first neuropeptide discovered, is now recognised as one of the tachykinins, along with eledoisin, and neurokinin A (NKA) and B (NKB). These peptides are formed by cleavage of preprotachykinins and are characterised by a terminal 'canonical' sequence, FXGLM-NH₂. They are found in the spinal ganglia, show sequence homology to opioid peptides and are generally faster acting than BK. Transportation to the dorsal horn and peripheral endings, and tissue-specific post-translational splicing control their abundance and distribution (Zubrzycka *et al.*, 2000). SP is expressed in approximately 50% of C-fibre afferents (predominantly polymodal) and 20% of A δ -fibres but not at all in A α /A β -fibre neurones. It is a co-transmitter with other peptides and glutamate in response to both nociceptive and non-nociceptive inputs, and its actions are mediated through the tachykinin receptor, NK1.

NK1 receptors are found generally on post-synaptic membranes, in the dorsal horn of the spinal cord in lamina I, the outer part of lamina II and in laminae III-V. Other subtypes include NK2 and NK3, which bind NKA and NKB respectively. All these are GPCRs and act by increasing intracellular calcium so triggering gene transcription.

SP can be released, along with CGRP, from nociceptors to cause neurogenic inflammation of the local area, including pre-capillary vasodilation and post-capillary plasma extravasation. The effects of SP are concentration-dependent in that a small amount may produce analgesia whereas high concentrations can induce hyperalgesia. This can be explained by SP stimulating opioid peptide release at low concentrations thereby mediating analgesia. In contrast at high concentrations, neuronal transmission in nociceptive pathways is activated.

1.7.2 Calcitonin gene-related peptide

CGRP is widely distributed throughout the nervous system and has an important role in inflammation and pain modulation. It is found in the majority of primary afferent nerves (in approximately 50% of polymodal C-afferents, 33% of A δ -fibres, and 20% of A α /A β -fibre neurones). In the periphery, CGRP release potentiates the excitatory effects of SP and increases intracellular calcium release. In the rat, N/OFQ has been documented to inhibit CGRP and SP release from the terminals of primary afferents (Helyes *et al.*, 1997).

Several subtypes of CGRP receptors have been identified, as well as a calcitonin receptor-like receptor. These are all GPCRs and are localised in the nucleus accumbens, indicating a central role for CGRP in pain transmission. Interestingly, Li *et al.* (2001) reported that the CGRP1 antagonist, CGRP8-37, potentiates the effects of CGRP and that the roles of these modulators are opposing in the brain, compared to the spinal cord.

1.7.3 Glutamate

This is one of the most important pathways modulating nociception and it is closely co-localised in the CNS with the opioid system. Glutamate, released from central terminal afferents, is the major excitatory output along ascending nociceptive pathways, from the cortex and cerebellum to other brain areas (secondary response neurones). Several transmitters are co-released with glutamate, namely SP, NKA and CGRP, as a result of noxious thermal or mechanical stimuli, or electrical stimuli above the threshold level required to activate C- and A δ -fibres. The effects of N/OFQ on glutamate release are generally inhibitory (Nelson *et al.*, 2000; Nicol *et al.*, 2002) however recent evidence suggests that N/OFQ can also stimulate glutamate levels in the substantia nigra of the rat (Marti *et al.*, 2002). Interestingly, nocistatin (Noc), a bioactive neuropeptide from the same protein precursor as N/OFQ, has been reported to antagonise this inhibitory action *in vitro* (Nicol *et al.*, 1998). Similarly to glutamate, the pre-synaptic actions of N/OFQ inhibit the

release of GABA (section 1.7.4) though no reversal with nocistatin was reported in the rat (Meis *et al.*, 2001).

Glutamate and their receptors are found in particularly high abundance in the dorsal root ganglion, and laminae I and II. Fast neuronal transmission is mediated through both ionotropic and metabotropic receptors. Ionotropic receptors include (\pm)- α -amino-3-hydroxy-5-methylisoxazole-4-propionic acid (AMPA) and N-methyl-D-aspartate (NMDA) subtypes, named after their ligands, the latter being the most important in nociception. They have specific roles; AMPA receptors mediate the largest component of synaptic currents and are responsible for baseline activity whereas NMDA, when activated, induces windup (related to second order hyperalgesia where pain is localised at a remote site) and mediates long-term plastic changes.

Activation of voltage-dependent NMDA receptors only occurs when the noxious input is above threshold level and the pore blockade (by extracellular magnesium) is removed. Hence simultaneously, glutamate must bind to NMDA and an impulse must cause the depolarisation of the post-synaptic membrane, both of which cause several excitatory peptides acting at their own specific receptors to remove this pore block (Dickenson *et al.*, 2002). Activation of NMDA receptors causes elevation of intraneuronal calcium, which stimulates a series of transduction messengers (protein kinases, protein phosphatases, immediate early genes) within the post-synaptic cell.

The metabotropic receptors, mGlu, are GPCRs, which are present on peripheral primary afferents, suggesting a possible role in nociception (Yang *et al.*, 2002). These can be divided further into three groups based on pharmacology, signal transduction and sequence homology. Group I (mGlu1 and mGlu5) signalling involves activation of PLC thereby releasing calcium from intracellular stores and activating protein kinase C. Group II

(mGlu2 and mGlu3) and Group III (mGlu4, mGlu6, mGlu7 and mGlu8) receptors inhibit adenylyl cyclase through G_i .

1.7.4 γ -Aminobutyric acid

GABA is the most widely distributed inhibitory transmitter in the vertebrate CNS. It is stored in the vesicles of nerve terminals and on release into the synaptic cleft, travels to the post-synaptic membrane where it is detected by GABA receptors. GABA transaminase is responsible for the catabolism of GABA and regeneration of glutamate via the Krebs cycle. Hence the metabolism of the two principal neurotransmitters of the CNS – GABA (inhibitory) and glutamate (excitatory) are intricately related and found in abundance in the brain.

At least three subtypes of GABA receptors have been identified: $GABA_A$ which is a pentameric ligand-gated chloride channel, $GABA_B$, a GPCR which indirectly inhibits cyclic adenosine monophosphate (cAMP) formation and also, the recently discovered $GABA_C$, consisting of ζ subunits which form oligomeric chloride channels. All these bind GABA and other mediators, which potentiate the effects of GABA.

GABAergic neurones involved in pain transmission are mainly concentrated in the brain, particularly in the neocortex and cerebellum, though they are also found in the spinal cord (interneurones which mediate peptide release, controlling pituitary function) and retina, with long projections between the striatum and the substantia nigra, and between the hypothalamic nuclei and forebrain.

1.8 Opioid pharmacology

1.8.1 Endogenous opioids

Four main families of opioid peptides have since been identified, which bind selectively to particular receptor subtypes (Table 1.4) to induce a variety of physiological roles within

the body. These are not used as opioid drugs and are known to be derived from peptide precursors in mammals: proopiomelanocortin (from β -lipotropin), prodynorphin and proenkephalin. A fourth precursor, proendomorphin (endomorphins named after endogenous morphine) has been proposed but remains to be identified.

The precursors are synthesised in neuronal soma and then transported to the axon terminal. Here they are transcribed and cleaved into various fragments. The precursors are generally multi-hormone precursors, for example, proopiomelanocortin encodes for β -endorphin and several other bioactive peptides such as adrenocorticotropic hormone (ACTH) (Figure 1.14, Table 1.4).

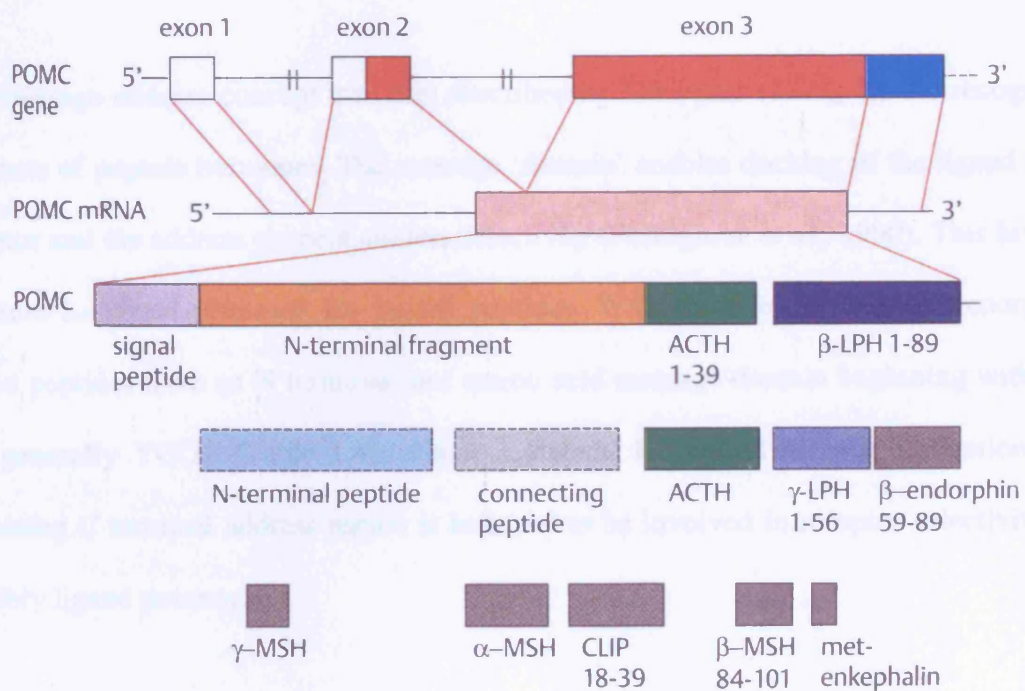


FIGURE 1.14 Proopiomelanocortin (POMC) system (Greenstein et al., 2000)

ACTH, adrenocorticotropic hormone; CLIP, corticotropin-like intermediary peptide; LPH, lipotropin; MSH, melanocyte stimulating hormone

TABLE 1.4 Structure of endogenous bioactive mammalian opioid ligands from specific opioid precursors (sequence homology shown in bold) and their specificity at opioid receptor subtypes

Precursor	Ligand	Sequence	MOP	DOP	KOP
?	Endomorphin-1	YPWF-NH ₂	+++	-	-
?	Endomorphin-2	YPFF-NH ₂	+++	-	-
<i>Pro-opiomelanocortin</i>	β -endorphin	YGGFMTSEKSQTPLVTLFK NAIKNAYKKGE	+++	+++	++
<i>Pro-enkephalin</i>	leu-enkephalin (Leu-E)	YGGFL YGGFMRF YGGFMRGL	+	+++	-
	met-enkephalin (Met-E)	YGGFM	++	+++	-
	Metorphamide	YGGFMRRV-NH₂			
<i>Pro-dynorphin</i>	D _a	YGGFLRRIRPKLKWDNQ	++	+	+++
	Dynorphin B	YGGFLRRQFKVVT			
	α -neoendorphin	YGGFLRKYPK			
	β -neoendorphin	YGGFLRKYP			

(- denotes no binding affinity through to high affinity +++; for amino acid single letter code, see Appendix section 12.1)

The message-address concept was first described by Schwyzer (1977) for the recognition elements of peptide hormones. The message 'domain' enables docking of the ligand to the receptor and the address element confers selectivity (Portoghese *et al.*, 1990). This bivalent structure has been proposed for opioid peptides. With the exception of endomorphins, opioid peptides have an N terminal four amino acid message domain beginning with Tyr¹ and generally YGGF (Table 1.4), which is critical for opioid receptor activation. The remaining C terminal address region is believed to be involved in receptor selectivity and possibly ligand potency.

1.8.2 Receptor subtypes

Three classical subtypes have been identified; μ (MOP) named after morphine, which induces analgesia, bradycardia, hypothermia, and indifference to environmental stimuli, κ (KOP) named after ketocyclazocine, which induces general sedation and depression of flexor reflexes, and δ (DOP) named after deferens since DOP was identified in mouse vas

deferens. Further opioid subtypes such as λ , ι , ζ , σ and ϵ , have been proposed though these are not generally accepted. Several classification systems (Table 1.5) for classical opioid receptor subtypes have been proposed. The most recent system uses DOP, KOP and MOP nomenclature (Cox *et al.*, 2000), and is adopted in this thesis.

TABLE 1.5 Recent IUPHAR classification systems for the opioid receptors

Before 1992	1992-1996	1996 IUPHAR (Dhawan <i>et al.</i> , 1996)	1999 IUPHAR (Cox <i>et al.</i> , 2000)
μ_1 μ_2 μ_3	μ_1 (MOR1/B)	OP3	MOP
δ_1 δ_2	δ_2 (DOR)	OP1	DOP
κ_1 κ_2 κ_3	κ_1 (KOR)	OP2	KOP

The receptors were identified as a result of advances in DNA techniques. Initial efforts to clone the receptors aimed to purify soluble protein from tissue though this proved difficult and unreliable. The first successful molecular cloning of DOP (Evans *et al.*, 1992; Kieffer *et al.*, 1992) used an expression screening method in which radioligand binding served as the screening assay. Subsequent clones of KOP (Yasuda *et al.*, 1993) and MOP (Thompson *et al.*, 1993) soon followed, obtained by hybridisation screening using homologous cDNA probes. Cloning provided information on receptor structure and allowed characterisation of each subtype in isolation.

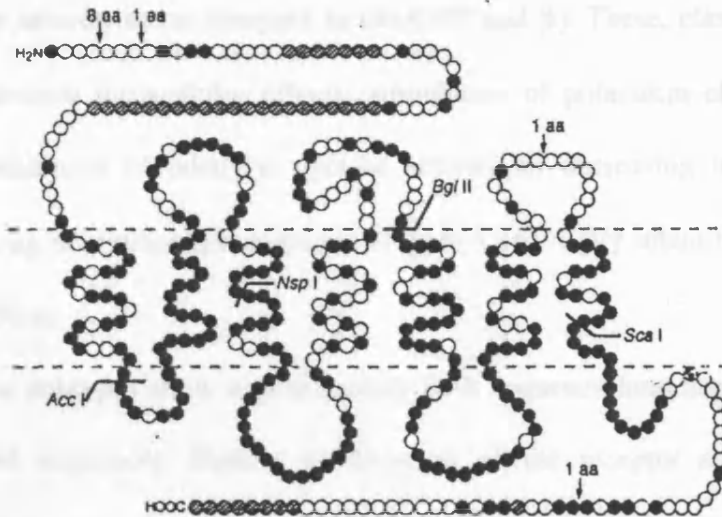


FIGURE 1.15 Proposed transmembrane topography of rat DOP subtype (Fukuda *et al.*, 1995). Note closed circles show homology with MOP and open circles represent non-identical amino acids

Classical opioid receptors are members of the seven-pass transmembrane receptor superfamily (Figure 1.15). These share common structural features of seven hydrophobic transmembrane domains, an extracellular N terminal region with several glycosylation sites, serine and threonine phosphorylation sites on an intracellular C terminal tail and a disulphide bond linking the first and second extracellular loops.

Phosphorylation sites found on the intracellular carboxyl tail of the MOP receptor, particularly Ser³⁶³, Thr³⁷⁰ and Ser³⁷⁵, are proposed to regulate agonist-induced receptor internalisation (El Kouhen *et al.*, 2001) and so control receptor activity. Substitution mutants of Ser³⁷⁵ have reduced receptor internalisation whereas the interchange of Ser³⁶³ and Thr³⁷⁰ to Ala resulted in accelerated internalisation kinetics.

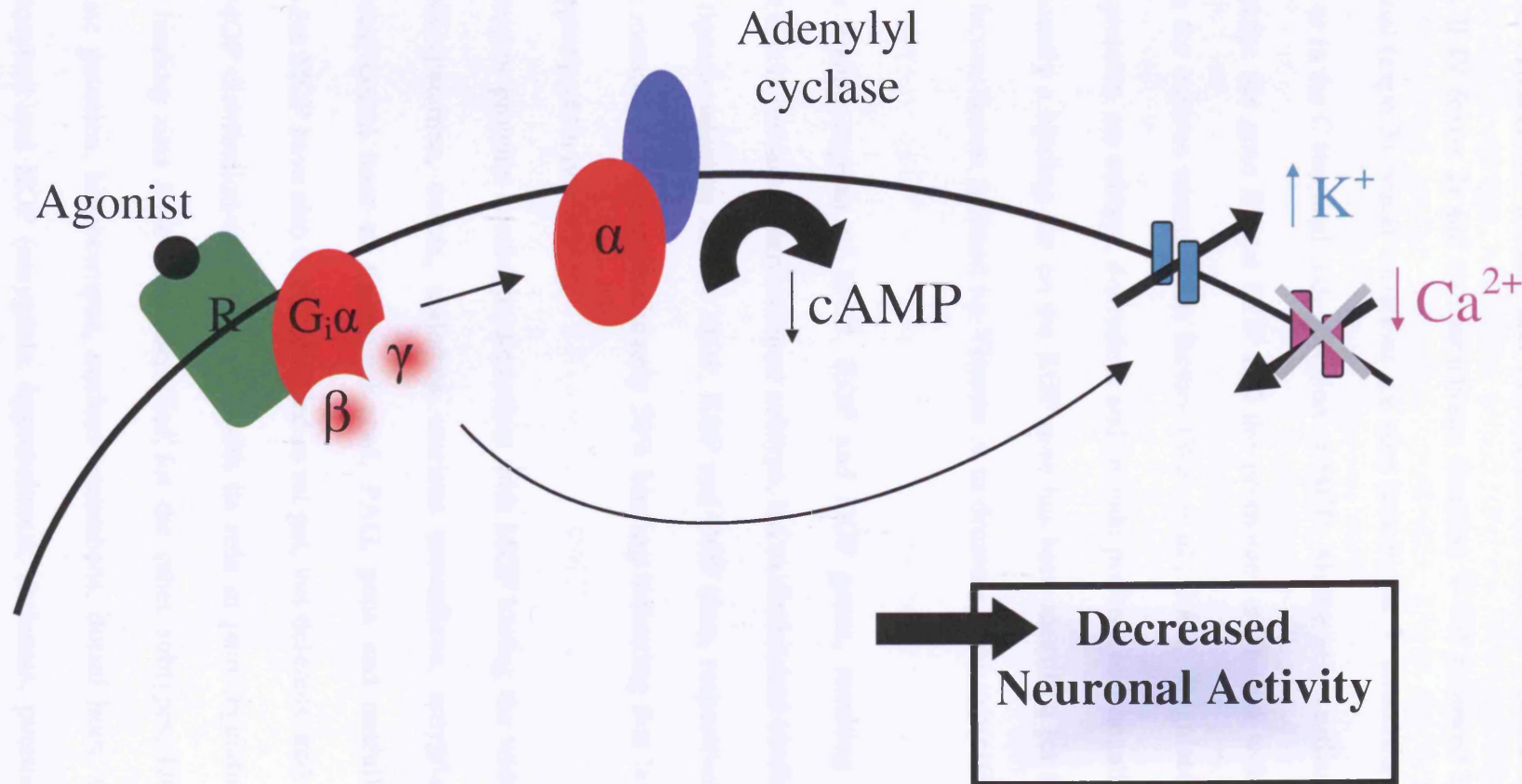
Opioid receptors couple to G proteins, G_o or G_i, which consist of three subunits, α , β and γ . On activation of MOP, DOP or KOP, a conformational change of the receptor protein occurs, leading to an interaction with diffusible G proteins. Guanosine diphosphate (GDP) is exchanged for guanosine triphosphate (GTP) on the α subunit thus promoting the

cleavage of the heterotrimeric complex to $G\alpha$ -GTP and $\beta\gamma$. These, classically $G_{i/o}\alpha$ -GTP, then mediate several intracellular effects: stimulation of potassium efflux, inhibition of VSCCs and inhibition of adenylyl cyclase activity so decreasing intracellular cAMP thereby inhibiting neurotransmitter release (Figure 1.16). $G\beta/\gamma$ subunits can also mediate intracellular effects.

Opioid receptor subtypes show approximately 60% sequence homology on alignment of the amino acid sequences. Further subdivisions of the receptor subtypes have been proposed on pharmacological grounds to include MOP-1, MOP-2, MOP-3, DOP-1, DOP-2, KOP-1, KOP-2 and KOP-3; this is controversial as each subtype arises from a single gene (Dhawan *et al.*, 1996; Mogil *et al.*, 2001). Moreover, there is now evidence to demonstrate that the subtypes, MOP, DOP and KOP, can exist as homo- and hetero-dimers (Jordan *et al.*, 1999) and several splice variants have been postulated. It is important to remember that despite pharmacological and behavioural evidence (e.g. a dissociation of the respiratory depressant and antinociceptive effects of morphine) to suggest the existence of subtypes of the classical MOP/DOP/KOP (i.e. pharmacologically distinct receptors), particularly of MOP, no such subtypes have been identified. However it is possible that some post-translational modification of a common MOP gene product or association with receptor activity modifying proteins may explain this pharmacology.

Interestingly, there are currently 15 splice variants of MOP, some with distinct regional distribution in the CNS. However, pharmacological analysis of these variants when expressed in Chinese hamster ovary (CHO) cells does not reveal any major differences (Pan *et al.*, 2001) and these do not correspond to the pharmacologically characterised MOP-1-3.

FIGURE 1.16 Schematic representation of signal transduction events resulting from opioid agonist interaction with either classical or NOP receptors (R in diagram) in neurones. Receptor (R) activation leads to G-protein interaction and eventual α -subunit dissociation. $G_i\alpha$ can then inhibit adenylyl cyclase to decrease cAMP formation, activate voltage-sensitive potassium channels to produce hyperpolarisation or close voltage-sensitive calcium channels decreasing intracellular calcium. The net effect is decreased neuronal activity



1.8.3 Expression and localisation

Genes for the opioid receptor subtypes share a common structure with coding regions over three major exons for the extracellular domain and transmembrane domain I (exon 1), transmembrane domains II-IV (exon 2) and transmembrane domains V-VII followed by the cytoplasmic C terminal (exon 3). Small variations are seen here in the 5' untranslated region of the KOP gene or in the C terminal coding region of MOP. All the genes utilise a TATA-less promoter except the gene for rat KOP and the promoters are found within clusters of binding sites for various transcription factors (Wei *et al.*, 2002). Regulatory mechanisms of gene expression are subtype dependent and include positive and negative transcription factors. Recently a binding site on the KOP gene has been identified for the inhibitory transcription factor, Ikaros, induced by Vitamin A to decrease gene expression (Wei *et al.*, 2002).

Gene disruption in the coding regions of MOP, KOP and DOP genes, resulting in 'knockout' animals deficient in the subsequent receptor subtype, led to diminished binding of radiolabelled opioid ligands selective for the MOP, KOP and DOP sites, respectively. Heterozygous knockout mutants showed approximately 50% binding indicating that both alleles contribute to receptor protein production.

Localisation of these receptor proteins is subtype dependent with MOP having the widest distribution in the CNS (putamen, cortex, thalamus, nucleus accumbens, amygdala, pallidum, locus coeruleus, dorsal horn of the spinal cord, PAG, pons and medulla). Peripheral binding sites for MOP have also been identified in rat gut, vas deferens, and on lymphocytes. Overall MOP distribution correlates well with its role in pain regulation. Central and peripheral binding sites have been identified for the other subtypes, DOP (olfactory cortex, caudate putamen, hippocampus, nucleus accumbens, dorsal horn, vas deferens and on lymphocytes) and KOP (amygdala, hypothalamus, thalamus, putamen, cortex, nucleus accumbens, pons, medulla, hippocampus and brainstem), which exhibit

great interspecies variation. These patterns of distribution are again consistent with their roles in water balance, food intake, pain perception and neuroendocrine modulation.

Whilst there is some overlap in subtype distribution (distribution for MOP and DOP generally appears complementary), precise anatomical localisation differs markedly (Dhawan *et al.*, 1996; Harrison *et al.*, 2000). Opioid receptors are localised with other neuromodulators: KOP immunoreactive neurones are sometimes co-localised with immunostaining for CGRP, nitric oxide synthase, vasoactive intestinal peptide and choline acetyltransferase (Poonyachoti *et al.*, 2002).

1.8.4 Effects of opioids

Opioids modulate transduction in two ways; indirect action on the dorsal horn by pre-synaptic inhibition of excitatory peptide release from afferent fibres, or by direct post-synaptic actions on dorsal horn neurones.

Enkephalins, key neurotransmitters of the opioid family, are present in cell bodies, fibres and nerve endings in many areas of the CNS. These bind to the MOP opioid receptor subtype and are thought to be of major importance in pain modulation through the descending efferent pathways. Neutral endopeptidase (NEP) is a zinc metalloendopeptidase, which degrades many neuropeptides such as SP, BK and indeed, enkephalin. Its importance has been investigated using knockout studies. When NEP is inhibited pharmacologically, increased concentrations of enkephalin result in antinociception. In contrast in knock out mice, hyperalgesia was observed in the hot-plate, tail withdrawal and the writhing tests (Fischer *et al.*, 2002). This indicates NEP-knockout results in BK-induced hyperalgesia, instead of enkephalin-mediated analgesia. NO is also thought to be required.

Endorphins are also key neuropeptides, which are synthesised in the brain and are particularly concentrated in brain areas involved in pain perception. They exert their

effects by blocking pre-synaptic glutamate release and hyperpolarisation of post-synaptic membranes. Neurones containing endorphins are in abundance in the spinal cord and brain stem and prevent ascending nociceptive signals from the dorsal horn to higher brain centres.

The classical response to opioid agonists is analgesia however other physiological and pathological effects reported include respiratory depression, inhibition of reproductive functions, endocrine and immune modulation, gastrointestinal motility and stress responses. The wide range of effects indicates the complex central role of the opioid system.

Analgesic effects are mediated through all receptor subtypes, but particularly MOP. MOP and KOP are also responsible for addiction and dysphoria, respectively. Interactions between the MOP and DOP systems possibly occur to elicit some responses though KOP receptors generally act independently. MOP activation produces primary analgesia followed by the accompanying secondary hyperalgesia. If the stimuli are prolonged, then the 2nd order effect increases and can eventually surpass the analgesic properties. This explains tolerance associated with the opioid system (Colpaert, 2002). There is also evidence that opioid peptides modulate the release of other mediators of the pain pathway. D_a, for example, acts on KOP receptors to suppress release of SP, which is associated with nociceptive transmission, and so diminishes the perceived intensity of noxious stimuli (Pertwee, 2001).

It is also well documented that opioids have a central role in cardiovascular modulation. Previous studies generally report an increase in sympathetic tone and hence increased heart rate and blood pressure. This is controversial as responses are dose dependent – low intracerebroventricular doses (0.2nmol) of Tyr-D-Ala-Gly-MePhe-Gly(ol)-enkephalin (DAMGO), the MOP agonist, induced increased arterial pressure, but 2 or 20nmol

DAMGO significantly decreased pressure and effects persisted for up to 100min (Rao *et al.*, 2003). In contrast, administration of low or high doses of D_a significantly decreased arterial pressure. These effects may be explained by the ability of high agonist concentrations to reach brain areas involved in cardiovascular function or to non-selectively stimulate other receptor subtypes. Opioids can also modulate respiratory functions (Szeto *et al.*, 1999; McQueen, 1983). If opioid drugs are administered to a subject with no pain then the pharmacology suggests respiratory depression. In contrast, when giving appropriate doses to patients with chronic pain, respiratory depression is minimal suggesting that nociceptive inputs oppose the respiratory effects (McQuay, 1999). Such non-pain effects must be noted when developing analgesics acting at opioid receptor subtypes.

1.9 Nociceptin pharmacology

The molecular cloning of MOP, DOP and KOP receptors defined three 'classical' opioid receptor subtypes. Hybridisation screening with opioid receptor probes led to the discovery of cDNA for a possible further opioid subtype, which was named ORL-1. Unsurprisingly, this receptor shows 63-65% homology to the opioid subtypes when considering cDNA from rat, human and mouse though recent evidence may indicate a distinct receptor system.

1.9.1 Nociceptin receptors

Similarly to opioid receptors, these orphan receptors were identified as seven pass receptors with the ability to couple G_{i/o} protein. Several groups cloned the murine and human receptor so various names exist for the nociceptin receptor (Table 1.6). NOP shall be used hereon in this thesis as suggested by IUPHAR.

Activation of NOP by N/OFQ (section 1.9.2) mediates a similar sequence of events to that observed on activation of classical opioid receptors - activation and dissociation of the heterotrimeric G protein, which subsequently modulates signal transduction. Amplification of this ligand-receptor signal is possible in that each receptor may activate several G proteins (Hawes *et al.*, 2000). Effects observed depend on effectors present in the cell with some differences seen using recombinant systems. Generally effects are mediated through $G_{i/o}\alpha$ -GTP, resulting in stimulation of potassium efflux, inhibition of VSCCs and of adenylyl cyclase activity, thereby decreasing cellular cAMP (Figure 1.16). The overall effect is inhibition of neurotransmitter release, such as glutamate, GABA, dopamine, noradrenaline and acetylcholine (Schlicker *et al.*, 2000), pre- and post-synaptically. In general, a depression of neuronal activity is observed.

Other transduction pathways, which can be activated through NOP, include PLA and PLC, and the extracellular signal-regulated kinase/mitogen-activated protein cascade so modulating transcription factors and long-term genetic control although this remains controversial (Hawes *et al.*, 2000). Effects can also be independent of G protein coupling; for example, N/OFQ can act to suppress low-voltage activated transient calcium current in rat dorsal root ganglia (Abdulla *et al.*, 1997).

TABLE 1.6 Initial reports of the cloning of NOP (Mogil et al., 2001)

SPECIES	NOMENCLATURE	REFERENCE
Mouse	KOR-3	Pan <i>et al.</i> (1995)
	MOR-C	Nishi <i>et al.</i> (1994)
Rat	LC132	Bunzow <i>et al.</i> (1994)
	XOR1	Wang <i>et al.</i> (1994)
	Ratxor1	Chen <i>et al.</i> (1994)
	C3	Lachowicz <i>et al.</i> (1995)
	ROR-C	Fukuda <i>et al.</i> (1994)
Human	ORL1	Mollereau <i>et al.</i> (1994)

The gene for NOP was identified from these three species and the homology of the species variants is high at >90% (Henderson *et al.*, 1997). In terms of intron-exon arrangement, it is identical to the genes for DOP, KOP and MOP suggesting a common ancestor (Meunier, 1997) though expression patterns and regulatory mechanisms are not well conserved. Genomic sequences have been discovered in teleost and cartilaginous fish suggesting that the receptor is ~400 million years old. No NOP isoforms have yet been reported despite the presence of several splice variants in peripheral sensory and sympathetic ganglia (Mogil *et al.*, 2001; Xie *et al.*, 1999).

1.9.2 Endogenous nociceptin

N/OFQ was the first novel bioactive substance, isolated from porcine hypothalamic extracts and rat brain, identified using the orphan receptor strategy (Meunier *et al.*, 1995; Reinscheid *et al.*, 1995). This 17 amino acid neuropeptide is derived in mammals from post-translational processing of its precursor, preproN/OFQ. The gene for preproN/OFQ has been partially characterised (Mollereau *et al.*, 1996). It has at least four exons interspersed by three introns with an N terminal 20 amino acid signal sequence and has been mapped to the short arm of human chromosome 8 (8p21). Murine and human nucleotide sequences show similar structural and organisational features to the genes encoding the precursors of the endogenous opioid peptides.

The preproN/OFQ protein consists of 181, 176 and 187 amino acids in rat, human and mouse, respectively. There are several basic cleavage sites in the sequence, upstream and downstream of N/OFQ itself indicating that preproN/OFQ may code for further biologically active peptides. Indeed these peptides are brought to maturation by enzymes of the furin group, which cut the precursor at pairs of cationic amino acid residues. A short bioactive fragment, Noc has been isolated from bovine brain and is reported to exhibit opposing roles to N/OFQ in the CNS (Okuda-Ashitaka *et al.*, 2000). There is an additional

novel heptadecapeptide (residues 160-176 in rat) to the carboxyl end of preproN/OFQ, which has the same terminal amino acids as N/OFQ and is wrapped in paired basic residues; its function is currently unknown. This position corresponds to that of dynorphin B in preprodynorphin. The sequence for N/OFQ appears in the C terminal of preproN/OFQ and it is here where the greatest homology is observed between the murine and human species. Hence it is not surprising that the amino acid sequence of N/OFQ is identical in human, rat and mouse.

N/OFQ was proposed to have message/address domains (Figure 1.17) similar to those proposed for opioid peptides, particularly D_a, though ligand-binding experiments involving truncated versions of this peptide indicate that its architecture may be different. Dynorphins do show considerable structural and sequence homology with N/OFQ but interestingly D_a binds to hNOP with very low affinity (K_i 386nM compared to 0.8, 1.8 and 2.9 for hKOP, hDOP and hMOP, respectively; Zhang *et al.*, 1998) and its receptor, KOP, shows very little affinity for N/OFQ. Ligands for NOP have Phe¹ as the receptor recognising pharmacophore, with Phe⁴ as the dominant pharmacophore responsible for receptor activity. Replacing Phe¹ with Leu has no effect but replacing Phe⁴ with aliphatic amino acids eliminates activity and drastically reduces affinity (Guerrini *et al.*, 1997). Opposite effects are seen if the same substitutions are carried out in opioids i.e. substitution of amino acids in position 1 lead to inactivity. Replacing Phe¹ with Tyr gives a compound, which acts on NOP, as well as KOP and MOP (Calo *et al.*, 1997; Varani *et al.*, 1999). Another important amino acid in the N/OFQ sequence is Arg⁸, which is required for receptor occupation and cannot be replaced. Amino acids in positions 9, 12 and 13 are also important though they are interchangeable.

The presence of paired basic amino acids in the N/OFQ sequence suggest the possibility of post-translational processing to give a truncated 11 amino acid peptide. This peptide has

been identified and shows unique pharmacology as it binds with a distinct pattern in rat brain compared to full sequence N/OFQ (Letchworth *et al.*, 2000).

N/OFQ is inactivated (Figure 1.17) by aminopeptidase N which cleaves the peptide to release N/OFQ(2-17), a fragment inactive at NOP, and endopeptidase 24.15 which acts on the bonds Ala⁷-Arg⁸ (A-R in Figure 1.17), Ala¹¹-Arg¹² (A-R) and Arg¹²-Lys¹³ (R-K), again producing inactive products.

1.9.3 Expression and localisation

Northern blot analysis of NOP mRNA produced a hybridising species of ~3.5kb in rat brain with two or three other fragments also found. Distribution of this receptor proved to be particularly abundant throughout the CNS in the cortical and cortico-limbic areas, brain stem and the dorsal and ventral horns of the spinal cord. Highest expression is observed in the hypothalamus, amygdala, piriform cortex, dorsal raphe nuclei and the locus coeruleus (Henderson *et al.*, 1997).

Moderate levels were observed in the cortex, thalamus, hippocampus, PAG and spinal cord and this pattern of expression was similar to that observed in the mouse brain. Very low levels of mRNA were found in the striatum where high levels of expression were observed for the MOP, DOP and KOP subtypes.

NOP mRNA is also found in peripheral tissues including; intestine, liver and spleen of the rat, mouse vas deferens (Calo *et al.*, 1996), human lymphocytes (Arjomand *et al.*, 2002) and guinea pig sympathetic ganglia (Kummer *et al.*, 1997) though no mRNA was reported in the skeletal muscle, kidney, oesophagus, testis or adrenal glands.

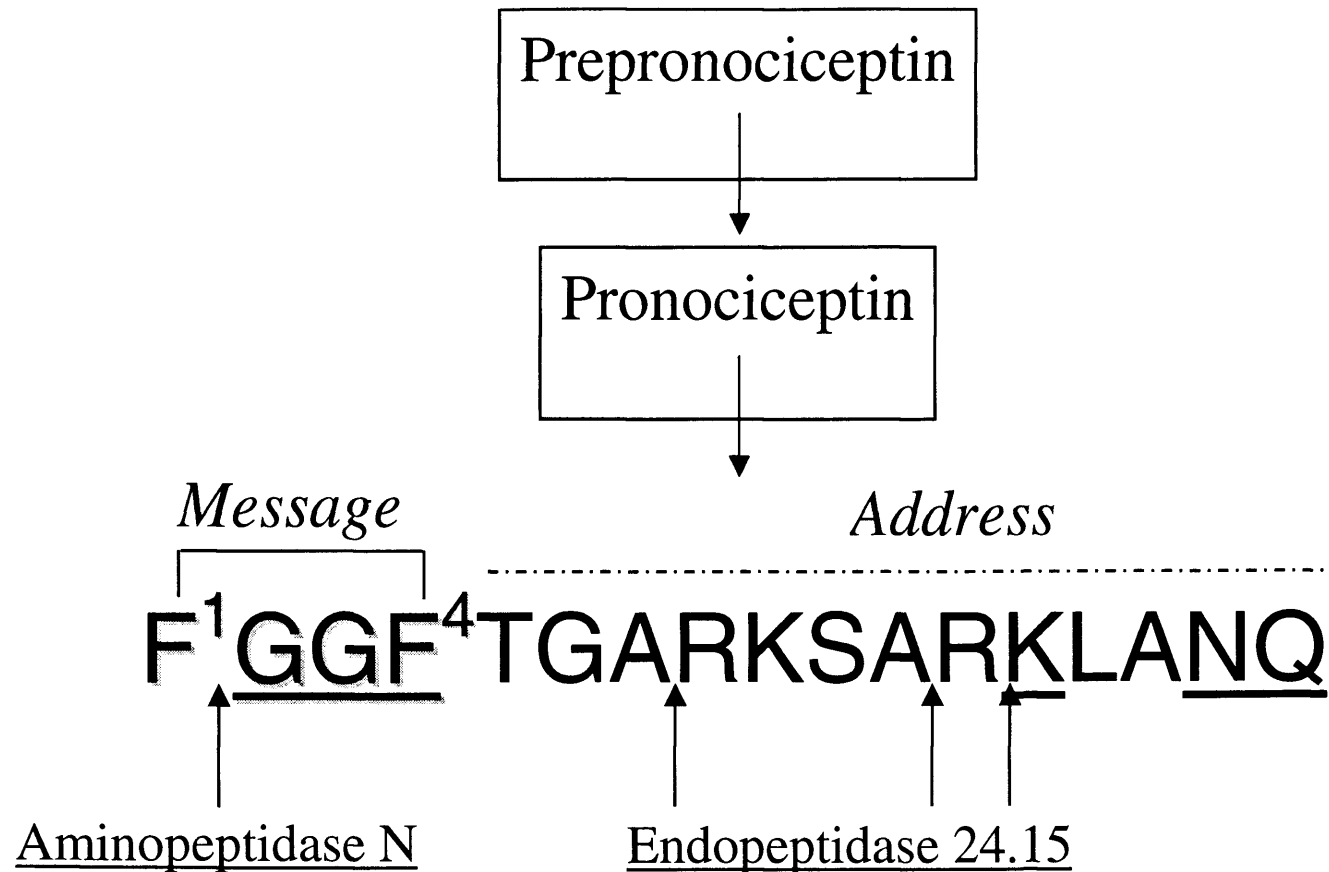


FIGURE 1.17 Schematic representation of the production and primary sites of metabolism of N/OFQ. The 17 amino acid peptide is drawn showing the message/address domains responsible for functional activity and binding affinity, respectively. Also noted in the message domain are the two pharmacophores, Phe¹ and Phe⁴

Receptor protein expression was also confirmed in these areas using immunohistochemical techniques and NOP localisation was found to be generally consistent with that of the other opioid receptor subtypes. Some differences in immunostaining for NOP and MOP were observed, consistent with their sometimes opposing effects (Monteillet-Agius *et al.*, 1998). This wide distribution of NOP indicates functional significance for this system in a variety of physiological areas. For example, localisation in the basal ganglia indicates a role in locomotor activity and indeed N/OFQ has a dose dependent effect on spontaneous activity (Rizzi *et al.*, 2001). The presence of N/OFQ in the hippocampus is consistent with its documented role in learning and memory (Goda *et al.*, 1998), and localisation in the pons and hypothalamic nuclei with its depressive effects on cardiovascular function (Salis *et al.*, 2000).

NOP receptors are found pre-synaptically on sympathetic, parasympathetic and sensory nerves similar to classical opioid receptors, where on activation they can trigger release of neuropeptides, particularly SP. Indeed, recent evidence shows co-expression of SP (72%) and CGRP (82%) in dorsal root ganglion primary afferents, supporting a role of N/OFQ in pre-synaptic modulation. Interestingly, in the majority of dorsal root ganglion neurones, preproN/OFQ expression was also observed on neurons juxtapositioned to those expressing these neuromodulators (Mika *et al.*, 2003).

Radioligand binding studies have also documented a wide distribution for NOP, including localisation in the striatum, retina and hypothalamus in the rat. Characterisation of these receptors show they exhibit similar binding properties despite receptor density being tissue type dependent - mean B_{max} values were 51.6 ± 7.7 , 44.0 ± 4.5 and 127.0 ± 28 fmol mg^{-1} protein respectively (Makman *et al.*, 1997b). Binding data does alter depending on the radioligand, tissue preparation and assay conditions, for example truncated ligands show

dense autoradiograms in different brain areas to full sequence N/OFQ (Letchworth *et al.*, 2000).

Distribution of NOP also correlates with the anatomical localisation of the preproN/OFQ gene. Northern blot analysis shows the expression of a 1.3kb preproN/OFQ mRNA fragment predominantly found in the brain and spinal cord of rat and human (Mogil *et al.*, 2001; Mollereau *et al.*, 1996). N/OFQ peptide was also localised in similar areas (cortex, hypothalamus and spinal cord).

The distribution of preproN/OFQ transcripts and N/OFQ in the CNS differs to that for opioid precursors and peptides. This difference in localisation could explain the opposite effects of opioids and N/OFQ on pain threshold since they activate similar signal transduction mechanisms.

1.9.4 Effects of N/OFQ

Numerous effects have been proposed for N/OFQ probably due to its wide distribution and are dependent on the route of administration and dose used (Mogil *et al.*, 2001). Spinally, N/OFQ mediates similar cellular effects to opioids i.e. analgesia. However, supraspinally, hyperalgesia/anti-opioid actions are observed. Pan *et al.* (2000) proposed a bi-directional mechanism for N/OFQ to explain its contrasting actions on pain. Two cell types, primary and secondary, occur in the raphe nuclei of the brain to produce analgesia and hyperalgesia, respectively. MOP opioids act by inhibiting secondary cells and disinhibiting the major primary cell type so producing analgesia. N/OFQ mediates hyperalgesia by inhibiting the primary cell. During opioid withdrawal, inhibition on the secondary cell is lost and this contributes to hyperalgesia. However N/OFQ inhibits the secondary cell types and therefore there is a net analgesic effect. These actions are dependent on behavioural state.

Other N/OFQ effects documented include control of neuroendocrine functions, inhibition of epilepsy, water balance, adaptive responses in stress and anxiety, regulation of sensory perception and memory, feeding, locomotor impairment and hearing (Calo *et al.*, 2000c; Mogil *et al.*, 2001).

N/OFQ also exerts central and peripheral effects on cardiovascular control. Under normal physiological conditions ($\sim 10\text{pg ml}^{-1}$ in plasma), this neuropeptide does not affect cardiovascular function but if levels are elevated, then modulation is noted. If N/OFQ is injected supraspinally into the medulla of anaesthetised rats, then significant reduction in heart rate and blood pressure is observed. These effects were not antagonised by naloxone (Salis *et al.*, 2000), indicating these actions were mediated through NOP and not via classical opioid receptors. Giuliani *et al.* (2000) also reported hypotension and bradycardia in anaesthetised rats caused by indirect modulation of neurotransmitter release.

An *in vitro* rat brainstem-spinal cord model also demonstrated modulatory effects of N/OFQ on respiration. A dose dependent decrease in respiratory frequency (firing frequency of ventral C4 activity) was observed with N/OFQ and this was competitively antagonised by J-113397, a NOP antagonist, indicating that these effects on medullary structures were not mediated through classical opioid receptors (Takita *et al.*, 2003). Removal of the dorsal half of the spinal cord did not alter the response to N/OFQ.

1.10 Current research ligands

Effective therapeutic treatments firstly rely on acquiring knowledge about the molecular mechanisms of a specific pain pathway so that a particular target might be identified. In the case of receptor modulation, isolation of endogenous ligands is generally imperative for progression in elucidating the roles of neurotransmitters. Essential moieties and binding domains within endogenous compounds can be determined and this knowledge used to

design synthetic replacements. Several synthetic peptide and non-peptide ligands for opioid and NOP receptors have been developed to date, based on the structural and pharmacological properties of endogenous peptides. There are several compounds available commercially with differing selectivities. The search for novel ligands with high potency and selectivity for these receptors is of paramount importance in developing understanding of these complex systems, and for the future development of potential therapeutic drugs for use in veterinary medicine and man. Table 1.7 shows the various research tools and clinical drugs available for the opioid and N/OFQ receptor systems involved in the pain pathways.

1.11 Clinical analgesics

Generally four major drug classes for the treatment of pain are acknowledged: those which directly inhibit sensory neurotransmission, drugs that block central plasticity, drugs mimicking descending inhibitory modulators and drugs affecting spinal inhibition of excitatory transmission. Combining drugs of different mechanisms of action and class is a common technique to achieve the desired level of analgesia, with minimal adverse effects.

Opioid drugs

Opioid drugs act specifically on opioid receptor subtypes to mimic endogenous opioids. Activation of MOP/KOP/DOP produces varying degrees of analgesia but despite a wealth of pre-clinical pharmacology indicating alternative analgesic targets, MOP receptor agonists (Table 1.7) still remain the drug of choice for acute, and some chronic, pains. Some adverse central effects have been documented on administration of opioid drugs, including euphoria (generally non-beneficial, reason for drug misuse), respiratory depression, constipation, nausea and vomiting. There are various routes of administration

for opioids (for example, oral, intramuscular, subcutaneous, intrathecal, transdermal) and tolerance to their effects develops so requiring progressive increasing doses for the same clinical effect.

TABLE 1.7 Summary of research tools and clinical drugs for opioid and nociceptin receptor classes

RECEPTOR	ENDOGENOUS LIGAND	RESEARCH AGONIST	RESEARCH ANTAGONIST	CLINICAL DRUG	
Opioid	MOP	β -Endorphin Endomorphin 1 Endomorphin 2	DAMGO PL017 Dezocine	Naloxone DPN Naltrexone CTOP Cyprodime β -funaltrexamine Quadazocine	Morphine Fentanyl Diamorphine (heroin) Hydromorphone Codeine Sufentanil Oxymorphone Dextropropoxyphene Methadone Pethidine Buprenorphine Etorphine (vet. med.)
	DOP	Leu-E Met-E	DPDPE DSLET DADLE	Naltrindole ICI174864	
	KOP	D _a	U50488H U69593	norBNI	Pentazocine
N/OFQ	N/OFQ	N/OFQ1-13 Ro 64-6198 <i>rac</i> -5a ZP120 CTD ALOH	[Nphe ¹] JTC-801 J-113397 UFP-101		

ALOH, [Arg¹⁴Lys¹⁵]N/OFQ(1-17)OH; CTD, Ac-RYYRWK-NH₂; CTOP, D-Phe-Cys-Tyr-D-Trp-Orn-Thr-Pen-Thr-NH₂; DADLE, [D-Ala², D-Leu⁵] enkephalin; DAMGO, Tyr-D-Ala-Gly-MePhe-Gly(ol)-enkephalin; DPDPE, [D-Pen², D-Pen⁵] enkephalin; DPN, diprenorphine; DSLET, [D-Ser², Leu⁵] enkephalin-Thr⁶; JTC-801, N-(4-amino-2-methylquinolin-6-yl)-2-(4-ethylphenoxymethyl) benzamide monohydrochloride; [Nphe¹], [Nphe¹]N/OFQ(1-13)NH₂; PL017, N-MePhe³, D-Pro⁴-morphiceptin; *rac*-5a, hexahydropyrrolo[3,4-*c*]pyrrole; UFP-101, [Nphe¹, Arg¹⁴, Lys¹⁵]N/OFQ-NH₂; ZP120, Ac-RYYRWK KKKKKK-NH₂; Red denotes non-selective

Opioid analgesics are widely used in both human and veterinary medicine (horses, sheep, dogs, cats, rabbits and swine). Caution must be noted since in animals, there are examples of species differences in response to opioid drugs. For example, the clinical therapeutic index of opioid analgesics is much higher in dogs than horses (Hellyer *et al.*, 2003). In horses experiencing acute pain, opioid drugs tend to cause increased locomotor activity and excitement whereas in the dog, particularly debilitated animals, a similar dose would cause sedation. Since there is evidence to indicate similar opioid systems within these species, it is not clear why the clinical effects differ so markedly; this could be attributed to different levels of receptor expression (Hellyer *et al.*, 2003).

There is also potential for abuse of opioids in animals, for example Remifentanil could be abused in race horses (Lehner *et al.*, 2000) since MOP agonists produce a good running response, due to increase locomotor activity as mentioned above, and analgesia (Kamerling *et al.*, 1989).

Clear similarities are illustrated in this thesis between classical opioid and NOP systems in terms of receptor and peptidic precursor genomic structure, amino acid sequence homology, receptor and ligand distribution in CNS, signal transduction mechanisms and mRNA expression levels, suggesting a common family although opposing effects are sometimes observed.

From a neurobehavioural stand point, opioids produce not only analgesia but also respiratory depression and dependence. N/OFQ produces analgesia spinally and anti-opioid effects supraspinally but there is no evidence for dependence. Hence, N/OFQ antagonists by reducing central N/OFQ tone may represent a novel class of clinically useful analgesics and an alternative to the traditional use of morphine (Calo *et al.*, 2002).

1.12 Age-related diseases in dogs

Inhibitory modulation is now a major key for treating diseases causing dysfunction of the periphery and CNS. In veterinary medicine, this includes targeting areas such as pain, anxiety and cardiovascular changes, which are particularly associated with geriatric animals. Changes observed with ageing are a major problem and a potential therapeutic area for new drugs. Veterinary diagnosis describes temporary illnesses and specific changes such as tumours, diseases of the heart, kidney or lung, and metabolic diseases, which become more pronounced with age. These are associated with increasing concern on the owners' part due to lifestyle observations such as no appetite, lethargy, unhealthy appearance. Common signs of pain observed by owners include whimpering, urinating, awkward posture and decreased social interaction or activity. In the case of dogs, the process of ageing depends generally on the size and species of the dog. Table 1.8 illustrates the approximate time involved for progression from senior to geriatric.

TABLE 1.8 The ageing process of dogs

Size	Weight (kg)	Senior (yr)	Geriatric (yr)
Small	<9	9-13	14+
Medium	9.5-23	7-11	12+
Large	23-41	6-9	10+
Giant	>41	5-7	8+

Beagle dogs represent an important species for studying *in vivo* cardiovascular parameters following drug administration (Greaves, 1998), and it is likely that N/OFQ modulates central effects such as cardiovascular activity in this species. Indeed as stated by Greaves (2000) “*the dog remains a relevant species because of the long experience in its use in toxicology and cardiovascular pharmacology*” (Greaves, 2000). This species also represents an important model with which to study anaesthetic action (Hirota *et al.*, 2001; Sato *et al.*, 2002) as there are many similarities to man.

1.13 Thesis aims

N/OFQ is a potential therapeutic target for debilitating diseases as via NOP it can modulate various physiological parameters such as cardiovascular function (exerts vasodilatory and bradycardia effects) (Kapusta *et al.*, 2002) and pain. Developing a suitable compound with affinity and potency at its receptor could reduce excitability within the ageing animal and hence render the animal less susceptible to disease. This could lead to a prolonged life and also ease any symptoms of ageing (hypertension, renal failure) so providing a better quality of life for the animal. Further research into N/OFQ action is therefore required, as this has not yet been investigated in the dog. In order to examine N/OFQ in this species, and as an intermediate between small laboratory mammals and man, a basic understanding of NOP receptor pharmacology is required. This information will enable more detailed autoradiographic and functional analyses to be performed with a view to eventually producing a therapeutic compound for veterinary medicine.

The primary aim of this thesis is to characterise native Beagle dog NOP, more specifically to:

- Determine NOP density using classical radioligand binding techniques with NOP selective radioligands in dog brain membranes. This data will be compared to that obtained in rat
- Ascertain whether the NOP binding sites correspond to a functional receptor using GTP γ ³⁵S binding
- Characterise various ligands, including Pfizer compound, CJ-X, for selectivity and efficacy at NOP in dog brain membranes. Compare any data with that determined in rat to investigate any pharmacological similarity in NOP between these species and identify any possible target ligands for further research

- Determine neuroanatomical localisation of NOP using autoradiography to determine if its distribution correlates with its various physiological roles, particularly pain
- Determine colocalisation of N/OFQ with its receptor, NOP, using anti-N/OFQ antibodies in immunohistochemistry (IHC). Compare the distribution of the peptide and relate to physiological function and distribution of NOP

2 Materials and Methods

2.1 Sources of materials

Abcam Ltd, UK: Abcam anti-N/OFQ antibody (rabbit polyclonal)

Agar Scientific, UK: Dog brain matrix, Tissue Slicer blades, large cover slips

Amersham BioSciences, UK: XK16 column, [*leucyl*-³H]N/OFQ (~149Ci mmol⁻¹ specific activity (SA)), [¹²⁵I](Tyr¹⁴)N/OFQ (~2000Ci mmol⁻¹ SA), Hyperfilm ECL[™], Hyperfilm[™] MP[™]

BDH, UK: DPX mountant

CytRx® Corporation, USA: TitreMax[®] Gold

Dako Corporation, USA: Envision[™]+ System, Peroxidase (3,3'-diaminobenzidine-HCl (DAB)) kit, hydrophobic PAP pen

DuPont (UK) Ltd: GTPγ³⁵S (1250Ci mmol⁻¹ SA)

Fisher Scientific UK Ltd: CaCl₂, glacial acetic acid, KCl, KH₂PO₄, methanol, MgCl₂, MgSO₄, NaCl, Na₂CO₃, NaOH, Wallac Optiphase 'Safe' scintillation fluid, Tris HCl, Whatman GF/B filters, large glass slides, xylene, CrK(SO₄).2H₂O, acetone, industrial methylated spirits (IMS)

Fisons Plc, UK: CuSO₄, Folin & Ciocalteu's Phenol Reagent, KOH

Invitrogen Life Sciences, UK: Dulbecco's medium, Hams F12 medium, foetal bovine serum, fungizone, geneticin (G418 sulphate), hygromycin B, penicillin-streptomycin, trypsin-EDTA, SeeBlue pre-stained standard markers

Marvel, UK: low fat milk

Merck, UK: PdO/BaSO₄ catalyst (10% Pd), LiChrospher^R 100 RP-18 column

National Diagnostics, UK: Ultra pure Protogel (30% acrylamide (w/v): 0.8% bisacrylamide (w/v))

NEN, UK: [³H]diprenorphine ([³H]DPN; 56Ci mmol⁻¹ SA)

Neosystem, France: III-BTD

Pall Gelman Laboratories, USA: Acrodisc Syringe filter 0.45µm

Pharmacia Biotech, Sweden: PD10 columns, Protein G Sepharose® 4 fast flow

Pierce Biotechnology, USA: Imject® Mariculture Keyhole Limpet Haemocyanin (KLH), *m*-Maleimidobenzoyl-*N*-hydroxysulfosuccinimide ester (Sulfo-MBS), SuperSignal® West Pico chemiluminescent substrate,

RA Lamb Ltd, UK: Accu-Edge® Low Profile Blades, Cool-jet, Tissue-Tek®, Eosin (1% aqueous)

Shandon, UK: haematoxylin, Shandon blueing reagent

Sigma, UK: ammonium persulphate (APS), alkaline phosphatase (AP) conjugated goat anti-rabbit antibody, amastatin, antifoam A, 2,2-azino-(3-ethylbenzthiazoline)-6-sulfonic acid, bacitracin, 5-bromo-4-chloro-3-indolylphosphate/nitro blue tetrazolium (BCIP/TNBT), bestatin, bovine serum albumin (BSA), Brilliant Blue, bromophenol blue, captopril, carbonate-bicarbonate buffer tablets, phosphate-carbonate buffer tablets, Cresyl Fast Violet, dialysis tubing, dithiothreitol, D_a, Leu-E, Met-E, ethylenediamine-tetraacetic acid (EDTA), ethyleneglycol-bis(β-aminoethyl ether) N,N,N',N'-tetraacetic acid (EGTA), glucose, glycerol, glycine, GDP, GTP, guanosine 5'-O-(3-thiotriphosphate) tetralithium salt (GTPγS), N-2-hydroxyethylpiperazine-N'-2-ethanesulphonic acid (HEPES), horseradish peroxidase (HRP) conjugated goat anti-rabbit antibody, H₂O₂, naloxone, naloxone benzoylhydrazone (NalBzOH), pertussis toxin (PTx), phosphate buffer saline (PBS) tablets, phosphoramidon, polyethylenimine (PEI), poly-L-lysine solution, Ponceau S, sodium dodecyl sulphate (SDS), Na₃PO₄, Tris buffered saline (TBS), NNN'N'-tetramethyl-1,2-diaminoethane (TEMED), trifluoroacetic acid (TFA), Tris base, Tween-20

Schleicher & Schuell, Germany: nitrocellulose membrane

TAAB Laboratories Equipment Ltd, UK: 3M tape

Tocris Cookson Ltd, UK: naltrindole, *nor*-binaltorphimine (*nor*BNI), cyprodime

Vector Laboratories, USA: Vectabond™ Reagent

2.2 Buffers, media and reagents

ABC colour reagent (for protein assay): A: 2% Na₂CO₃ in 0.1M NaOH; B: 1% CuSO₄; C: 2% Na⁺/K⁺ tartrate. Combine in a ratio of 100:1:1 respectively

Antibody buffer (for antibody dilutions in IHC): 0.05M Tris + 1% BSA, pH7.6

Binding buffer (for radioligand binding and autoradiography): wash buffer (below) supplemented with 0.5% BSA (w/v)

Blocking buffer (blocks non-specific sites in enzyme linked immunosorbent assays (ELISAs) and Western blots): 5% low fat milk (w/v) in 20mM Tris, 0.5M NaCl, 0.05% Tween-20, 0.01% Antifoam A

Conjugation buffer (for conjugation of hapten to antigen): 0.083M Na₃PO₄, 0.9M NaCl, 0.1M EDTA, pH7.2

GTPγ³⁵S assay buffer (for GTPγS binding experiments): 50mM Tris, 0.2mM EGTA, 100mM NaCl, 1mM MgCl₂, pH7.4 with NaOH

GTPγ³⁵S homogenisation buffer (for cells used in GTPγ³⁵S binding): 50mM Tris, 0.2mM EGTA, pH7.4 with NaOH

Harvest buffer (for cell harvesting without trypsinising): 10mM HEPES buffered saline (0.9%), 0.05% EDTA, pH7.4

IHC buffer (for washing in IHC): 0.05M TBS + 0.1% Tween 20, pH7.6

Incubation buffer (for autoradiography): binding buffer supplemented with 5mg ml⁻¹ bacitracin, 10μM of each amastatin, bestatin, captopril and phosphoramidon

Krebs-HEPES buffer (for cAMP assays): 143mM NaCl, 12mM glucose, 10mM HEPES, 4.7mM KCl, 1.2mM KH₂PO₄, 1.2mM MgSO₄, 2.6mM CaCl₂, pH7.4

Loading buffer (for diluting samples for SDS polyacrylamide gel electrophoresis (PAGE)): 50mM Tris, pH6.8, 100mM dithiothreitol, 2% SDS, 0.1% bromophenol blue, 10% glycerol

Running buffer (for SDS PAGE): 0.5M Tris, 0.38M glycine, 0.01% SDS, pH8.3

Selection media (for cell culture): Dulbecco's medium/Hams F12 medium (v/v, 50:50) supplemented with 5% foetal bovine serum (v/v), 100U ml⁻¹ penicillin, 100µg ml⁻¹ streptomycin, 2.5µg ml⁻¹ fungizone, 200µg ml⁻¹ geneticin and 200µg ml⁻¹ hygromycin B

Transfer buffer (for semi-dry blot): 0.25M Tris, 0.19M glycine, 20% methanol, pH8.3

Wash buffer (for radioligand harvesting): 50mM Tris, 5mM MgSO₄, pH7.4 with KOH

2.3 Peptide synthesis

N/OFQ, N/OFQ(1-17)NH₂ (N/OFQ-NH₂), CFGGFTGARKSARKLANQ-NH₂ (cysN/OFQ), N/OFQ(1-5)NH₂ (N/OFQ5), N/OFQ(1-9)NH₂ (N/OFQ9), N/OFQ(1-11)NH₂ (N/OFQ11), N/OFQ(1-12)NH₂ (N/OFQ12), N/OFQ(12-17)OH (N/OFQ12-17), N/OFQ13, [Phe¹ψ(CH₂-NH)Gly²]N/OFQ(1-13)NH₂ ([F/G]), [Nphe¹]N/OFQ(1-13)NH₂ ([Nphe¹]), [Arg¹⁴,Lys¹⁵]N/OFQ(1-17)OH (ALOH), [(pF)Phe⁴]N/OFQ(1-13)NH₂ ([pF)Phe⁴]), AcRYRQK-NH₂ (CTD), Noc, CAEPVADEADEVEQKQLQ-NH₂ (cysNoc), CGVQPGSETAVAILR-NH₂ (cysNOP), GVQPGSETAVAILR (NOP epitope) and J-113397 were kindly synthesised by Dr R. Guerrini (University of Ferrara, Italy). The synthesiser in this department is a continuous flow instrument for the Fmoc method of solid-phase peptide synthesis (Merrifield, 1963). Ro64-6198 was from Dr F. Jenck and Dr J. Wichmann of F. Hoffmann-La Roche AG, Switzerland and CJ-X was provided by Pfizer Ltd, UK.

2.4 Synthesis of novel radioligand [³H]N/OFQ(1-13)NH₂

Radioligand synthesis was carried out at one of our collaborative institutions in Hungary. The novel NOP radioligand, [³H]N/OFQ(1-13)NH₂ ([³H]N/OFQ13) was prepared by catalytic dehalogenation of a precursor peptide, p-iodo-Phe¹-N/OFQ(1-13)NH₂ using solid phase peptide synthesis methodology employing tritium gas and PdO/BaSO₄. Briefly ~2μmol p-iodo-Phe¹-N/OFQ(1-13)NH₂ was labelled using 10mg PdO/BaSO₄ catalyst (10% Pd) and 9μmol of triethylamine with tritium gas (555GBq, 15Ci), produced by heating in a closed glass manifold (Toth *et al.*, 1997). The mixture was stirred at room temperature for 60min and excess tritium removed using pyrophoric uranium. Filtration through Whatman GF/C filters and repeated vacuum evaporation followed to remove the catalyst and labile tritium. Total radioactivity was determined as 44.8mCi (1.657GBq) with a Searle-Delta-300 liquid scintillation counter and toluene-Triton X-100 scintillation cocktail. The crude tritiated product was then purified by high pressure liquid chromatography (HPLC) on a LiChrospher^R 100 RP-18 (5μm) column, using 0.1% TFA in water/acetonitrile (gradient condition: 5-25% acetonitrile, for 20min (k'=3.74)) as an eluant. Detection was with a Jasco UV-975 detector at 220nm and a Packard Flow-one/β A-500 radiodetector. Purity of the final radioligand was >95%. Specific activity of N/OFQ(1-13)NH₂,[phenylalanyl¹-4-³H]trifluoroacetic acid salt was determined from the mass by HPLC using a calibration curve prepared with unlabelled N/OFQ13 and radioactivity yielding 30Ci mmol⁻¹ (1110GBq mmol⁻¹).

2.5 Animal care and ethics

Male and female Beagle dogs were housed at Pfizer Ltd. and female Wistar rats and male New Zealand White rabbits at the University of Leicester in accordance with the Animal Act 1996. All animal work was carried out in compliance with UK law and was approved

by local animal ethical review as appropriate. All animals were subject to appropriate dark-light cycles, and both food and water were offered *ad libitum*.

2.6 Brain membrane preparation

Brains from dogs (9-14kg), humanely killed by pentobarbital overdose, and rats (200-250g), killed by stunning and cervical dislocation, were used. Dog brain membranes were prepared at Pfizer Ltd and shipped to Leicester in dry ice. Crude rat cortical preparations were made in-house as follows: brains from 2 animals were rapidly dissected, the cerebellum and brain stem removed and the remaining tissue (i.e. cortical and midbrain tissue) processed further by homogenisation (~10s, 13500rpm with Ultra Turrax T25) and centrifugation (13500rpm for 10min at 4°C in Biofuge 28RS) in wash buffer (section 2.2). This process was repeated three times and the pellet finally resuspended in wash buffer (Okawa *et al.*, 1998; 1999). Total protein concentration was determined (section 2.10) and 1ml stocks frozen at -70°C until further use.

2.7 Cell culture

The CHO cell line used here is an example of an adherent culture, which grows *in vitro*. These cells are transfected with DNA coding for human NOP (CHO_{hNOP}; expressing 1.72pmol mg⁻¹ protein (Okawa *et al.*, 1999)), mouse DOP (CHO_{mDOP}), rat MOP (CHO_{rMOP}) or rat KOP (CHO_{rKOP}). Stock flasks (selection media) and experimental flasks (media without geneticin and hygromycin B) were maintained at 37°C in 5% CO₂ humidified air. For CHO_{hNOP} selection media, see section 2.2. CHO_{rMOP/rKOP/mDOP} selection media were similar but contained 10% foetal bovine serum, 250µg ml⁻¹ geneticin and hygromycin B was omitted. All stock flasks were subcultured when confluent.

For subculturing, media was removed by pouring and the flasks rinsed twice with 1.5ml trypsin. Cells were incubated at 37°C with a further 2ml trypsin for 2-3min until the cells could be removed from the flask bottom by gentle tapping. Media (~3ml) was added to inhibit trypsinisation and 1ml of cells was passaged into each of 4 new flasks containing 10ml fresh media (1 stock flask and the other 3 containing experimental media) before incubating as previously. Experimental flasks were used when confluent (2-3 days).

In GTP γ ³⁵S (section 2.17) and forskolin stimulated cAMP (section 2.18) assays investigating PTx sensitivity, 100ng ml⁻¹ PTx was added to the cell culture media 20h prior to harvesting as below.

2.8 Cell membrane preparation

Media was removed from the culture flasks and the flasks rinsed twice with harvest buffer (section 2.2). Cells were incubated at 37°C for ~5min with sufficient harvest buffer to cover the flask bottom to chelate cations and hence loosen the cell monolayer from the flask bottom. The suspension was then transferred into a 25ml container and the flasks rinsed with harvest buffer. No trypsin was used in cell harvesting to avoid digestion of cell surface receptors. Cells were centrifuged at 1500rpm for 2min (Labofuge 400R) and then resuspended in the residual volume. The suspension was homogenised at 24000rpm for 3s 10 times before centrifuging further in buffer (section 2.2, wash buffer for competition binding or homogenisation buffer for GTP γ ³⁵S binding) at 13500rpm for 10min at 4°C (Biofuge 28RS). This process was repeated until three cycles had been completed and the pellet finally resuspended in appropriate assay buffer. Total protein concentration was determined (section 2.10) and the suspension stored on ice until diluting to the required assay concentration. Cell membrane preparations were made fresh as required.

2.9 Whole cell preparation

For whole cell preparations of CHO_{hNOP}, cells were harvested using harvest buffer and centrifuged as in section 2.8. For forskolin stimulated cAMP assays (section 2.18), the pellet was then resuspended in Krebs-HEPES buffer (section 2.2) as no homogenisation was carried out. Three cycles of centrifugation and resuspension were completed and the pellet finally resuspended in appropriate volume of buffer. Whole cell preparations were made fresh as required. These experiments were performed in collaboration with Tim Barnes.

2.10 Protein assay

The method used is a modification of that described by Lowry *et al.* (1951) to measure total protein concentration. Proteins are solubilised in alkali before reacting with copper ions. The copper-treated protein then reduces the Folin's reagent resulting in the development of a blue colour.

ABC colour reagent (2.5ml, section 2.2) was added to 0.5ml BSA standards (50-250 mg ml⁻¹, made previously in 0.1M NaOH and stored at 4°C) and appropriately diluted samples (generally 1:10, 1:20, 1:50 and 1:100), mixed well and incubated for 10min at room temperature. 250µl of Folin's reagent (Folin:dH₂O, 1:3) was added, the solutions vortexed and incubated for a further 30min before reading absorbance at 750nm on a Corning spectrophotometer. This was zeroed to a blank of 0.1M NaOH treated as described for samples. GraphPad Prism version 3.0 (GraphPad Software, San Diego California USA, www.graphpad.com, accessed November 2003; referred to as Prism hereafter) was used to plot a linear standard curve (Figure 2.1) and the unknown protein concentrations were extrapolated from this. Samples giving absorbance values outside of the standard curve

range were excluded and the remaining values averaged to give the total protein concentration of the solution.

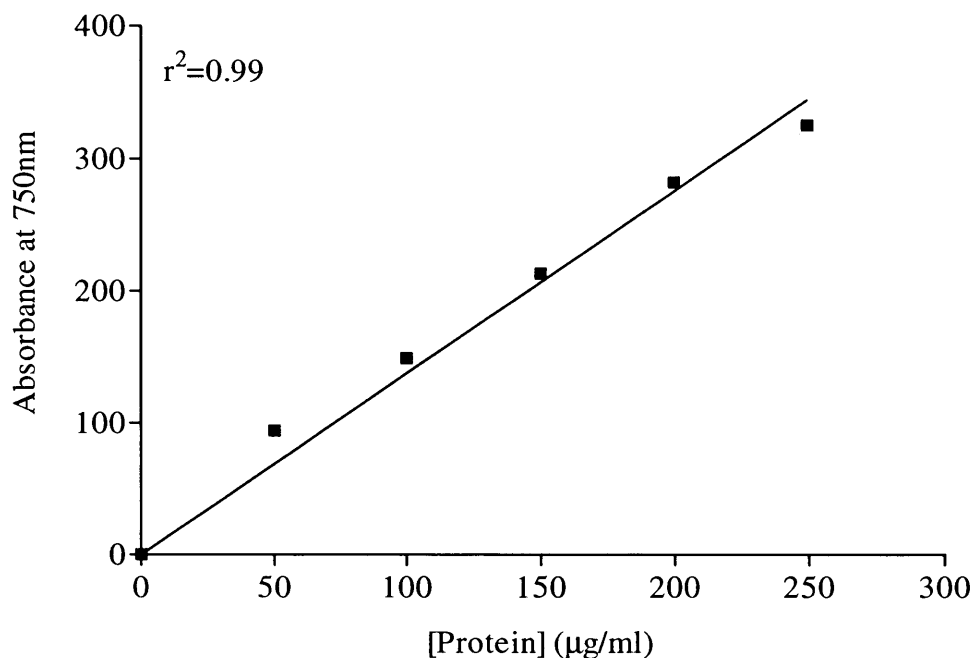


FIGURE 2.1 Specimen protein standard curve

2.11 Theory of radioligand binding

2.11.1 Radioactive decay

Incorporating the radioactive isotope, tritium, into a molecule should not alter its structure or biological function. Hence radioligand binding assays represent a true interaction of the ligand with a binding site and are a reliable method for investigating receptor characteristics.

The decay of a radioligand is a random event and $t_{1/2}$ is the time taken for half of the radioactive isotope to decay. In the case of tritium, $t_{1/2}$ is 12.43 years and the fraction remaining can be calculated using:

$$\text{Fraction remaining} = e^{-K_{\text{decay}} \cdot \text{Time}}$$

(where K_{decay} is the rate constant of decay expressed in units of inverse time)

An important thing to note is that the concentration of labelled ligand changes with time though the specific activity remains constant. The decomposition of the ligand is controversial, thought to be caused by the energy released in radioactive decay. Analyses of radioligand binding assume that the unlabelled decay products do not affect binding in the experiments however it is clearly better to be sure by using newly synthesised radioisotopes.

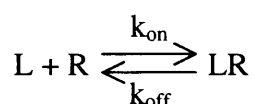
2.11.2 Efficiency of detecting radioactivity

Efficiency relates to the fraction of radioactive disintegrations actually detected by the radioactivity counter and is usually much lower with [^3H] isotopes (β radiation hence efficiency approximately 40%) than [^{125}I] (γ radiation hence over 90%) since the latter are high energy.

The decay of a radioactive atom is a random process and a tritium neutron decomposes into a proton, producing an electron and a neutrino. The decay energy released is always consistent though may be distributed differently between the electron and neutrino. If the electron has sufficient energy, it collides with a fluor molecule in the scintillation fluid. This amplifies the radioactive signal by producing luminescence, which is then detected by the β -counter. The intensity of the luminescence i.e. number of photons produced on activation of the fluor molecule is proportional to the energy of the electron. If the electron has low energy, it may not be able to activate the fluor molecules, or on colliding, the luminescence from only a few photons may be insufficient to be detected. Counting efficiency is affected by colour in the scintillation vials and a homogeneity of the mixture.

2.11.3 Law of mass action

The binding characteristics of a targeted receptor are probed using three basic protocols: kinetic, saturation and competition experiments. Analysis of radioligand binding is based on the law of mass action, a simple model used to explain experimental data:



(where L is ligand, R receptor and LR the ligand-receptor complex)

Binding is a simple bimolecular process involving ligand diffusion and collision within a population of receptors. Collisions must occur in the correct orientation and with sufficient energy. The number of binding events per unit of time is represented by the association rate constant, k_{on} (units $M^{-1} \text{min}^{-1}$). Once bound, the complex stabilises for a random length of time, influenced by the affinity of the ligand for the receptor, and then dissociates as determined by k_{off} (units min^{-1}). The probability of dissociation is the same over time and when this occurs, the receptor and ligand return to the same configuration as previously. If this is not the case, then the binding does not follow the law of mass action.

Equilibrium is reached when the rate of the ligand associating with the receptor equals the rate of dissociation of the LR complex. At equilibrium, this can be represented as:

$$[L] \cdot [R] \cdot k_{\text{on}} = [L \cdot R] \cdot k_{\text{off}}$$

This can then be rearranged to define the equilibrium dissociation constant K_d , the inverse of the association constant:

$$\frac{[L] \cdot [R]}{[L \cdot R]} = \frac{k_{\text{off}}}{k_{\text{on}}} = K_d$$

So the dissociation constant K_d (units M) can be considered as the concentration of ligand, which will bind to half the total number of receptors at equilibrium. K_d can be converted into pK_d using the following equation:

$$pK_d = -\log_{10} K_d$$

The law of mass action can also be used to predict the fractional occupancy of a receptor at equilibrium from the following equation:

$$\text{Fractional occupancy} = \frac{[L]}{[L] + K_d}$$

The law of mass action does have limitations and is not useful in the some experimental conditions since it assumes that:

- all receptors are equally accessible
- receptors are either free or bound to their ligand – there is no partial binding
- ligands and receptors are not modified in any way
- binding of a ligand to a receptor is reversible
- no cooperativity or depletion of free radioligand.

2.11.4 Non-specific binding

Ligands can bind to sites other than at the binding pocket being investigated and this is known as non-specific binding (NSB). These interactions may be at a site distinct from but linked to the receptor, such as a separate allosteric site located on the receptor, an effector molecule or other macromolecule.

NSB must be quantified in order to define specific binding. A cold, or unlabelled, ligand at a saturating concentration competes with the radioligand for the receptor binding sites and hence all the receptors are occupied by the cold ligand. The binding of radioligand is

therefore much reduced and correlates to binding at sites other than the receptor i.e. non-specific sites. The concentration of cold ligand should be at a sufficient concentration to block all specific binding, approximately 100 times the K_d of the radioligand. NSB, determined experimentally, is directly proportional to the amount of radioligand used and is required to define the amount of specific binding since:

$$\text{Total} - \text{NSB} = \text{Specific binding}$$

Using the same ligand for the 'hot' radioligand and cold in determining NSB is an example of homologous competitive binding. This is advantageous since it is likely that the receptor has the same affinity for both ligands hence an increased accuracy in receptor density estimates.

2.11.5 Calculating radioactive concentration

From the SA of a given radioligand, disintegrations per minute (dpm) bound expected in a 1ml assay at 1nM can be calculated. For example, if SA is 150Ci mmol⁻¹, then:

- $1/150\text{Ci mmol}^{-1} = 6.667 \times 10^{-3} \text{mmol Ci}^{-1}$
- Change units - $6.667 \times 10^{-3} \times 1 \times 10^{-3} \times 1 \times 10^{-6} = 6.667 \text{pmol } \mu\text{Ci}^{-1}$
- As 1 pmol in 1ml = 1000pmol in 1L = 1nM, then $6.667 \text{pmol } \mu\text{Ci}^{-1} = 6.667 \text{nM } \mu\text{Ci}^{-1}$
- As $1 \mu\text{Ci} = 2.22 \times 10^6 \text{dpm}$, then $2.22 \times 10^6 / 6.667 = 332983 \text{dpm}$ in 1ml assay
- If a 0.5ml assay requires 0.2nM, expect $\sim 33298.2 \text{dpm}$ if 100 μl of standard is counted
- Conversely if a sample has 143278dpm, this equals $\sim 0.86 \text{nM}$

2.12 Assay conditions

All assays described in sections 2.13-2.16 were performed in a total volume of 0.5ml binding buffer (section 2.2) with 10 μ M peptidase inhibitors (amastatin, bestatin, captopril and phosphoramidon) for 60min at room temperature (Okawa *et al.*, 1998; 1999). All protocols separated bound and free radioligand by rapid vacuum filtration using a Brandel 24 place harvester with ice cold wash buffer onto Whatman GF/B filters. Filters were soaked for 1h in 0.5% PEI to reduce NSB and loaded onto the harvester wet. Bound radioactivity was extracted for at least 8h in 4.5ml Wallac Optiphase 'Safe' scintillation fluid before assessing radioactivity by standard scintillation spectroscopy. Counts were measured using a Packard 1900TR Liquid Scintillation Analyzer and results were recorded as dpm.

2.13 Time course assays

As mentioned above, the probability that ligand and receptor associate is given by $k_{on} \cdot [R][L]$ and the probability of dissociation by $k_{off} \cdot [RL]$. The rate of change is therefore represented as the difference between these:

$$\frac{d[RL]}{dt} = k_{on} [R][L] - k_{off} [RL]$$

No catalytic processes are involved in binding so L and R should be conserved and when there is no ligand depletion, the following represents the time course of formation:

$$[RL] = [RL]_{eq} (1 - e^{-(k_{on} \cdot [L] + k_{off})t})$$

[RL] initially rises exponentially to its equilibrium value $[RL]_{eq}$ with a time course determined by the net rate constant $k_{on} \cdot [L] + k_{off}$.

Using Prism's one phase exponential association equation to analyse specific binding from time course data enables the value of K to be determined. This variable K is the observed rate constant, k_{ob} , expressed in units of inverse time. Since X-axis data in these experiments are generally entered in min, then k_{ob} is expressed in min^{-1} . This can be converted to the association rate constant, k_{on} , using the equation below though this was not deemed necessary for data presented in this thesis:

$$k_{on} = \frac{k_{ob} - k_{off}}{[R]}$$

In order to investigate the stability of the NOP receptor system, brain membranes (100 μ g rat or 200 μ g dog) were incubated with a fixed concentration of $\sim 0.2\text{nM}$ [*leucyl*-³H]N/OFQ for various times (0-60min). NSB was determined in all experiments by the addition of 1 μ M unlabelled N/OFQ. Assay conditions and harvesting were as described in section 2.12.

2.14 Saturation binding

A common experimental way of determining receptor density is saturation binding. At equilibrium, the equations governing association and dissociation can be used to predict a hyperbolic curve dependent on the concentrations of [RL] and [L]. When the concentration of free ligand is equal to the K_d , then half the receptor sites are occupied. Conversely, the free ligand at 50% receptor saturation, or IC_{50} , is a measure of K_d .

Scatchard plots are frequently used for analysing B_{max} and K_d but are not the method of choice in our laboratory. Firstly a Langmuir isotherm or rectangular hyperbola (fmol mg^{-1}

protein vs [radioligand], analysed using one site binding hyperbola in Prism) is plotted to visualise data, specifically the saturation of the receptor system. The equation for this analysis also describes enzyme kinetics and assumes only one population of receptors:

$$\text{Specific binding} = \frac{B_{\max} \cdot [L]}{K_d + [L]}$$

For a more mathematically accurate estimate of B_{\max} and K_d , a semi-log transformation of specific binding data (fmol mg^{-1} protein vs log [radioligand], analysed using sigmoidal dose-response curve with a variable slope) is performed with Prism. This is the chosen method in this thesis to estimate B_{\max} and K_d .

The radioligand concentration bound (section 2.11.5) is required to convert the dpm values of samples to fmol mg^{-1} protein, or B_{\max} , depending on the amount of protein in the assay, using the equation below:

$$\left(\frac{\text{dpm in sample}}{\text{radioligand bound}} \right) \times 0.5 \times 1000 \times \text{mg}/\mu\text{g protein used} = \text{fmol mg}^{-1} \text{ protein}$$

For example, if the filter gave 1070dpm after 8hr extraction, the initial radioligand added was 332983dpm and the protein used in assay was 200 μg , then the bound radiolabel in the sample would be:

$$1070/332983 \times 0.5 \times 1000 \times 5 = 8.03 \text{fmol mg}^{-1} \text{ protein}$$

In order to determine opioid receptor density for comparison with NOP expression, membranes (100 μg rat or 200 μg dog) were incubated with various concentrations of either [*leucyl*- ^3H]N/OFQ, the novel truncated [^3H]N/OFQ13 or [^3H]DPN (Harrison *et al.*, 1999; Smart *et al.*, 1997). NSB was determined in all experiments by the addition of either 1 μM

unlabelled N/OFQ (for [*leucyl*-³H]N/OFQ), N/OFQ13 ([³H]N/OFQ13) or naloxone ([³H]DPN). Assay conditions and harvesting were as described in section 2.12.

2.15 Competition binding

These experiments measure the binding of a radioligand in the presence of various concentrations of unlabelled competing ligand to determine the affinity of the unlabelled compound. Firstly a semi-log transformation (sigmoidal curve as in section 2.14 with constants set: bottom 0 and top 100) of the specific data is plotted in Prism to estimate the IC₅₀ i.e. the concentration of unlabelled ligand, which competes for half of the specific binding. The curve can be described by the following equation:

$$\text{Total} = \text{NSB} + \frac{(\text{Total} - \text{NSB})}{1 + 10^{\log[\text{displacer}] - \log(\text{IC}_{50})}}$$

The Cheng Prusoff equation (Cheng *et al.*, 1973) is then used to predict K_i, the affinity for the unlabelled ligand:

$$K_i = \frac{\text{IC}_{50}}{1 + [L]/K_d}$$

Prism also measures the slope factor of a curve when the ‘sigmoid dose-response variable slope’ is selected. A standard competitive binding curve has a slope factor of 1.0. If the slope factor is greatly reduced then the binding observed does not follow the law of mass action with a single site as lower slopes are indicative of two affinity sites. When such data is fitted to a two site competition model, IC₅₀ and K_i values for the respective high and low affinity states can be calculated. The proportion of sites with ‘high’ affinity is estimated as

Fraction_{HIGH} by Prism, and the low affinity proportion may be deduced as the remaining portion.

A comparison of NOP and opioid receptors in dog, rat and CHO cell membranes was performed in a series of competition studies. In these studies, [*leucyl*-³H]N/OFQ was used at a fixed concentration of ~0.2nM with 200µg dog/rat or 20µg CHO cell membranes, plus increasing concentrations of ligands as described in section 2.19 and chapter 3 results. In similar experiments with ~0.4nM [³H]DPN, 300µg dog/rat or 20µg CHO membranes were used with all other assay conditions as described above. NSB was determined in the presence of 1µM unlabelled N/OFQ or naloxone as appropriate. Assay conditions and harvesting were as described in section 2.12.

2.16 NaCl/GTPγS shift experiments

As discussed in section 2.15, a standard competitive binding curve with a reduced slope factor could be indicative of high and low affinity binding sites. This could be used to show that the receptor involved is able to couple to G proteins.

In NaCl/GTPγS shift experiments, the protocol used was similar to that described for [*leucyl*-³H]N/OFQ competition studies (section 2.15). Dog brain membranes (200µg) were incubated as previously with a fixed concentration of ~0.2nM [*leucyl*-³H]N/OFQ and increasing concentrations of N/OFQ, in the presence and absence of 120mM NaCl and 100µM GTPγS. These data were analysed with sigmoid (variable slope) or two site competition curves as appropriate.

2.17 GTPγ³⁵S binding

GTPγ³⁵S binding is another useful assay for investigating the functional properties of a receptor. Essentially the agonist in the system induces conformational changes within the

receptor, which results in stimulation and dissociation of the coupled G protein. On activation, GDP on the α subunit is interchanged for GTP, or in this case $\text{GTP}\gamma^{35}\text{S}$, and since this activated complex is stable, the amount of $\text{GTP}\gamma^{35}\text{S}$ bound is a measurement of agonist stimulation.

These studies can also be used to characterise antagonists. If a ligand shows no efficacy, then it can be investigated simultaneously with various concentrations of a known agonist. If a parallel shift in the curve is seen, with no changes in the maximum response and slope value, then reversible competitive antagonism is assumed. The potency of the antagonist or the negative log of the molar concentration, which at equilibrium and in the absence of an agonist would occupy 50% of receptors, can be calculated using the Gaddum-Schild equation (assuming a slope of unity). This is known as the pK_B value:

$$\text{pK}_B = \log_{10} \frac{\text{CR} - 1}{[\text{antagonist}]}$$

(where concentration ratio, CR refers to the EC_{50} of the agonist in the presence of an antagonist divided by that of the agonist in the absence)

pA_2 is theoretically equal to pK_B and can be defined as the negative log of the antagonist molar concentration that makes it necessary to double the agonist concentration to elicit the original submaximal response. pA_2 values were calculated if a minimum of three concentrations of antagonist were investigated and are extrapolated as the intercept on the X-axis on a Schild plot ($\log(\text{concentration ratio} - 1)$ vs $\log[\text{antagonist}]$). pA_2 or pK_B values for antagonists were calculated as appropriate.

$\text{GTP}\gamma^{35}\text{S}$ binding experiments were performed essentially as described by Berger *et al.* (2000b). 20 μg of CHO, dog or rat membrane preparations were incubated in 0.5ml $\text{GTP}\gamma^{35}\text{S}$ assay buffer (section 2.2) supplemented with 100 μM GDP, 0.15mM bacitracin

(previously heated to 70°C for 1 hour before use to remove any enzymatic activity), 1mg ml⁻¹ BSA and 10μM peptidase inhibitors (cocktail as in section 2.12) containing ~150pM GTPγ³⁵S and various concentrations of agonists/antagonists as described in section 2.19 and chapter 4 results. NSB was defined with 10μM unlabelled GTPγS.

All assays were incubated for 1h at 30°C with gentle shaking before harvesting with ice cold GTPγS assay buffer using rapid vacuum filtration on a Brandel Harvester (section 2.12). For this experiment, filters were not soaked in PEI as this attracts GTPγ³⁵S to filters. Bound radioactivity was extracted and counted as previously. Results are expressed as dpm or stimulation factor (agonist stimulated specific/basal specific) E_{max}, this being the maximum possible effect that the ligand produces under given conditions.

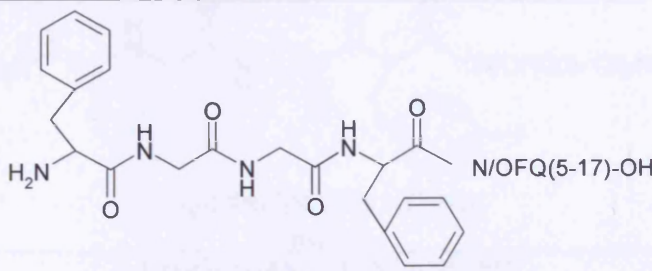
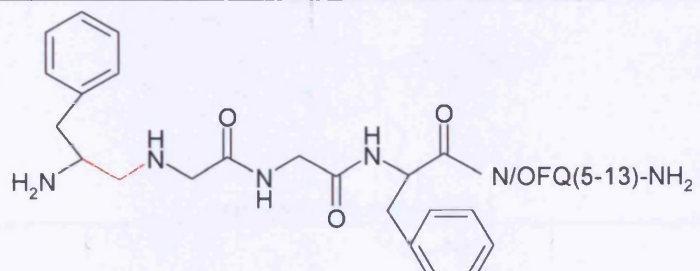
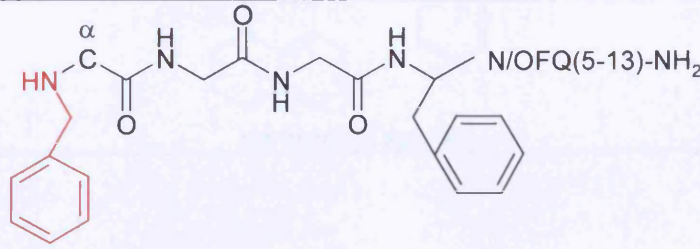
2.18 Forskolin stimulated cAMP formation

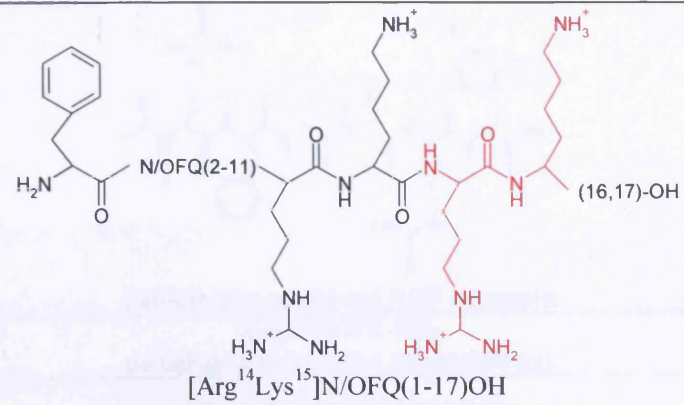
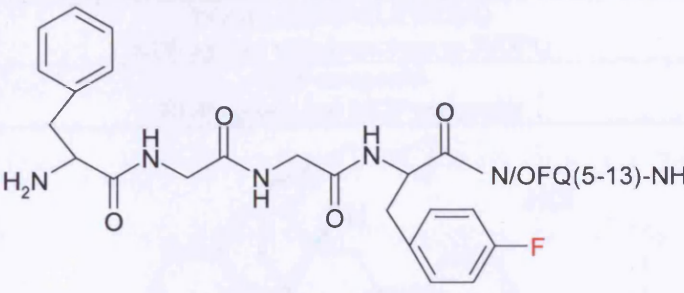
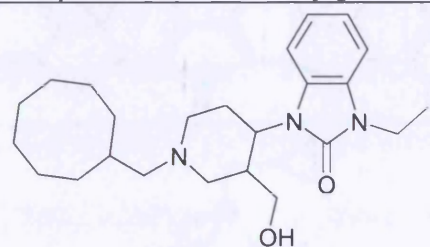
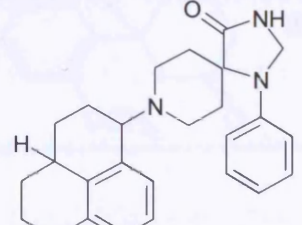
Activation of NOP results in inhibition of adenylyl cyclase, thereby reducing cellular cAMP levels. In this assay, forskolin stimulates cAMP production and hence this formation will be inhibited if NOP is activated by the ligands being investigated. CHO_{hNOP} cells were suspended in Krebs-HEPES buffer (section 2.2) supplemented with 0.5% BSA. Formation of cAMP was measured in 0.3ml volumes of whole cell suspensions as described above in Krebs-HEPES buffer supplemented with 1mM isobutylmethylxanthine and 1μM forskolin at 37°C for 15 minutes. Peptidase inhibitors were not included, as they do not influence the response to N/OFQ (Hashimoto *et al.*, 2002). Ligands were included in various combinations. The reaction was terminated using 10M HCl, neutralised with 10M NaOH and buffered with 1M Tris, pH7.4. cAMP was assayed using a protein binding assay as described by Brown *et al.* (1971) and Okawa *et al.* (1999). cAMP data is presented as a percentage inhibition of forskolin stimulated response. These experiments were performed in collaboration with Tim Barnes.

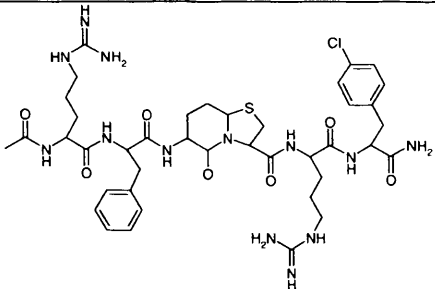
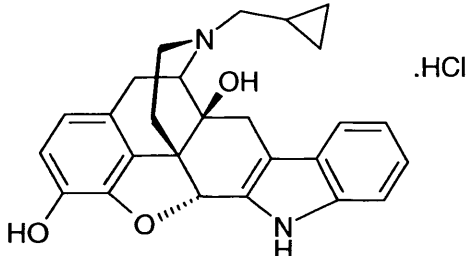
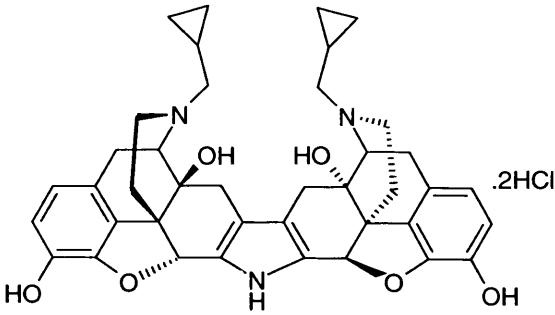
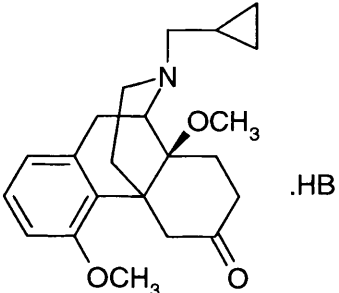
2.19 Ligands investigated

The following ligands (Table 2.1) were investigated in the experiments described above at various concentrations as indicated in the appropriate methods and results sections. The structures of N/OFQ, analogues of N/OFQ, J-113397, Ro64-6198, III-BTD, naltrindole, *nor*BNI and cyprodime are also shown.

TABLE 2.1 Ligands used in this study. *Red* shows important modifications

LIGAND	ACTIVITY/STRUCTURE	REFERENCE
N/OFQ	 <p>N/OFQ(5-17)-OH endogenous NOP ligand</p>	Meunier <i>et al.</i> (1995); Reinscheid <i>et al.</i> (1995)
N/OFQ-NH ₂	amidated N/OFQ	Guerrini <i>et al.</i> (1997)
N/OFQ5	truncated analogues of N/OFQ	Guerrini <i>et al.</i> (1997)
N/OFQ9		
N/OFQ11		
N/OFQ12		
N/OFQ13		
[F/G]	 <p>N/OFQ(5-13)-NH₂ [Phe¹ψ(CH₂-NH)Gly²]N/OFQ(1-13)NH₂ pseudo-peptidic partial agonist</p>	Butour <i>et al.</i> (1998); Guerrini <i>et al.</i> (1998)
[Nphe ¹]	 <p>N/OFQ(5-13)-NH₂ [Nphe¹]N/OFQ(1-13)NH₂ first selective peptide antagonist</p>	Calo <i>et al.</i> (2000b); Guerrini <i>et al.</i> (2001a)

ALOH	 <p>[Arg¹⁴Lys¹⁵]N/OFQ(1-17)OH first peptide with greater potency than N/OFQ</p>	Okada <i>et al.</i> (2000)
[(<i>p</i> F)Phe ⁴]	 <p>[(<i>p</i>F)Phe⁴]N/OFQ(1-13)NH₂ peptide</p>	Guerrini <i>et al.</i> (2001b)
cysN/OFQ	CFGGFTGARKSARKLANQ-NH ₂ Cys added to N/OFQ for conjugation	
Noc	bioactive fragment from N/OFQ precursor	Costentin <i>et al.</i> (1998); Okuda-Ashitaka <i>et al.</i> (1998)
cysNoc	CAEPVADEADEVEQKQLQ-NH ₂ Cys added to Noc for conjugation	
J-113397	 <p>non-peptidyl antagonist</p>	Kawamoto <i>et al.</i> (1999); Bigoni <i>et al.</i> (2000a)
Ro64-6198	 <p>non-peptidyl agonist</p>	Jenck <i>et al.</i> (2000)

III-BTD	 <p>non-selective opioid and NOP antagonist</p>	Bigoni <i>et al.</i> (2000b); Hashiba <i>et al.</i> (2001)
CTD	AcRYYRWK-NH ₂ partial agonist (complex pharmacology)	Dooley <i>et al.</i> (1997)
naloxone	non-selective opioid antagonist	Pert <i>et al.</i> (1973)
D _a	YGGFLRRIRPKLKWDNQ KOP agonist with homology to N/OFQ	Chavkin <i>et al.</i> (1982)
NalBzOH	NOP antagonist KOP agonist and MOP antagonist	Bigoni <i>et al.</i> (2002a)
naltrindole	 <p>.HCl</p>	Rogers <i>et al.</i> (1990)
norBNI	 <p>.2HCl</p>	Stein <i>et al.</i> (1989)
cyprodime	 <p>.HB</p>	Schmidhammer <i>et al.</i> (1989)

2.20 Tissue sectioning

For tissue sectioning, staining methods and results, see chapter 6.

2.21 Autoradiography

For autoradiographical methods and results, see chapter 7.

2.22 Immunological techniques

For antibody production, IHC and other immunological techniques (ELISA, Western blotting) and results, see chapter 8.

2.23 Data analysis and statistical tests

All data are presented as mean \pm s.e.m from a minimum of three experiments as indicated. Concentration response curves were analysed using non-linear or linear regression in Prism as described in appropriate methodology. In competition studies, IC₅₀ values were corrected for the competing mass of radiolabel using the Cheng and Prusoff equation (Cheng *et al.*, 1973) where the K_d used was determined in this study. In GTP γ ³⁵S binding, data is presented either as dpm or stimulation factor, E_{max}. pA₂ or pK_B values for antagonists were calculated as appropriate using the Gaddum Schild equation and Schild plot. cAMP data is presented as a percentage inhibition of forskolin stimulated response. ELISA absorbance values were corrected and analysed using Microsoft Excel 2000 (Excel; Microsoft Corporation, USA). Antibody titres were estimated by plotting a graph (absorbance vs 1/serum dilution) where the titre is half the maximum absorbance extrapolated on the X-axis. Autoradiograms were analysed as appropriate using MCID Analysis Evaluation 7.0 (referred to as MCID hereon) to identify brain areas containing NOP receptors. Where appropriate, data have been analysed for statistical significance using ANOVA, Wilcoxon signed rank test or Students t-test (two tailed), with p<0.05 considered as significant.

3 Results: Radioligand binding

3.1 Introduction

NOP is a member of the GPCR superfamily. Activation of NOP receptors by N/OFQ results in stimulation of potassium efflux, inhibition of VSCCs and of adenylyl cyclase activity, thereby decreasing cellular concentrations of cAMP. Depending on cellular NOP localisation, pre-synaptic inhibition of neurotransmitter release or post-synaptic inhibition of neuronal excitability will result (Mogil *et al.*, 2001). Due to homology with the classical opioid system, this novel receptor-transmitter system is of high analgesic relevance.

Many studies have examined the pharmacology and distribution of NOP in rodents, the group in which there is most evidence that N/OFQ acts as an important neuromodulator and, in which NOP was initially identified. However, the characteristics of this receptor and its peptide in the dog have yet to be determined. It is important to determine basic radioligand binding as species differences on administration of opioid drugs have been observed (Hellyer *et al.*, 2003). These effects have been attributed to differences in receptor density and hence expression levels are important clinically.

Therefore in this chapter, a series of classical radioligand binding experiments, namely time course, saturation and competition studies, with two selective NOP radioligands, [*leucyl*-³H]N/OFQ and [³H]N/OFQ13, were used to investigate the density, stability and characteristics of the NOP receptor system. Data for the dog were compared to that for NOP in rat, the identity of which has been confirmed in both cloning and pharmacological studies. In addition, NOP receptor densities were compared with those of classical MOP, DOP and KOP receptors. The methodology of these studies is described in sections 2.13-2.15 and for brain preparations in section 2.6.

The aims of this chapter are to characterise:

- Binding of [*leucyl*-³H]N/OFQ over time in dog and rat
- NOP receptor density using the radioligands [*leucyl*-³H]N/OFQ and [³H]N/OFQ13
- Total opioid receptor population using [³H]DPN for comparison with NOP
- Properties of various common NOP and opioid receptor ligands to investigate any pharmacological correlation between dog and rat
- Competition binding of [³H]DPN by selective opioid ligands in order to estimate the proportion of the receptor subtypes within the total opioid population

3.2 Time course of [*leucyl*-³H]N/OFQ

The binding of [*leucyl*-³H]N/OFQ was observed to be time dependent such that at ~0.2nM, an apparent equilibrium was reached after 15min. This saturation was observed for both dog and rat membrane preparations and was stable for at least 1h (Figure 3.1). Hence subsequent binding experiments were incubated for 1h to ensure equilibrium was reached at lower radioligand concentrations.

Data for NSB was subtracted from the total binding and then fitted to a one phase exponential association curve using Prism. The mean observed rate constant of association, k_{ob} , was estimated to be 0.133 and 0.196min⁻¹ ($n=3$) for dog and rat, respectively.

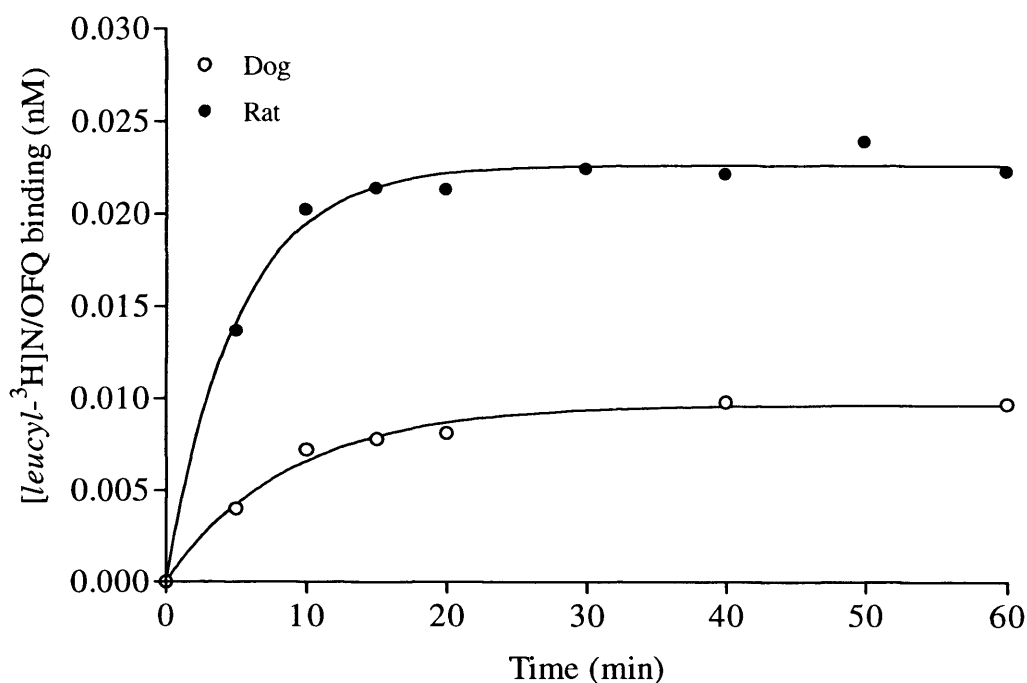


FIGURE 3.1 Typical one phase exponential association time course for [*leucyl*-³H]N/OFQ binding in dog and rat membranes illustrates a saturable stable receptor system

3.3 Saturation binding of [*leucyl*-³H]N/OFQ, [³H]N/OFQ13 and [³H]DPN

[*leucyl*-³H]N/OFQ binding was found to be concentration dependent and saturable in both dog and rat. This data was initially plotted as a hyperbola (Figure 3.2) and then transformed into a sigmoidal plot (Figure 3.3) to calculate B_{\max} and pK_d values.

Four different dog brain preparations were compared and small differences in B_{\max} were observed between these preparations (Table 3.1). There were significantly fewer ($p=0.0002$) N/OFQ binding sites in dog compared to rat with B_{\max} values of 28.7 ± 2.8 and $137.0 \pm 12.9 \text{ fmol mg}^{-1}$ protein, respectively. There were no differences in the pK_d values of [*leucyl*-³H]N/OFQ for both species (Table 3.1) and the data from rat agrees well with that measured previously in our laboratory ($157.0 \pm 4.0 \text{ fmol mg}^{-1}$ protein; Hashiba *et al.*, 2002a).

The differences in B_{\max} between species could not be attributed to loss of receptor over time since the storage of membranes at -70°C for approximately 5 months resulted in an approximate 6% decrease in receptor density. This failed to reach statistical significance when compared to fresh samples. There was no change in pK_d with time (Table 3.1). Changes in receptor density in dog preparations were also investigated in a freeze-thaw cycle (thaw for 1h and refreeze overnight) and the B_{\max} here was observed to significantly ($p=0.0019$) decrease by approximately 25% from 35.8 ± 1.2 to 26.3 ± 1.2 (Table 3.1). Hence repeat freeze thaw cycles were avoided.

The novel truncated radiolabel, [^3H]N/OFQ13, also bound in a concentration dependent and saturable (Figure 3.4) manner with values as shown in Table 3.1. This radioligand confirmed a significantly ($p<0.0001$) lower density of binding sites in dog (B_{\max} $23.7\pm 2.0\text{fmol mg}^{-1}$ protein) compared to rat (B_{\max} 130.4 ± 1.1) and there was also a small (~3 fold) but significant ($p<0.005$) difference in pK_d , with lower affinity seen in the dog.

The binding of the non-selective opioid radioligand, [^3H]DPN, was used to assess total classical opioid receptor (MOP, DOP and KOP) density for comparison with NOP data. The binding of this radioligand was concentration dependent and saturable. Data were initially plotted as a hyperbola and then transformed into a sigmoidal semi-log plot (Figure 3.5) with B_{\max} and pK_d values as in Table 3.1. There was a much higher (~3 fold) density of total opioid receptors in dog brain preparations compared to N/OFQ binding sites. In contrast, in the rat there were half as many opioid as NOP receptors.

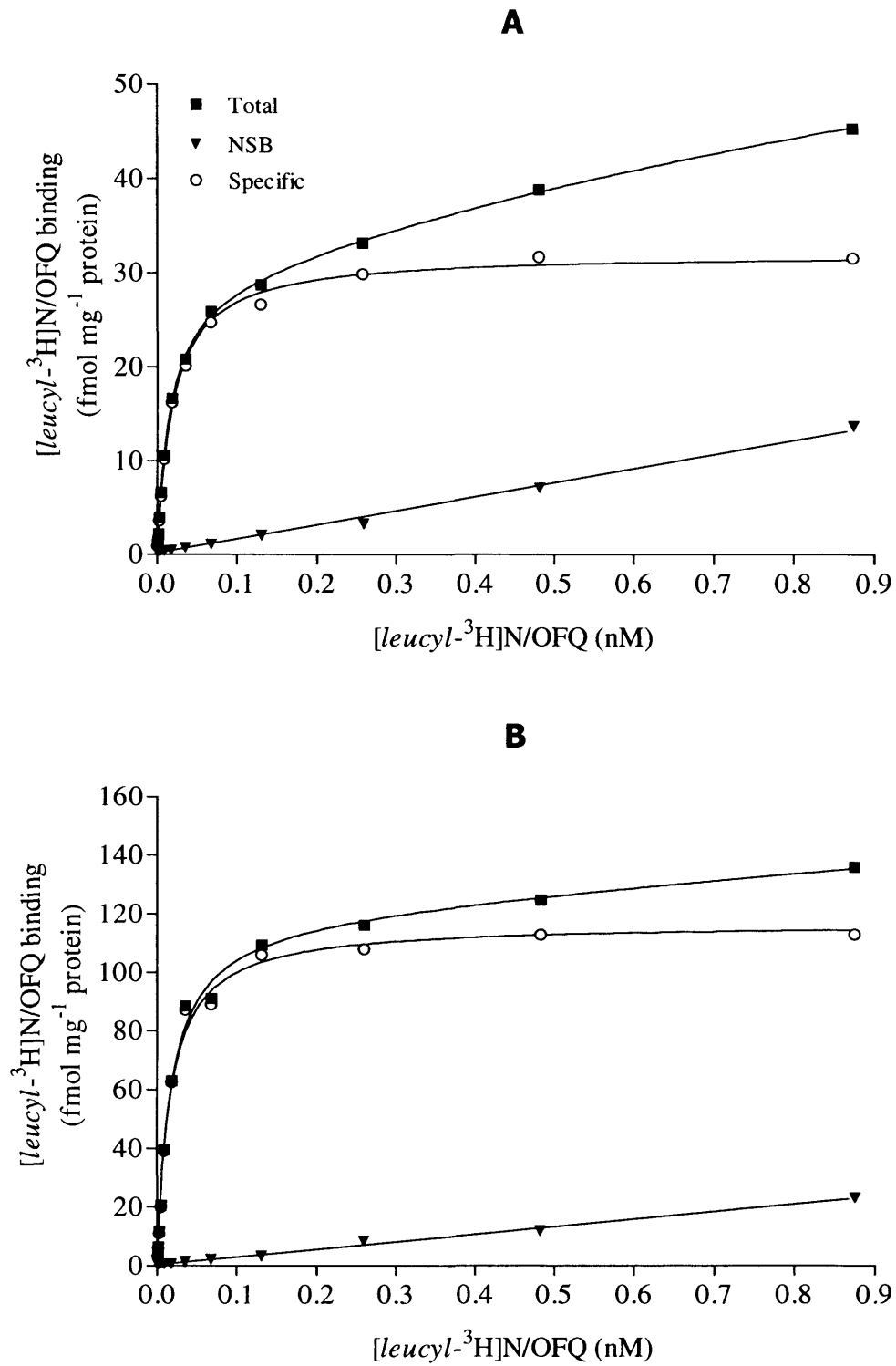


FIGURE 3.2 Typical saturation isotherms for [leucyl-³H]N/OFQ binding in dog (A) and rat (B) brain membranes

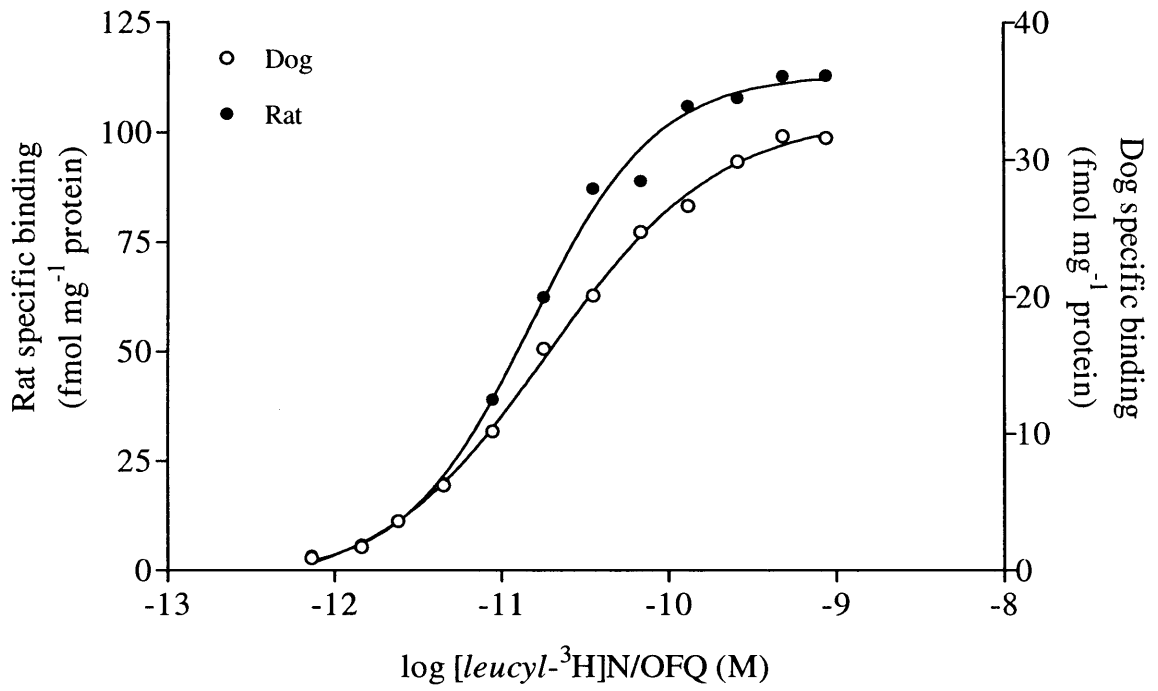


FIGURE 3.3 Typical sigmoidal transformation of specific binding data for [leucyl-³H]N/OFQ binding in dog and rat brain membranes

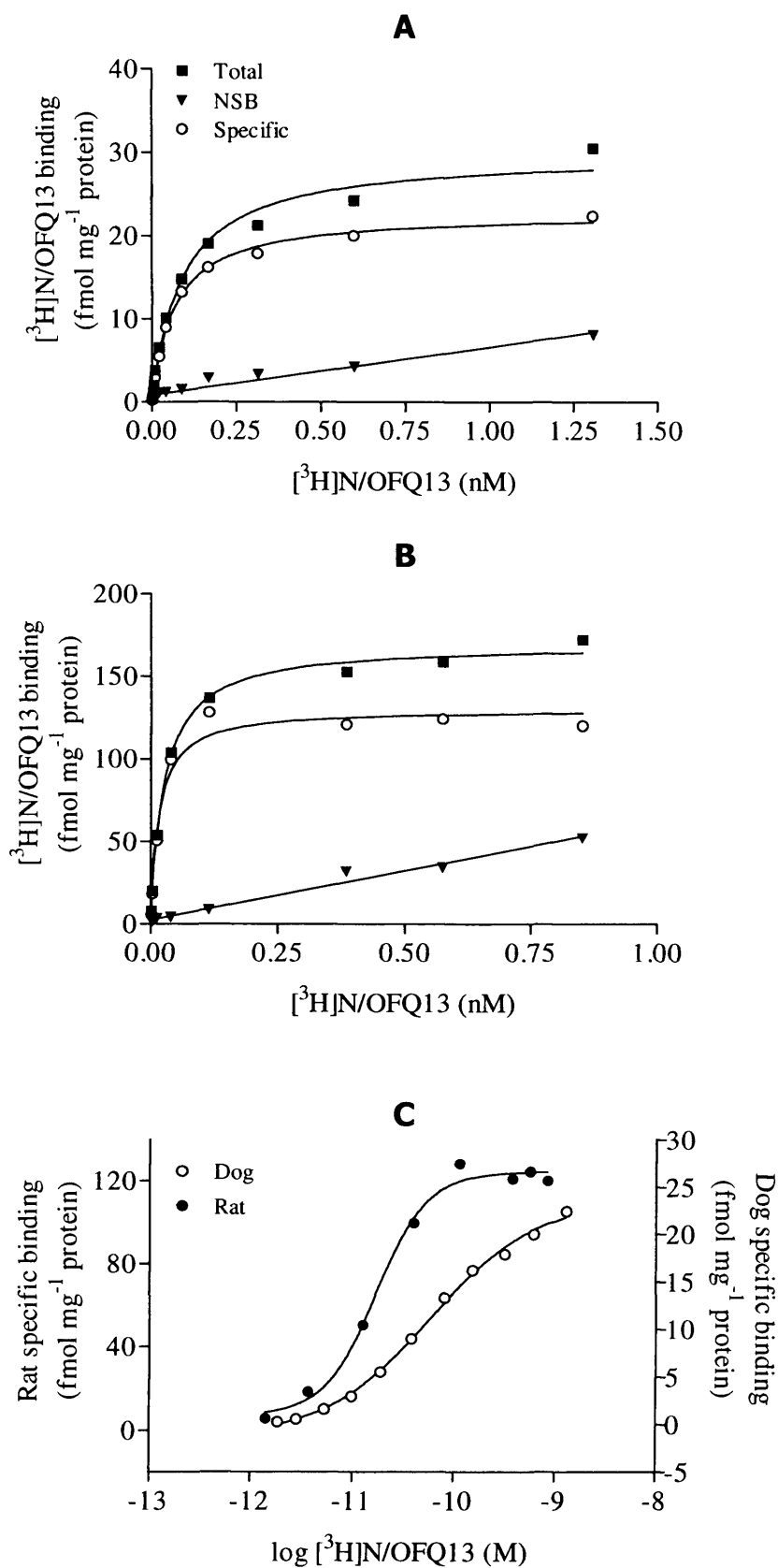


FIGURE 3.4 Typical saturation binding isotherms for $[^3\text{H}]\text{N/OFQ13}$ in the dog (A) and rat (B). Sigmoidal transformations of specific binding data are depicted in C

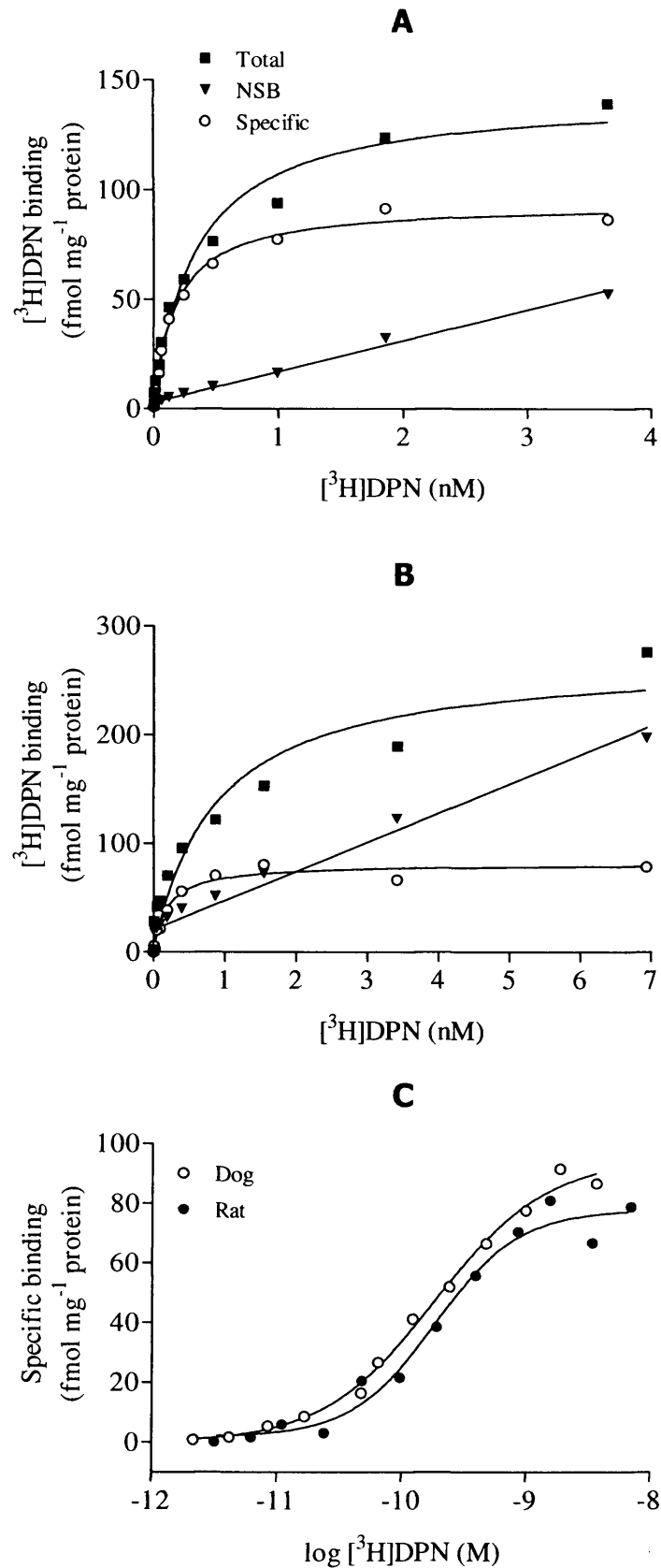


FIGURE 3.5 Specimen saturation binding isotherms for $[^3\text{H}]\text{DPN}$ in the dog (A) and rat (B). Sigmoidal transformations of specific binding data are depicted in C

TABLE 3.1 B_{max} (fmol mg^{-1} protein) and pK_d values obtained in saturation binding experiments with [*leucyl*- 3H]N/OFQ, [3H]N/OFQ13 and [3H]DPN. Data are mean \pm s.e.m (n=3-5)

		B_{max}	pK_d	K_d (pM)
$[leucyl-^3H]N/OFQ$	Preparation 1	35.8 \pm 1.2	10.44 \pm 0.08	36
	Preparation 1 ^a	33.6 \pm 6.1	10.38 \pm 0.12	42
	Preparation 1 ^b	26.3 \pm 1.2	10.35 \pm 0.09*	45
	DOG Preparation 2	23.5 \pm 0.7	9.97 \pm 0.13	107
	Preparation 3	24.9 \pm 1.9	10.43 \pm 0.11	37
	Preparation 4	30.8 \pm 2.7	10.23 \pm 0.07	59
	<i>Mean (excludes 1^a 1^b)</i>	28.7 \pm 2.8	10.27 \pm 0.11	54
RAT <i>Mean</i>	137.0 \pm 12.9 [#]	10.41 \pm 0.05	39	
$[^3H]N/OFQ13$	DOG Preparation 4	23.7 \pm 2.0 ⁺	10.16 \pm 0.12	69
	RAT ^c	130.4 \pm 1.1 [#]	10.70 \pm 0.03 ^o	20
$[^3H]DPN$	DOG	77.7 \pm 5.3	9.74 \pm 0.09	182
	RAT	79.1 \pm 18.2	9.51 \pm 0.04	309

^asamples tested ~5 months after original determination resulted in no change in either B_{max} or pK_d ;

^bsamples tested after a freeze-thaw cycle showed 25% decrease (^{*} $p < 0.05$) in B_{max} but no change in pK_d ; ^cHashiba *et al.* (2002a); [#] $p < 0.05$, ~5 fold more than dog B_{max} ; ⁺ $p < 0.05$, smaller compared with B_{max} in same preparation using [*leucyl*- 3H]N/OFQ; ^o $p < 0.005$, higher affinity than dog

3.4 Competition Binding of [*leucyl*-³H]N/OFQ

The binding of [*leucyl*-³H]N/OFQ was displaced in a concentration dependent manner in both dog (Figure 3.6) and rat (Figure 3.7) brain membranes by a range of NOP and classical opioid ligands, encompassing both peptide and non-peptide structures.

pK_i values for these data were estimated using the Cheng and Prusoff equation (section 2.15) where the K_d used was determined in this study (Table 3.2.). NalBzOH and N/OFQ9 displaced with relatively low affinity. Naloxone, N/OFQ5, cysNoc and Noc were inactive over the range of concentrations used. A small but significant ($p=0.03$) difference for [F/G] pK_i values (10.00 ± 0.16 and 10.74 ± 0.24 for dog and rat, respectively) was observed between the two species.

TABLE 3.2 pK_i values obtained in competition binding of [*leucyl*-³H]N/OFQ by a range of ligands with activity at NOP and classical opioid receptors in dog and rat brain membranes. Data are mean \pm s.e.m ($n=3-15$)

	LIGAND	DOG	RAT
<i>Agonists</i>	N/OFQ	10.98 \pm 0.20	10.99 \pm 0.10
	cysN/OFQ	10.11 \pm 0.21	10.27 \pm 0.06
	N/OFQ5	<7	<7
	N/OFQ9	7.99 \pm 0.11	8.20 \pm 0.06
	N/OFQ12	10.43 \pm 0.15	10.63 \pm 0.02
	N/OFQ13	11.69 \pm 0.21	11.94 \pm 0.23
	Ro64-6198	9.07 \pm 0.37	9.11 \pm 0.21
<i>Partial agonists</i>	[F/G]	10.00 \pm 0.16	10.74 \pm 0.24*
	CTD	10.79 \pm 0.23	10.75 \pm 0.19
<i>Antagonists</i>	[Nphe ¹]	8.79 \pm 0.18	8.90 \pm 0.23
	J-113397	9.21 \pm 0.07	9.67 \pm 0.04
<i>Mixed pharmacology</i>	III-BTD	8.28 \pm 0.06	8.28 \pm 0.06
	NalBzOH	7.32 \pm 0.23	7.87 \pm 0.08
	Noc	<7	<7
	cysNoc	<7	<7
	Naloxone	<7	<7

* $p=0.03$

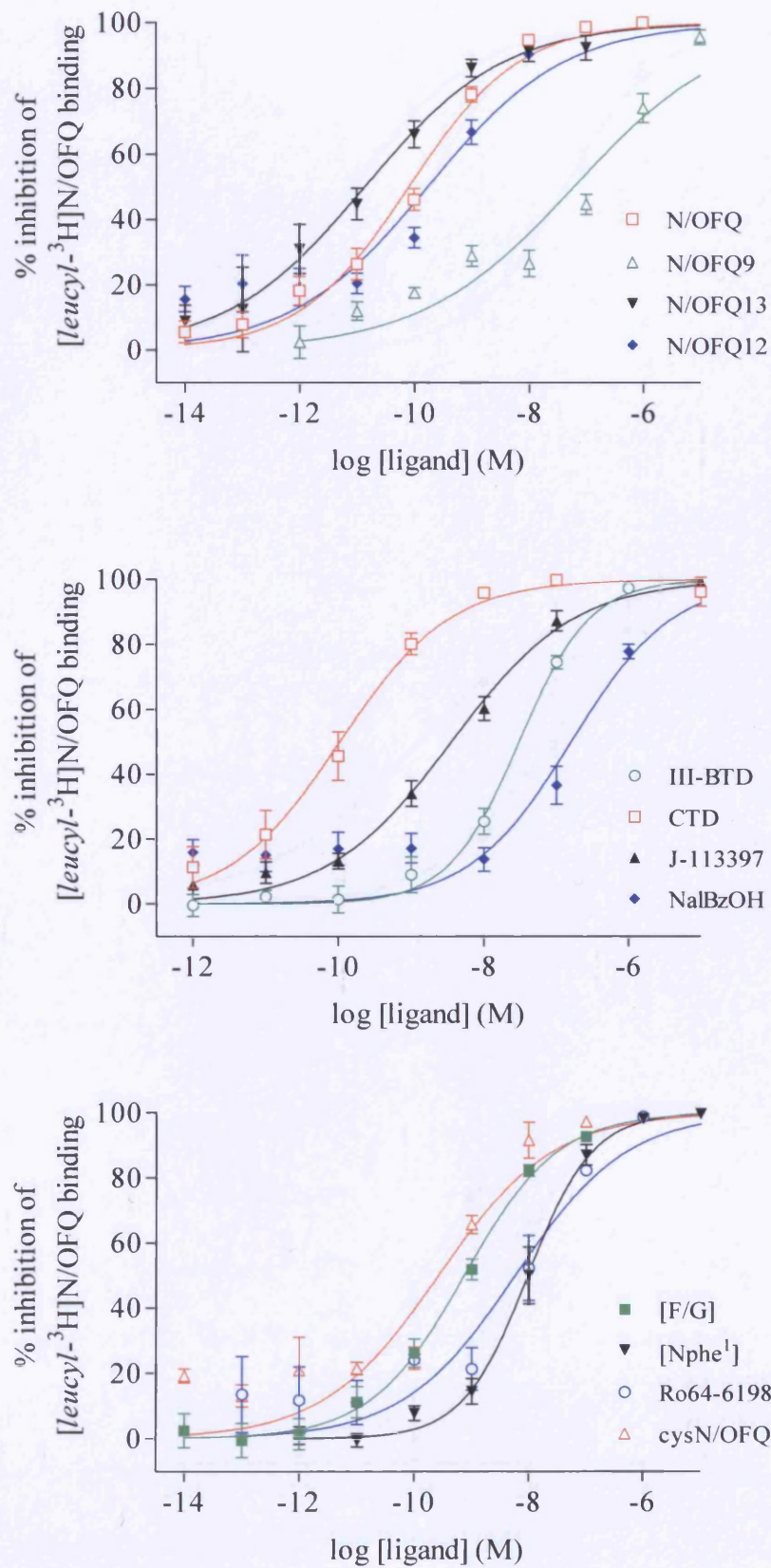


FIGURE 3.6 Competition curves of [³H]N/OFQ for a range of unlabelled ligands in dog brain membranes. Data are mean \pm s.e.m (n=3-15)

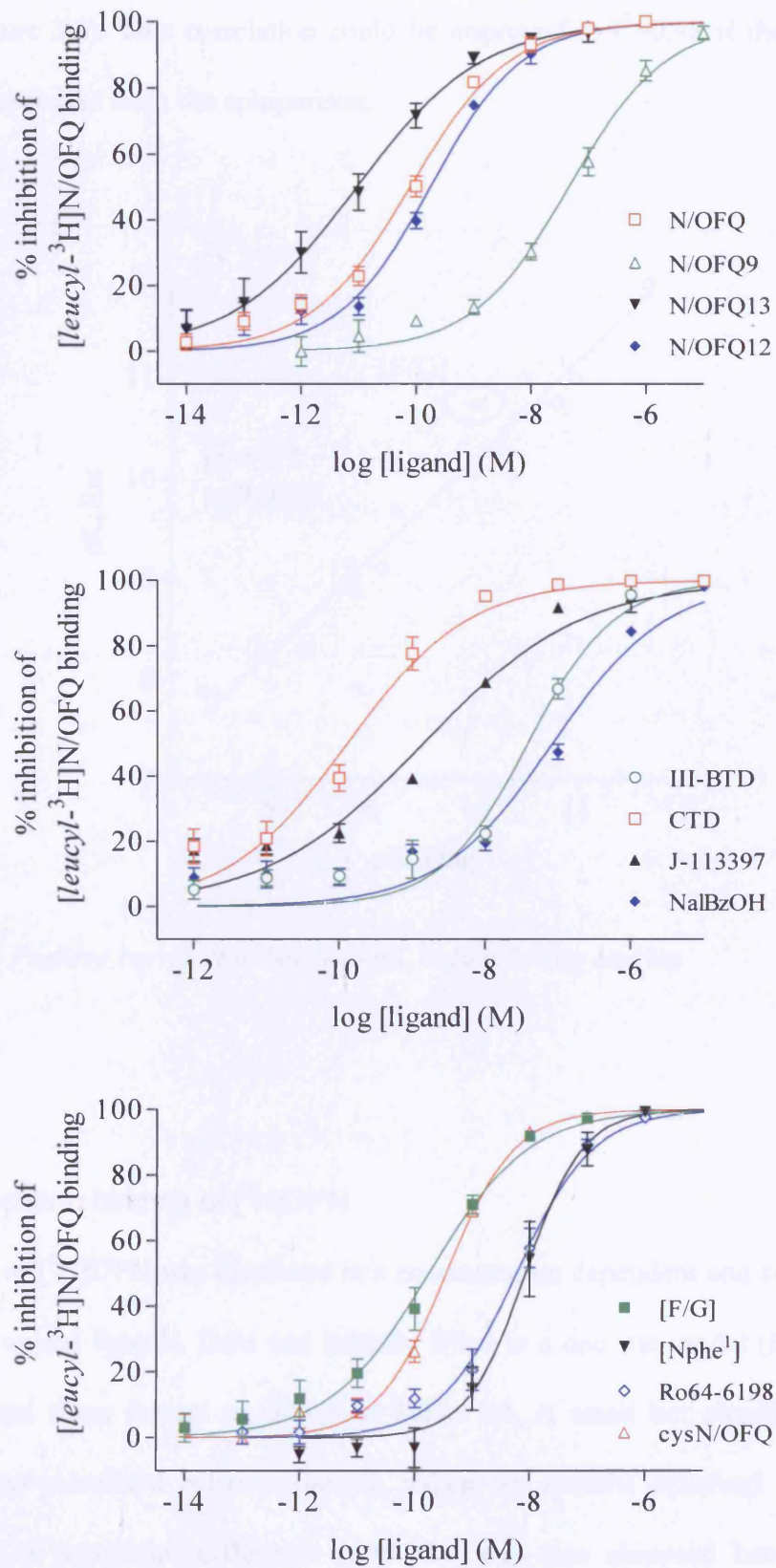


FIGURE 3.7 Competition curves of [³H]N/OFQ for a range of unlabelled ligands in rat brain membranes. Data are mean \pm s.e.m (n=3-15)

There was a strong positive correlation ($r^2=0.97$; $p<0.0001$) between pK_i values in both species (Figure 3.8). This correlation could be improved to $r^2=0.98$ if the pK_i values for [F/G] were excluded from the comparison.

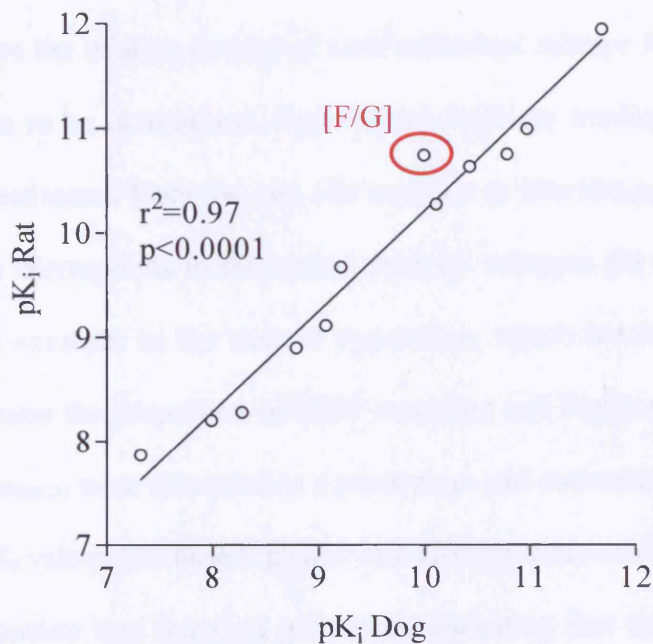


FIGURE 3.8 Positive correlation between pK_i values in dog and rat

3.5 Competition binding of [³H]DPN

The binding of [³H]DPN was displaced in a concentration dependent and saturable manner by selective opioid ligands. Data was initially fitted to a one site model (Figure 3.9) with pK_i values and slope factors as shown in Table 3.3. A small but significant difference ($p=0.002$) was calculated between the pK_i values for *nor*BNI observed in dog and rat. Interestingly, a significant difference ($p=0.001$) was also observed between the slope factors for cyprodime in dog and rat.

The curve for naloxone has a slope of approximately 1 (0.96) since this ligand is non-selective i.e. it binds to the different opioid receptor subtypes with the same affinity. Slopes of less than unity were observed (indicating binding to more than one affinity group) for the other ligands as they are known to be selective; cyprodime for MOP, naltrindole for DOP and *nor*BNI for KOP. Modelling this data to a two site curve (section 2.15) thereby allows the relative density of each individual subtype within the total opioid receptor population to be determined. Each ligand displaces binding from its 'selective' receptor subtype, estimated from the two site analysis as Fraction_{HIGH} (Figure 3.10). The remaining fraction corresponds to the opioid receptor subtypes for which the ligand has lower affinity, for example in the case of cyprodime, which binds selectively to MOP, Fraction_{HIGH} estimates the proportion of MOP receptors and Fraction_{LOW}, DOP and KOP. Values for Fraction_{HIGH} were corrected to a percentage and converted to fmol mg⁻¹ protein as in Table 3.4. pK_i values for these high and low affinity states can be found in Table 3.3. No statistical difference was found in pK_i values indicating that these displacers bind to their high affinity sites in dog and rat with similar affinity.

From the estimated high affinity fraction, the proportions of the individual subtypes were estimated to be; KOP (42%) > DOP (34%) > MOP (24%) in dog, and DOP (49%) > MOP (34%) > KOP (17%) in rat brain membranes.

TABLE 3.3 pK_i values for one and two site competition of [3 H]DPN with selective opioid ligands in dog and rat brain membranes. Data are mean \pm s.e.m (n=3-10). For Fraction_{HIGH} values see Table 3.4

Ligand	Receptor	One/ Two site	DOG				RAT			
			pK_i	pK_i H	pK_i L	Slope	pK_i	pK_i H	pK_i L	Slope
Naloxone	All classical opioid	One	8.39 \pm 0.17	-	-	0.96 \pm 0.03	8.37 \pm 0.16	-	-	0.88 \pm 0.03
N/OFQ	NOP	One	<6.0	-	-	-	<6.0	-	-	-
Naltrindole	DOP	One	8.73 \pm 0.10	-	-	0.56 \pm 0.04	8.81 \pm 0.12	-	-	0.55 \pm 0.07
		Two	-	9.35 \pm 0.15	7.75 \pm 0.07	-	9.85 \pm 0.45	8.77 \pm 0.42	-	-
Cyprodime	MOP	One	7.66 \pm 0.60	-	-	0.84 \pm 0.03*	7.85 \pm 0.37	-	-	0.58 \pm 0.01
		Two	-	7.68 \pm 0.15	6.48 \pm 0.22	-	7.29 \pm 0.77	6.62 \pm 0.44	-	-
norBNI	KOP	One	8.91 \pm 0.20*	-	-	0.55 \pm 0.06	7.46 \pm 0.05	-	-	0.76 \pm 0.09
		Two	-	10.91 \pm 1.40	8.17 \pm 0.43	-	9.96 \pm 1.11	7.29 \pm 0.13	-	-

* $p < 0.002$ compared to rat

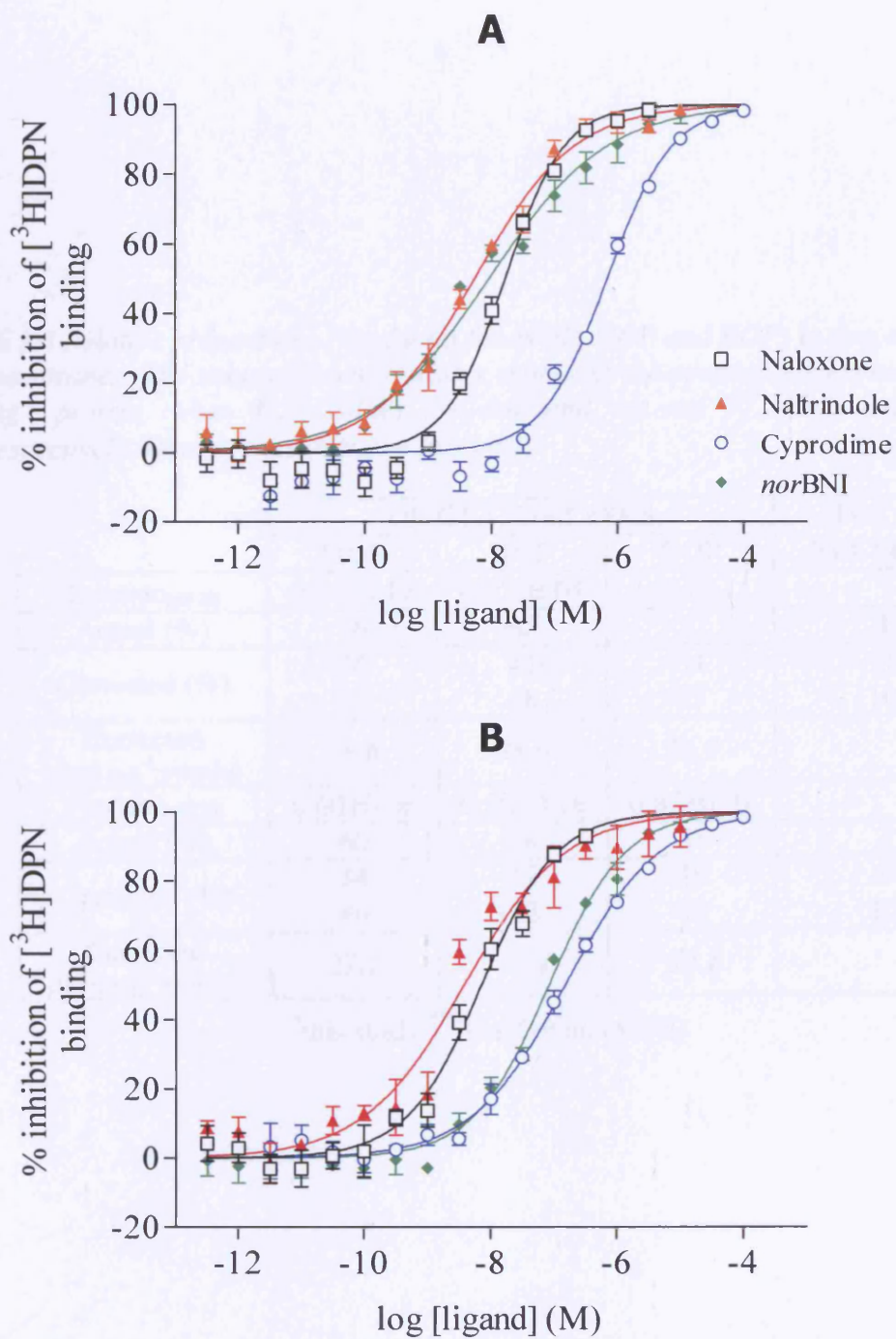


FIGURE 3.9 One site competition curves of [³H]DPN for a range of opioid ligands in dog (A) and rat (B) brain membranes. Data are mean \pm s.e.m (n=3-8)

TABLE 3.4 Relative proportions (% of total for MOP, DOP and KOP) in dog and rat brain membranes. The values shown in italics represent the proportions expressed as fmol mg⁻¹ protein, when B_{max} values for dog and rat are 77.7±5.3 and 79.1±18.2, respectively. Data are mean±s.e.m (n=3-10)

		OPIOID SUBTYPES			TOTAL % RECEPTORS
		MOP	KOP	DOP	
DOG	Fraction _{HIGH}	0.36±0.17	0.65±0.04	0.52±0.11	-
	Actual (%)	36	65	52	153
	Corrected (%)	24	42	34	100*
		5	58	37	100**
Corrected (fmol mg ⁻¹ protein)	<i>18.6</i>	<i>33.0</i>	<i>26.4</i>	-	
RAT	Fraction _{HIGH}	0.60±0.06	0.28±0.16	0.85±0.07	-
	Actual (%)	60	28	85	173
	Corrected (%)	34	17	49	100*
		46	12	42	100**
Corrected (fmol mg ⁻¹ protein)	<i>27.1</i>	<i>13.4</i>	<i>39.1</i>	-	

* this study ** Sharif *et al.* (1990)

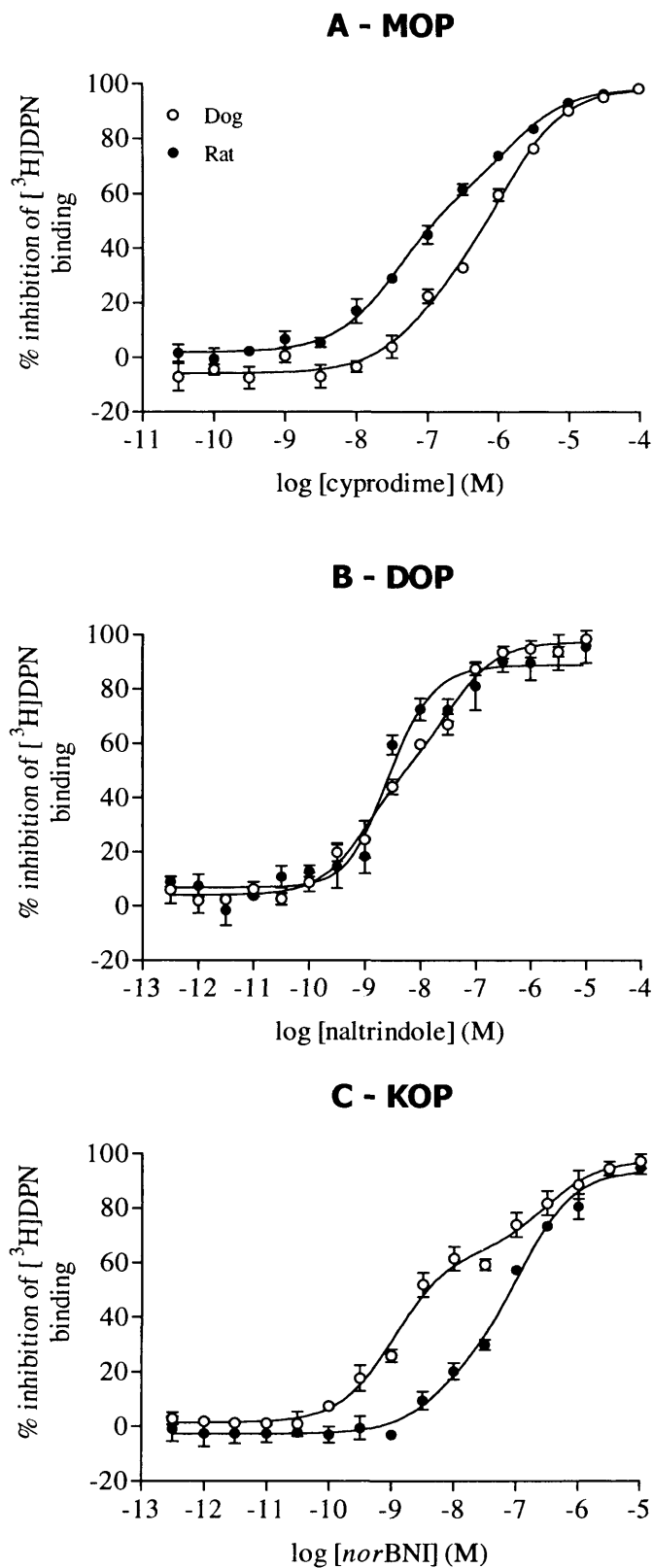


FIGURE 3.10 Two site competition of [³H]DPN by cyprodime (A), naltrindole (B) and norBNI (C) in dog and rat brain membranes. Data are mean \pm s.e.m (n=3-4)

3.6 Discussion

The data presented in this chapter has clearly demonstrated that dog brain possesses a relatively low density of N/OFQ binding sites compared to rat, and compared to the total MOP, DOP and KOP opioid receptor population. It is probable that these binding sites correspond to NOP identified by Reinscheid *et al.* (1995) and Meunier *et al.* (1995).

The levels of receptor expression in dog and rat membrane preparations assessed using [*leucyl*-³H]N/OFQ differ markedly with B_{max} values of some 29 and 137fmol mg⁻¹ protein respectively. The binding affinity of this ligand was species independent. There have been several studies examining the binding of both [³H]N/OFQ(1-17)OH and [¹²⁵I]Y¹⁴N/OFQ(1-17)OH in a range of species, which generally demonstrated a significantly higher density of NOP in these species compared to the dog.

This work has also examined NOP receptor density in dog and rat using a novel radioligand, [³H]N/OFQ13. Truncation of N/OFQ from 17 to 13 amino acids results in an agonist with essentially the same activity (in binding and functional assays) as the full sequence peptide (Calo *et al.*, 2000b; Okawa *et al.*, 1999). In addition, amidation may protect the molecule from enzymic degradation, although in the present study peptidase inhibitors were included in all our assays. Increased functional potency of the amidated peptide has been shown in isolated vas deferens (Calo *et al.*, 2000b). Data obtained in the dog with this radioligand essentially confirm the relatively low density of NOP in this species though the number of N/OFQ binding sites was lower (~23%) than with the full sequence radioligand in paired membrane preparations. No difference in binding affinity was observed for these two radioligands in dog. Interestingly there was a small (~3 fold) but significant (p<0.005) difference in [³H]N/OFQ13 pK_d observed when comparing dog to rat, with the higher affinity obtained in the rat.

In competition studies with [*leucyl*-³H]N/OFQ, there was a statistically significant positive correlation between pK_i values obtained in both species, indicating a high degree of similarity in N/OFQ binding sites. In experiments using [*leucyl*-³H]N/OFQ as the primary labelling ligand, a range of molecules with affinity for NOP produced a concentration-dependent displacement. The rank order of pK_i obtained in both species is essentially identical and agrees with that reported by our laboratory (Okawa *et al.*, 1999) and others (Calo *et al.*, 2000a; 2000c) for the rat and human NOP. However, one discrepancy with our previous data is the higher affinity of [F/G], although notably, previous data was obtained using the radioligand, [¹²⁵I]Y¹⁴N/OFQ(1-17)OH. Affinity values for the antagonists, [Nphe¹] (Calo *et al.*, 2000b), J-113397 (Ozaki *et al.*, 2000), III-BTD (Bigoni *et al.*, 2000b), and agonist Ro64-6198 (Dautzenberg *et al.*, 2001) are essentially identical with values obtained using recombinant human NOP and [³H]N/OFQ(1-17)OH as the radioligand (Hashiba *et al.*, 2001). Ligands with variable activity at NOP receptors and classical opioid receptors displayed weak affinity at NOP in both dog and rat. Indeed, NalBzOH which is a mixed opioid agonist/antagonist and a partial agonist at NOP (Bigoni *et al.*, 2002a) displaced with relatively low affinity (similar to that of N/OFQ9). Noc was also inactive. Further comment is required on the binding of [³H]DPN; the results presented in this thesis indicate that there is a similar total opioid receptor population in dog and rat brain membranes. Data reported here for the rat are higher than the B_{max} values observed by other groups - Tao *et al.* (1988) report 54.0 and Sadee *et al.* (1982) 30.0fmol mg⁻¹ protein. Variation is also observed in K_d values – 0.309 in this thesis, 2.60 (Tao *et al.*, 1988) and 0.16nM (Sadee *et al.*, 1982), respectively. Such intraspecies variation cannot be explained though it is common in radioligand binding studies, depending on the tissue investigated and the assay conditions.

Despite similar total opioid receptor populations, the proportions of each opioid receptor subtype in dog and rat preparations differ. For dog, the rank order was KOP > DOP > MOP, compared to DOP > MOP > KOP in rat. These proportions are important when characterising particular selective agonists since receptor density is known to affect intrinsic properties.

In conclusion, this chapter has compared the binding of NOP and opioid receptor ligands in rat and dog brain. Despite the almost identical pharmacology between dog and rat NOP, dog brain contains approximately one fifth the density of NOP receptors found in rat, and has ~3 fold higher density of total opioid receptors, compared to NOP.

4 Results: Functional Binding

4.1 Introduction

NOP exhibits ~60% sequence homology to classical opioid receptor subtypes hence there are several similarities between NOP and opioid receptors that extend past this molecular identification. However, NOP binds opioid peptides with low affinity and activation of NOP *in vivo* can produce contrasting effects to those observed on activation of classical opioid receptors, especially MOP (Calo *et al.*, 2000c).

Studies of receptor distribution are of great value in revealing the specific structures in which the receptor is present, aiding rationalization of the effects seen from systemic or local drug administration. Nevertheless, the mere presence of a receptor gives little information of functional activity. Many studies have examined the pharmacology and distribution of NOP in a range of species and thus data presenting receptor density and pharmacological characteristics is in abundance (Mollereau *et al.*, 2000; Okawa *et al.*, 1998; Pettersson *et al.*, 2002). Chapter 3 reported the ligand binding characteristics of native dog NOP and detailed a particularly low level of expression in the brain. Further studies investigating whether these NOP receptors are functionally active species were therefore warranted.

This chapter presents results from a series of functional binding experiments, the methods of which can be found in sections 2.16 and 2.17. Brain preparation methodology and cell culture can be found in sections 2.6, 2.7 and 2.8. Data for a limited number of comparative studies using CHO_{hNOP} cells are also included.

The aims of this chapter are to characterise:

- The affinity states of dog NOP using a series of [*leucyl*-³H]N/OFQ competition studies in the absence and presence of NaCl/GTP γ S
- Agonist stimulation of GTP γ ³⁵S binding to dog and CHO_{hNOP} membranes
- Whether the stimulation of GTP γ ³⁵S binding to dog and CHO_{hNOP} membranes could be antagonised by various selective NOP ligands

4.2 NaCl/GTP γ S Shift

In the absence of NaCl and GTP γ S, N/OFQ produced a concentration dependent and saturable displacement of [*leucyl*-³H]N/OFQ (Figure 4.1) with a low slope factor (0.38) and pK_i of 9.62±0.07 (Table 4.1). These data were best modelled to a two site competition curve, indicative of two receptor affinity states where High=LRG and Low=LR (Figure 4.2; where L represents N/OFQ, R NOP and G G protein). Approximately 33% of the receptors displayed high affinity for N/OFQ with the remaining 67% showing lower affinity. Addition of 120mM NaCl and 100 μ M GTP γ S produced a significant (p=0.009) increase in the slope (0.95), which was then best modelled to single site binding. As illustrated in Figure 4.2, there was an absence of high affinity N/OFQ binding sites in the presence of NaCl/GTP γ S due to the dissociation of LRG.

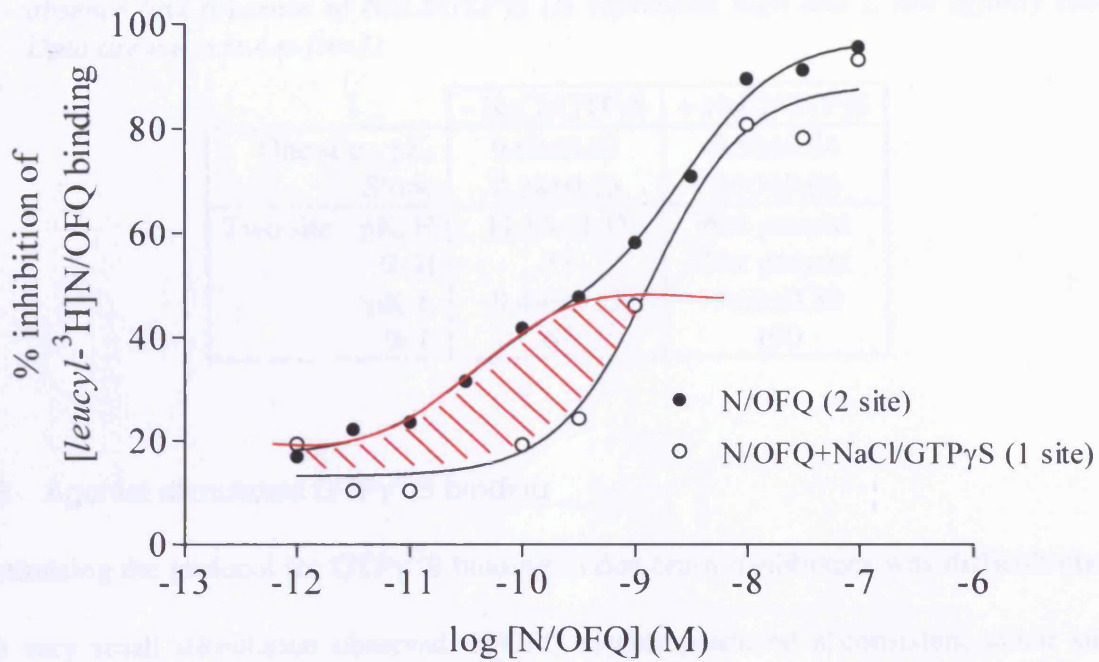


FIGURE 4.1 Specimen curves of [leucyl-³H]N/OFQ competition in dog brain membranes modelled to one and two sites. The area under the curve denoted in red illustrates the high affinity proportion of the two site curve



FIGURE 4.2 Allosteric regulation of NOP by non-hydrolysable GTP γ S indicates that NOP exists as two different affinity states, high (H), when N/OFQ-NOP couples to the trimeric G protein and low (L), when, in the presence of the GTP γ S, the G protein is activated and dissociates from the ternary complex

TABLE 4.1 One and two site analysis of [*leucyl*-³H]N/OFQ competition curves in the absence and presence of NaCl/GTP γ S (*H* represents high and *L* low affinity sites). Data are mean \pm s.e.m (*n*=3)

	- NaCl/GTP γ S	+ NaCl/GTP γ S
One site - pK _i	9.62 \pm 0.07	9.58 \pm 0.24
Slope	0.38 \pm 0.05	0.95 \pm 0.06
Two site - pK _i H	11.64 \pm 0.37	Not present
% H	33	Not present
pK _i L	9.44 \pm 0.15	9.68 \pm 0.30
% L	67	100

4.3 Agonist stimulated GTP γ ³⁵S binding

Optimising the protocol for GTP γ ³⁵S binding in dog brain membranes was difficult due to the very small stimulation observed. N/OFQ (1 μ M) produced a consistent albeit small stimulation of GTP γ ³⁵S binding to dog in a concentration dependent and saturable manner (Figure 4.3), with pEC₅₀ and E_{max} (stimulation factor) values shown in Table 4.2. In CHO_{hNOP} membranes (included as a positive control), a larger stimulation (~7 fold) was observed (Figure 4.3; Table 4.2). Ro64-6198 produced a similar stimulation (E_{max} 1.22 \pm 0.03) to N/OFQ in dog, with a reduced pEC₅₀ value of 6.58 \pm 0.40 (Figure 4.3), consistent with full agonism (Hashiba *et al.*, 2002b). As is clearly illustrated, the net stimulation in dog was a small fraction of that seen in CHO_{hNOP} with some 259 dpm specific binding observed in the dog at a saturating N/OFQ concentration. Due to this low stimulation there was some inherent variation in the data.

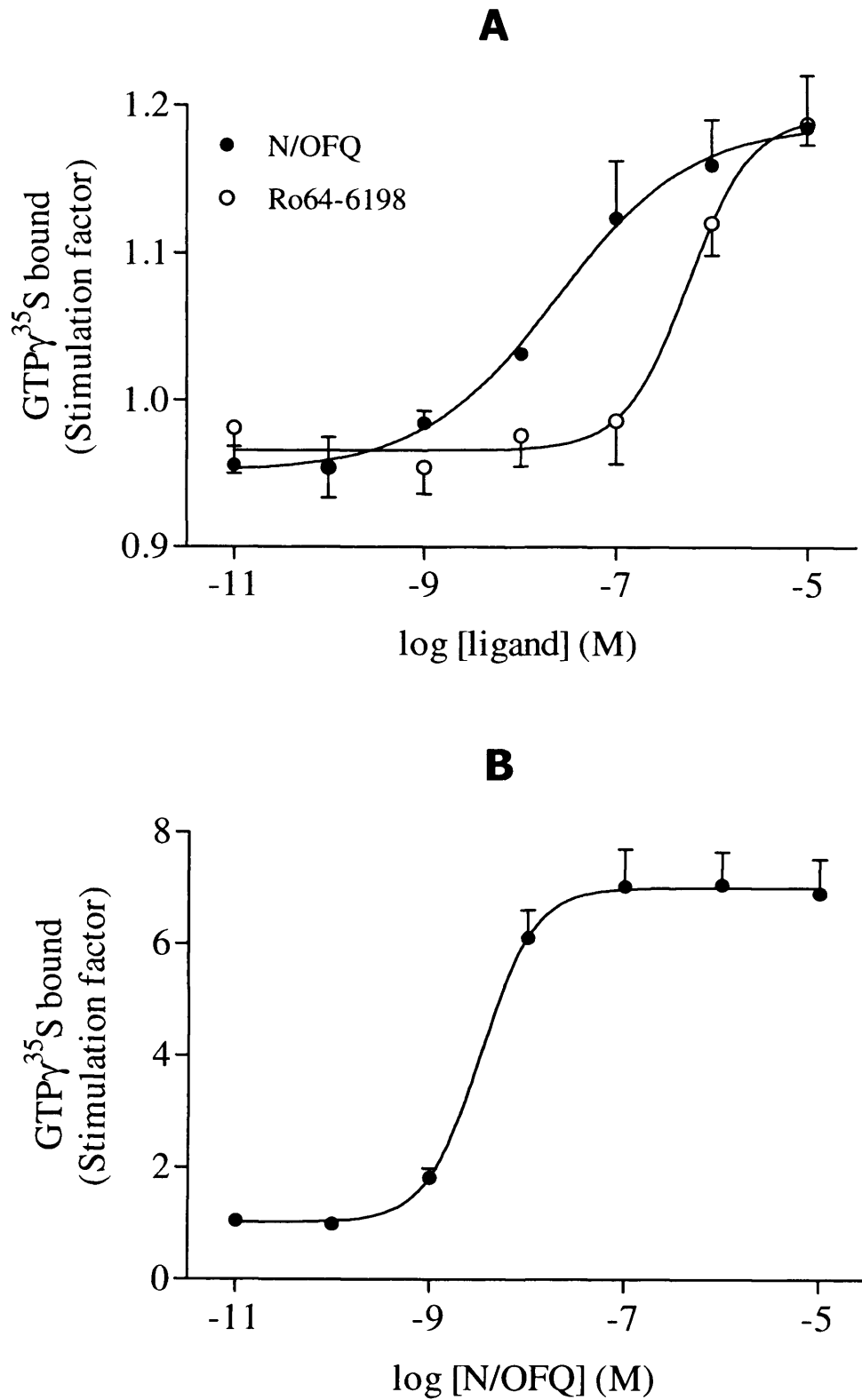


FIGURE 4.3 Stimulation of $GTP\gamma^{35}S$ binding to dog (A) and CHO_{hNOP} cell (B) membranes. Data are mean \pm s.e.m ($n=4-6$)

TABLE 4.2 Comparison of estimated N/OFQ potency and efficacy at native NOP expressed in dog brain and CHO_{hNOP} cells. Data are mean±s.e.m (n=3-12)

	DOG	CHO _{hNOP}
N/OFQ pEC ₅₀	8.21±0.17	8.47±0.01
N/OFQ E _{max}	1.17±0.01	7.01±0.63*
GTPγ ³⁵ S bound (dpm)	259±39	3577±120*
B _{max} [<i>leucyl</i> - ³ H]N/OFQ (fmol mg ⁻¹ protein)	28.7±2.8	1348±44*#

*p<0.05, greater than dog; #from Hashiba *et al.* (2002a)

Single concentration data at 10μM for a range of ligands related to N/OFQ are presented in Table 4.3. N/OFQ is included at 1μM for comparative purposes. N/OFQ5, CTD and Noc all failed to stimulate GTPγ³⁵S binding. However, it should be noted that these data give no information on agonist potency.

TABLE 4.3 Effects of a range of N/OFQ ligands at single concentrations on GTPγ³⁵S binding to dog brain membranes. Data are stimulation factor at 10μM (except N/OFQ, 1μM) presented as mean±s.e.m (n=3-12)

LIGAND	E _{max}
N/OFQ	1.16±0.02*
N/OFQ5	1.03±0.04
N/OFQ9	1.09±0.03*
N/OFQ11	1.14±0.05*
N/OFQ12	1.16±0.07*
N/OFQ13	1.19±0.06*
ALOH	1.28±0.04*
[(<i>p</i> F)phe ⁴]	1.31±0.07*
CTD	0.94±0.02
Noc	0.92±0.07

*p<0.05 compared with unstimulated basal GTPγ³⁵S binding

4.4 Antagonism of $\text{GTP}\gamma^{35}\text{S}$ stimulation

N/OAQ stimulated $\text{GTP}\gamma^{35}\text{S}$ binding to dog brain membranes was competitively antagonised by 100nM J-113397 (selective non-peptide NOP antagonist) such that the concentration response curve for N/OAQ was shifted to the right with no significant depression of the maximum response (Figure 4.4). Similar data was obtained for CHO_{hNOP} (Figure 5.4).

Analysis of these data using the Gaddum Schild equation yielded pK_B values of 8.58 and 8.34 for dog and CHO_{hNOP} , respectively (Table 4.4). In a similar series of experiments in dog only, N/OAQ stimulated $\text{GTP}\gamma^{35}\text{S}$ binding was competitively antagonised by the low potency peptide antagonist, $[\text{Nphe}^1]$ and the partial agonist $[\text{F/G}]$, both at 1 μM (Figure 4.5). pEC_{50} and pK_B values are shown in Table 4.4.

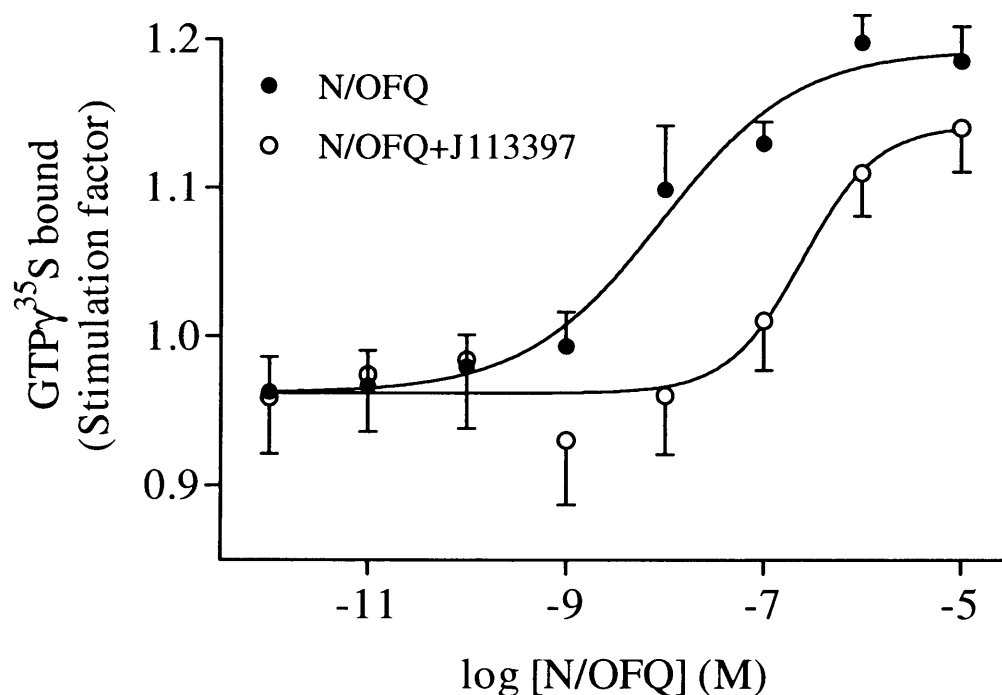


FIGURE 4.4 N/OAQ stimulated $\text{GTP}\gamma^{35}\text{S}$ binding to dog ($n=5$) membranes is competitively antagonized by the selective NOP antagonist J-113397 (100nM). Data are mean \pm s.e.m ($n=4$)

TABLE 4.4 J-113397 (100nM), [Nphe¹] and [F/G] (both at 1μM) competitively antagonised N/OFQ stimulated GTPγ³⁵S binding to dog brain membranes. Comparative data with J-113397 in CHO_{hNOP} membranes are also shown. Data are mean±s.e.m from paired experiments (n=3-5)

Antagonist		pEC ₅₀		pK _B
		-Antagonist	+Antagonist	
J-113397	Dog	8.09±0.23	6.50±0.17*	8.58±0.21
	CHO _{hNOP}	8.47±0.01	7.12±0.02*	8.34±0.02
[Nphe ¹]	Dog	8.01±0.32	6.72±0.12*	7.06±0.59
[F/G]	Dog	8.25±0.12	6.86±0.38*	7.32±0.41

*p<0.05 lower than in the absence of antagonist

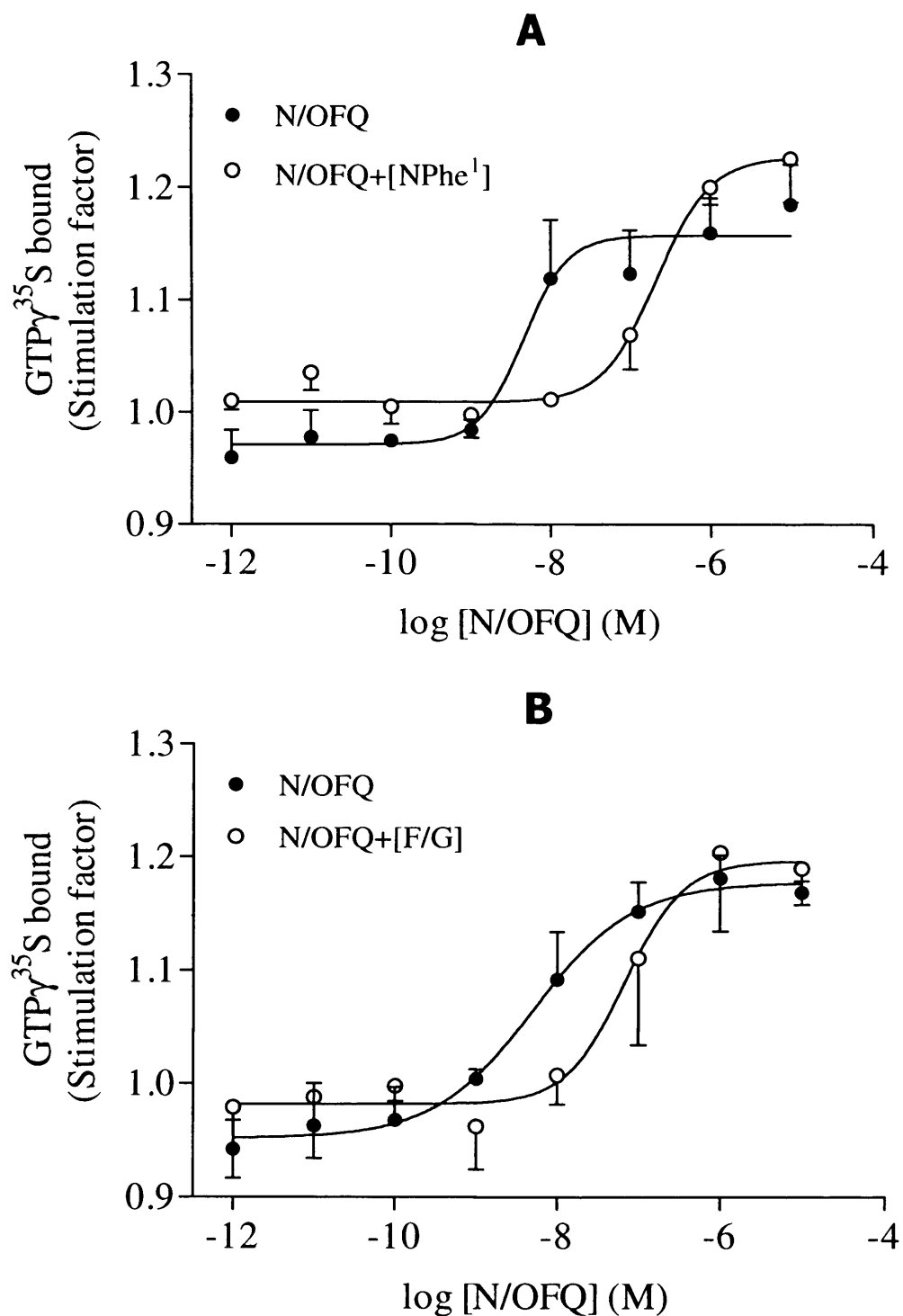


FIGURE 4.5 N/OFQ stimulated GTP γ^{35} S binding to dog membranes is competitively antagonized by 1 μ M [Nphe¹] (A) and 1 μ M [F/G] (B). Data are mean \pm s.e.m (n=4)

4.5 Discussion

Despite extremely low expression of NOP in dog brain ($\sim 29 \text{ fmol mg}^{-1}$ protein, chapter 3), functional activity was still detectable using a series of “GTP-shift” studies and agonist stimulated $\text{GTP}\gamma^{35}\text{S}$ binding assays.

In competition studies in dog brain membranes, binding of N/OFQ was sensitive to a combination of NaCl and $\text{GTP}\gamma\text{S}$. NOP existed in two different affinity states evidently regulated by G protein association i.e. receptor coupled or uncoupled to its respective G protein. In the absence of elements which promote dissociation of the G protein heterotrimer, and therefore of the ternary complex (e.g. sodium ions and $\text{GTP}\gamma\text{S}$), 33% of dog NOP exist in a high affinity state (pK_i 11.64) with the remaining 67% in a lower affinity state (pK_i 9.44). In the presence of NaCl/ $\text{GTP}\gamma\text{S}$, a steepening of the competition curve is observed, signifying dissociation of the ternary complex, and there is a shift to the low affinity receptor conformation (pK_i 9.68). Allosteric regulation of N/OFQ binding by sodium and non-hydrolysable GTP analogues has been shown previously with recombinant NOP (Butour *et al.*, 1997) and is akin to that of opiate binding to opioid receptors (Pert *et al.*, 1973). There is a critical Asp residue in NOP, which is the putative site for sodium sensitivity, and this appears to be conserved in opioid and other receptors, which are also sensitive to sodium (Butour *et al.*, 1997). This highlights the ability of native dog NOP to functionally couple to its respective G protein in a manner expected for an opioid-like GPCR.

GDP for GTP exchange represents the earliest opportunity at which receptor activation and functional coupling can be measured. $\text{GTP}\gamma^{35}\text{S}$ binding assays were used to further evaluate that native NOP in dog could stimulate guanine nucleotide exchange. These data were compared to our well-characterised CHO_{hNOP} model (Hashiba *et al.*, 2001; Okawa *et al.*, 1999).

Supra-maximal concentrations of peptide and peptoid analogues of N/OFQ had mixed action with regard to their ability to stimulate GTP γ ³⁵S binding to dog brain membranes. Those ligands previously characterised as full agonists i.e. N/OFQ (Meunier *et al.*, 1995; Reinscheid *et al.*, 1995), N/OFQ13 (Calo *et al.*, 1997), ALOH (Okada *et al.*, 2000) and [(pF)Phe⁴] (Bigoni *et al.*, 2002b; McDonald *et al.*, 2002) all produced significant increases in GTP γ ³⁵S binding relative to basal. Amidated analogues of N/OFQ truncated to 1-9 also produced significant GTP γ ³⁵S binding (but it should be re-emphasised that no information on potency can be obtained from single concentration studies) although the degree of stimulation at equimolar concentrations apparently decreased as the C-terminus was shortened. This is similar to the loss of binding affinity seen with increasing C-terminal truncation and has been demonstrated in an earlier study (Calo *et al.*, 1997) using mouse vas deferens and guinea pig ileum preparations. Though the maximal stimulation (E_{\max} 1.16 with N/OFQ) observed in dog is small, it is representative of very low NOP expression in dog brain.

Indeed, the stimulation seen in dog parallels that recently observed in our laboratory in an inducible expression system with CHO_{INDhNOP} (cells transfected with an ecdysone inducible plasmid, thereby allowing for the control of gene transcription and hence receptor density) expressing ~25fmol mg⁻¹ receptor (E_{\max} of 1.28; McDonald *et al.*, 2003). Higher stimulation seen in CHO_{hNOP} is merely a function of greater receptor density (~1348fmol mg⁻¹; Hashiba *et al.*, 2002a), which is typical of transfected systems. Importantly, it can be seen that potency values for N/OFQ are comparable in both tissues. To further characterise the pharmacology of NOP in dog, N/OFQ stimulated GTP γ ³⁵S binding was antagonised by the NOP selective antagonists, [Nphe¹] and J-113397 (Guerrini *et al.*, 2000; Kawamoto *et al.*, 1999). pK_B values for both are similar to those reported previously for these antagonists in other systems, and additionally, for J-113397 at

hNOP in this study. In addition, the agonist [F/G], whilst being inactive *per se*, also antagonised N/OFQ stimulated $\text{GTP}\gamma^{35}\text{S}$ binding. We have clearly shown previously that the efficacy of this ligand is dependent on receptor density and would have predicted [F/G] to be antagonistic in dog given the low receptor expression (McDonald *et al.*, 2003; Okawa *et al.*, 1999).

Using a modified $\text{GTP}\gamma^{35}\text{S}$ binding assay and immunoprecipitation of individual $\text{G}_{\alpha\text{i}1-3}$ subunits, it was possible to measure NOP receptor coupling specifically to $\text{G}_{\alpha\text{i}1-3}$ subunits. The data in Table 4.5 is presented with the permission of John McDonald and shows that $1\mu\text{M}$ N/OFQ stimulated the binding of $\text{GTP}\gamma^{35}\text{S}$ to $\text{G}_{\alpha\text{i}1-3}$ subunits in both dog and CHO_{hNOP} membranes. Immunoprecipitated stimulation factors in dog are comparable with those from standard $\text{GTP}\gamma^{35}\text{S}$ binding, which suggest that $\text{G}_{\alpha\text{i}1-3}$ represents the majority of G protein coupling. In CHO_{hNOP} , N/OFQ also stimulated the binding of $\text{GTP}\gamma^{35}\text{S}$ to $\text{G}_{\alpha\text{i}1-3}$ subunits although stimulation factors were lower than in standard (non-immunoprecipitated) $\text{GTP}\gamma^{35}\text{S}$ binding assays. However, differences in buffer (low GDP, high magnesium ions and high protein) and efficiency of the respective assays may account for this variation in response.

These studies show specific coupling of NOP to $\text{G}_{\alpha\text{i}1-3}$ subunits, which suggests the classical PTx sensitive pathways are also activated by dog NOP. Activation of such G proteins in dog indicates that NOP most likely regulates potassium conductance, VSCCs and adenylyl cyclase as reported for NOP in other species.

TABLE 4.5 N/OAQ (1 μ M) stimulated GTP γ ³⁵S binding to G α ₁₋₃ subunits. Differences in total dpm bound represent the different mass of tissue used, lower GDP (5 μ M) and higher magnesium ions (5mM). Data are mean \pm s.e.m (n=3) and is presented here with kind permission of John McDonald

	Tissue Origin	
	Dog (150 μ g)	CHO _{hNOP} (40 μ g)
Total dpm	8321 \pm 1021	1488 \pm 144
NSB dpm	375 \pm 37	280 \pm 21
1 μ M N/OAQ dpm	10632 \pm 1531	4629 \pm 786
Net DPM	2311 \pm 605	3140 \pm 912
E _{max}	1.28 \pm 0.06	3.90 \pm 1.18

(Methodology (Cordeaux *et al.*, 2000): 40 μ g CHO_{hNOP} or 150 μ g dog membranes in 0.5ml 50mM Tris-HCl, 100mM NaCl, 0.2mM EGTA, 5mM MgCl₂, pH7.4 with 1mg ml⁻¹ BSA, 150 μ M bacitracin, 10 μ M peptidase inhibitors, 5 μ M GDP, ~150pM GTP γ ³⁵S and 1 μ M N/OAQ for 1h, 30°C with gentle shaking. NSB defined in presence of 10 μ M GTP γ S. Reactions terminated with 1ml ice-cold buffer and centrifugation for 5min at 16000g. Pellets resuspended in 100 μ l solubilisation buffer (50mM Tris-HCl, 150mM NaCl, 5mM EDTA, 1.25% (v/v) Igepal, pH7.4) with 0.2% (w/v) SDS and protease inhibitors, and incubated for 5min. Further 100 μ l solubilisation buffer (SDS free) added before further 5min incubation. Samples pre-cleared with 15 μ l protein-A agarose for 30min, 4°C. Anti-G α ₁₋₃ antibody (4 μ g) then added for 13h, 4°C. Antibody precipitated with 30 μ l of protein-A agarose for 2h, 4°C and 5min centrifugation at 16000g. Samples resuspended in 750 μ l solubilisation buffer (protease inhibitor free), centrifuged for 5min at 16000g, resuspended in scintillation cocktail and counted after 8h extraction.)

In conclusion, this chapter shows that NOP in dog is functionally active with a basic pharmacological profile analogous to that reported in other species, including the recombinant hNOP presented here as a positive control.

5 Results: *In vitro* characterisation of CJ-X

5.1 Introduction

N/OFQ is structurally related to the opioid peptides but displays very low affinity for the classical MOP/DOP/KOP receptor subtypes and has been implicated in many roles within the CNS, including modulation of pain perception, anxiety, locomotion, and the cardiovascular system (Calo *et al.*, 2000c; Mogil *et al.*, 2001). The search for novel ligands with high potency and selectivity for this receptor is of paramount importance in developing an understanding of this system in health and disease. To date there are several compounds available (section 2.19) encompassing both peptide and non-peptide structures including; [Nphe¹] (Calo *et al.*, 2000b), its derivative UFP-101 (Calo *et al.*, 2002), JTC-801 (Yamada *et al.*, 2002), J-113397 (Kawamoto *et al.*, 1999), III-BTD (Becker *et al.*, 1999) and Ro64-6198 (Jenck *et al.*, 2000).

In chapter 3, a unique binding site for NOP selective radioligands, [*leucyl*-³H]N/OFQ and [³H]N/OFQ13 was identified in dog brain membranes though maximal binding was much reduced compared to that observed in rat and, to total opioid receptor population. Chapter 4 used functional assays to highlight that this binding site was indeed a functional receptor, with the ability to couple to G_i proteins. Its endogenous ligand, N/OFQ, has been characterised and can stimulate specific coupling of NOP to G_{αi1-3} subunits. This suggests that the NOP system has a role in various PTx sensitive intracellular pathways; potassium conductance, VSCCs and inhibition of adenylyl cyclase.

This chapter describes the basic pharmacological characterisation of the novel synthetic non-peptidic ligand synthesised by Pfizer Ltd in a series of radioligand binding and functional assays. Due to confidentiality and intellectual property issues, this ligand is referred to as CJ-X hereon. The methods for cell culture and membrane preparation are described in sections 2.6-2.9 and those for binding assays in sections 2.13-2.15, 2.17 and

2.18. Data is presented for dog and rat brain membranes, and also membranes and whole cell preparations from CHO_{hNOP}, CHO_{mDOP}, CHO_{rMOP} and CHO_{rKOP}. N/OFQ, naloxone, cyprodime, naltrindole and *nor*BNI were included in these studies as reference ligands.

The aims of this chapter are to characterise:

- Competition of [*leucyl*-³H]N/OFQ and [³H]DPN by CJ-X in dog and rat, and in CHO cells expressing recombinant hNOP and opioid receptor subtypes rMOP, mDOP and rKOP
- CJ-X stimulation of GTPγ³⁵S binding to CHO_{hNOP} membranes
- CJ-X effects on cAMP formation in whole CHO_{hNOP} cell preparations

5.2 Competition of [*leucyl*-³H]N/OFQ and [³H]DPN in dog and rat

In membranes prepared from rat and dog brain, both N/OFQ and CJ-X produced a concentration dependent displacement of [*leucyl*-³H]N/OFQ binding (Figure 5.1), yielding pK_i values as shown in Table 5.1. CJ-X displaced [³H]DPN binding (Figure 5.1) to classical opioid receptors in both preparations with much reduced affinity (Table 5.1). Naloxone was included as a high affinity non-selective reference compound and displaced with a K_i in the nM range. From these data it is possible to estimate a crude selectivity of CJ-X for NOP over the total opioid population as 2455 fold in rat and 1820 fold in dog.

*TABLE 5.1 Interaction of CJ-X with NOP and classical opioid receptors in [*leucyl*-³H]N/OFQ and [³H]DPN competition binding with dog and rat brain membranes. Data are mean ± s.e.m (n=3-5)*

Species	Radioligand	CJ-X pK _i	Reference Ligand pK _i
Rat	[<i>leucyl</i> - ³ H]N/OFQ	10.31±0.09	N/OFQ 10.99
	[³ H]DPN	6.92±0.16	Naloxone 8.58
Dog	[<i>leucyl</i> - ³ H]N/OFQ	10.27±0.11	N/OFQ 10.98
	[³ H]DPN	7.01±0.06	Naloxone 8.37

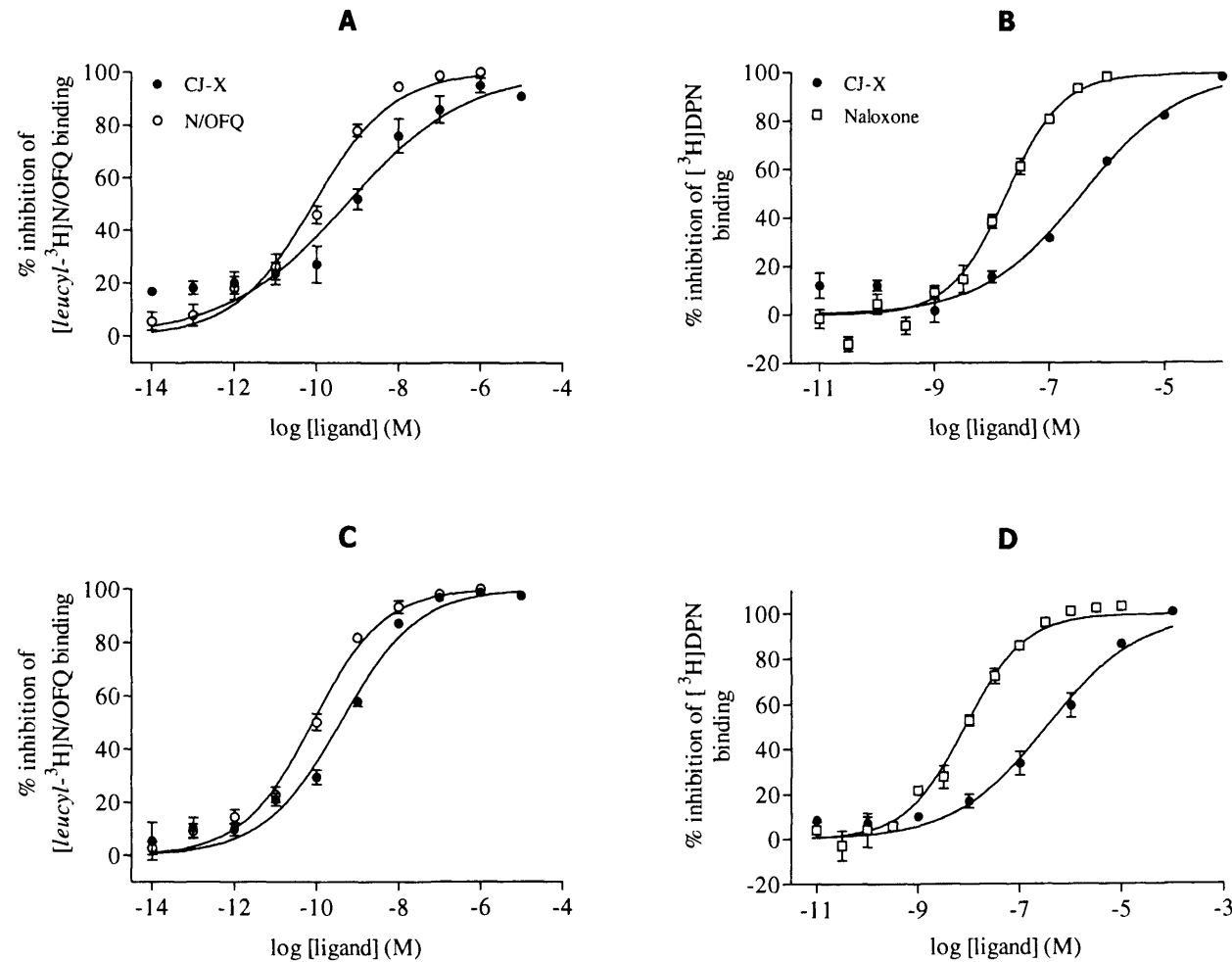


FIGURE 5.1 Competition curves of [leucyl- ^3H]N/OFQ and [^3H]DPN for CJ-X in dog (A and B) and rat (C and D) membranes. N/OFQ and naloxone are included as reference ligands. Data are mean \pm e.m (n=6-15)

5.3 Competition of [*leucyl*-³H]N/OFQ and [³H]DPN in CHO membranes

Displacement of [*leucyl*-³H]N/OFQ and [³H]DPN in CHO cells expressing recombinant hNOP or rMOP/mDOP/rKOP subtypes (Figure 5.2) provided more detailed information on selectivity, with pK_i values shown in Table 5.2. The binding of both radioligands was displaced in a concentration dependent and saturable manner by various selective ligands. Estimated selectivity of CJ-X for hNOP over mDOP, rMOP and rKOP is 19496, 416 and 63 fold, respectively. It should be noted that these estimated selectivities are based on comparing receptors from different species.

TABLE 5.2 Interaction of CJ-X with NOP and classical opioid receptors in [*leucyl*-³H]N/OFQ and [³H]DPN competition binding assays using membranes prepared from CHO cells expressing recombinant receptors. Data are mean \pm s.e.m (n=3-6)

Receptor	Radioligand	pK _i CJ-X (selectivity)	Reference pK _i
CHO _{hNOP}	[<i>leucyl</i> - ³ H]N/OFQ	9.76 \pm 0.10	N/OFQ: 9.85
CHO _{mDOP}	[³ H]DPN	5.47 \pm 0.28 ₍₁₉₄₉₆₎	Naltrindole: 10.24
CHO _{rMOP}		7.14 \pm 0.17 ₍₄₁₆₎	Cyprodime: 7.71
CHO _{rKOP}		7.96 \pm 0.11 ₍₆₃₎	<i>nor</i> BNI: 8.18

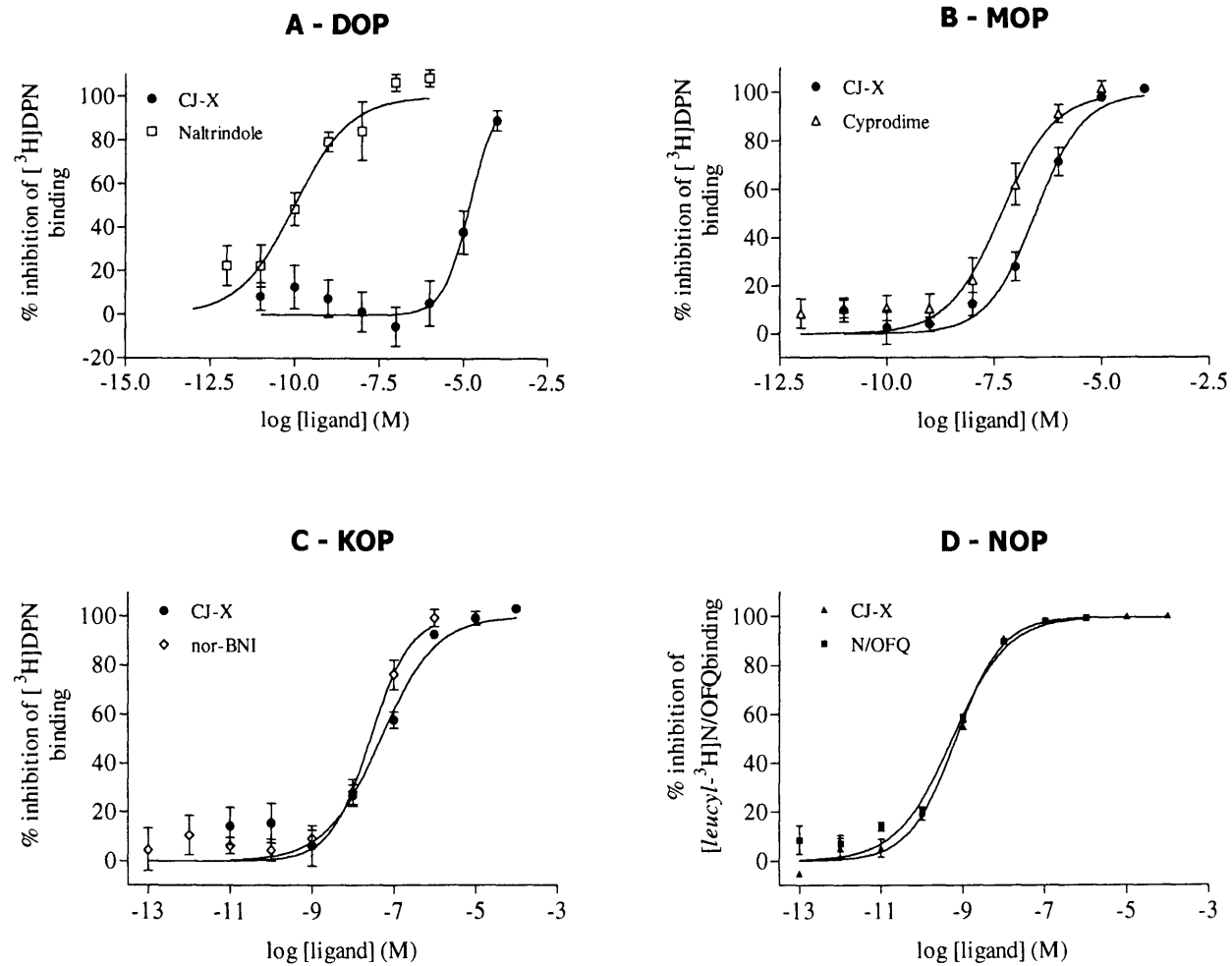


FIGURE 5.2 Competition curves of [leucyl-³H]N/OFQ and [³H]DPN for CJ-X in *CHO*_{mDOP} (A), *CHO*_{rMOP} (B), *CHO*_{rKOP} (C) and *CHO*_{hNOP} (D) membranes. N/OFQ, cyprodime, naltrindole and norBNI are included as reference ligands. Data are mean ± s.e.m (n=3-6)

5.4 GTP γ^{35} S binding in CHO_{hNOP} membranes

In CHO_{hNOP} membranes, CJ-X and N/OFQ stimulated GTP γ^{35} S binding in a concentration-dependent and saturable manner (Figure 5.3) with pEC₅₀ and E_{max} values shown in Table 5.3. Whilst there was a small reduction in E_{max} for CJ-X, this did not reach statistical significance, hence both are considered full agonists. The effects of CJ-X and N/OFQ were PTx sensitive (Table 5.4). The partial agonist activity of CJ-X may be masked at a low B_{max} hence these experiments were repeated in an inducible system of CHO_{INDhNOP} cells (data included here with thanks and kind permission of John McDonald). In CHO_{INDhNOP} cells, induced with 5 μ M ponasterone and with a reduced B_{max} of ~190fmol mg⁻¹ protein, the efficacy of CJ-X remained unchanged with pEC₅₀ of 8.48 \pm 0.01 and E_{max} of 2.80 \pm 0.01 (Figure 5.3).

TABLE 5.3 pEC₅₀ and E_{max} values for CJ-X and N/OFQ stimulated GTP γ^{35} S binding to CHO_{hNOP} membranes and inhibition of forskolin stimulated cAMP formation in whole CHO_{hNOP} cells. Data are mean \pm s.e.m (n=3-6)

Assay/Agonist	pEC ₅₀	E _{max}
<i>CHO_{hNOP} GTPγ^{35}S binding (E_{max}, stim factor)</i>		
CJ-X	8.46 \pm 0.07	8.17 \pm 0.52
N/OFQ	8.48 \pm 0.10	9.25 \pm 0.40
<i>CHO_{hNOP} cAMP inhibition (E_{max}, %)</i>		
CJ-X	9.35 \pm 0.06	102.3 \pm 1.9
N/OFQ	9.51 \pm 0.08	103.3 \pm 2.0

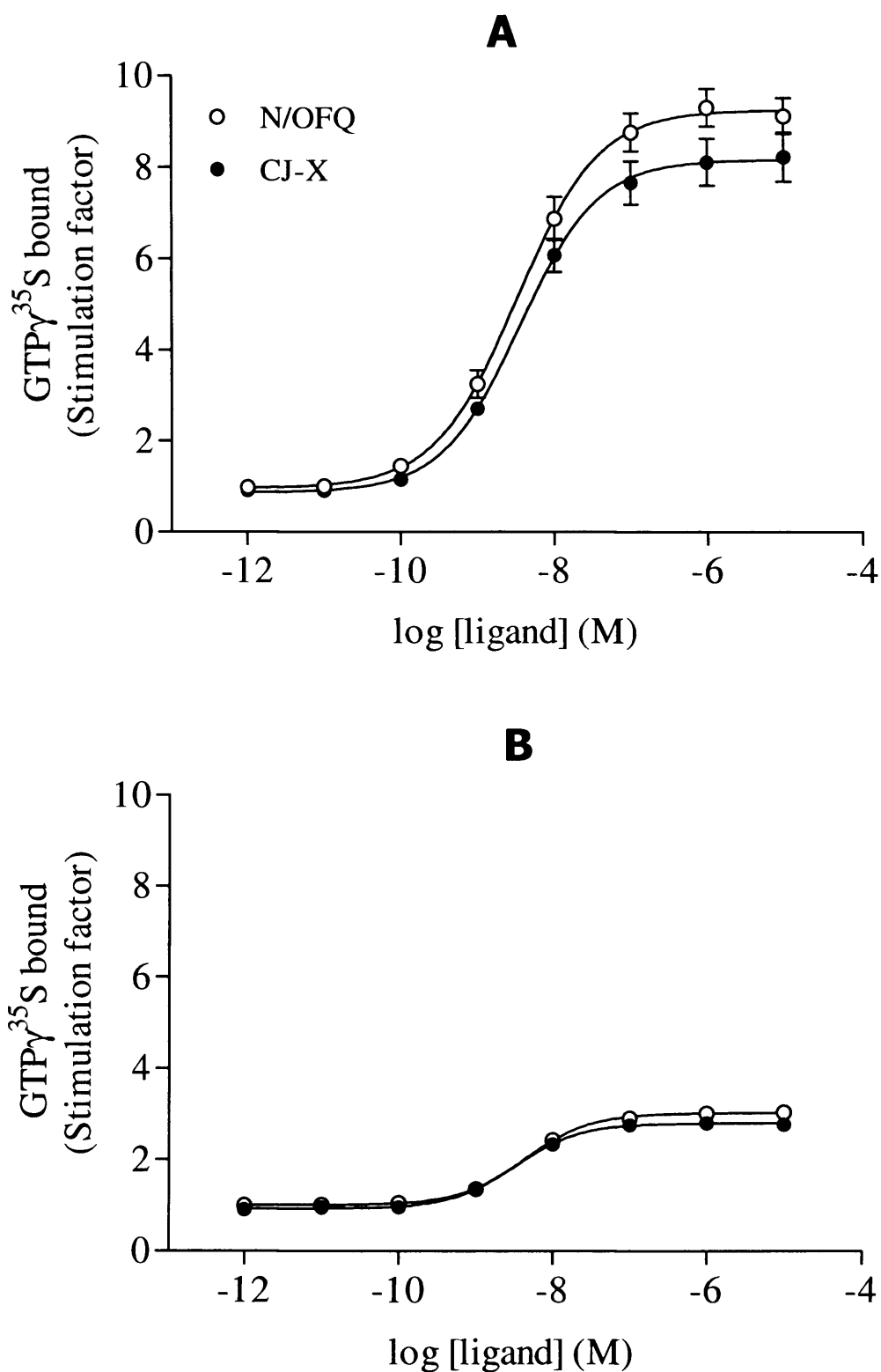


FIGURE 5.3 Effects of CJ-X and N/OFQ on the binding of GTP γ^{35} S to membranes prepared from CHO_{hNOP} (A) and CHO_{INDhNOP} (B) cells (included with kind permission of John McDonald). Data are mean \pm s.e.m (n=3-6)

In addition, the effects of CJ-X in CHO_{hNOP} were competitively antagonised by various concentrations of J-113397, which caused a parallel, concentration-dependent rightward shift in the agonist concentration response curve (Figure 5.4). Schild analysis yielded a pA₂ value for J-113397 of 8.57±0.05 with a slope of 1.08±0.02 (*n*=5) indicating competitive antagonism. In this assay, J-113397 was devoid of residual agonist activity. This data is comparable with those described in section 4.4 and Table 4.4.

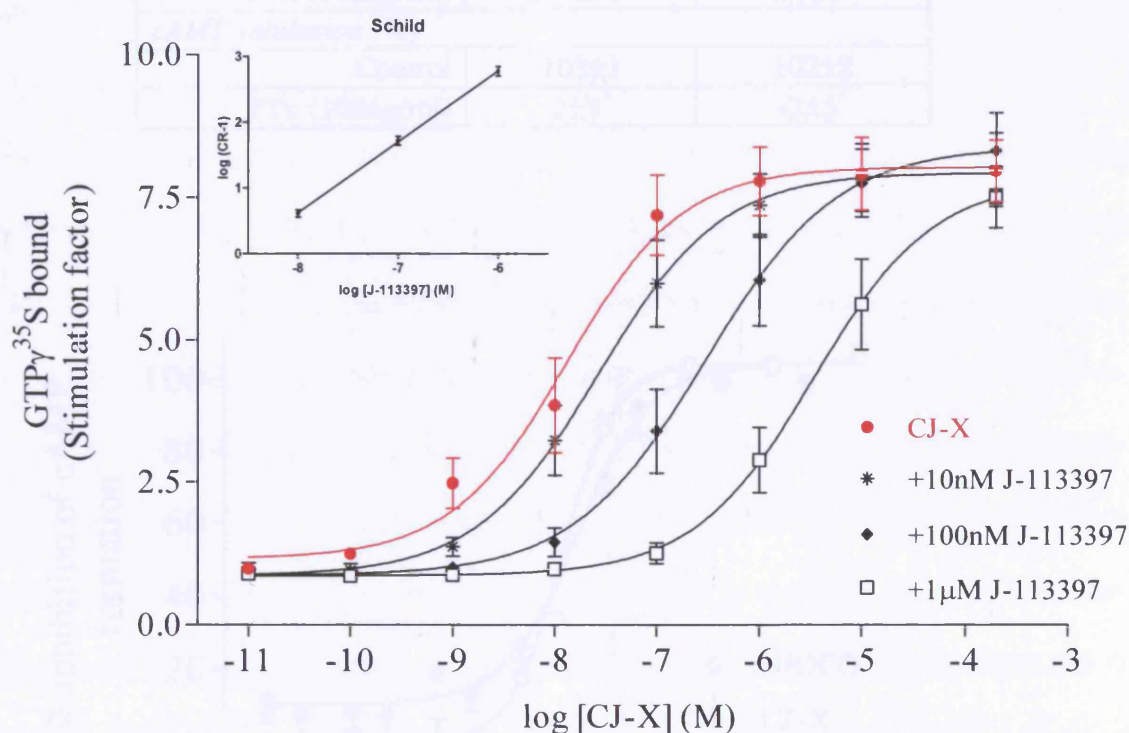


FIGURE 5.4 CJ-X stimulation of GTP γ^{35} S binding to membranes prepared from CHO_{hNOP} cells is competitively antagonized by the selective NOP antagonist J-113397. Inset shows Schild analysis yielding a pA₂ of 8.57, CR is concentration ratio (section 2.17). Data are mean \pm s.e.m (*n*=5)

5.5 CJ-X effects on cAMP formation

In whole CHO_{hNOP} cells, CJ-X and N/OFQ inhibited forskolin stimulated cAMP formation in a concentration dependent and saturable manner (Figure 5.5), with pEC₅₀ and E_{max} values shown in Table 5.3. The effects of CJ-X and N/OFQ were PTx sensitive (Table 5.4).

TABLE 5.4 CJ-X and N/OFQ (10 μ M) stimulated GTP γ ³⁵S binding and inhibition of forskolin stimulated cAMP formation in CHO_{hNOP} cells is PTx sensitive. Data are mean \pm s.e.m (n=3)

Assay/treatment	N/OFQ	CJ-X
<i>GTPγ³⁵S bound (dpm)</i>		
Control	5935 \pm 89	6289 \pm 20
PTx (100ng/ml)	399 \pm 10*	635 \pm 5*
<i>cAMP inhibition (%)</i>		
Control	103 \pm 1	102 \pm 2
PTx (100ng/ml)	2 \pm 3*	-2 \pm 5*

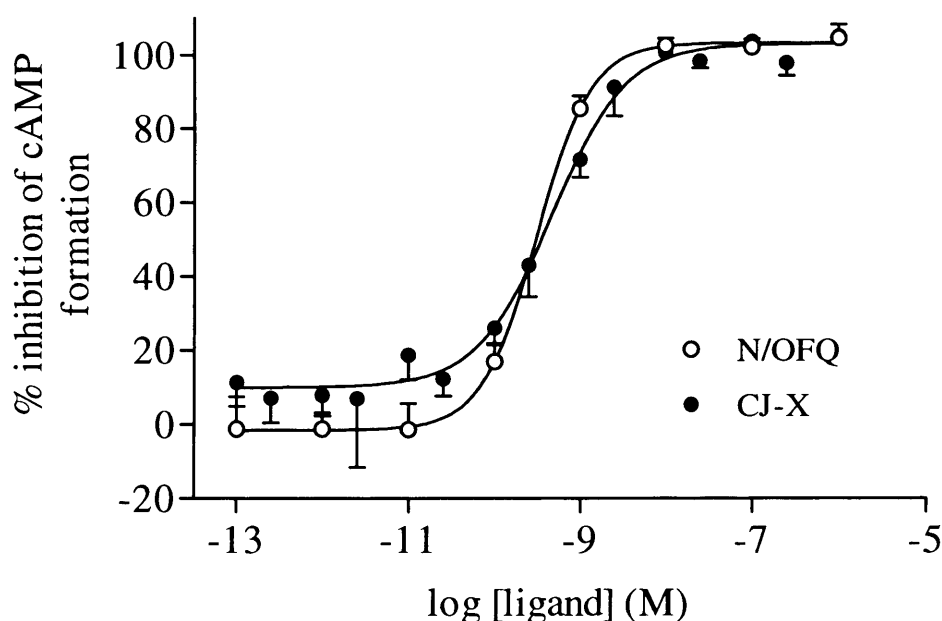


FIGURE 5.5 Effects of CJ-X and N/OFQ on forskolin stimulated cAMP formation in whole CHO_{hNOP} cells. Data are mean \pm s.e.m (n=5)

5.6 Discussion

This chapter illustrates that CJ-X stimulated $\text{GTP}\gamma^{35}\text{S}$ binding and inhibited forskolin-stimulated cAMP formation in CHO_{hNOP} cells. In both assays, CJ-X was equipotent and displayed similar intrinsic activity to the endogenous NOP ligand, N/OFQ. Moreover, the actions of this non-peptide ligand were PTx sensitive and competitively antagonised by J-113397, with a pA_2 consistent with chapter 4 and our laboratory value (8.53; McDonald *et al.* 2002); as such these results suggests that CJ-X is a NOP agonist.

In a series of binding experiments to native receptors in brain tissue, the crude selectivity of CJ-X for NOP over total classical opioid receptors is ~2000 fold. However, this selectivity may be incorrect due to the mixed opioid population in dog and rat brain, although on investigating individual subtypes, selectivities of 19496 fold for mDOP, 416 fold for rMOP and 63 fold for rKOP were estimated.

Whilst there appears to be a small reduction in intrinsic activity for CJ-X (compared to N/OFQ) in the $\text{GTP}\gamma^{35}\text{S}$ binding assay, possibly suggesting very high “efficacy” partial agonist activity, this failed to reach statistical significance. Increasing receptor density can affect the relative intrinsic activity of partial agonists (Kenakin, 2002). Indeed, in an inducible system of $\text{CHO}_{\text{INDhNOP}}$ cells, our laboratory has recently shown that the activity of [F/G] can be manipulated to encompass antagonism, partial agonism through to full agonism, merely by increasing receptor density (McDonald *et al.*, 2003). In order to further explore the intrinsic activity issue for CJ-X, $\text{GTP}\gamma^{35}\text{S}$ binding assays were repeated in this inducible $\text{CHO}_{\text{INDhNOP}}$ cell line. In cells induced with 5 μM ponasterone, a NOP density of ~190fmol mg^{-1} protein was obtained, some 10 fold lower than that seen in CHO_{hNOP} cells. Under the conditions of reduced receptor density, the profile of CJ-X remained unchanged with pEC_{50} of 8.48 ± 0.01 and E_{max} of 2.80 ± 0.01 . The relative intrinsic activity is 0.93 compared to N/OFQ (pEC_{50} 8.36 ± 0.01 , E_{max} 3.02 ± 0.08 in $\text{CHO}_{\text{INDhNOP}}$) with no significant

difference observed in pEC_{50} or E_{max} values ($p > 0.05$, Wilcoxon signed rank test) and as such, we are confident that this non-peptide is indeed a full agonist. Table 5.4 also supports this as the counts bound at a saturating concentration observed in $GTP\gamma^{35}S$ binding were similar for these agonists, with the slightly higher response observed for CJ-X.

When considering down-stream events such as an inhibition of cAMP formation where there is considerable amplification of the initial signal, the presence of a coupling reserve often returns full agonism (Figure 5.6) for agonists that display partial agonist activity in a $GTP\gamma^{35}S$ binding assay (Berger *et al.*, 2000a; Kenakin, 1997). As previously, our laboratory would recommend caution when defining intrinsic activity of an agonist in a single functional screen particularly when amplification is an issue.

Since the identification of NOP and its ligand N/OFQ (Meunier *et al.*, 1995; Reinscheid *et al.*, 1995) there has been intense activity in the identification of novel ligands for this system. Indeed, our laboratory (as a collaboration with the University of Ferrara) has described several peptide molecules including the recently identified antagonist UFP-101 (Calo *et al.*, 2002). However, peptide molecules are disadvantaged by their susceptibility to peptidase activity (Calo *et al.*, 2000a; Terenius *et al.*, 2000) but have improved solubility characteristics. In contrast non-peptide molecules are likely to be more stable *in vivo*. There are several non-peptide agonists currently available and these are summarised in Table 5.5. A major problem with many of these is low selectivity. This is particularly true for NalBzOH and buprenorphine, which were originally designed as classical opioid agonists (Bigoni *et al.*, 2002a; Bloms-Funke *et al.*, 2000).

TABLE 5.5 Comparison of the activity of CJ-X and a range of currently available non-peptide NOP agonists at recombinant receptor systems

Agonist	NOP (K _i)	Minimum selectivity	Functional activity (pEC ₅₀)		Reference
			GTPγ ³⁵ S binding	cAMP inhibition	
CJ-X	0.17nM	63 (Rat/Dog brain 49-54pM)	Full agonist: 3.5nM (N/OFQ: 3.3nM)	Full agonist: 0.45nM (N/OFQ: 0.31nM)	This thesis
NNC 63-0532	7.3nM	12	Full agonist: 305nM (N/OFQ: 2.0nM)	Full agonist: 109nM (N/OFQ: 0.83nM)	Thomsen <i>et al.</i> (2000a)
Ro65-6570	2.5nM	5	Full agonist: NA (N/OFQ: NA)	Full agonist: 2.1nM (N/OFQ: 0.28nM)	Hashiba <i>et al.</i> (2001)
Ro64-6198	0.39nM	120	Full agonist: 39nM (N/OFQ: 43nM)	Full agonist: 0.32nM (N/OFQ: NA)	Jenck <i>et al.</i> (2000)
(+)-5a (Roche)	0.49nM	562	Full agonist: 65.4nM (N/OFQ: 38nM)	Full agonist: 9.1nM (N/OFQ: 0.36nM)	Kolczewski <i>et al.</i> (2003)
NalBzOH	24nM	LOW ¹	Antagonist/partial agonist (pK _b : 6.93)	Partial agonist (44%): 1μM (N/OFQ: 0.14nM)	Bigoni <i>et al.</i> (2002a)
Buprenorphine	9.8nM ²	LOW ¹	Partial agonist (50%): 7.9nM (N/OFQ: 1.3nM)	Full agonist: 39nM ² (N/OFQ: 0.24nM) ²	Bloms-Funke <i>et al.</i> (2000)

¹Originally introduced as a classical opioid, ²from Hashiba E, Hashimoto Y and Lambert DG (2003, unpublished). Where possible complete studies have been selected. NA, not available

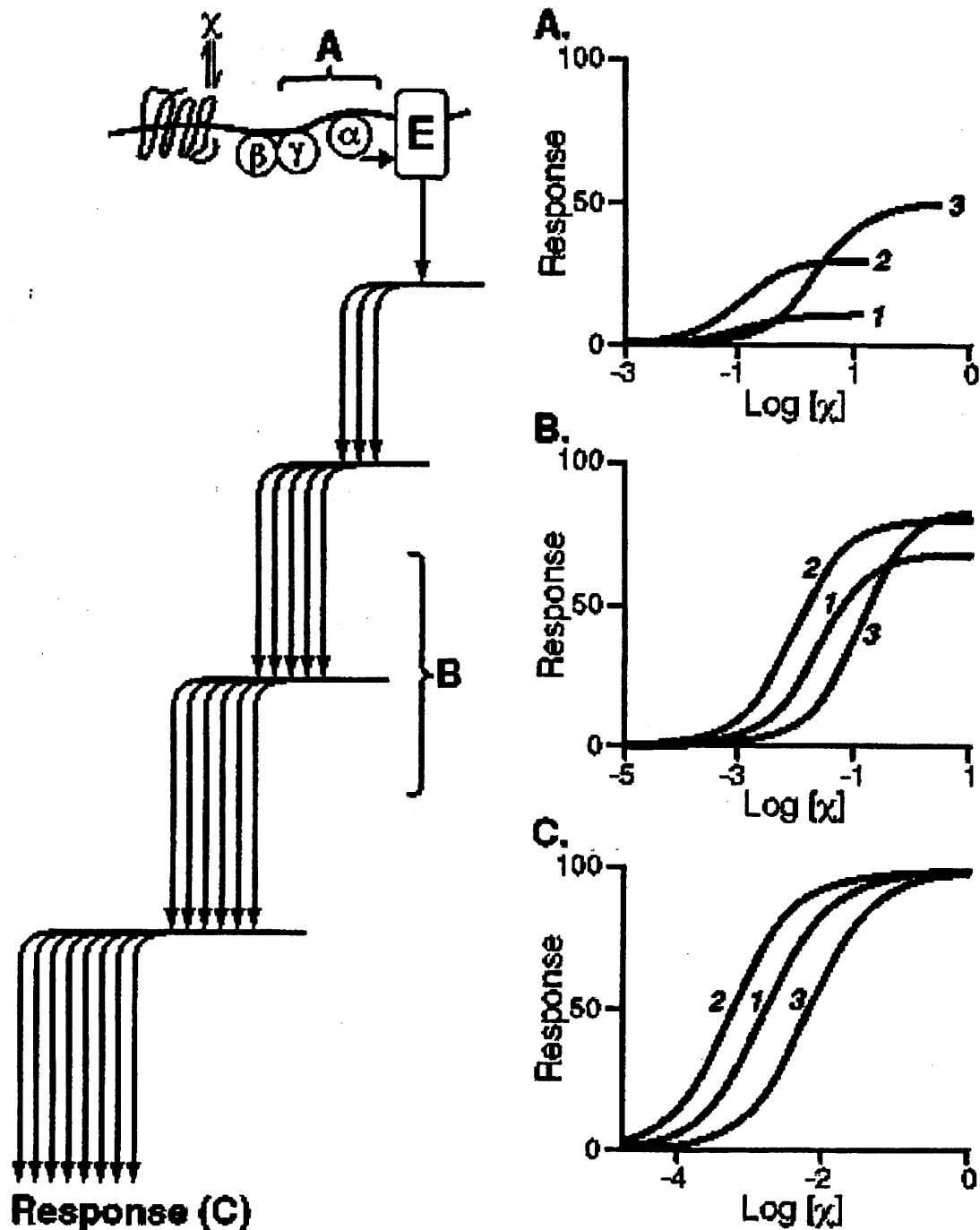


FIGURE 5.6 Saturation steps in the stimulus-response mechanisms of receptor systems obscure the ability to observe differences in efficacy. (Panel A) The stimulus to three hypothetical agonists of relative efficacy Agonist 3=1, Agonist 2=0.6, and Agonist 1=0.2 (as measured by maximal stimulation of GDP-GTP exchange) is shown. (Panel B) The stimulus produced in panel A is processed through a hyperbolic saturable stimulus-response function of output = input/(input+3). (Panel C) The output of Panel B is further processed through another saturable stimulus-response function output = input/(input+0.03) (Kenakin, 2002)

A major contribution regarding synthetic agonists has been made by researchers at Roche who followed the rather poor (in terms of selectivity) Ro65-6570 with the much improved Ro64-6198, both in terms of affinity and selectivity (Hashiba *et al.*, 2002b; Jenck *et al.*, 2000). Earlier this year, a third agonist was described which displayed similar affinity for NOP but some 562 fold selectivity (Kolczewski *et al.*, 2003).

As a novel agonist, CJ-X shows some similarities to Ro64-6198 but displays just over 2 fold greater binding affinity for NOP. Indeed, of the non-peptides with high selectivity, CJ-X displays the highest affinity for NOP. Moreover, in comparison with Ro64-6198 (and the other non peptides) CJ-X displays the highest functional potency, at least in the GTP γ ³⁵S binding assay, although differences in receptor expression could be a confounding factor. However, to address this issue there were no differences in potency for CHO_{hNOP} and CHO_{INDhNOP}, despite some 10 fold difference in receptor density. Moreover, using the same cell line, our laboratory has described the activity of Ro64-6198 in GTP γ ³⁵S binding and cAMP inhibition assays (Hashiba *et al.*, 2002) so a direct comparison can be made. In the GTP γ ³⁵S binding assay, the pEC₅₀ for CJ-X was 8.46 (Table 5.3) and Ro64-6198 was 7.61. Similarly for cAMP inhibition, pEC₅₀ of 9.35 for CJ-X (Table 5.3) and 8.45 for Ro64-6198 were obtained.

In summary, this chapter reports the *in vitro* characteristics of a novel NOP agonist CJ-X, which displays high affinity, potency, intrinsic activity and selectivity for hNOP over classical rMOP, mDOP and rKOP. This molecule will be a further useful addition to the range of NOP ligands and further *in vivo* studies in dogs are clearly warranted.

6 Tissue sectioning and staining

This chapter presents methodologies involved in optimising the sectioning of a whole dog brain. Initially microtome sectioning was tested, however a more standardised procedure was later developed with a cryostat. The resulting whole brain sections cut here are important for use in autoradiography (chapter 7) and IHC (chapter 8). The sections were also stained with two common histological stains; haematoxylin/eosin and Cresyl Fast Violet, to determine basic dog brain morphology and also more specifically, neuronal structure. The findings of the histological staining are presented below.

6.1 Microtome sectioning

This methodology is similar to that described by Gillberg *et al.* (1986). Whole dog brains were frozen at -80°C and then mounted on end i.e. frontal cortex upwards, in a 0.5% carboxymethyl cellulose block on the moving belt of the microtome (PMV, Palmistiernas; Figure 6.1). The blocks were left in the chamber overnight to set. The internal environment of the microtome is maintained at -25°C except during freeze-drying. Ideally for IHC and autoradiography, sections approximately $5\mu\text{m}$ thick are required but it was impossible to cut thinner than $25\mu\text{m}$. Therefore coronal sections of $25\mu\text{m}$ thickness were cut and captured onto 3M tape. The strips of tape were adhered to racks and left inside the microtome overnight to freeze dry. They were then stored in a folder and kept at -20°C .

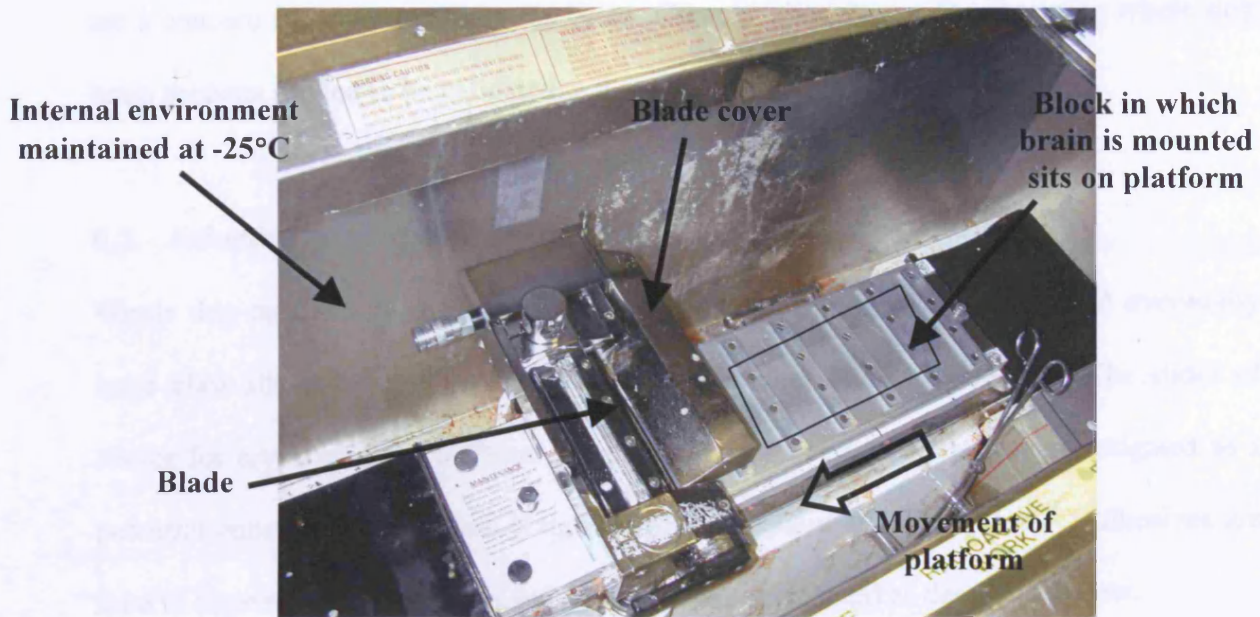


FIGURE 6.1 A microtome is used for whole brain sectioning. 3M tape is pressed along the top of the block, over the mounted sample, so collecting the section as it is cut

6.2 Removal of sections from tape

Initially it was proposed to secure the tape and perform autoradiography on the sections whilst still attached to the tape. The logistics of this were not feasible and also small pieces of the sections floated off the tape, if submerged in dH_2O . A method developed for whole body autoradiography (Watanabe *et al.*, 1975) for transferring sections from tape to glass slides (<http://www.instrumedics.com/mtts.htm>, accessed November 2003) was too expensive and not possible within the time limit of this work.

The sections could not be transferred by rubbing against a poly-L-lysine slide (though some transfer occurred if the slide was warmed with finger heat) or by submersing in dH_2O as the liquid dispersed the section. A section placed against a coated slide put into the incubator for a few minutes showed some tissue transfer, which could be improved by using a slide at $-20^{\circ}C$ and rolling hard against the tape. It was clear that the whole section would never be transferred accurately using this method and also the temperature extremes

are a concern for the proteins in the brain. Other methodologies for obtaining whole dog brain sections needed to be validated.

6.3 Adhesive coating of glass slides

Whole dog brain sections were too large for common microscope slides and eventually large glass slides (3" x 2") were located from Fischer Scientific UK Ltd. The slides of choice for cryosectioning at Pfizer are poly-L-lysine coated so this was investigated as a potential adhesive for the glass plates, as well as gelatin and Vectabond™. Adhesives are used to improve tissue adhesion and so the slides were coated as described below.

6.3.1 Poly-L-lysine

The slides were cleaned with acid alcohol (1% HCl in 70% ethanol) before placing them into poly-L-lysine solution (0.1% w/v; 1:10 dilution with dH₂O) for 5min. The slides were drained and allowed to dry overnight at room temperature.

6.3.2 Gelatin

Gelatin (4.0g) and 0.4g CrK(SO₄).2H₂O were added to 800ml dH₂O and warmed gently whilst stirring. The solution was cooled before dipping each slide individually into the gelatin. The slides were left upright overnight to drain and dry.

6.3.3 Vectabond™

The slides were cleaned in a detergent and then rinsed thoroughly before soaking in acetone for 5min. Vectabond™ reagent was prepared by adding 14ml Vectabond™ to 700ml acetone, sufficient to coat approximately 1000 slides. The slides were removed from the acetone and placed immediately into the Vectabond™ bath for 5min. The slides were slowly rinsed in dH₂O for 30s and left to dry.

6.4 Cryosectioning

Cryosectioning with a cryostat (CM1900 Leica, USA; Figure 6.2) is generally used for sectioning small tissue samples. The sample is mounted onto a disc, sliced and the cut section falls onto the collection platform. This is then picked up onto a coated adhesive slide.

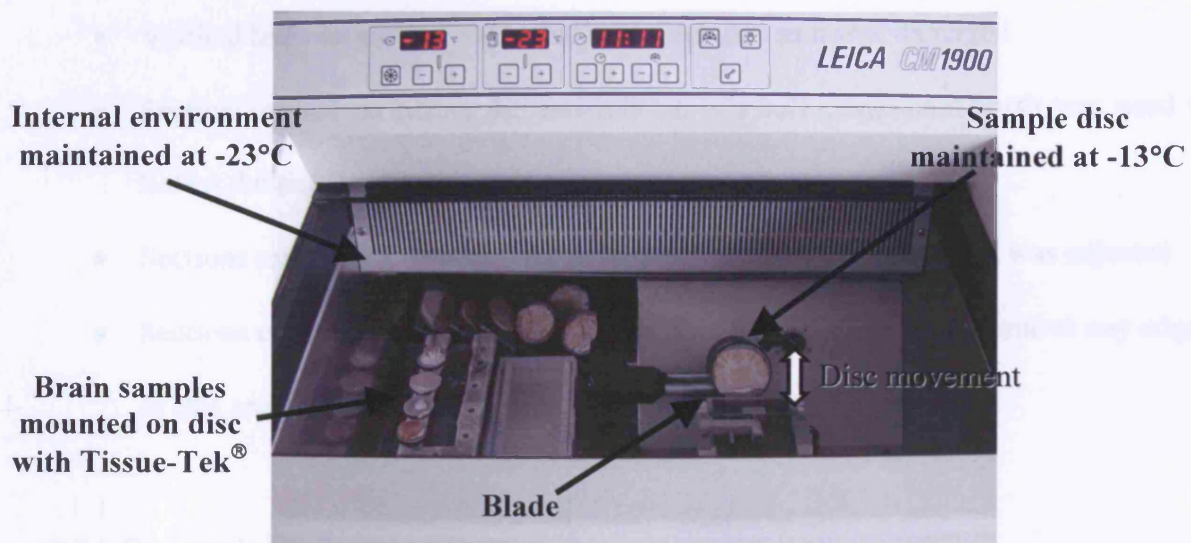


FIGURE 6.2 A cryostat used to section small tissue samples

Fresh dog brains were cut to fit onto a sample disc so initially non-standardised random coronal sections were cut using a scalpel. These were frozen at -20°C until required. Cutting the brain was extremely difficult and needed to be optimised so that in future experiments, the same sections could be taken. It was also important to cut even flat sections, which was particularly difficult with fresh brain tissue.

The frozen slices were mounted individually using an adhesive, Tissue-Tek[®], onto a round sample disc, sprayed with Cool-jet (to set quickly) and left in the cryostat to dry and equilibrate for approximately 30min. The cryostat chamber temperature was maintained at -23°C , with the specimen mount at -13°C . These were the optimum temperatures for tissue

sections of this size. Accu-Edge[®] Low Profile blades (new blade was used for each session) were used to cut 15µm sections. These were thaw mounted using finger heat onto coated slides, equilibrated to the cryostat chamber temperature. Initially, sections were cut onto ten slides of each adhesive and these then stored at -20°C until use.

Several problems were encountered during cryosectioning:

- Vertical lines on section – the blade was replaced as it was damaged
- Sections curled on lifting the anti-roll bar – a soft camel-hair brush was used to flatten the tissue
- Sections tear during cutting – space between anti-roll bar and blade was adjusted
- Sections crease in one area – due to the Tissue-Tek[®] so better to remove any edges of this around the section

6.5 Comparing adhesive coatings

The adhesives were compared depending on how well the tissue remained on the slides. Ease of coating a large number of slides was also taken into account. For the methodology, gelatin coating was the messiest and most time consuming, whereas Vectabond[™] and poly-L-lysine protocols were both straightforward. For comparison of stickiness, the slides onto which brain sections were mounted, were submersed in dH₂O overnight (some were allowed to dry first at room temperature for 30min). Following submersion without initial drying, small and large pieces of tissue floated off randomly. This was observed with all adhesives however the gelatin coat retained more tissue on the slide and poly-L-lysine the least. After drying, some tissue pieces floated off the slides but this was less than previously. The tissue sections were also subjected to autoradiography (section 7.1) with dH₂O as a test run. No differences were observed here. Overall no obvious major

differences were observed between the adhesives, though gelatin seemed stickier. From these tests, and the ease of coating a large number of slides, it was concluded that the Vectabond™ coating was most suitable for this study. 500 glass slides were therefore coated with this solution (section 6.3.3) and once dry, were stored in boxes ready for use.

6.6 Optimised cyrosectioning

To overcome the problems of cutting fresh brain slices manually, a dog brain matrix (Figure 6.3) was purchased. This enabled brain structure to be retained during slicing and also provided a standardised method of cutting.

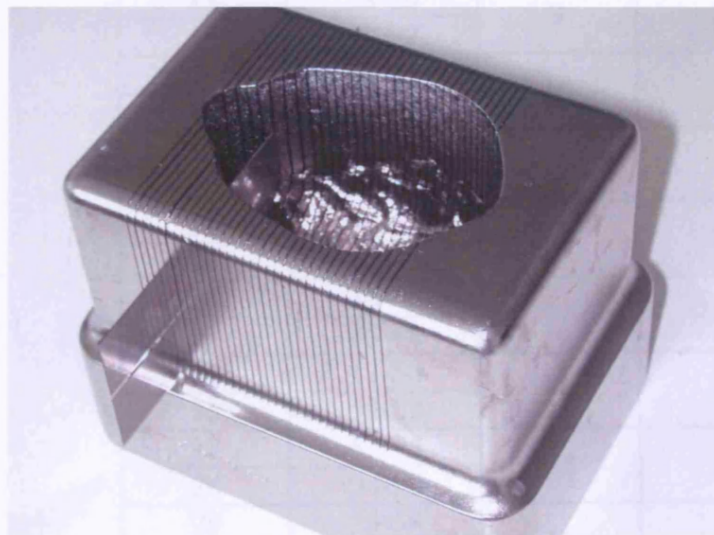


FIGURE 6.3 A dog brain matrix

A fresh female dog brain was placed ventral side upwards into the matrix and frozen inside it at -20°C for 45min. This does not completely freeze the brain but helps to maintain rigidity when cutting into slices. Slices of 4mm were cut using Tissue Slicer Blades through alternate grooves (each groove is 2mm) in the matrix. These 19 coronal slices were removed carefully and stored flat (with orientation noted i.e. anterior and posterior) at -80°C in bioassay trays until further sectioning (Table 6.1).

TABLE 6.1 Sectioning pattern for dog brain

	MATRIX GROOVE	Distance (mm)	Section	
			Number	Thickness (mm)
ANTERIOR (frontal cortex)	1	0-2	1	0-4
	2	2-4		
	3	4-6	2	4-6
	4	6-8	3	6-8
	5	8-10	4	8-12
	6	10-12		
	7	12-14	5	12-16
	8	14-16		
	9	16-18	6	16-20
	10	18-20		
	11	20-22	7	20-24
	12	22-24		
	13	24-26	8	24-28
	14	26-28		
	15	28-30	9	28-32
	16	30-32		
	17	32-34	10	32-36
	18	34-36		
	19	36-38	11	36-40
	20	38-40		
	21	40-42	12	40-44
	22	42-44		
	23	44-46	13	44-48
	24	46-48		
25	48-50	14	48-52	
26	50-52			
27	52-54	15	52-56	
28	54-56			
29	56-58	16	56-60	
30	58-60			
31	60-62	17	60-64	
32	62-64			
POSTERIOR (cerebellum)	33	64-66	18	64-66
		66-76	19	66-76

The frozen slices were then mounted, sliced as previously (section 6.6) onto Vectabond™ coated slides and stored at -20°C. For each section in Table 6.1, 10 slices were taken from the anterior end and a further 10 from the posterior, with the number of discarded slices in

between noted. This allowed the distance between each slice to be estimated. Approximately 306 slides were obtained from the whole brain and their usage is described in Appendix section 12.4. Two sections were mounted onto each slide if space allowed. Sections of dog vas deferens and mid-coronal rat brain section were mounted onto a slide for comparison, along with dog skeletal muscle as a negative control.

6.7 Histological staining

The desired slides (Appendix section 12.4) of whole dog brain sections were stained using two different methods suitable for frozen sections to show tissue morphology. Staining results were used in conjunction with autoradiography (chapter 7) and IHC (chapter 8) results to identify the brain areas labelled.

6.7.1 Haematoxylin and Eosin

This stain is the most commonly used in animal histology and has been around for over one hundred years. Haematoxylin stains nuclei and the endoplasmic reticulum blue, as these are acidic structures (due to high DNA/RNA content respectively), for which the dye has a high affinity. In contrast, eosin stains basic structures, for example the cytoplasm, within tissues a pinkish red colour.

The desired slides (Appendix section 12.4) were selected for staining and allowed to dry for 90min at room temperature. The slides were incubated in IMS for 5min to fix the tissue before rehydrating under running dH₂O for at least 5min. A 10min incubation with haematoxylin preceded further washing in dH₂O. The slides were then differentiated by dipping 10 times in acid alcohol (removes excess haematoxylin) and then into Blueing reagent (blues haematoxylin stained nuclei) for 2min. Further washing in dH₂O followed before staining the sections in eosin for 5-15min. The slides were washed in dH₂O for 3min and dehydrated through a series of steps: IMS (30s), absolute alcohol (45s) and xylene

(5min). They were then placed into mounting xylene before mounting large cover slips with DPX permanent mountant. The slides were left to dry overnight before handling. Digital images were taken using a Nikon D1x camera. These were cropped and unsharpened using Adobe Photoshop version 7 (Adobe Systems, USA).

6.7.2 Cresyl Fast Violet

This stain is used routinely in neurohistology to demonstrate the neuronal cellular pattern. Nissl granules (rough endoplasmic reticulum) contain RNA and are found in the soma of neurones. All cells contain endoplasmic reticulum hence Cresyl Fast Violet will stain both neuronal and glial cell bodies deep violet. The nuclei appear pale violet whereas any myelinated areas stain a pale blue-turquoise.

The desired slides (Appendix section 12.4) were dried, fixed and rehydrated as previously described (section 6.7.1). A working solution of Cresyl Fast Violet was made from 96ml 1% aqueous Cresyl Fast Violet stock solution plus 720ml dH₂O and 8ml 10% acetic acid. This was heated to 56°C and the slides stained in the solution maintained at this temperature for 8min. They were rinsed in dH₂O and then dehydrated, mounted and recorded as above (section 6.7.1).

6.8 Staining results

6.8.1 Haematoxylin and Eosin

Slides were successfully stained with an even distribution of haematoxylin and eosin. Examples of the stained slides can be found in Figure 6.4. The nuclei of cells are stained with haematoxylin so they appear dark blue, and the cytoplasm is coloured by the eosin hence a purple-pink appearance. All other stained sections are presented as the base layer in section 7.3.2 in conjunction with [*leucyl*-³H]N/OFQ autoradiography results.

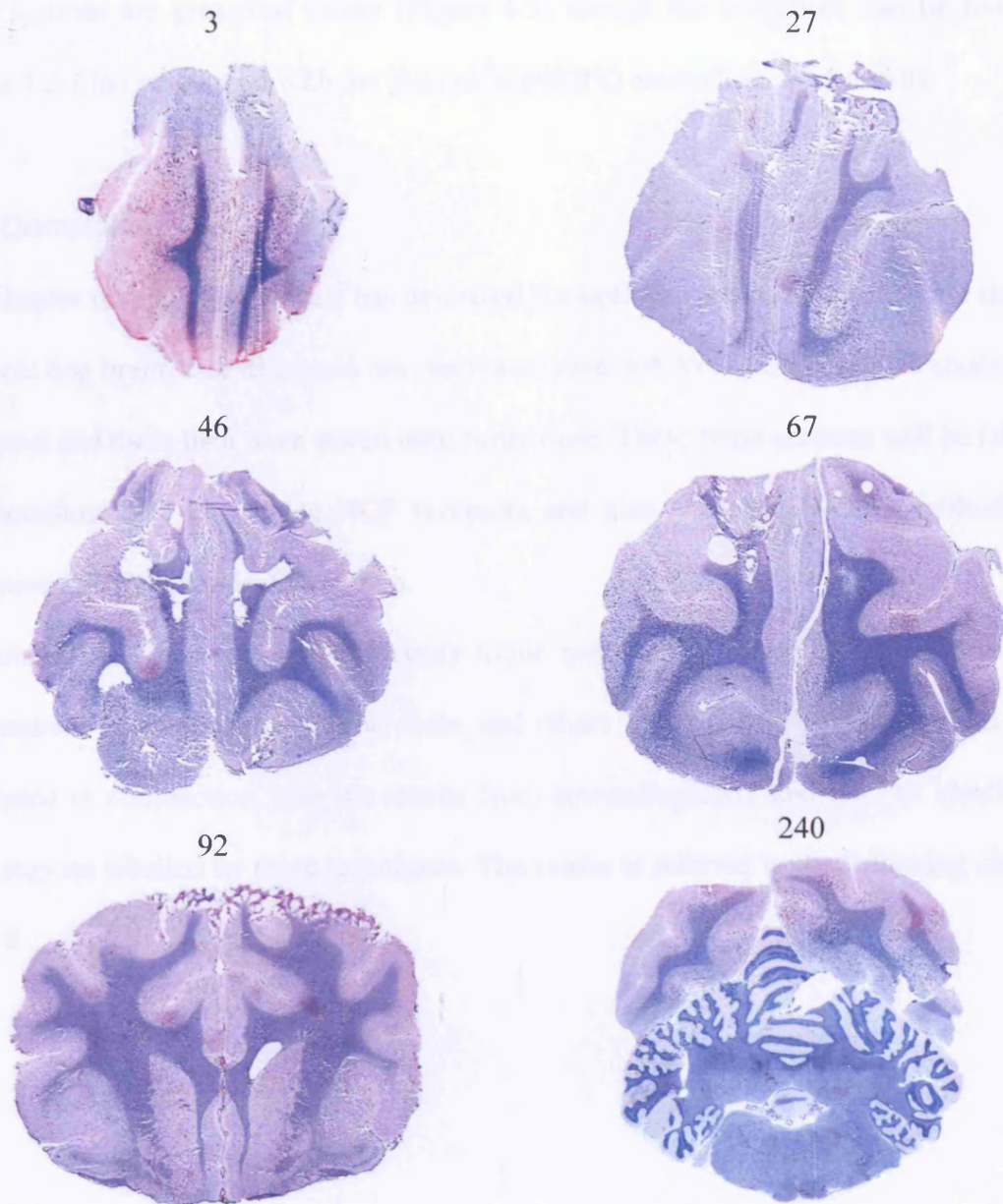


FIGURE 6.4 Slides showing a typical haematoxylin and eosin stain. The sections are in order from anterior to posterior and the number refers to slide number (Appendix section 12.4)

6.8.2 Cresyl Fast Violet

Sections were successfully stained with Cresyl Fast Violet. The soma containing grey matter showed violet/blue staining due to the presence of Nissl granules, whereas myelinated white matter appeared pale blue-turquoise. The sections of cerebellum showed the most pronounced staining with the cerebellar layers appearing a very dark blue/violet.

Some sections are presented below (Figure 6.5) though the remainder can be found in section 7.3.2 in conjunction with the [*leucyl*-³H]N/OFQ autoradiography results.

6.9 Discussion

This chapter (using 7 dog brains) has described the optimisation of sectioning and staining of whole dog brain. One dog brain was sectioned onto 306 Vectabond™ coated slides using a cryostat and these then were stored until further use. These brain sections will be labelled in autoradiography to localise NOP receptors and also with anti-N/OFQ antibodies to determine N/OFQ peptide distribution.

For comparative purposes and to identify tissue morphology, some of the brain sections were stained with haematoxylin and eosin, and others with Cresyl Fast Violet. Both stains were used in conjunction with the results from autoradiography and IHC to identify the brain regions labelled by these techniques. The reader is referred to the following chapters 7 and 8.

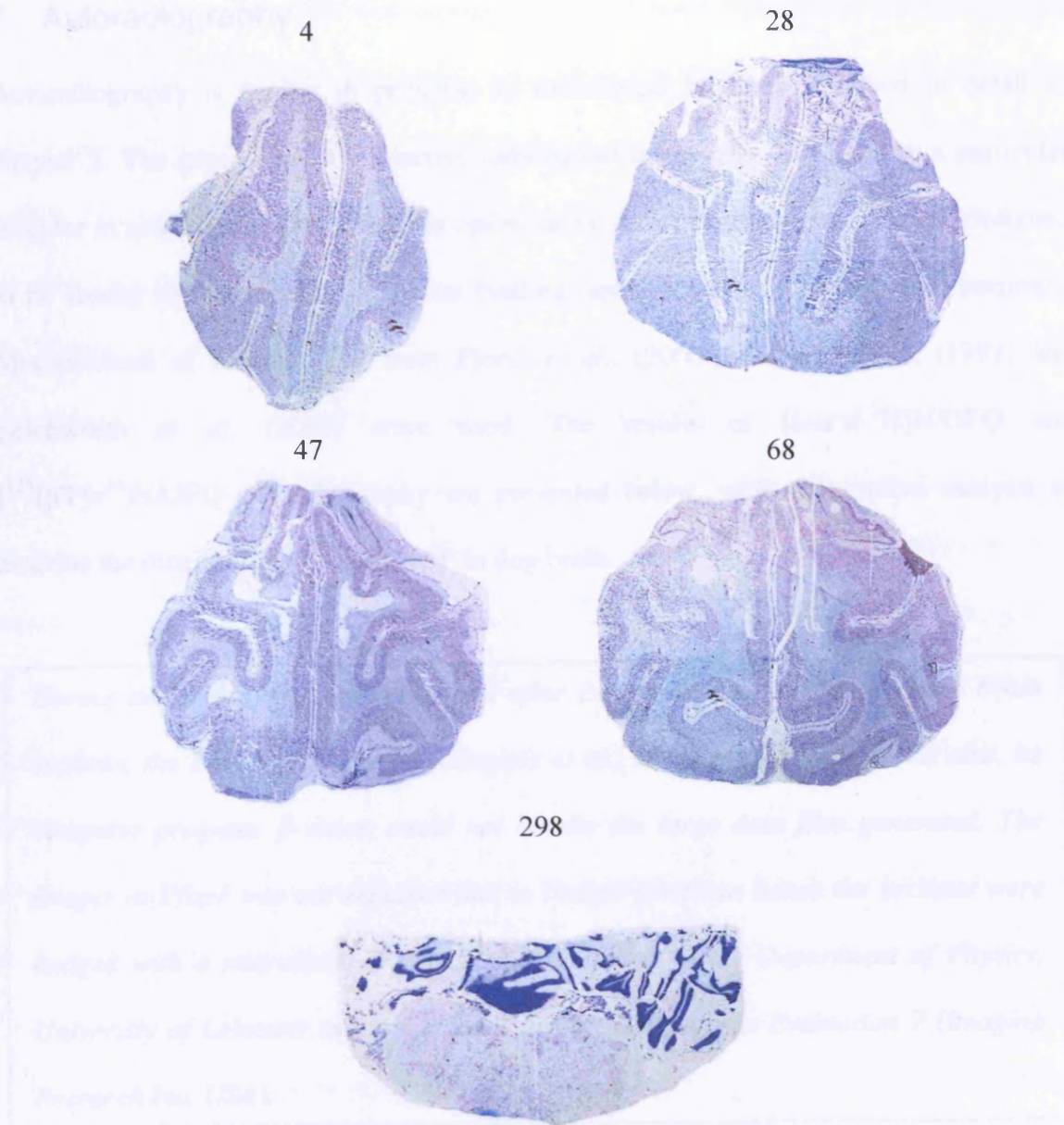


FIGURE 6.5 Cresyl Fast Violet staining showing neuronal distribution in whole dog brain sections. The sections are in order from anterior to posterior and the number refers to slide number (Appendix section 12.4)

7 Autoradiography

Autoradiography is similar in principle to radioligand binding, described in detail in chapter 2. The process uses a selective radioligand to quantify and localise a particular receptor *in situ*. This chapter describes optimisation of the experimental protocol, designed to be similar to that used in saturation binding (section 2.14) for comparative purposes. Modifications of methodology from Florin *et al.*, (2000), Kitchen *et al.*, (1997) and Letchworth *et al.* (2000) were used. The results of [*leucyl*-³H]N/OFQ and [¹²⁵I](Tyr¹⁴)N/OFQ autoradiography are presented below, with quantitative analysis to describe the distribution of native NOP in dog brain.

*During this phase of the project, and after cutting and processing the dog brain sections, the Biospace β -imager (Langlois *et al.*, 2001) malfunctioned and also, its computer program, β -vision could not handle the large data files generated. The imager at Pfizer was not repaired due to budget problems hence the sections were imaged with a microchannel plate (MCP) detector in the Department of Physics, University of Leicester and analysed using MCID Analysis Evaluation 7 (Imaging Research Inc, USA).*

7.1 [*leucyl*-³H]N/OFQ labelling *in situ*

Slides from coronal cryosectioning of a whole dog brain (section 6.6) were selected for these experiments (Appendix section 12.4). Mid-coronal rat brain sections, and also dog skeletal muscle and vas deferens were included for comparative purposes since chapter 3 indicated that rat brain contains almost three times more NOP receptors than dog. It is also well documented that vas deferens contains functional NOP (Calo *et al.*, 1996) and that skeletal muscle has no NOP receptors.

The sections were placed flat and air-dried for 2h at room temperature. A hydrophobic reservoir was created around each using a specialised pen. The sections were pre-incubated with binding buffer (section 2.2) for 30min at 4°C to remove endogenous peptides. This buffer was tipped off and the sections blotted dry. A 1h incubation in incubation buffer (section 2.2) supplemented with ~5nM [*leucyl*-³H]N/OFQ (saturating concentration based on Figure 3.2) then followed at room temperature. Adjacent sections were used to determine NSB in the presence of 1µM unlabelled N/OFQ. The volume of buffer applied to the sections depended on section size, generally 1ml was sufficient. Four 5min washes in binding buffer at 4°C preceded a 5min wash in ice-cold dH₂O. This last wash in dH₂O removes any buffer salts, which may crystallise out and ruin sections during drying. The sections were dried for 15min under a cold air stream and the pen barrier removed with IMS. The slides were imaged 'real time' over 24h using a novel radioisotope free, low noise MCP detector.

MCP detectors were originally developed for photon counting in astronomical X-ray telescopes though Lees *et al.* (2001; 1999) recently suggested their use in radiolabelled biological assays. This system is capable of detecting most of the commonly used isotopes (³H, ¹⁴C, ³⁵S and ¹²⁵I) with high electron detection efficiency. One slide is inserted into the chamber of the detector (Figure 7.1) and as β particles are low energy (average energy 6keV), measurement of electron emission is performed under vacuum (<10⁻⁶mbar operating pressure). Data was acquired using an in-house program, β Autorad and after imaging, all images were standardised to the same scale and size (tif file, 2048x2048 pixel image) to allow for a direct comparison. The images were analysed as appropriate using MCID.

[³H]microscales (0.97-23.22nCi mg⁻¹) were imaged in the MCP detector. The MCID square tool, which samples a selected area, was used to measure intensity levels (nCi mg⁻¹)

for each radioactive concentration. For the calibration, a 3rd degree polynomial curve (Appendix section 12.5) was chosen as this type gave the best relative error for each standard (ideally error should be below 10%). As the [³H]microscales were measured in nCi mg⁻¹ then no further spatial calibration was required hence no correction for the area of the square tool was required. This calibration was used in any further analysis of the autoradiograms.

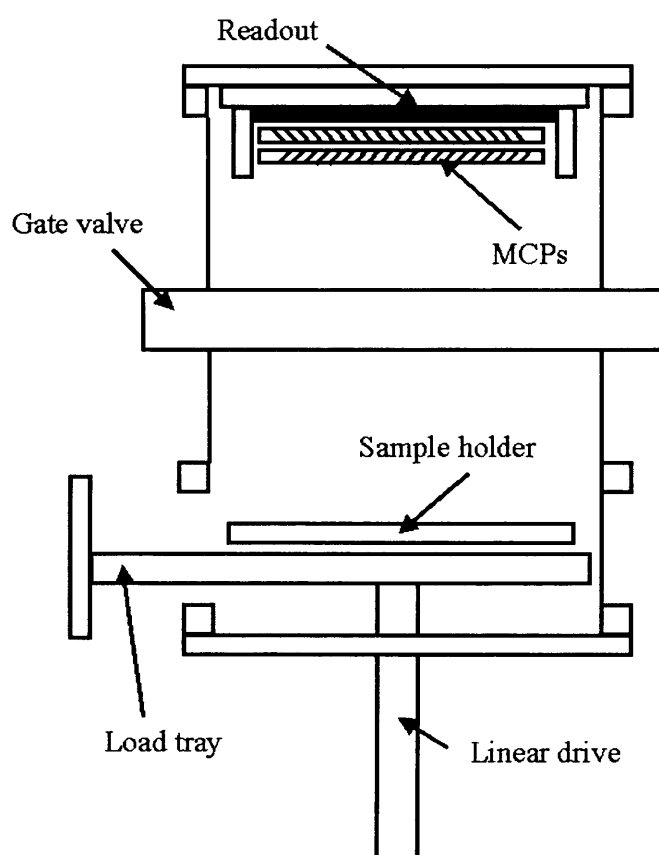


FIGURE 7.1 Schematic diagram of microchannel plate detector. Slides are placed in the sample holder and imaged under vacuum

Due to financial constraints, only twenty of the dog brain slides labelled were imaged with the MCP detector, four of which were NSB. These brain sections and the slide containing rat brain and various dog tissues were analysed with MCID as follows:

- A random area of interest within the NSB sections was selected using the square tool and the binding (nCi mg⁻¹) recorded (overlap of analysis area could not always

be avoided). This was sampled so $n=3$ per section ($n=5$ for dog vas deferens as analysis repeated in five different sections) and an average determined

- The area of interest in the total binding section was sampled and binding recorded as for the NSB section
- Analysis was repeated on the same slide so $n=3$ for all areas of interest ($n=5$ for dog vas deferens i.e. 1 analysis per section)
- NSB binding was subtracted from total values to give specific binding for particular brain region/tissue type (section 2.11.4)
- Averages were then calculated for each brain area/tissue type and are presented as specific binding (nCi mg^{-1})

To identify brain areas of interest, each image was printed, traced and labelled to produce a canine brain atlas. Brain areas were identified using the atlases from Miller's Anatomy of the dog (Evans, 1993), from Gross brain anatomy (<http://vanat.cvm.umn.edu/grossbrain/>, accessed November 2003) and from Canine brain atlas (<http://vanat.cvm.umn.edu/brainsect/section0.html>, accessed November 2003). The rat brain section was identified using a rat brain atlas (Zilles, 1985).

Note that some of the images have been modified aesthetically for inclusion as figures in this chapter but for analytical purposes, all images were used in their original format.

7.2 [^{125}I](Tyr 14)N/OFQ labelling *in situ*

This technique was optimised in case the slides labelled with [^3H]N/OFQ could not be imaged in a suitable manner after the breakdown of the β -imager. [^{125}I](Tyr 14)N/OFQ film autoradiography is advantageous compared to [^3H]N/OFQ as it gives rapid

results with better resolution.

This methodology is exactly the same as in section 7.1 except a non saturating concentration of ~0.4nM [^{125}I](Tyr¹⁴)N/OFQ is used for 100min in the main incubation step. After drying the sections under cold air for 15min, they are placed into a film cassette (sections facing up) with Hyperfilm ECL™ and exposed for the desired length of time. The film was then developed using an Amersham Hyperprocessor. This was scanned and the images saved.

7.3 Results

7.3.1 [^{125}I](Tyr¹⁴)N/OFQ autoradiograms

As the slides labelled with [*leucyl*-³H]N/OFQ were successfully imaged using a MCP detector, no analysis was performed on the sections labelled with [^{125}I](Tyr¹⁴)N/OFQ. A representative sample of the [^{125}I](Tyr¹⁴)N/OFQ autoradiograms is presented below. NSB slides can be found in Figure 7.2 and total binding slides, and their corresponding brain atlases, in Figure 7.3.

These sections confirm the localisation of native NOP in dog brain as similar areas are labelled with [^{125}I](Tyr¹⁴)N/OFQ to those observed in [*leucyl*-³H]N/OFQ autoradiography (see later). For example the cortex is labelled consistently and shows higher intensity than that seen in the mid brain. This is also consistent with [^{125}I](Tyr¹⁴)N/OFQ binding observed in the rat (Letchworth *et al.*, 2000). The cerebellum and basal ganglia also contain some NOP receptors. For further discussion on these and other brain areas the reader is referred to section 7.3.2.

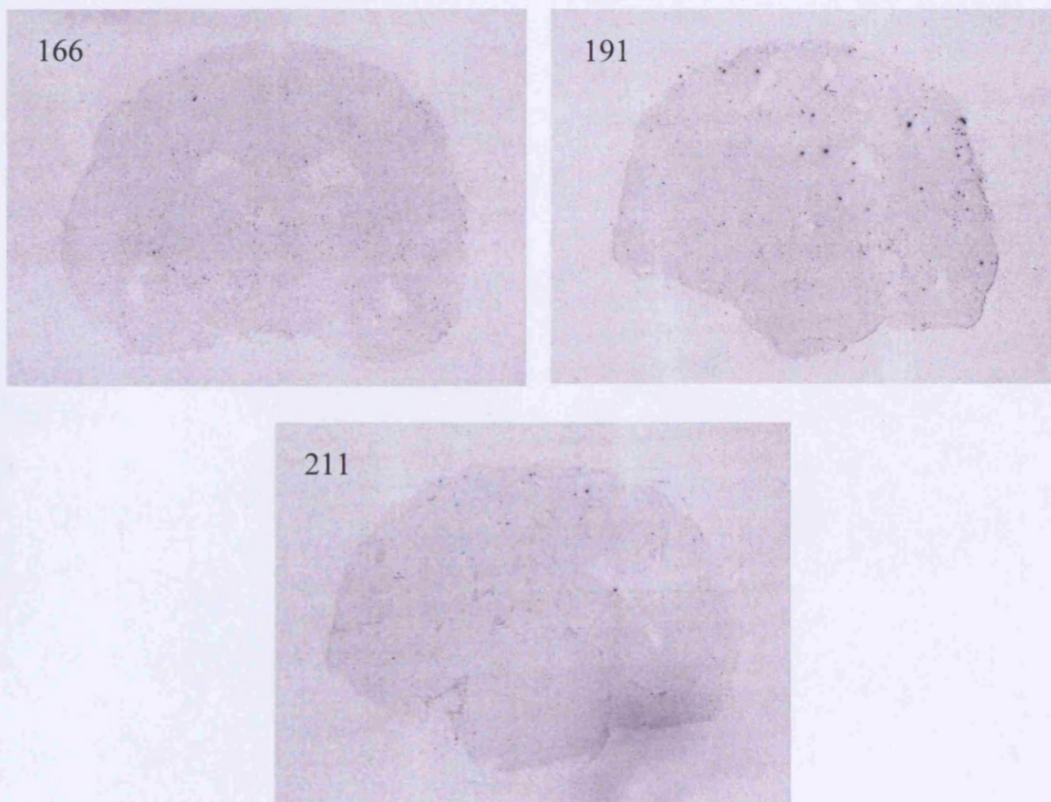
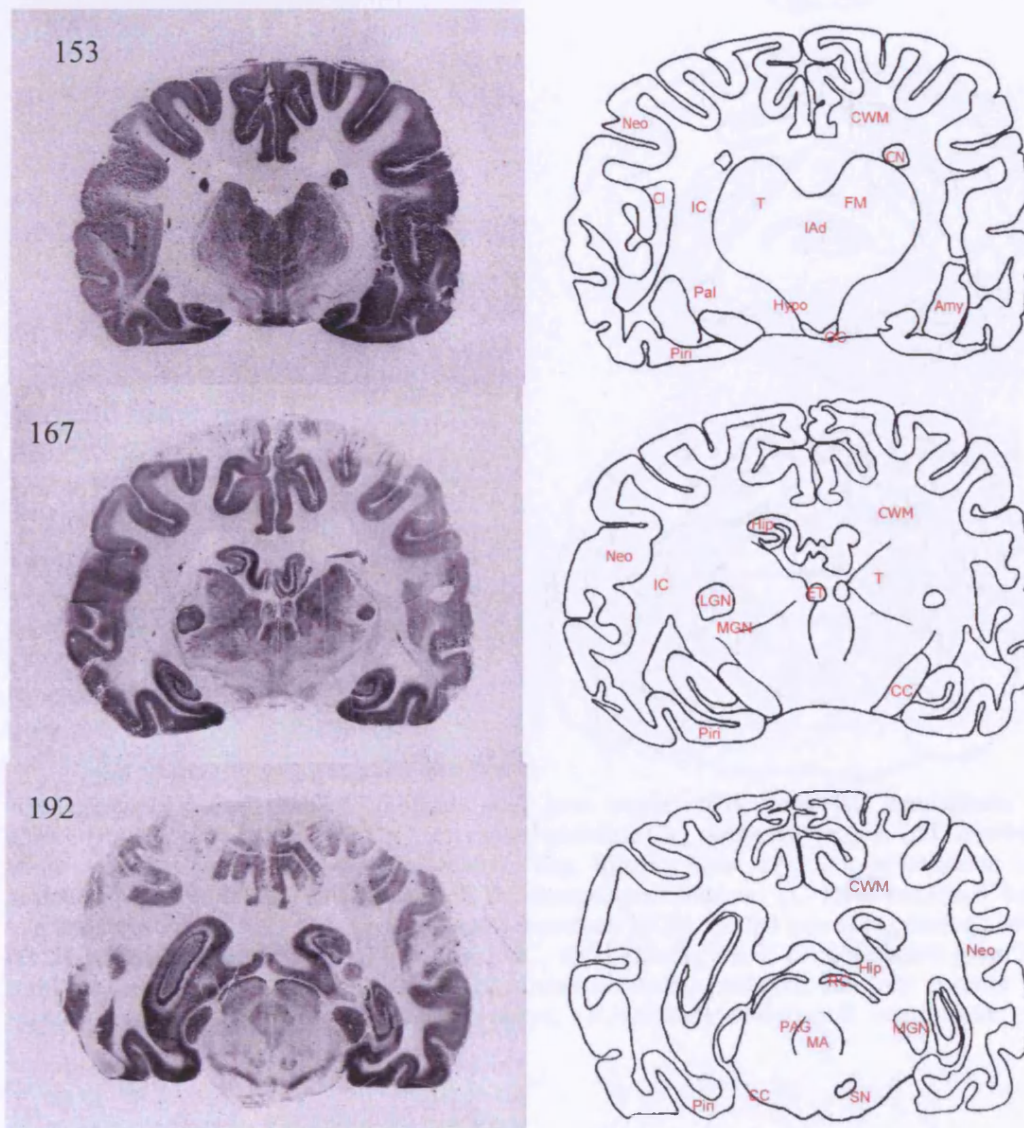
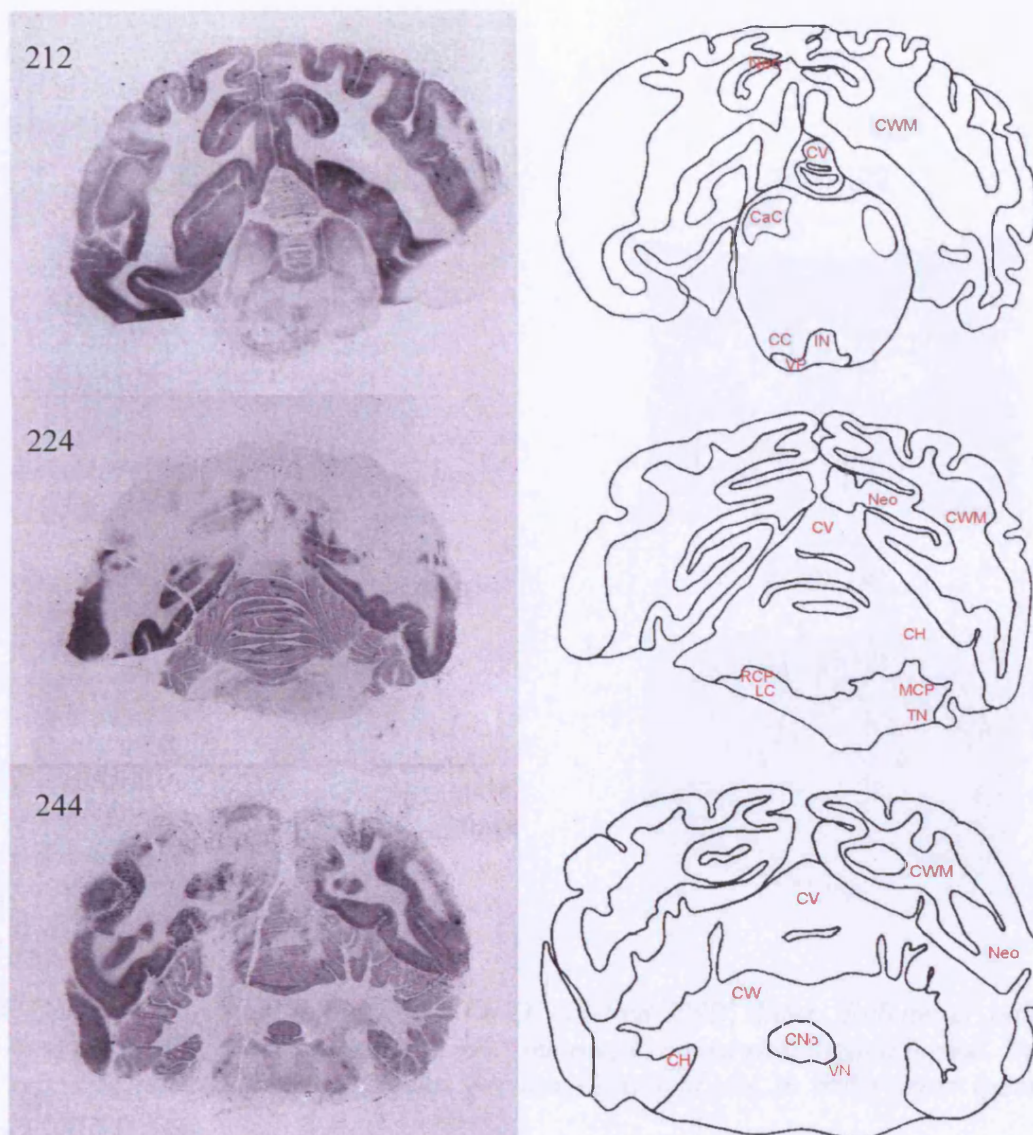


FIGURE 7.2 [^{125}I](Tyr 14)N/OFQ autoradiograms of NSB slides 166, 191 and 211. Numbers refer to slide number (Appendix section 12.4) and are in order from anterior to posterior

TABLE 7.1 Images of [125 I](Tyr 14)N/OFQ autoradiography in whole dog brain sections exposed against film for 48hr. Numbers refers to slide number (Appendix section 12.4) and are in order from anterior to posterior





Amy, amygdala; CaC, caudal colliculus; CC, crus cerebri; CH, cerebellar hemisphere; Cl, claustrum; CN, caudate nucleus; CNo, cerebellar nodulus; CV, cerebellar vermis; CW, cerebellar white matter; CWM, cerebral white matter; Hip, hippocampus; Hypo, hypothalamus; IAd, interthalamic adhesion; IC, internal capsule; IN, interpeduncle nucleus; LC, locus coeruleus; LGN, lateral geniculate nucleus; MA, mesencephalic aqueduct; MGN, medial geniculate nucleus; MCP, middle cerebellar peduncle; Neo, neocortex; OC, optic chiasm; PAG, periaqueductal grey; Piri, piriform cortex; RC, rostral colliculus; RCP, rostral cerebellar peduncle; RN, red nucleus; SN, substantia nigra; T, thalamus; TN, trigeminal nerve; VN, vestibular nucleus; VP, ventral pons

7.3.2 [*leucyl*-³H]N/OFQ autoradiograms

Three values were recorded from each of the four NSB sections of dog brain cortex (Figure 7.3) and averaged to give NSB of $0.49 \pm 0.25 \text{ nCi mg}^{-1}$, used in all future analysis. An example of MCID analysis for slide number 111 can be found in Appendix section 12.6.

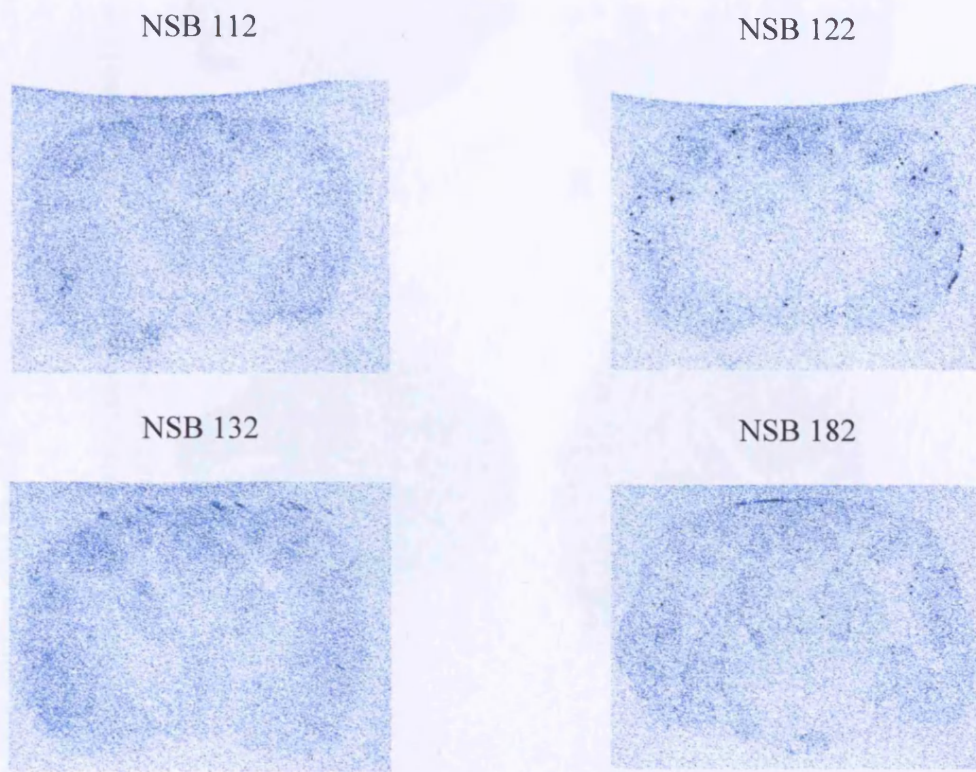
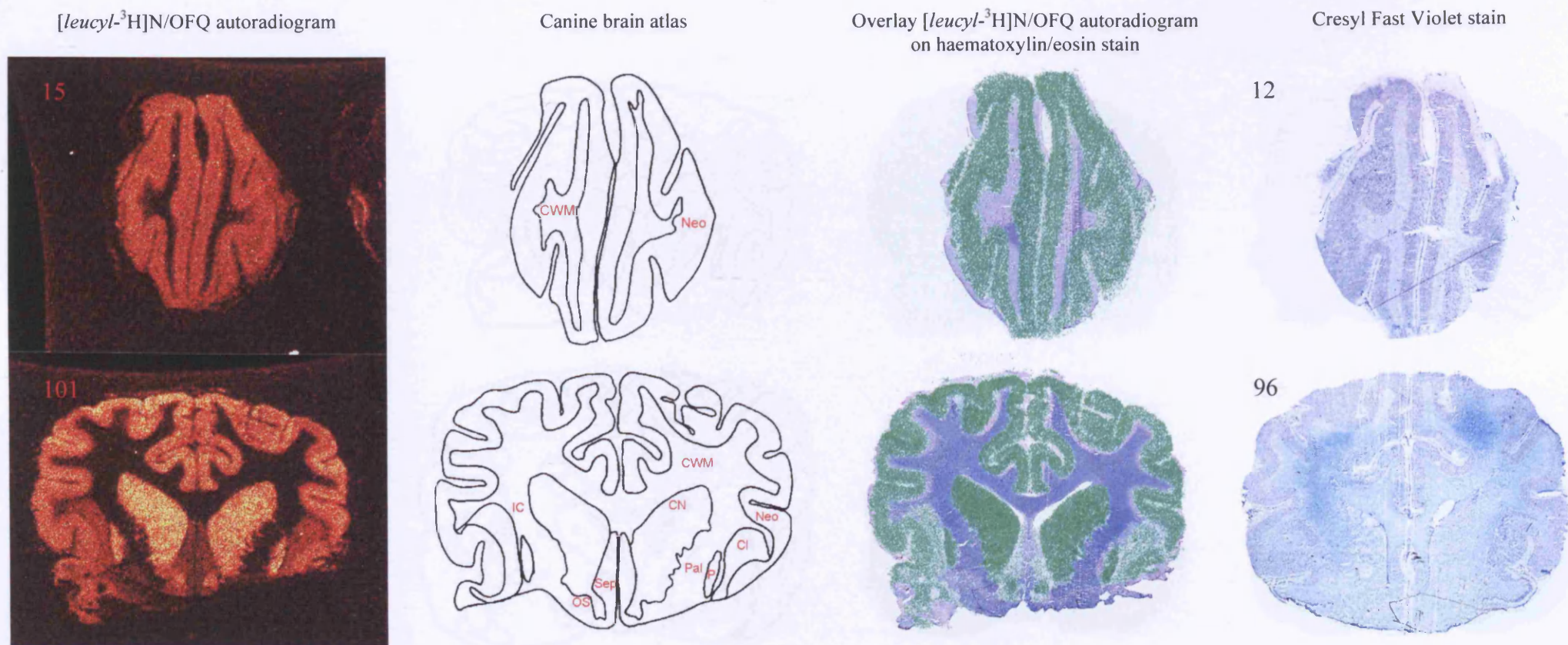


*FIGURE 7.3 Images of [*leucyl*-³H]N/OFQ labelled NSB slides. Palette is pale blue through to black with black being most intense, i.e. most radioligand bound. Numbers refers to slide number (Appendix section 12.4) and are in order from anterior to posterior*

The [*leucyl*-³H]N/OFQ autoradiograms of coronal whole dog brain sections are presented in Table 7.2, along with a brain atlas, an overlay of the autoradiogram over an adjacent haematoxylin and eosin stained section, and a section stained with Cresyl Fast Violet. The binding of [*leucyl*-³H]N/OFQ differed markedly over different brain regions and values for this binding, presented as specific intensity, can be found in Table 7.3.

TABLE 7.2 [*leucyl*-³H]N/OFQ autoradiograms of whole dog brain depicting NOP binding sites *in situ*

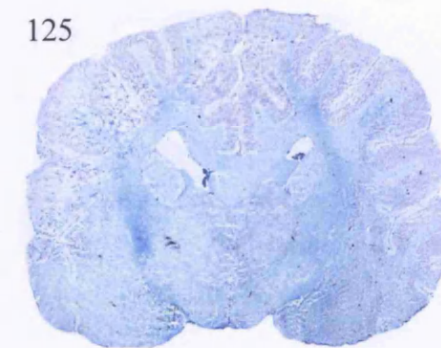
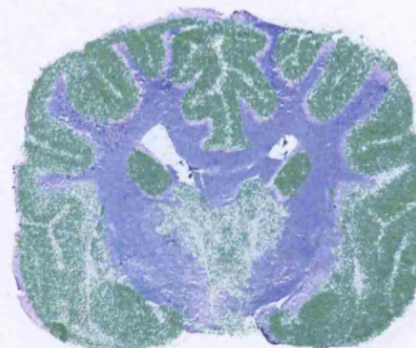
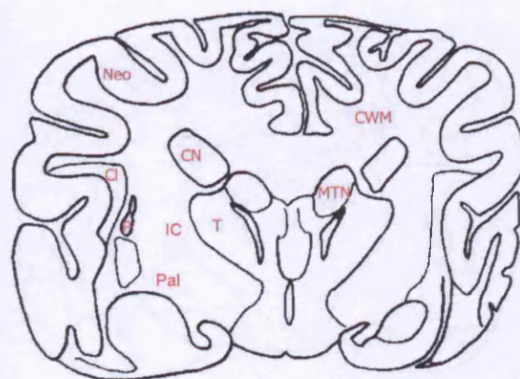
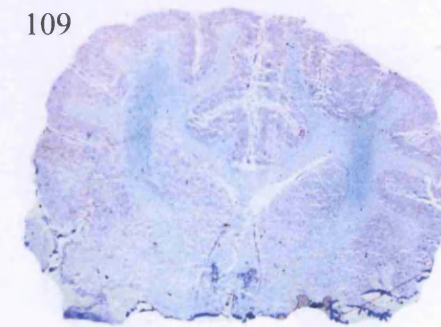
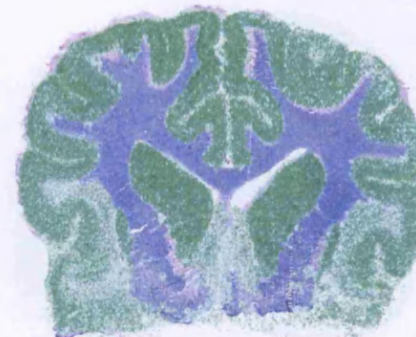
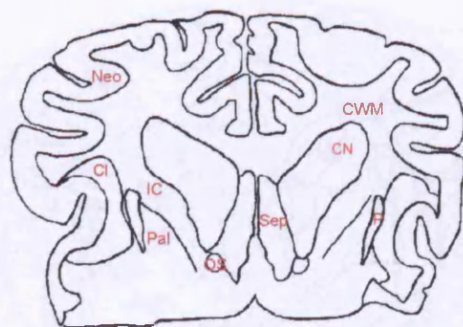
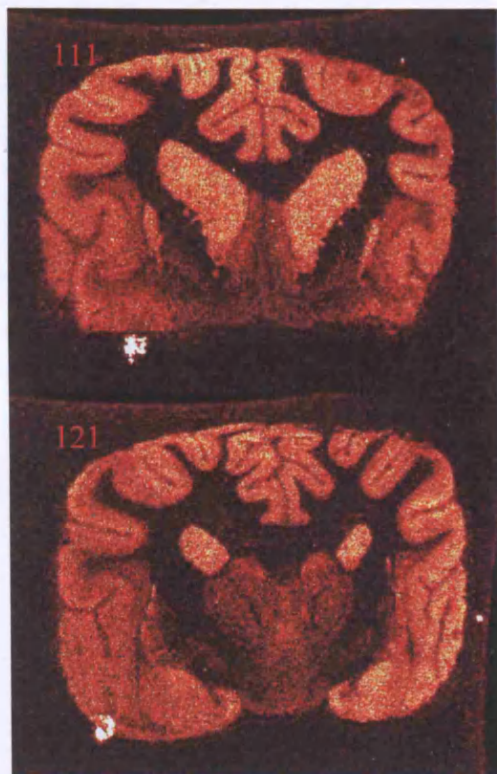


[*leucyl-³H*]N/OFQ autoradiogram

Canine brain atlas

Overlay [*leucyl-³H*]N/OFQ autoradiogram
on haematoxylin/eosin stain

Cresyl Fast Violet stain

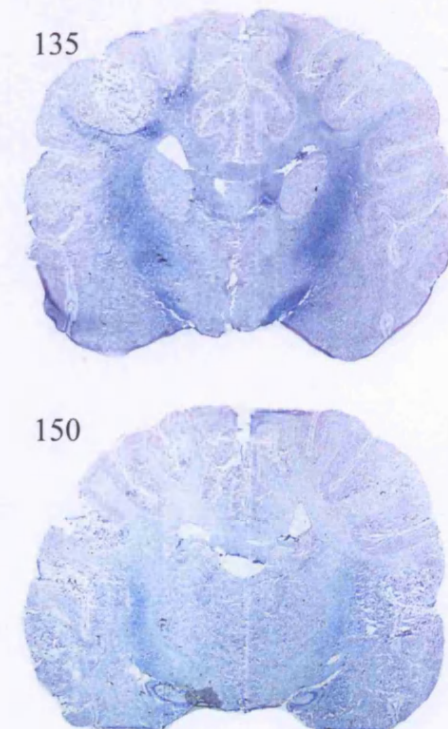
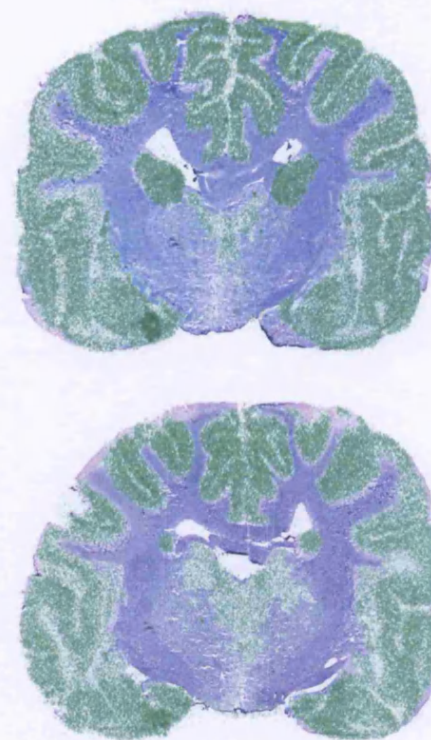
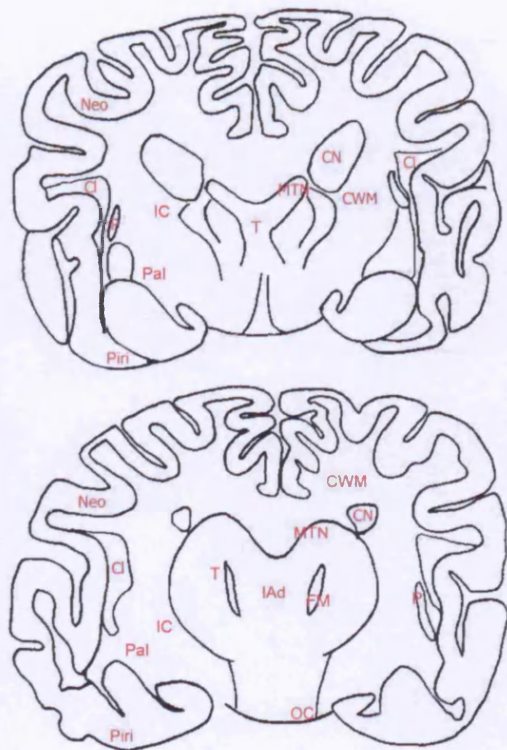


[leucyl-³H]N/OFQ autoradiogram

Canine brain atlas

Overlay [leucyl-³H]N/OFQ autoradiogram
on haematoxylin/eosin stain

Cresyl Fast Violet stain

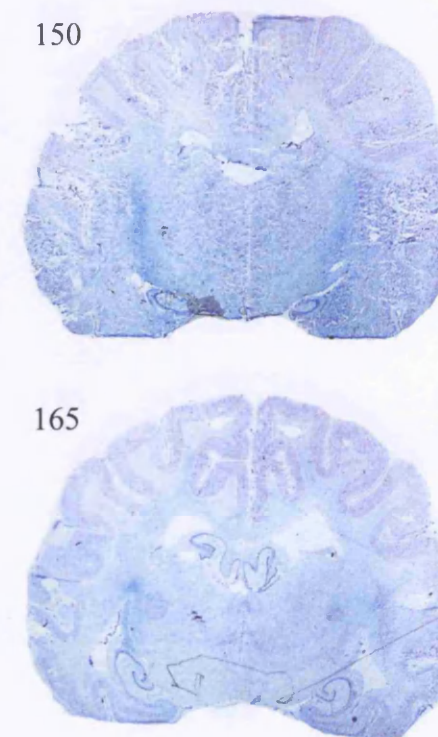
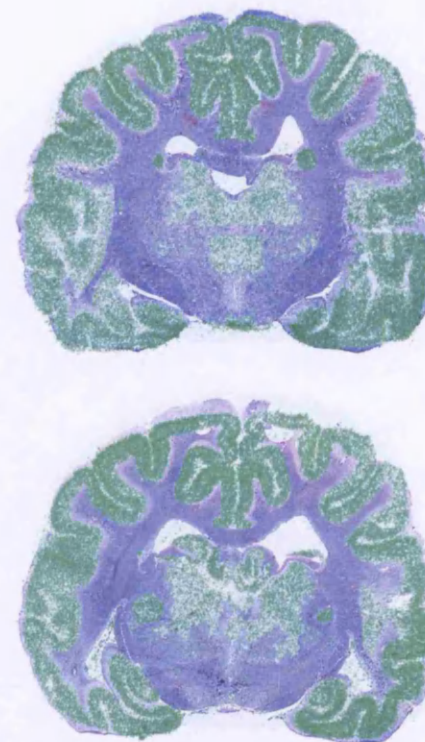
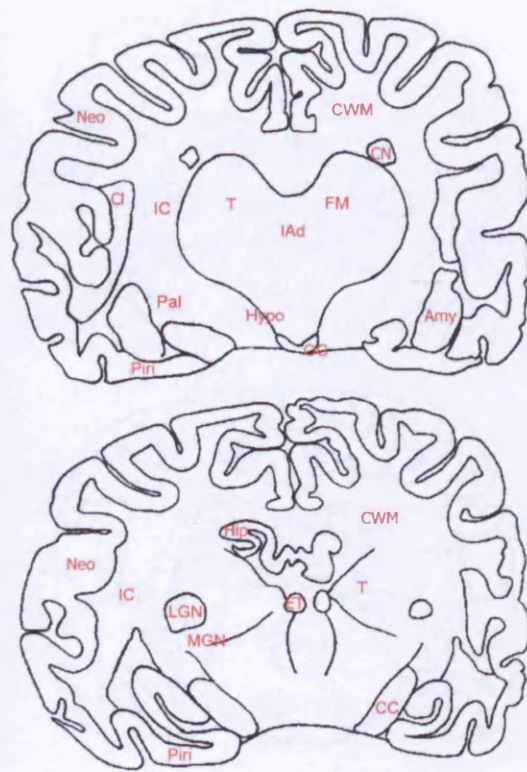


[*leucyl-³H*]N/OFQ autoradiogram

Canine brain atlas

Overlay [*leucyl-³H*]N/OFQ autoradiogram
on haematoxylin/eosin stain

Cresyl Fast Violet stain

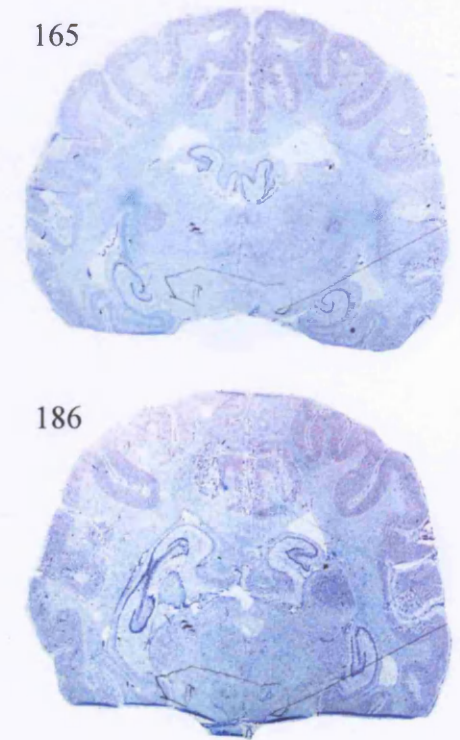
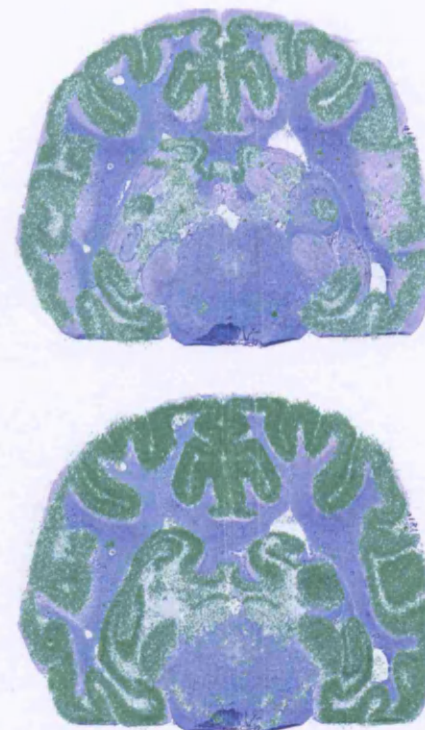
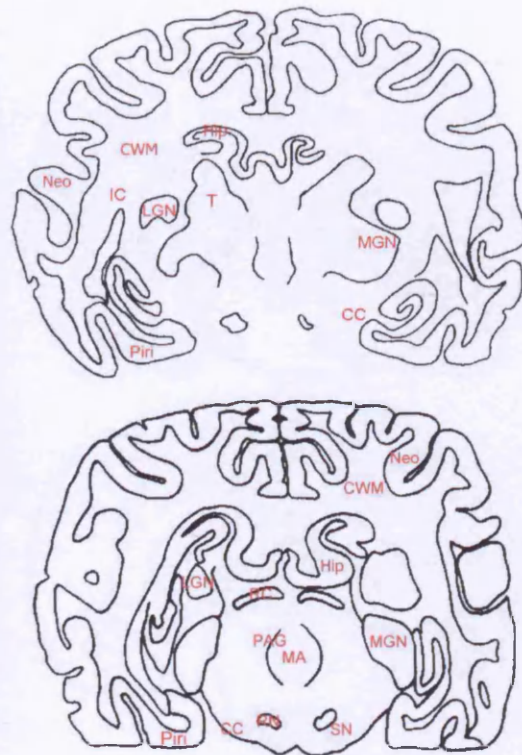
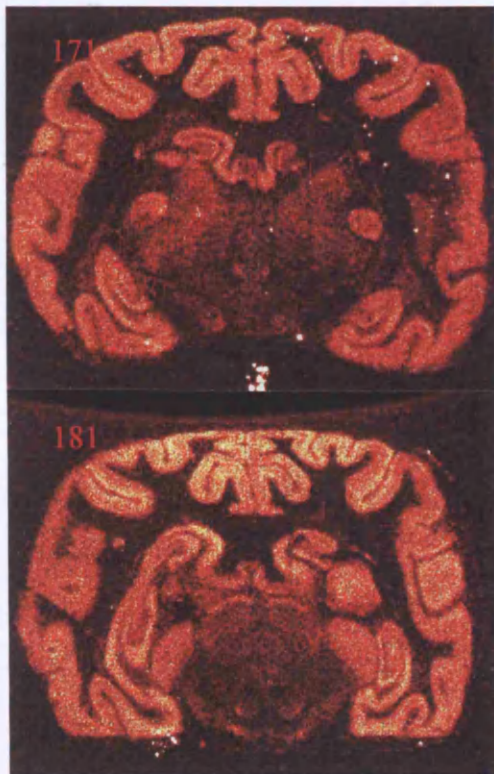


[*leucyl*-³H]N/OFQ autoradiogram

Canine brain atlas

Overlay [*leucyl*-³H]N/OFQ autoradiogram
on haematoxylin/eosin stain

Cresyl Fast Violet stain

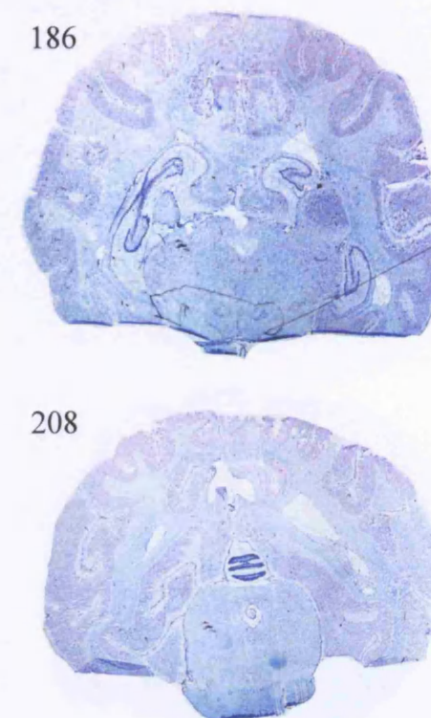
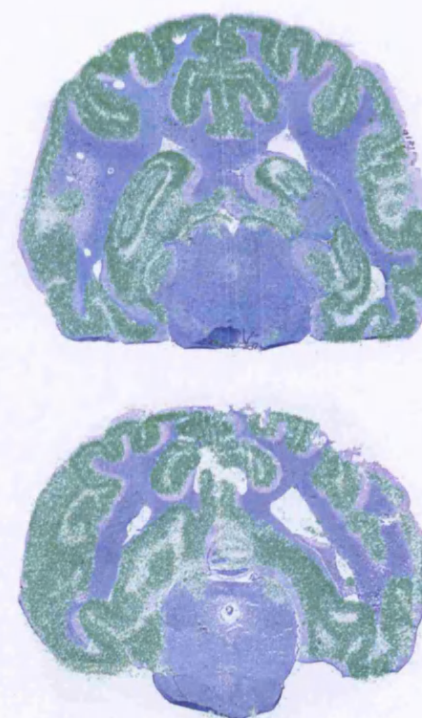
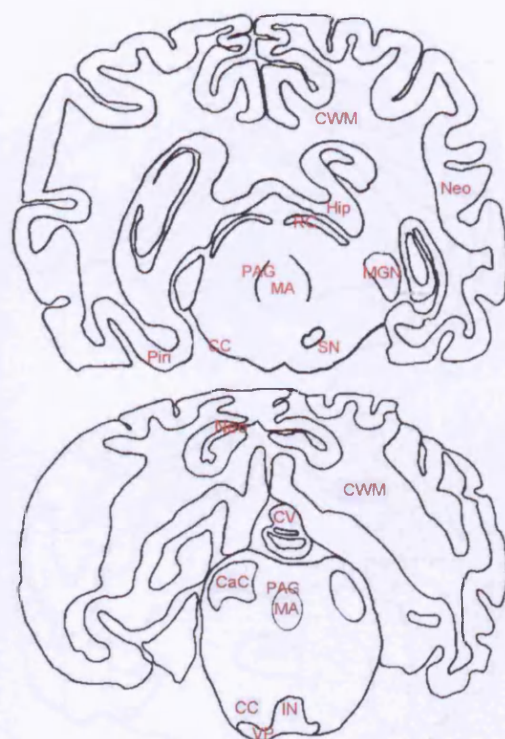


[*leucyl*-³H]N/OFQ autoradiogram

Canine brain atlas

Overlay [*leucyl*-³H]N/OFQ autoradiogram
on haematoxylin/eosin stain

Cresyl Fast Violet stain

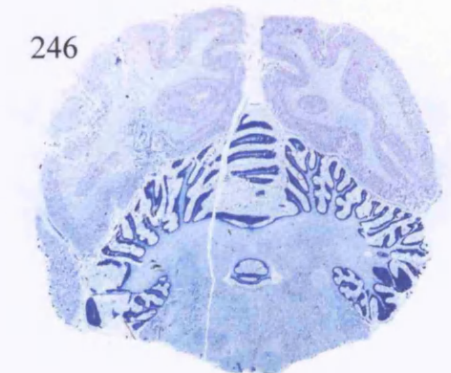
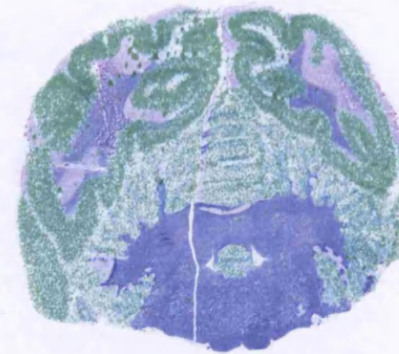
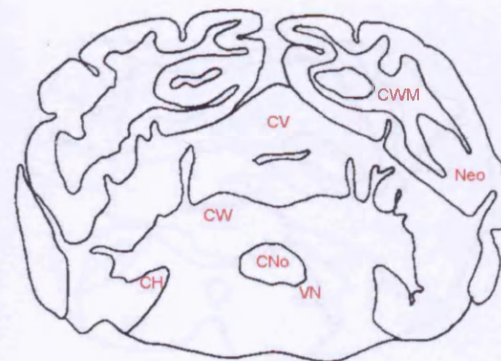
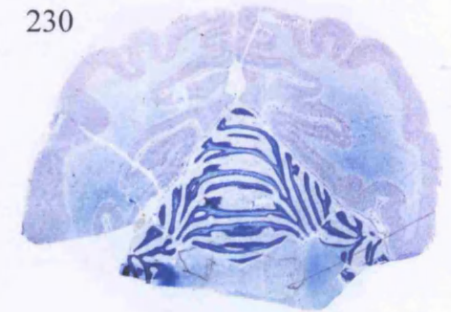
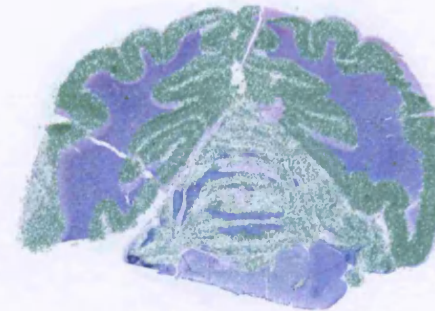
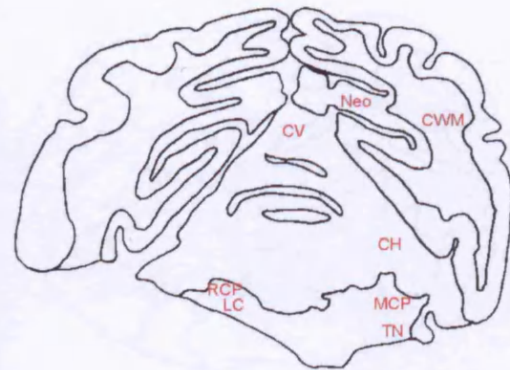


[*leucyl*-³H]N/OFQ autoradiogram

Canine brain atlas

Overlay [*leucyl*-³H]N/OFQ autoradiogram
on haematoxylin/eosin stain

Cresyl Fast Violet stain



[*leucyl*-³H]N/OFQ autoradiogram

Canine brain atlas

Overlay [*leucyl*-³H]N/OFQ autoradiogram
on haematoxylin/eosin stain

Cresyl Fast Violet stain

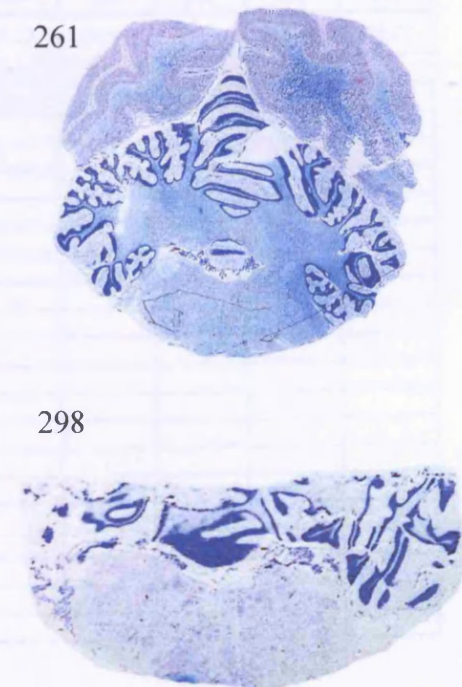
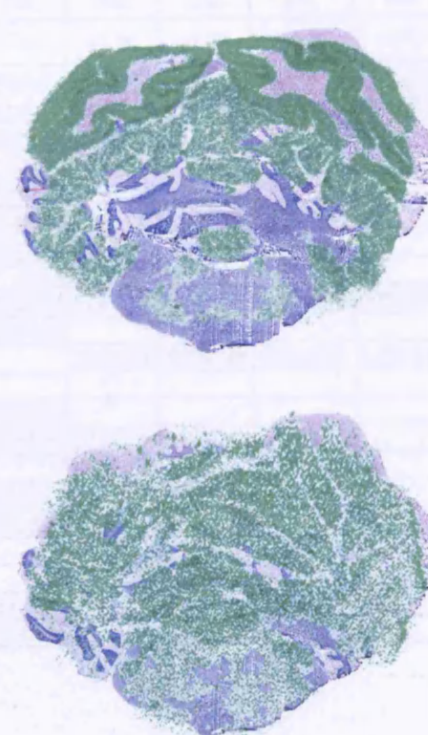
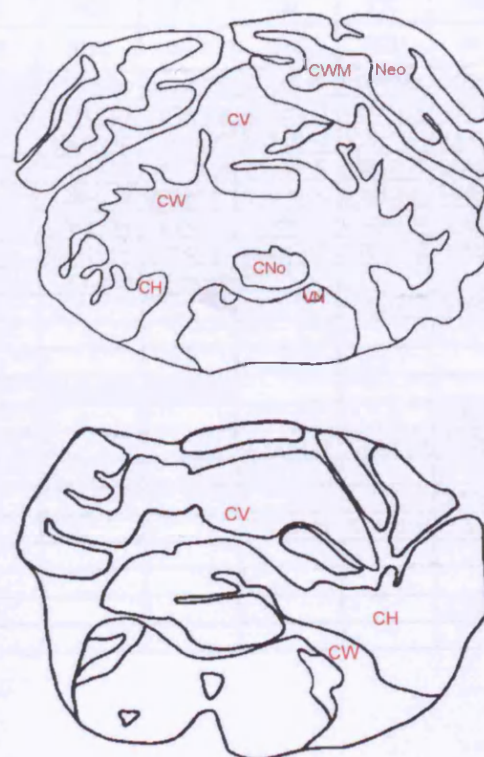
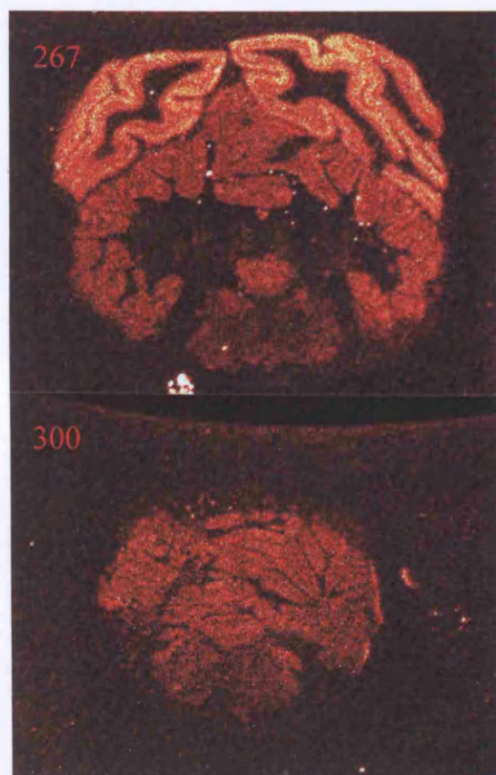


TABLE 7.3 Expression of NOP receptors (quoted as specific intensity in $n\text{Ci mg}^{-1}$) in various brain areas as determined in [*leucyl*- ^3H]N/OFQ autoradiography. Note blanks in table denote area not tested ($n=3$)

SLIDE NUMBER		SPECIFIC INTENSITY ($n\text{Ci mg}^{-1}$)															
		15	101	111	121	131	143	151	161	171	181	194	209	225	251	267	300
<i>Distance from anterior (mm)</i>		5.37	29.38	30.30	32.95	34.01	36.96	37.68	41.14	41.89	44.39	45.23	49.22	54.34	57.55	61.04	68.27
TELENCEPHALON	Cerebral white matter CWM	0.00±0.10	0.08±0.01	0.03±0.00	0.00±0.01	0.00±0.00	0.02±0.00	0.00±0.01	0.00±0.00	0.00±0.03	0.00±0.00	0.00±0.00	0.09±0.01	0.04±0.00	0.07±0.02	0.06±0.02	
	Neocortex Neo	4.66±0.10	6.53±0.03	7.02±0.08	4.58±0.05	4.39±0.18	6.18±0.10	5.61±0.06	6.96±0.03	6.49±0.16	9.29±0.05	6.50±0.07	3.72±0.02	5.98±0.04	5.14±0.11	5.86±0.09	
	Caudate nucleus CN		9.98±0.10	7.69±0.10	6.79±0.02	5.39±0.14	5.63±0.08	6.26±0.08	0.03±0.04								
	Putamen P		8.11±0.10	5.48±0.06	2.71±0.02	3.89±0.12	2.38±0.10										
	Pallidum Pal		0.28±0.12	0.71±0.07	0.27±0.04	0.02±0.02	0.05±0.05	0.03±0.02									
	Clastrum Cl		3.04±0.18	2.81±0.02	1.74±0.05	1.50±0.04	2.06±0.25	1.76±0.03									
	Internal capsule IC		0.11±0.06	0.05±0.01	0.00±0.01	0.00±0.02	0.00±0.04	0.04±0.02	0.03±0.05	0.02±0.02							
	Septum Sep		1.57±0.03	1.73±0.06													
	Piriform cortex Piri					3.20±0.25	6.00±0.10	4.11±0.33	4.84±0.08	4.50±0.05	7.90±0.15	6.40±0.07					
	Amygdala Amy							5.29±0.06									
Hippocampus Hip								5.77±0.08	5.75±0.01	4.03±0.09	3.75±0.04						
Olfactory stria OS		0.20±0.06	0.03±0.05														
DIENCEPHALON	Optic chiasm OC						1.32±0.00	4.99±0.55									
	Thalamus T				2.37±0.10	1.88±0.14	2.42±0.06	2.27±0.28	2.26±0.07	1.64±0.16							
	Epithalamus ET								3.12±0.16								
	Interthalamic adhesion IAd						2.33±0.04	1.61±0.07									
	Medial thalamic nuclei MTN				2.02±0.02	2.44±0.04	2.20±0.02	2.67±0.28									
	Lateral geniculate nucleus LGN								2.20±0.08	1.46±0.07	6.14±0.21						
	Medial geniculate nucleus MGN								3.72±0.13	4.64±0.08	5.13±0.01	3.17±0.04					
	Mammillothalamic bundle FM						1.30±0.06	0.54±0.13									
Hypothalamus Hypo							0.46±0.02										

SLIDE NUMBER		SPECIFIC INTENSITY (nCi mg ⁻¹)															
		15	101	111	121	131	143	151	161	171	181	194	209	225	251	267	300
<i>Distance from anterior (mm)</i>		5.37	29.38	30.30	32.95	34.01	36.96	37.68	41.14	41.89	44.39	45.23	49.22	54.34	57.55	61.04	68.27
MESENCEPHALON	Crus cerebri CC								0.00±0.01	0.02±0.01	0.00±0.01	0.00±0.01	0.03±0.02				
	Mesencephalic aqueduct MA										0.75±0.09	0.66±0.01					
	Periaqueductal grey PAG										0.86±0.05	0.62±0.03	0.19±0.06				
	Rostral colliculus RC										4.26±0.10	3.53±0.09					
	Substantia nigra SN										2.35±0.11						
	Red nucleus RN										1.18±0.11						
	Caudal colliculus CaC												1.77±0.11				
	Trigeminal nerve TN													0.06±0.00			
METENCEPHALON	Locus coeruleus LC													0.00±0.04			
	Rostral cerebellar peduncle RCP													0.01±0.05			
	Middle cerebellar peduncle MCP													0.00±0.01			
	Interpeduncular nucleus IN												0.46±0.03				
	Ventral pons VP												1.30±0.07				
	Cerebellar vermis CV												1.58±0.03	2.09±0.01	3.01±0.05	2.88±0.04	2.58±0.38
	Cerebellar hemisphere CH													1.55±0.03	1.97±0.07	2.12±0.10	1.91±0.03
	Cerebellar nodulus CNo														2.46±0.02	2.77±0.04	
MYELENCEPHALON	Cerebellar white matter CW													0.00±0.01	0.00±0.01	0.13±0.03	
	Vestibular nucleus VN													0.77±0.05	1.70±0.03		

Slides 15-300 cover the whole dog brain from the anterior cortex to the posterior cerebellum and medulla. The most notable feature from Table 7.3 is the wide distribution of [*leucyl*-³H]N/OFQ binding, indicating diverse localisation of NOP in dog brain. Relatively high intensity binding is observed in the neocortex, piriform cortex, hippocampus, amygdala, caudate nuclei and putamen with moderate binding in the epithalamus, geniculate nuclei and rostral colliculus. The claustrum, septum, optic chiasm, thalamus, interthalamic adhesion, medial thalamic nuclei, PAG, substantia nigra, red nuclei, caudal colliculus, cerebellar vermis and cerebellar hemisphere show low levels of [*leucyl*-³H]N/OFQ binding with no binding observed at all in the pallidum, internal capsule, cerebral white matter, olfactory stria, crus cerebri, corpus callosum, trigeminal nerve or cerebellar peduncles.

The autoradiogram depicting various rat and dog tissues can be found in Figure 7.4. For the rat mid-coronal brain sections, three random areas from the piriform cortex were analysed in both total and NSB sections to give an average for specific binding of $20.86 \pm 2.52 \text{ nCi mg}^{-1}$ ($n=3$). Values from all five sections of both total and NSB dog vas deferens were averaged and exhibited specific binding of $2.14 \pm 0.56 \text{ nCi mg}^{-1}$. In dog skeletal muscle, three random areas were sampled and averaged from total and NSB sections though no specific binding ($0.22 \pm 0.20 \text{ nCi mg}^{-1}$) was observed.

The rat coronal brain section was identified using a rat brain atlas (Zilles, 1985) and was hypothesised to be in the region of dog brain slides 151 and 161 (Figure 7.4). Hence the binding observed for rat was compared to dog piriform. The specific binding values for the piriform from these two sections were averaged showing a specific intensity of $4.11 \pm 0.27 \text{ nCi mg}^{-1}$.

When comparing intensities for specific binding in the different tissues, Figure 7.5 shows that rat piriform cortex exhibits significantly higher binding, with approximately 5 and 10

fold more [*leucyl*-³H]N/OFQ binding sites compared to dog piriform and vas deferens, respectively. The higher binding observed in the rat cortex is of considerable significance as this result confirms the findings of chapter 3 that rat brain contains significantly more NOP than dog brain.

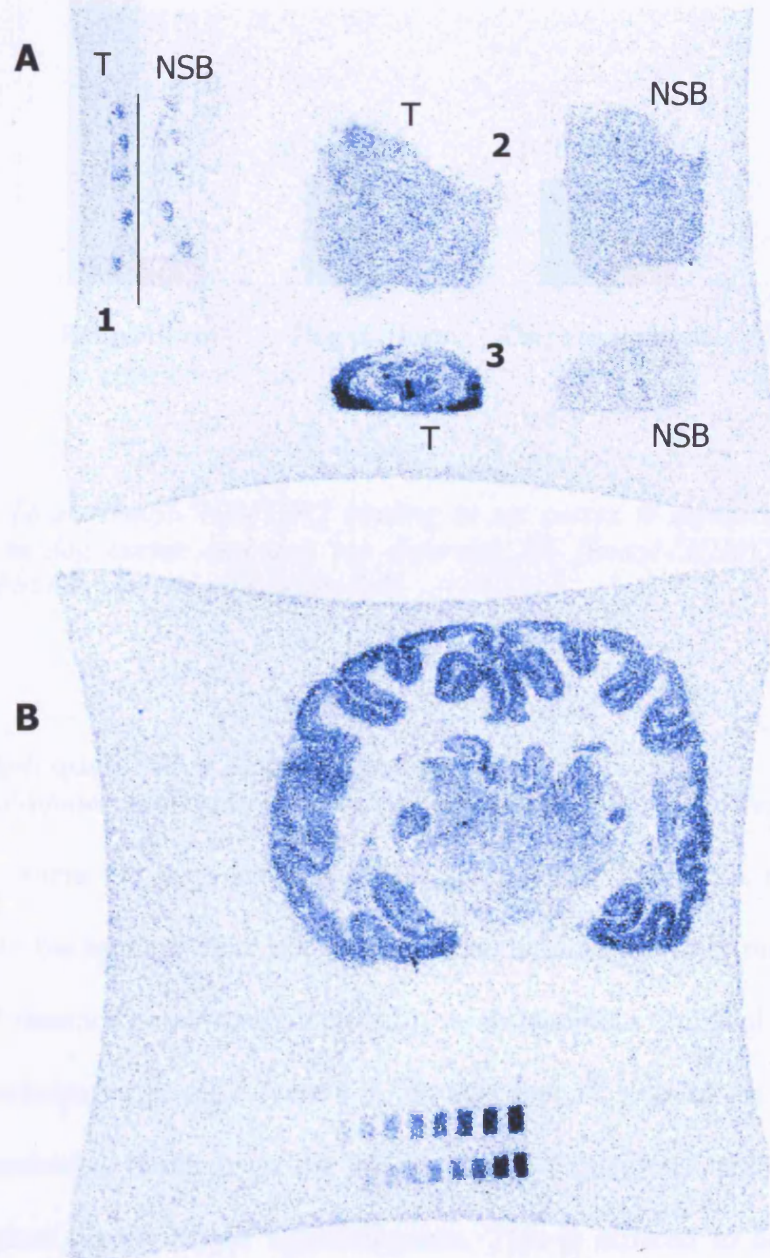


FIGURE 7.4 Autoradiogram A and B (actual field of view of MCP detector) show [*leucyl*-³H]N/OFQ binding in dog vas deferens (1; 10 sections), dog skeletal muscle (2), rat mid-coronal brain section (3) and dog mid-coronal brain section (B; total binding). Total binding (T) and NSB are as indicated. Palette is pale blue through to black with black being most intense, i.e. most radioligand bound

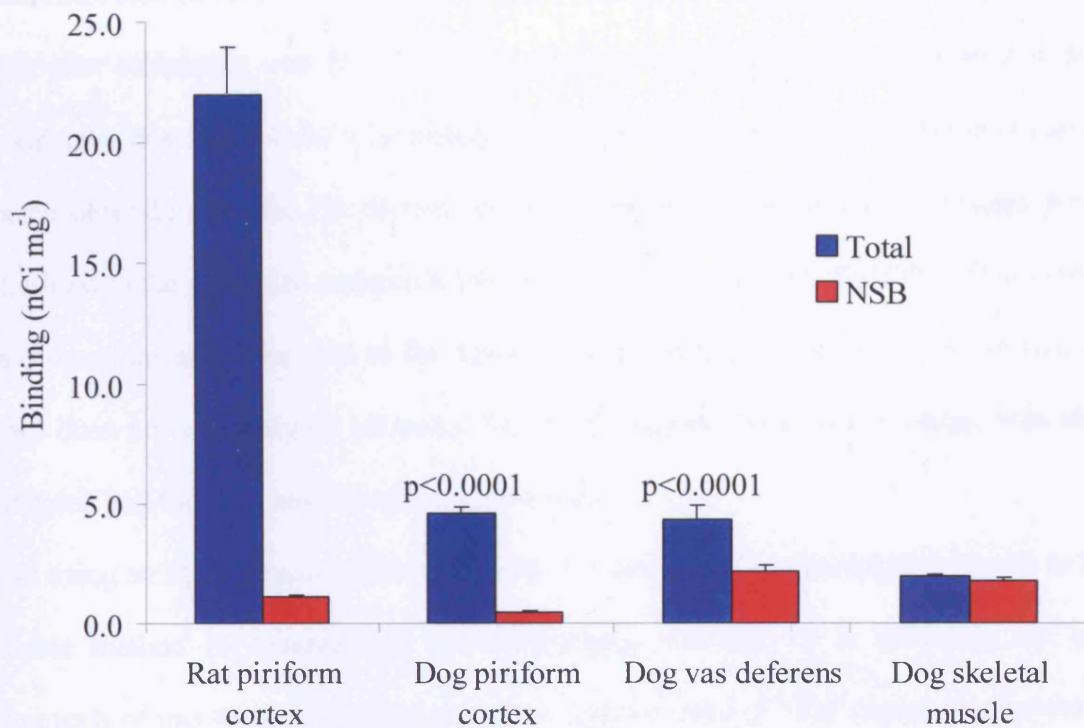


FIGURE 7.5 Total [*leucyl*-³H]N/OFQ binding in rat cortex is significantly higher than binding in dog cortex and dog vas deferens. No [*leucyl*-³H]N/OFQ binding was observed in dog skeletal muscle ($n=3-5$)

7.3.3 Errors in quantitative autoradiography

Errors are a common problem in quantitative autoradiography (Eilbert *et al.*, 1990; Lapin *et al.*, 1991). There are large errors involved in sampling intensities of different brain regions. Firstly the sections were not imaged simultaneously as only one slide would fit into the MCP detector hence there is probably some variation in signal for each section. This is counterbalanced in some respect by the fact that all sections are calibrated to the same [³H]microscales. Furthermore the images are not particularly 'smooth' due to great variation in pixel density of the autoradiograms. This is difficult to correct but longer exposure time might have given better resolution. Also the autoradiograms are slightly distorted and have a few 'hot spots' of contamination on the detector, which were avoided in the analysis.

Caution must also be taken when manipulating the format of the images from the detector. Initially after calibrating with the [³H]microscales, the curve appeared to saturate and this was originally postulated to be a limitation of the MCP detector. However this was easily corrected depending on the file format and pixel density chosen hence all images were standardised to the same size and pixels presented as an uncompressed tiff file. There were some discussions about the area of the square tool affecting readings however the size of the tool does not affect signal intensity. Similarly, magnification of the image was also investigated and found to have no effect on intensity.

Overall using an MCP detector followed by MCID analysis of autoradiograms seems to be a reliable method for quantitative autoradiography. Certainly it is sufficient for the requirements of this thesis for investigating the relative trend of NOP expression however a formal comparison between the MCP detector and traditional film method should be made.

7.4 Discussion

Although the anatomical localisation of NOP in rat has been well documented, no data describes expression in dog. This chapter uses autoradiography with two NOP selective radioligands to localise native dog NOP. Both [*leucyl*-³H]N/OFQ and [¹²⁵I](Tyr¹⁴)N/OFQ binding sites were abundant in dog brain and it is probable that these binding sites correspond to those identified in brain membrane preparations as functional receptor sites (chapters 3 and 4). No quantitative analysis was carried out on [¹²⁵I](Tyr¹⁴)N/OFQ autoradiograms. The pattern of distribution for NOP in these autoradiograms appeared similar to that observed with [*leucyl*-³H]N/OFQ (Figure 7.6). Florin *et al.* (1997) previously reported similar binding patterns in rat brain for [¹²⁵I](Tyr¹⁴)N/OFQ and [*leucyl*-³H]N/OFQ.

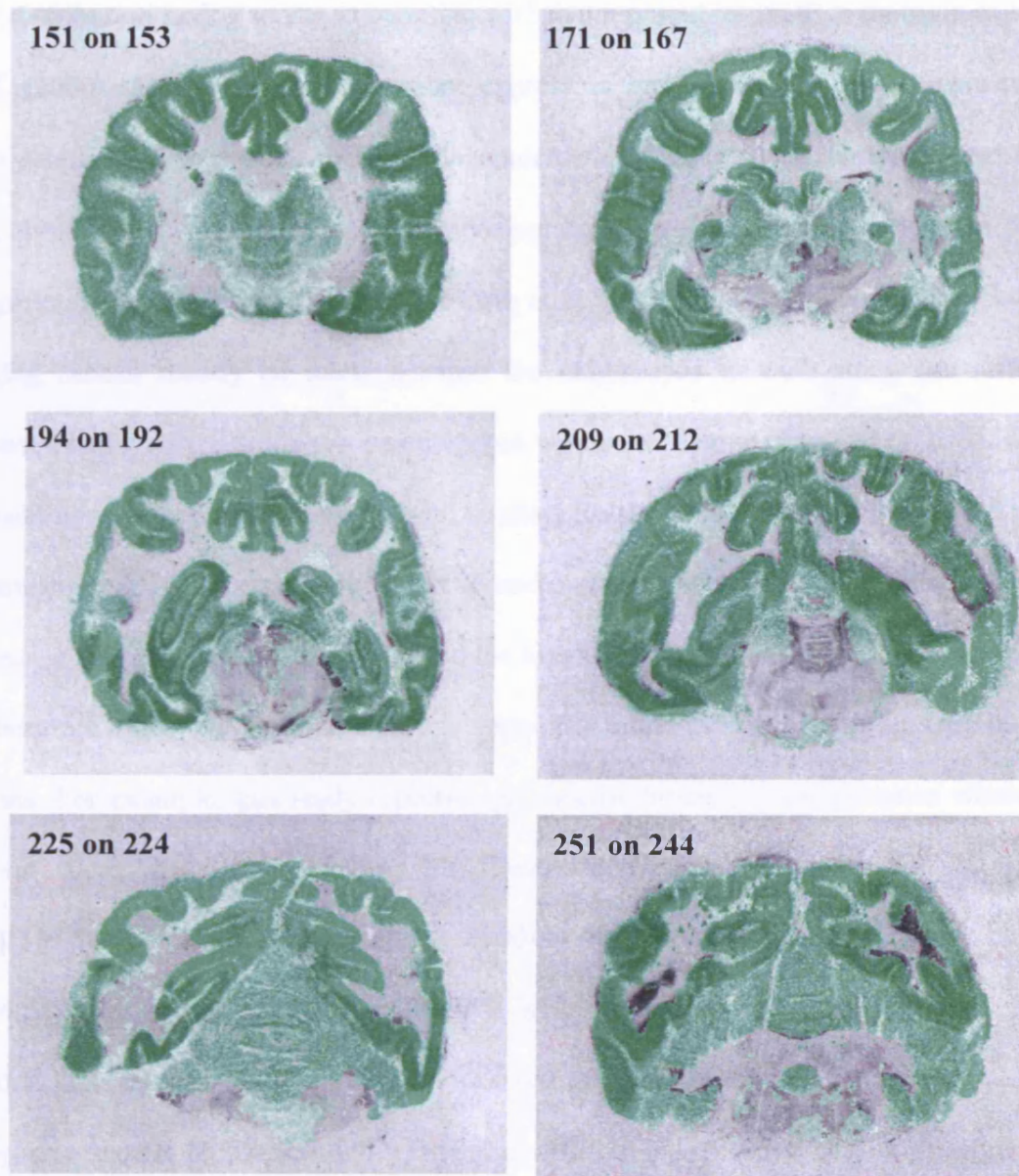


FIGURE 7.6 Overlay of $[leucyl-^3H]N/OFQ$ autoradiograms and $[^{125}I](Tyr^{14})N/OFQ$ autoradiograms

In $[leucyl-^3H]N/OFQ$ autoradiograms, the binding was widely distributed throughout the whole brain and specific intensity was brain structure dependent. The highest intensity was observed in the neocortex, piriform cortex, hippocampus, caudate nuclei and putamen with lower levels in the thalamic areas and mid brain. No binding was observed in corpus callosum, internal capsule, crus cerebri, and cerebral white matter.

NOP distribution in dog seems to correlate with that reported for NOP in rat brain as Florin *et al.* (2000) showed extensive receptor expression including the cortex, hippocampus, basal ganglia and mid brain regions. Receptor density within these areas differed in rat with the highest intensities seen in the cortex, amygdala, and thalamus. A direct comparison with the levels reported by Florin *et al.* (2000) for rat and those described here for dog cannot strictly be made because the calibrations in each study are different. However relative expression can be compared with some degree of accuracy, especially as the radioligand used is the same in both studies. Relative levels of expression in dog and rat are comparable, particularly in areas such as the substantia nigra, interpeduncular nucleus, claustrum, geniculate nuclei, and the hippocampus.

Furthermore there appears to be species-specific levels of expression in certain brain regions. For example, this study reports high specific binding in the putamen whereas in the rat brain, low level binding for [*leucyl*-³H]N/OFQ (Florin *et al.*, 2000) and [¹²⁵I](Tyr¹⁴)N/OFQ (Letchworth *et al.*, 2000) is documented. Indeed although only rat piriform cortex was sampled in this study it is apparent from the autoradiogram in Figure 7.7 that high intensity binding is also observed in the thalamic areas of rat brain. When comparing signals on the autoradiograms, this was not as intense in similar thalamic areas of the dog brain (Figure 7.7).

Chapter 3 showed markedly different levels of receptor expression in dog and rat membrane preparations with B_{max} values of 29 and 137fmol mg⁻¹ protein, respectively. The autoradiograms support these findings as there is significantly ($p < 0.0001$) greater [*leucyl*-³H]N/OFQ binding in the rat cortex (20.86 ± 2.52 nCi mg⁻¹) compared to dog (4.11 ± 0.27 nCi mg⁻¹).

Extensive distribution of NOP has been reported for a variety of species including mouse (Florin *et al.*, 1997), rat (Florin *et al.*, 2000), human (Berthele *et al.*, 2003) and other

primates (Bridge *et al.*, 2003). As species specific expression levels have been reported for other neuropeptides such as CGRP (Dennis *et al.*, 1991) then it is probable that interspecies differences will be observed for N/OFQ, though this can be influenced by the radioligand and assay conditions (Dooley *et al.*, 2000). Identical distribution is observed for NOP in dog and primate brain probably due to the homology between brain development and structures. Bridge *et al.* (2003) report differences between primates and rat, which support this. Distribution in dog also appears similar to that recently described for human brain (Berthele *et al.*, 2003) which documents receptor expression with colocalisation of NOP mRNA.

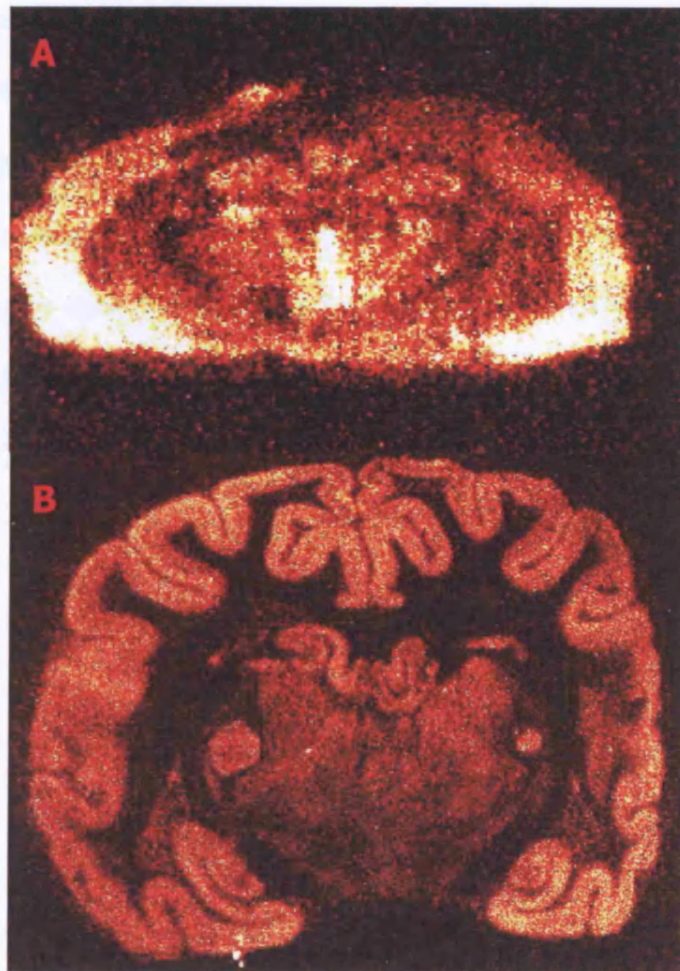


FIGURE 7.7 Significantly higher binding of [leucyl-³H]N/OFQ is observed in rat cortex (A) compared to dog cortex (B). Autoradiograms are not to scale and the intensity varies from black through to bright orange with orange being the most intense

The N/OFQ-NOP system has been reported to be involved in various roles and the distribution described here for dog brain supports several functions. For example, N/OFQ is known to impair spatial learning and memory in rats (Sandin *et al.*, 1997) and hence NOP is found in high levels in the hippocampus and the amygdala, both areas important for learning and memory. Low binding observed in the PAG, septum and hypothalamus indicate this system's role in stress and anxiety (Jenck *et al.*, 2000) and cardiovascular modulation. Of most interest here is the binding of [*leucyl*-³H]N/OFQ in the mid brain regions such as PAG, red nucleus and substantia nigra which implicate N/OFQ in pain modulation. N/OFQ as a pain modulator is well documented and it would be of particular interest to image autoradiography sections of the medulla to see if labelling is also observed in the raphe nucleus, another brain region involved in pain pathways.

This chapter concludes a widespread distribution for native NOP in dog brain, which is consistent with functional roles documented for N/OFQ in other species. Furthermore the dog piriform cortex contains approximately 5 fold less NOP receptors than rat cortex and these findings support those from chapter 3 which reported a fifth of NOP expression in dog brain membranes compared to rat.

8 Immunological techniques

Antibodies are unique molecules and essential tools in scientific research. This chapter describes the optimisation of protocols and progression from antibody production, through to determination of antibody specificity in ELISA and Western blotting, and finally their usage in IHC of whole dog brain sections to further characterise NOP. All methods are described below along with results for each technique.

8.1 Antibody production

The aim here was to produce antibodies against N/OFQ, rat Noc and an epitope in the third extracellular domain of NOP. These antibodies can then be used in further studies to localise their corresponding peptide antigens *in situ*. In order to obtain antibodies of specific selectivity, sequences with little or no homology were chosen, particularly in the case of the antigenic sequence from NOP. If the technique is successful, antibodies should mainly be generated towards the sequence of interest but this does rely on the synthetic peptide mimicking the conformation of the epitope within the native protein. This is more of a problem again with the NOP sequence, as the epitope needs to be surface-orientated as well as hydrophilic and flexible. Several computer programs are available for determining possible epitopes within proteins though these were not used here since the proteins of interest are generally short.

The following antigenic peptides were kindly synthesised in their amide form by Dr R. Guerrini, University of Ferrara, Italy, for use in antibody generation:

- CFIGGFTGARKSARKLANQ-NH₂ (cysN/OFQ; aa sequence for N/OFQ)
- CAEPVADEADEVEQKQLQ-NH₂ (cysNoc; aa116-132 rat nocistatin)
- CGVQPGSETAVAILR-NH₂ (cysNOP epitope; aa289-302 of rat NOP)

The cysteine residue at the N terminal of these continuous epitopes is for conjugation to KLH using Sulfo-MBS, a heterobifunctional crosslinking agent. Note that this residue has been added at the opposite end to the C terminal epitope so this is fully available to the immune system. The same peptides without N terminal cysteine and in the carboxy form were also synthesised for characterising the antibodies generated.

8.1.1 Conjugation of hapten to carrier

To raise antibodies against small antigenic molecules, such as peptides, it is necessary to couple these haptens to carrier proteins to render them immunogenic. This method used is a modification of that described in 'Example Protocol for Preparation of an Immunogen' (Appendix section 12.2) and has two steps: activation of KLH followed by coupling of the peptide to the carrier.

KLH is a dinuclear copper-containing protein (hence a characteristic bluish solution when dissolved) isolated from the haemolymph of giant keyhole limpets. This protein exists as a didecamer of approximately 8 million Da, composed of subunits of ~45kDa. It can be coupled to the peptide using a heterobifunctional crosslinker, the reaction of which is influenced by the number of lysine residues with $-NH_2$ groups available. KLH has a very high number (300-600) of these groups compared to BSA or ovalbumin, other common carrier proteins. A high degree of conjugation is required to increase the immunogenicity of the antigen.

NHS-esters-maleimide crosslinkers target primary amines, linking via an amide bond, and sulfhydryl groups ($-SH$), forming thioether linkages. The maleimide group favours reaction with the sulfhydryl group if pH is maintained at 6.5-7.5. Above this pH, reaction with primary amines, particularly the ϵ -amino group of lysine, becomes more significant. The coupling reaction favours dilute protein solutions and can be followed as change in absorbance at 280nm since absorbance increases with the release of the NHS-ester group

(Carlsson *et al.*, 1978). Hence the reaction is complete when no further change in absorbance is observed.

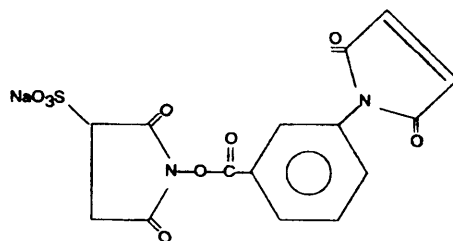


FIGURE 8.1 Chemical structure of Sulfo-MBS

Sulfonated forms of NHS-esters, such as non-cleavable Sulfo-MBS (Figure 8.1; Martin *et al.* (1982)), are water soluble due to the sulfonate group on the N-hydroxysuccinimide ring. The coupling reaction of Sulfo-MBS with a peptide is shown in Figure 8.2.

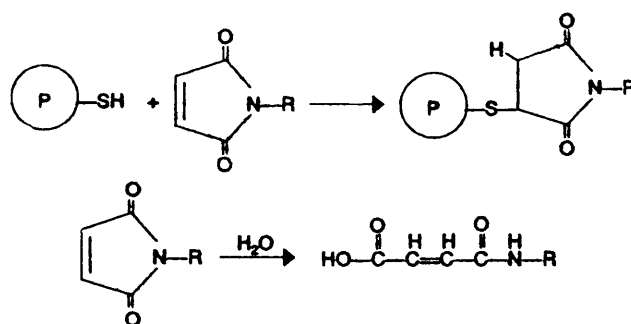


FIGURE 8.2 Reaction scheme of Sulfo-MBS with a sulfhydryl containing peptide

A whole vial of KLH was reconstituted in 2ml dH₂O to give a 10mg ml⁻¹ solution, pH7.2. Precisely 200μl of this was added to a test tube. Sulfo-MBS (2mg) was dissolved in 1ml conjugation buffer (section 2.2) and 100μl was then immediately transferred into the test tube containing KLH. The reaction was allowed to proceed for 1h at room temperature. To remove excess unbound KLH, the mixture was passed through a PD10 column that had been previously equilibrated with ~20ml conjugation buffer. Further conjugation buffer

was added to elute the active mixture and this was monitored using a spectrophotometer with the wavelength set to 280nm. The maleimide-activated KLH was eluted from the column in fractions 5-7 in the example shown in Figure 8.3 and these fractions were pooled.

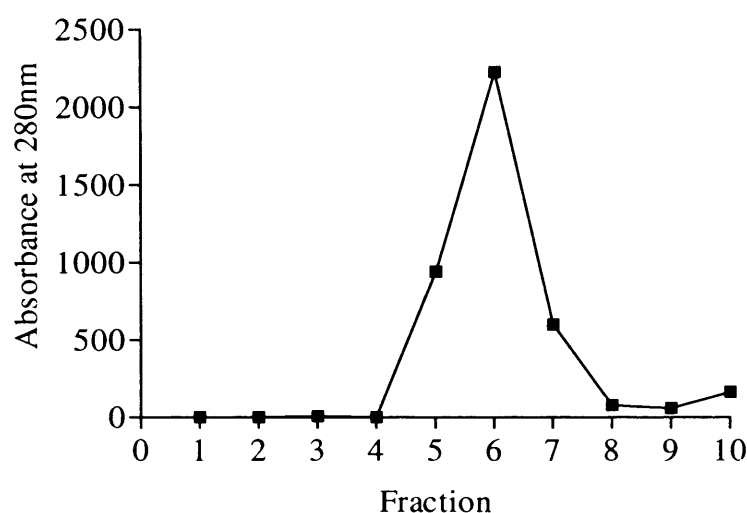


FIGURE 8.3 Graph showing the elution of maleimide-activated KLH complex from PD10 column

Approximately 2mg of the appropriate sulfhydryl-containing peptide was dissolved in 500 μ l conjugation buffer (solutions of each peptide were made such that there was at least 40 molar excess of peptide for KLH) and this solution was added drop wise to the subsequent pooled fractions of KLH. The mixture was incubated for 2h at room temperature before being dialysed to remove any free peptide against at least four buffer changes of ~2L PBS. The immunogen (Figure 8.4) was pipetted into 0.5ml aliquots and stored at -70°C until further use.

As anti-NOP antibodies were produced at a later date than anti-N/OFQ and anti-Noc, the conjugation procedure was repeated with a new batch of KLH so all components were fresh.

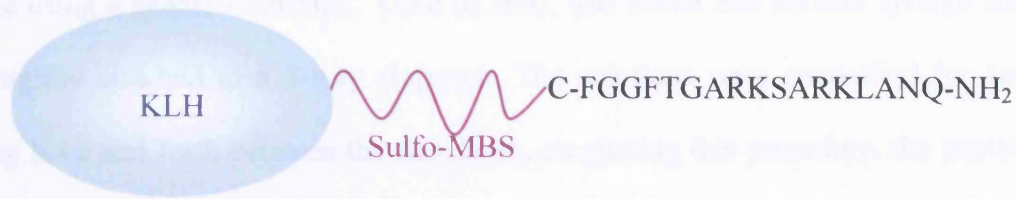


FIGURE 8.4 Immunogen (peptide conjugated to KLH via Sulfo-MBS crosslinker)

8.1.2 Emulsification of immunogen

Following the crosslinking reaction of a hapten to its carrier, the complex is taken up into an adjuvant to form an emulsion. Adjuvants influence the titre, duration and avidity of antibodies through their effects on cell mediated immunity. They also protect the immunogen from early catabolism and retain a high concentration at the injection site (slow release of immunogen occurs).

Block copolymers were noted for their adjuvant activity by Hunter *et al.* (1981) and the adjuvant chosen here, TitreMax[®] Gold, is an improved version of TitreMax[®] which consists of synthetic blocks of hydrophobic polyoxypropylene and hydrophilic polyoxyethylene. They also contain squalene, metabolisable oil, and a unique microparticulate stabiliser. These adjuvants work by inducing an immune response, representing all IgG isotypes, at the injection site; more specifically, they induce T helper cells (classes 1 and 2) and in some cases, also cytotoxic T lymphocytes. They do not contain proteins, mineral oils or microbial products so minimising the adverse effects sometimes observed with Freund's Complete Adjuvant (Bennett *et al.*, 1992). Water-in-oil emulsions are difficult to make and are generally unstable, despite this the TitreMax[®] formulation has been designed to produce a stable emulsion.

The method here is that described in 'Research Adjuvants' (Appendix section 12.3).

Immediately prior to immunisation, the required volume of conjugated peptide antigen was

emulsified. Briefly, 0.25ml of conjugated peptide solution was pipetted into a 2.5ml syringe using a needle. TitreMax[®] Gold (0.5ml), was added into another syringe and both were tightly attached to a 3-way stopcock. The solutions were emulsified for 1min by passing back and forth between the tips. Note, on starting this procedure, the peptide was always passed into the adjuvant first. A further 0.25ml of peptide solution was added and emulsification continued for a further minute. The emulsified immunogen was placed on ice until use.

8.1.3 Immunisation of animals

One rabbit (~2.5kg) was immunised per immunogen as described in Table 8.1 with approximately 200 μ l at four different subcutaneous injection sites. A test bleed was collected from the ear vein prior to the initial immunisation and then one week after each immunisation for determination of antibody titre. The test bleed samples were allowed to clot and were then centrifuged at 3000rpm for 10min at 4°C before removing the serum. This was stored at -70°C in 50 μ l aliquots until titre analysis. Exsanguination was carried out once titre was deemed sufficient.

TABLE 8.1 Timetable for immunisation of animal

DAY	INJECTION	BLOOD SAMPLE
0	Initial inoculation	Pre-immune
21	1 st boost	
28		1 st test bleed
35	2 nd boost	
42		2 nd test bleed
49	3 rd boost	
56		3 rd test bleed Exsanguination

Some evidence of local reaction was observed in one rabbit so the procedure was reviewed to see if sterility could be improved to ensure animal welfare. For future immunisations, the above protocol was therefore repeated in a sterile environment and all equipment was sterilised with 70%IMS before use. All buffers and solutions, where feasible, were passed through 0.45µm Acrodisc Syringe filters prior to use.

8.2 ELISA

Antibody titre and specificity were investigated using an ELISA. This indirect sandwich method (Figure 8.5) uses an unlabelled primary antibody, which is captured by a labelled secondary, in this case labelled with HRP. This secondary antibody is raised against the Ig of the species hosting the primary antibody. HRP is the most commonly used reporter enzyme for chemiluminescent substrates as it is small, stable and relatively inexpensive. The fast kinetics of the reaction provide a signal almost immediately. The indirect method (compared to direct labelling of antigen with HRP-conjugated primary antibody) is efficient and amplifies the signal.

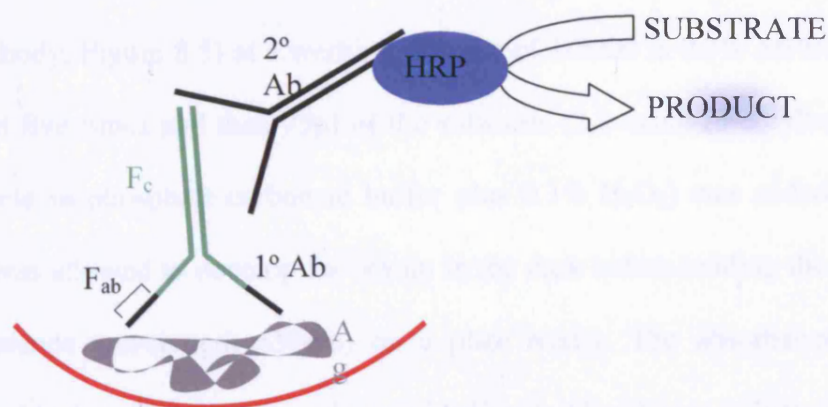


FIGURE 8.5 Basic principles of indirect ELISA. Note as there are two F_c binding sites on the primary antibody (1°Ab) then two or more secondary antibodies (2°Ab) can bind

A successful ELISA protocol was firstly determined using polyclonal anti-N/OFQ antibody purchased from Abcam (referred to as Abcam hereon). This antibody was raised to the C terminal of N/OFQ (CTGARKSARKLANQ) to avoid cross reactivity with N terminal four amino acid message domain of opioid peptides (section 1.8.1). A cysteine was added at the N terminal for conjugation to diphtheria toxin via the crosslinking agent, Maleimidocaproyl-N-hydroxysuccinimide.

96 well plates were incubated for 16h at 4°C with 200µl carbonate-bicarbonate buffer containing 2µg ml⁻¹ of antigen (as indicated in the results section). This was removed by flicking and the plates washed three times with PBS supplemented with 0.05% Tween-20 (PBST). To prevent non-specific binding, wells were blocked with 200µl of 5% non-fat dry milk in PBST (MPBST) per well for 1h at room temperature. Thorough washing, as previously, was carried out prior to the addition of 50µl primary antibody (antiserum or Abcam as positive control) at 1/200 in 0.5% MPBST. This was serially diluted in MPBST down the plate and incubated for 3h at room temperature. Several wells were used as controls in which 50µl 0.5% MPBST was added for the duration of the incubation instead of primary antibody. Five washes with PBST preceded 2h incubation with 200µl per well of HRP conjugated goat anti-rabbit secondary antibody (specific for the F_c region of the primary antibody, Figure 8.5) at a working dilution of 1/2000 in 0.5% MPBST. The plates were washed five times and then 75µl of the substrate (2,2-azino-(3-ethylbenzthiazoline)-6-sulfonic acid in phosphate-carbonate buffer plus 0.1% H₂O₂) was added to each well. The colour was allowed to develop for 30min in the dark before reading the absorbance at 405nm (reference wavelength 650nm) on a plate reader. The absorbance values were corrected for blank values before analysis with Excel. Absorbance values were plotted in Prism and points joined with a connecting line. In experiments investigating antibody titre, the titre is half the maximum absorbance extrapolated on the X-axis (Figure 8.6).

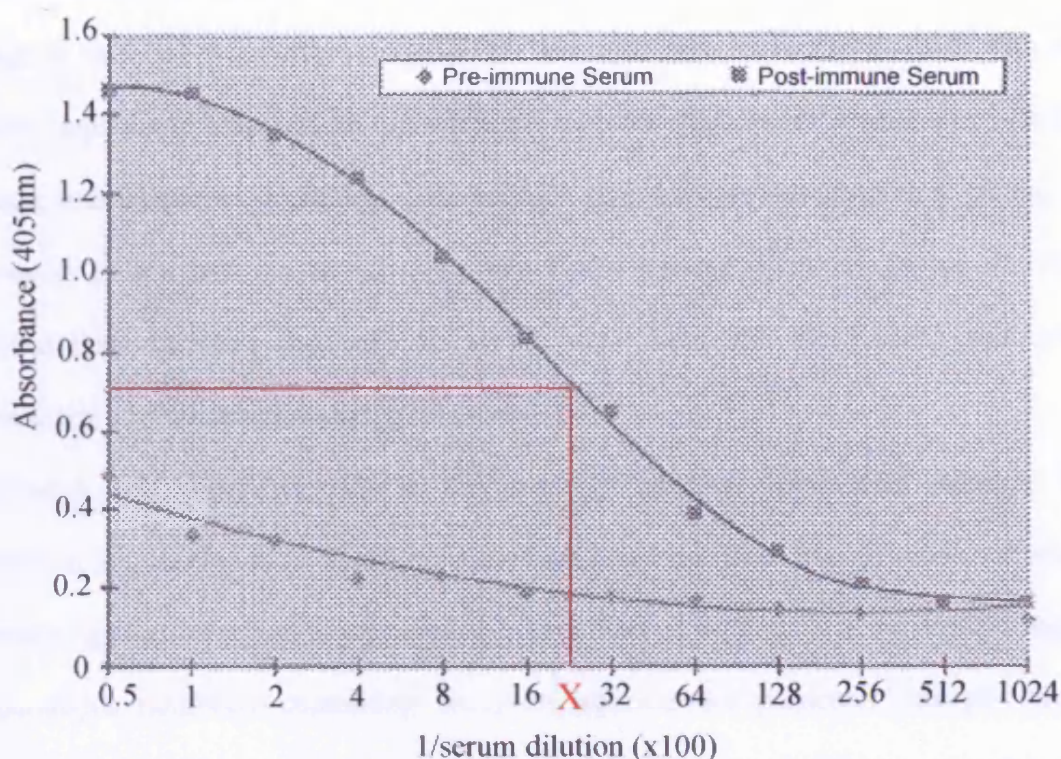


FIGURE 8.6 Sample graph of antibody titre – X dilution value corresponding to half the maximal absorbance is quoted as antibody titre (from *Antibodies: From Design to Assay* www.2.perkin-elmer.com/pa/3409/html/toc.html, accessed December 2000)

This immunoassay was repeated for each test bleed sample to show specificity and change in titre over the immunisation period, and with a range of peptides (N/OFQ, N/OFQ-NH₂, Leu-E, Met-E, D_a, N/OFQ9, N/OFQ11, N/OFQ13, [Nphe¹], N/OFQ12-17, Noc and NalBzOH) at various concentrations to investigate cross reactivity. Cross reactivity can be observed when part of a particular epitope is shared with another, resulting in antibodies of the first epitope binding to both sequences.

8.2.1 Results

A successful ELISA protocol was determined which gave reproducible results with the Abcam antibody. Control wells were also consistent, with absorbance values in the region of 0.015 to 0.027. All wells were corrected for these i.e. the average for control wells was

subtracted from all values before any further analysis. ELISAs were used to determine change in antibody titres after immunisation and these were shown to increase with each booster injection compared to pre-immune antisera (maximum absorbance ~ 0.025). Booster immunisations generally continue until titre increase has reached a plateau but University policy does not advise more than 3 or 4 booster injections. Hence all rabbits received three boosters and only the rabbit immunised with the N/OFQ immunogen showed any adverse reaction during this study.

Antibodies are multivalent and in this case are binding monovalent haptens. This interaction is a combination of non-covalent bonds and repulsive forces, which are vital in determining specificity and discrimination between antigens. The F_{ab} hypervariable regions of paratopes (antibody combining sites) are specific for particular epitopes though interaction extends beyond these areas; there must be suitable groupings on opposing parts of the antibody and antigen with an appropriate shape, hence allowing bond formation to hold the complex together (Roitt *et al.*, 1998).

Antiserum contains many antibodies with various paratopes, which react with a variety of epitopes, or even with different parts of the same epitope. The overall binding action of these antibodies contributes to specificity. They are capable of remarkable specificity due to their ability to recognise small differences in epitopes, as well as differences in charge, optical configuration and steric conformation.

ELISAs were used to show the increase in antibody titre after each immunisation. From the antibody titre graphs (Figure 8.7), the final titres of anti-N/OFQ and Abcam antibodies were estimated to be 1/3600 and 1/529, respectively (Table 8.2). Lower titres were achieved for anti-Noc and anti-NOP antibodies (Figure 8.8), which did slightly increase with subsequent booster injections (Table 8.2). The maximum absorbance values for these antibodies binding to cysNoc (~ 0.2) and the NOP epitope (~ 0.3) respectively, were also

lower, compared to anti-N/OFQ binding to N/OFQ (~0.5) though the reason for this is not known.

TABLE 8.2 Summary of titres for all antibodies. For comparison to anti-N/OFQ, the titre of Abcam was estimated to be 1/529

Antibody	Sample		
	1 st test bleed	2 nd test bleed	3 rd test bleed
Anti-N/OFQ	1/643	1/1161	1/3600
Anti-Noc	1/228	1/286	1/333
Anti-NOP	1/247	1/305	1/333

The final bleeds of anti-N/OFQ and anti-Noc were tested for cross reactivity against serial dilutions of various endogenous and synthetic ligands. The antibodies did not cross react with any analogues of N/OFQ or homologous opioid peptides (Figure 8.9).

Anti-N/OFQ antibodies showed specificity for N/OFQ and N/OFQ-NH₂ even at low antigen concentration (5ng). Slightly higher affinity was observed for N/OFQ-NH₂ at such concentrations, presumably because these antibodies were produced against the amidated peptide. The results of the same experiment with Abcam are presented for comparative purposes and show that this antibody does indeed have high affinity for N/OFQ. In contrast with this antibody, the higher affinity is observed for the carboxyl form of this peptide (absorbance value ~0.50) than for anti-N/OFQ with N/OFQ (~0.46). This is probably because this was the form used in the synthesis of Abcam antibodies.

Anti-Noc antibodies also showed high specificity for cysNoc (Figure 8.9) even at low concentration of antigen. These antibodies would not be expected to show non-specific binding with endogenous opioids, Leu-E, Met-E and D_a, and N/OFQ as sequence homology is minimal.

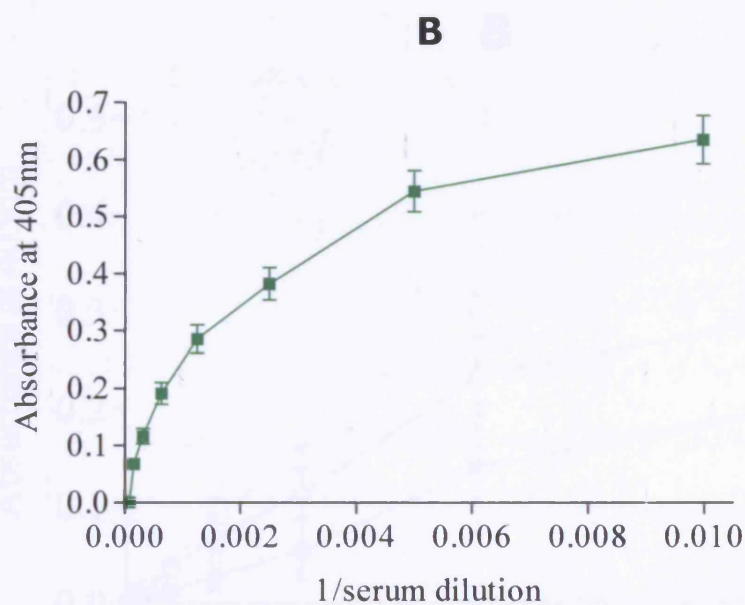
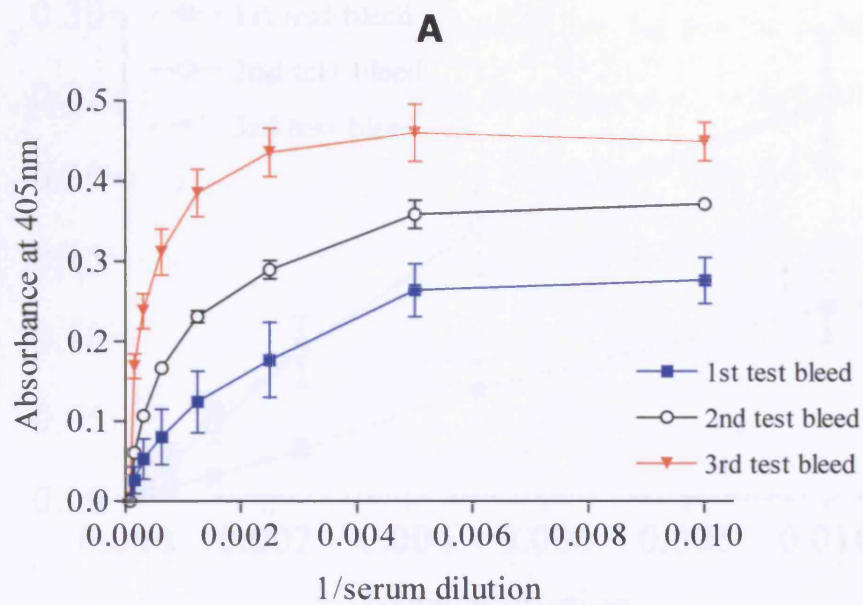


FIGURE 8.7 Increasing titres were observed with booster immunisations for anti-N/OFQ (A) antibodies tested in ELISAs using $2\mu\text{g ml}^{-1}$ N/OFQ as antigen. B shows the titre graph for Abcam antibodies. Data are mean \pm s.e.m ($n=3-5$)

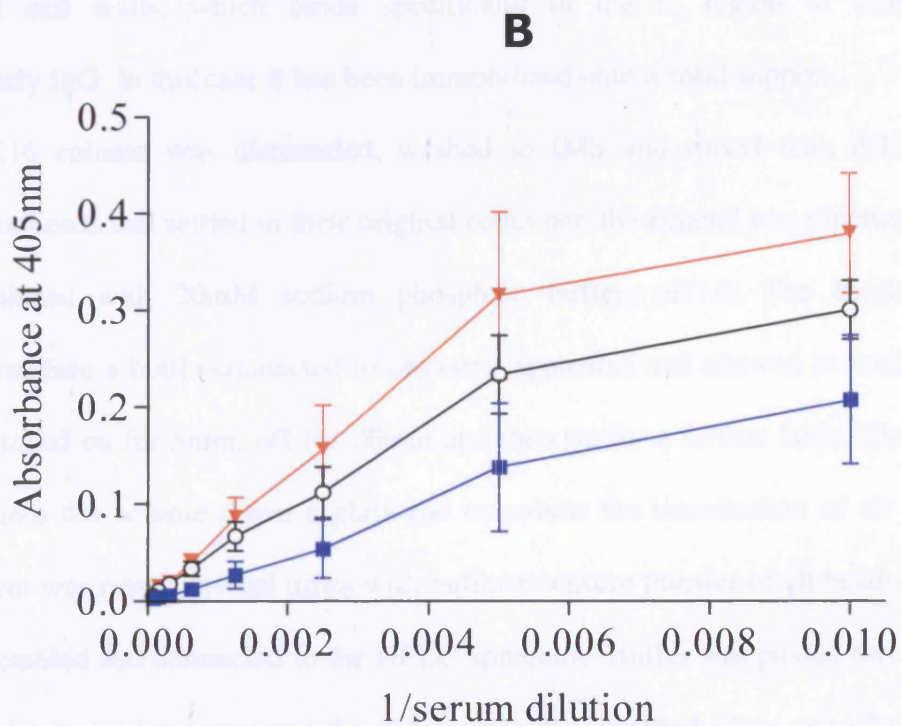
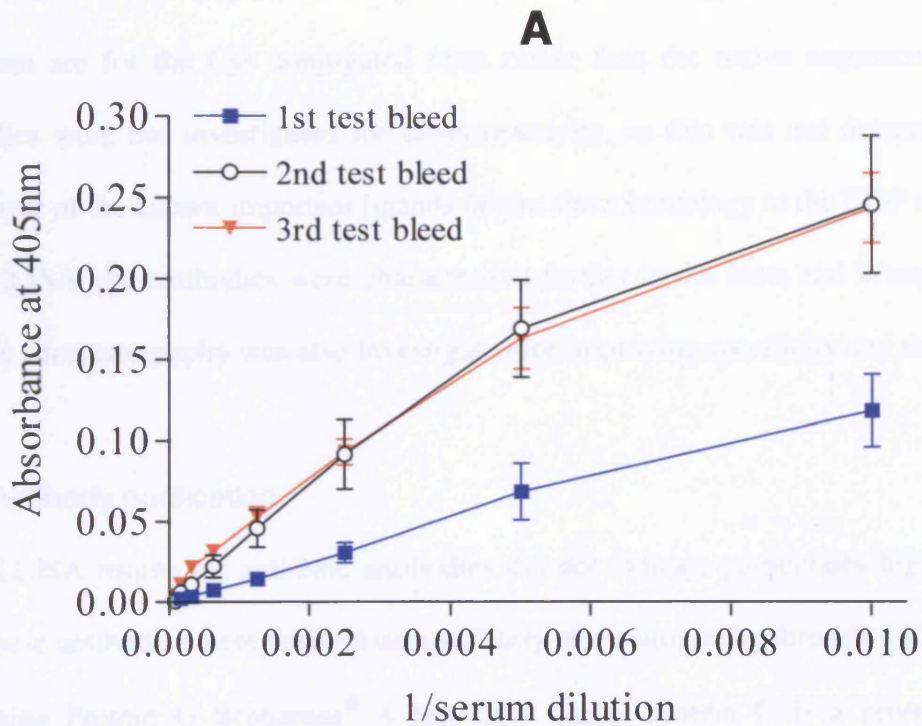


FIGURE 8.8 Increasing titres were observed with booster immunisations for anti-Noc (A) and anti-NOP (B) antibodies tested in ELISAs with $2\mu\text{g ml}^{-1}$ *cysNoc* or the NOP epitope. Data are mean \pm s.e.m ($n=3-5$)

Anti-Noc antibodies, surprisingly, also exhibited low affinity for Noc (maximum absorbance ~0.021) compared with cysNoc (~0.24). This suggests more paratopes in the antiserum are for the Cys conjugated form rather than the native sequence. Anti-NOP antibodies were not investigated for cross reactivity, as this was not deemed necessary since none of the known important ligands *in situ* show homology to the NOP epitope.

After ELISA, the antibodies were characterised further in dot blots and Western blotting. Affinity chromatography was also investigated for improving specificity and titre.

8.3 Antibody purification

Since ELISA results for anti-Noc antibodies did not indicate particularly high avidity for Noc, these antibodies were purified using affinity chromatography through a XK16 column containing Protein G Sepharose[®] 4 fast flow beads. Protein G is a protein found in bacterial cell walls, which binds specifically to the F_c region of immunoglobins, particularly IgG. In this case it has been immobilised onto a solid support.

The XK16 column was dismantled, washed in IMS and rinsed with dH₂O. Once the sepharose beads had settled in their original container, the ethanol was pipetted off and this was replaced with 20mM sodium phosphate buffer, pH7.0. The beads were then transferred into a bottle connected to degassing apparatus and allowed to settle. The pump was switched on for 5min, off for 20min and then on for a further 5min. The beads were poured into the column down a glass rod to reduce the introduction of air bubbles. All equipment was rinsed several times with buffer to ensure transfer of all beads. The column was assembled and connected to the HPLC apparatus. Buffer was passed through until the bed level remained constant and the column was then washed (flow rate ~2ml min⁻¹) with 3 bed volumes (~75ml) of buffer. A solution of 0.5% BSA in buffer was passed through the column to test the system.

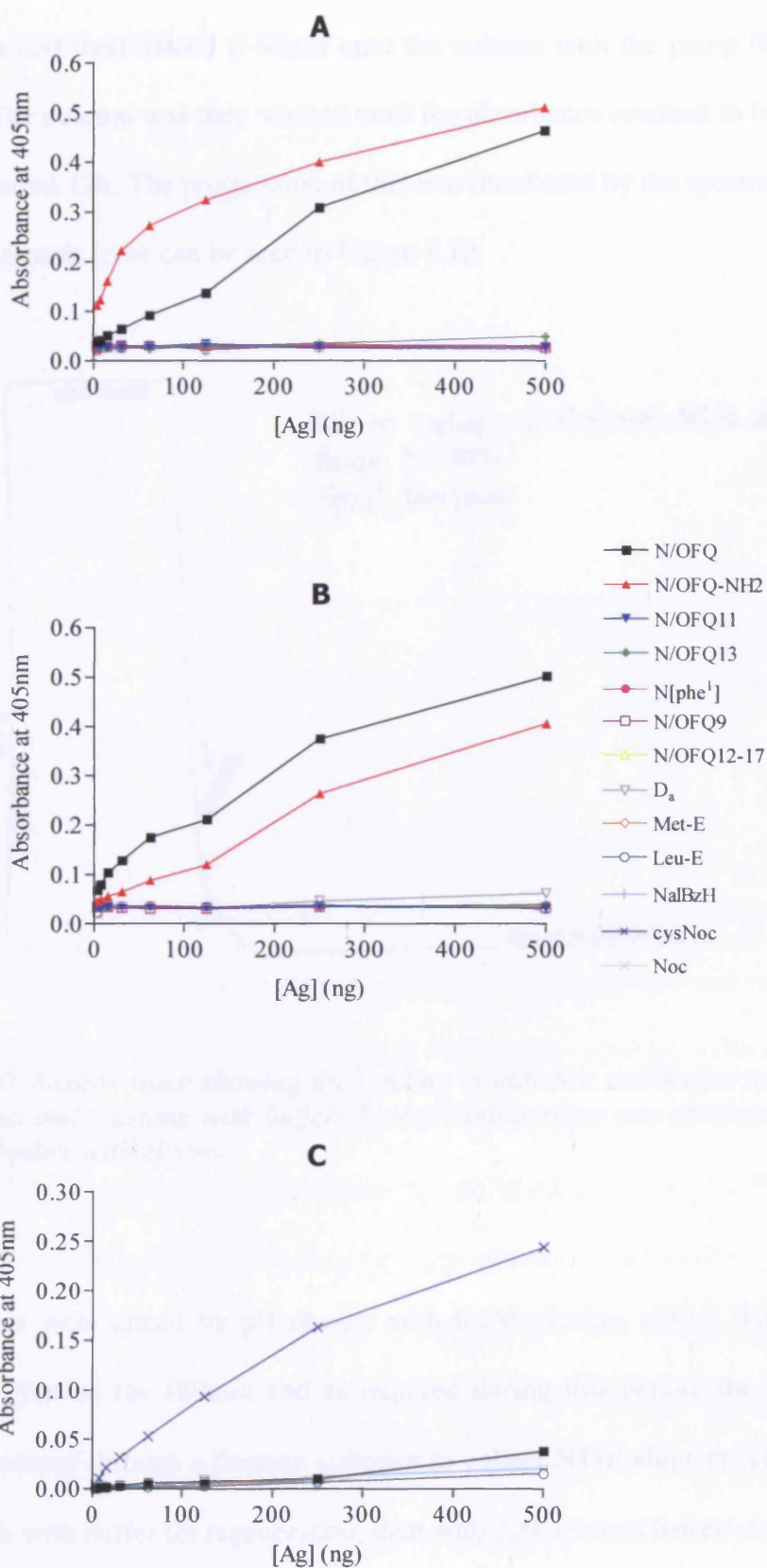


FIGURE 8.9 Cross reactivity of anti-N/OFQ (A), Abcam (B) anti-Noc (C) antibodies with a serial dilution of various antigens (Ag)

The antiserum collected for anti-Noc antibodies was filtered through 0.45µm Acrodisc syringe filters and then loaded (~50ml) onto the column with the pump flow rate set at ~2ml min⁻¹. The column was then washed until the absorbance returned to baseline, which generally required 12h. The progression of this was monitored by the spectrophotometer at 280nm and a sample trace can be seen in Figure 8.10.

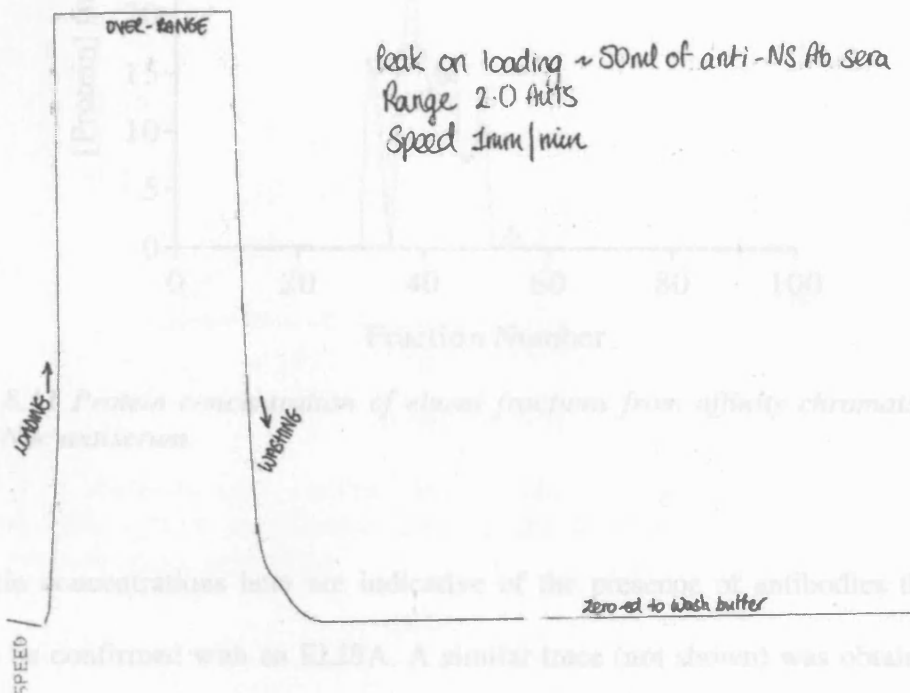


FIGURE 8.10. Sample trace showing the loading of anti-Noc antibodies to XK16 Protein G column and washing with buffer. A very similar trace was obtained on elution of the antibodies with glycine

The antibodies were eluted by pH change with 0.1M glycine, pH2.7. The column was washed with glycine for 180min and as required during this period, the outflow of the column was passed through a fraction collector to collect 500µl aliquots. The column was washed for 1h with buffer for regeneration, then with 20% ethanol before storing at 4°C. 100µl 1M Tris was added to each fraction to neutralise glycine and protect the antibodies. The elution trace was similar to that for loading in Figure 8.10. A protein assay was carried

out on the fractions to determine protein concentration (Figure 8.11) and they were also assayed for antibody specificity using an ELISA.

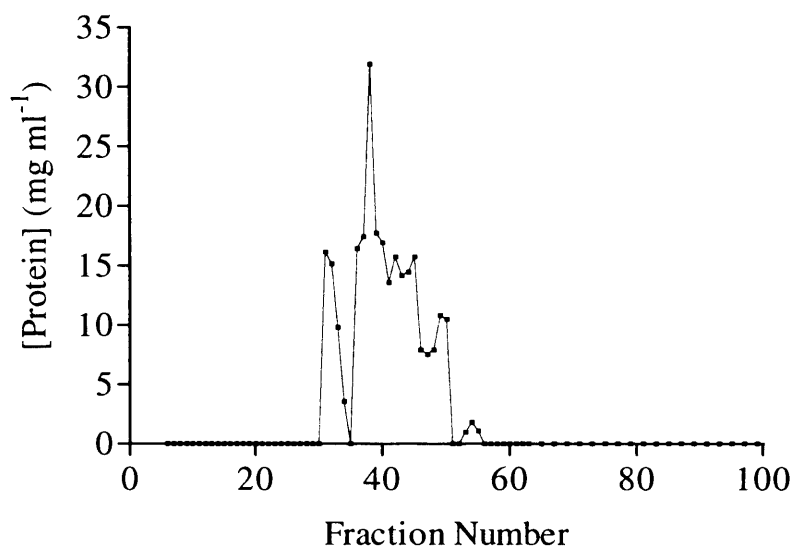


FIGURE 8.11 Protein concentration of eluted fractions from affinity chromatography of anti-Noc antiserum

The protein concentrations here are indicative of the presence of antibodies though this needed to be confirmed with an ELISA. A similar trace (not shown) was obtained for the ELISA results showing that the fractions did indeed contain antibody. The waste from the elution period i.e. liquid collected after the first 100 fractions, was also tested and the absorbance values were found to be similar to the blank controls - 0.027 compared to 0.024, respectively indicating that the waste did not contain any antibodies.

An ELISA against cysNoc was carried out comparing the final bleed sample (i.e. before purification) of anti-Noc antibodies with a sample after purification. Affinity purification with Protein G sepharose does indeed purify the antiserum giving a solution with higher titre than observed previously. The improvement was only small with an increase in titre from 1/333 to 1/383 (Figure 8.12). On comparing with the antibodies' avidity for Noc, this was not improved with affinity purification (Figure 8.12). These antibodies show high

affinity for the sequence against which they were raised though do not have high avidity for native rat Noc hence these are not investigated further in this thesis.

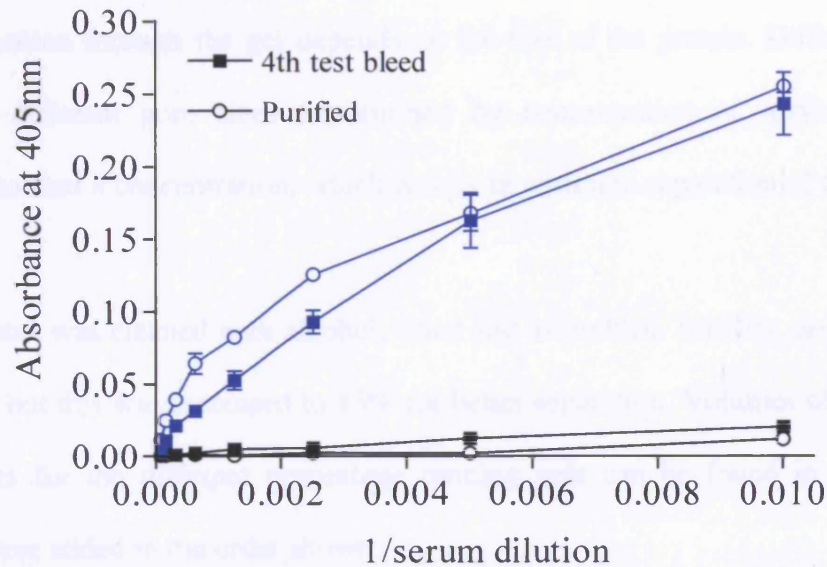


FIGURE 8.12 Antibody titre against *cysNoc* (blue) of anti-Noc antibodies increased slightly after affinity purification. Low affinity is observed for Noc (black) with no improvement after purification

8.4 Western Blotting

Towbin *et al.* (1979) described a method of transferring proteins from a gel onto a nitrocellulose membrane. It was named Western blotting as it parallels the process of Southern blotting (transferring DNA from gel onto membrane). It is a useful technique for identifying and quantifying proteins in a mixture; the molecular weights of these can also be determined. Here, the main objective was to further test and confirm the specificity of the produced antibodies. Before labelling with an antibody, the proteins must be separated using SDS PAGE and transferred to a nitrocellulose membrane. A semi-dry blot was used for the transfer.

8.4.1 SDS PAGE

Gel polymerisation is a chain reaction initiated by APS and TEMED. This process is inhibited by oxygen hence the need for butanol (see below) and freshly made solutions. The samples are denatured prior to separation and bind SDS in a manner proportional to the molecular weight of the protein. This gives the polypeptides a negative charge and hence migration through the gel depends on the size of the protein. Different percentage gels have different pore sizes (determined by concentration of acrylamide) so it is necessary to find a concentration, which results in optimum separation of the bands on the gel.

Gel apparatus was cleaned with alcohol, dried and assembled. Initially, an 8% running gel was tested but this was increased to 15% for better separation. Volumes of the appropriate components for the different percentage running gels can be found in Table 8.3. The reagents were added in the order shown.

TABLE 8.3 Composition of different percentage running gels (total volume 10.01ml)

Component	Percentage Gel		
	8%	12%	15%
Protogel (ml)	2.67	4.0	5.0
PAGE B (ml)	2.5	2.5	2.5
10% SDS (µl)	100	100	100
dH ₂ O (ml)	4.63	3.3	2.3
10% APS (µl)	100	100	100
TEMED (µl)	10	10	10

(PAGE B 1.5M Tris base pH 8.8)

APS was made fresh for each experiment and stored at 4°C. The running gel was mixed well and poured into the gel mould. 200µl water-saturated butanol was added to the top and the gel allowed to set before washing three times with dH₂O and blotting dry with

filter paper. The 4.5% stacking gel was then made using the volumes as shown in Table 8.4.

TABLE 8.4 Composition of 4.5% stacking gel (total volume 10.01ml)

Component	4.5% Gel
Protogel	1.5ml
PAGE D	2.5 ml
10% SDS	100µl
dH ₂ O	5.8 ml
10% APS	100µl
TEMED	10µl

(PAGE D 0.5M Tris base pH 6.8)

The components were combined and mixed well before pouring on top of the running gel and slowly inserting a 10mm 8 well comb. When the stacking gel had set, the comb was carefully removed and the gel washed three times with dH₂O. The gel was then secured into the electrophoresis tank and the tank filled with running buffer (section 2.2). Samples of peptides and cell membrane preparations were diluted to the appropriate protein concentration (~15µg) in loading buffer (section 2.2) before boiling in a water bath at 100°C for 5min. This buffer contained glycerol, which increases the density of the samples and so helps them to 'sink' to the well bottom and also bromophenol blue, which migrates with the electrophoresis front. The samples and SeeBlue pre-stained markers (Table 8.5) were loaded using gel loading tips (10µl per well) and electrophoresis carried out at 170V, ~0.38mA for approximately 90min or until dye front was 2-3mm from bottom of gel.

TABLE 8.5 Molecular weight (M_r) of SeeBlue markers used in SDS PAGE. N/OFQ and NOP are included for comparative purposes

Marker	M_r (kDa)
Myosin	250
BSA	98
Glutamic Dehydrogenase	64
Alcohol Dehydrogenase	50
NOP	~45.7
Carbonic Anhydrase	36
Myoglobin	30
Lysozyme	16
Aprotinin	6
Insulin, B chain	4
N/OFQ	~2.4

8.4.2 Immunoblotting

Before proceeding with Western blotting as described below, several dot blots were carried out to check antibody-antigen interactions and to optimise antibody dilutions and visualisation. These involved applying 15 μ l (3 μ l at a time and allowing to dry in between) of the peptides, N/OFQ, cysNOP and the NOP epitope, or CHO_{hNOP} membranes to nitrocellulose and then labelling this with primary and secondary antibodies as described below.

The gel was removed from the electrophoresis tank and placed into transfer buffer (section 2.2). Six filters and a piece of nitrocellulose membrane were cut to the size of the gel before soaking in transfer buffer and dH₂O, respectively. A Western blot sandwich was assembled as in Figure 8.13, pressed gently to remove air bubbles and placed into a semi-dry blotter at 6V, 60mA for 2.5h at 22°C.

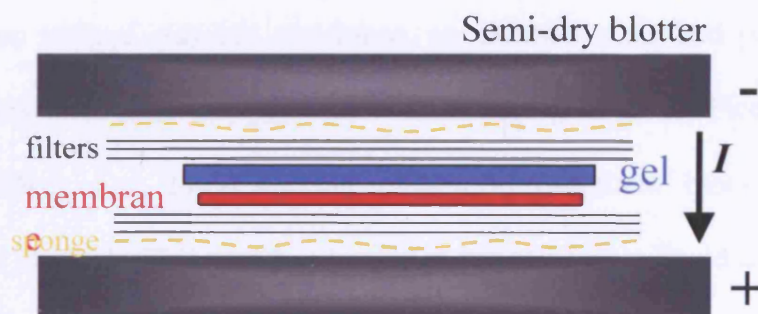


FIGURE 8.13 A Western blot sandwich

After semi-dry blotting, if required, gels could be stained in Brilliant Blue (0.25g in 45% dH₂O; 45% methanol; 10% glacial acetic acid) overnight to check for successful transfer of the proteins to the membrane. Gels were destained in 45% dH₂O, 45% methanol, 10% glacial acetic acid for ~6h. Another technique giving more rapid results was to stain the membrane with Ponceau S for ~30min, resulting in pink bands of protein on the nitrocellulose. This stain is reversible if incubated in excess dH₂O for ~30min allowing the Western blot to be continued without delay.

The nitrocellulose was blocked for 16h at 4°C in blocking buffer (section 2.2) with shaking (increases system efficiency). Sufficient volume should be added to ensure that the membrane does not dry out. The primary antibody (anti-N/OFQ or anti-NOP) at 1/2000 dilution in blocking buffer was added for 1h at room temperature with shaking. Six 10min washes in TBS with Tween-20 (TBST) followed before further 1h incubation with goat anti-rabbit secondary (AP conjugated if using BCIP/TNBT, or HRP conjugated for SuperSignal[®] West Pico chemiluminescent substrate) antibody at appropriate dilution in blocking buffer at room temperature with shaking. Six further 10min washes with TBST preceded incubation with the appropriate substrate.

A colorimetric method using BCIP/TNBT substrate was initially tested. Approximately 3-4ml (sufficient to cover) of BCIP/TNBT solution was added to the membrane and this then incubated in the dark for 15min. The membrane was then washed with copious dH₂O and any blue bands were noted as specific binding of the primary antibody.

As the above method was not consistent, an alternative method was optimised. The membrane was incubated for 5min with ~4ml SuperSignal[®] West Pico chemiluminescent substrate (Walker *et al.*, 1995) working solution (~0.125ml/cm² blot of equal volumes of enhancer and luminol). This was then blotted to remove excess liquid and wrapped in cling film before exposing to Hyperfilm[™] MP[™] in a film cassette. Exposure time initially was

5min and was then optimised to 1-5min. The film was then developed using an Amersham Hyperprocessor. The light generated with this substrate lasts for up to 8h, and the blot could be stripped and re-labelled if necessary. Any bands observed correspond to the specific binding of the primary antibody to the target protein. The gel, membrane and film were scanned and saved as a digital image.

8.4.3 Results

Running gels of 8 (Figure 8.14) and 12% did not give 9 bands for the markers, as separation was not sufficient. A 15% gel (Figure 8.15) separated the bands further particularly in the region of bands 4 and 5 where the band for the NOP receptor ($M_r \sim 45,500$) should lie. Resolution is not important here since this technique is being used to confirm specificity of antibodies rather than to determine actual M_r of NOP. Gels were stained to show successful transfer of protein (Figure 8.15) before continuing with immunoblotting.

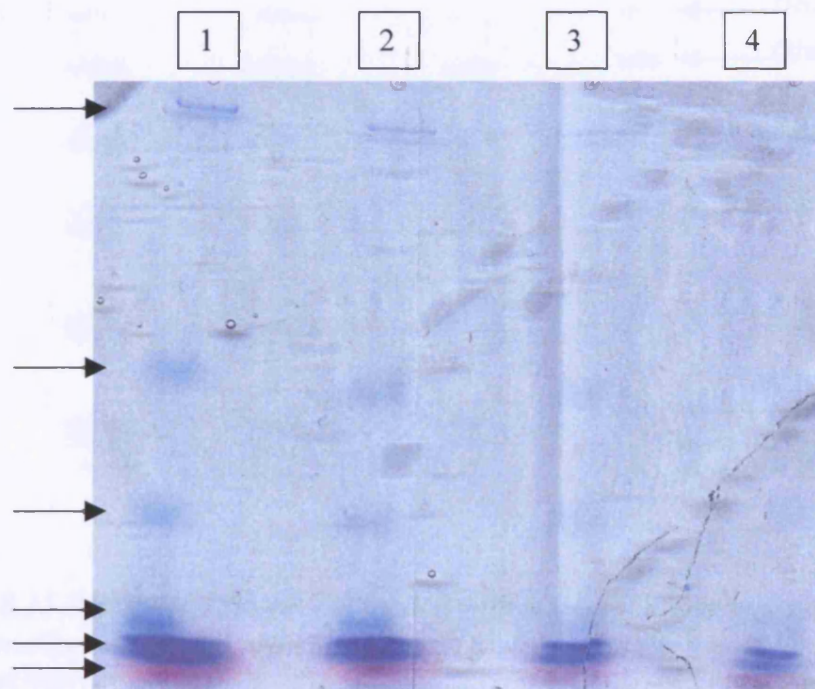


FIGURE 8.14 A 8% running gel did not separate the bands of the molecular markers sufficiently as only 6 bands (shown by arrows) are visible. Lanes 1 – 4 contain 20, 15, 10 and 5 µl of markers, respectively

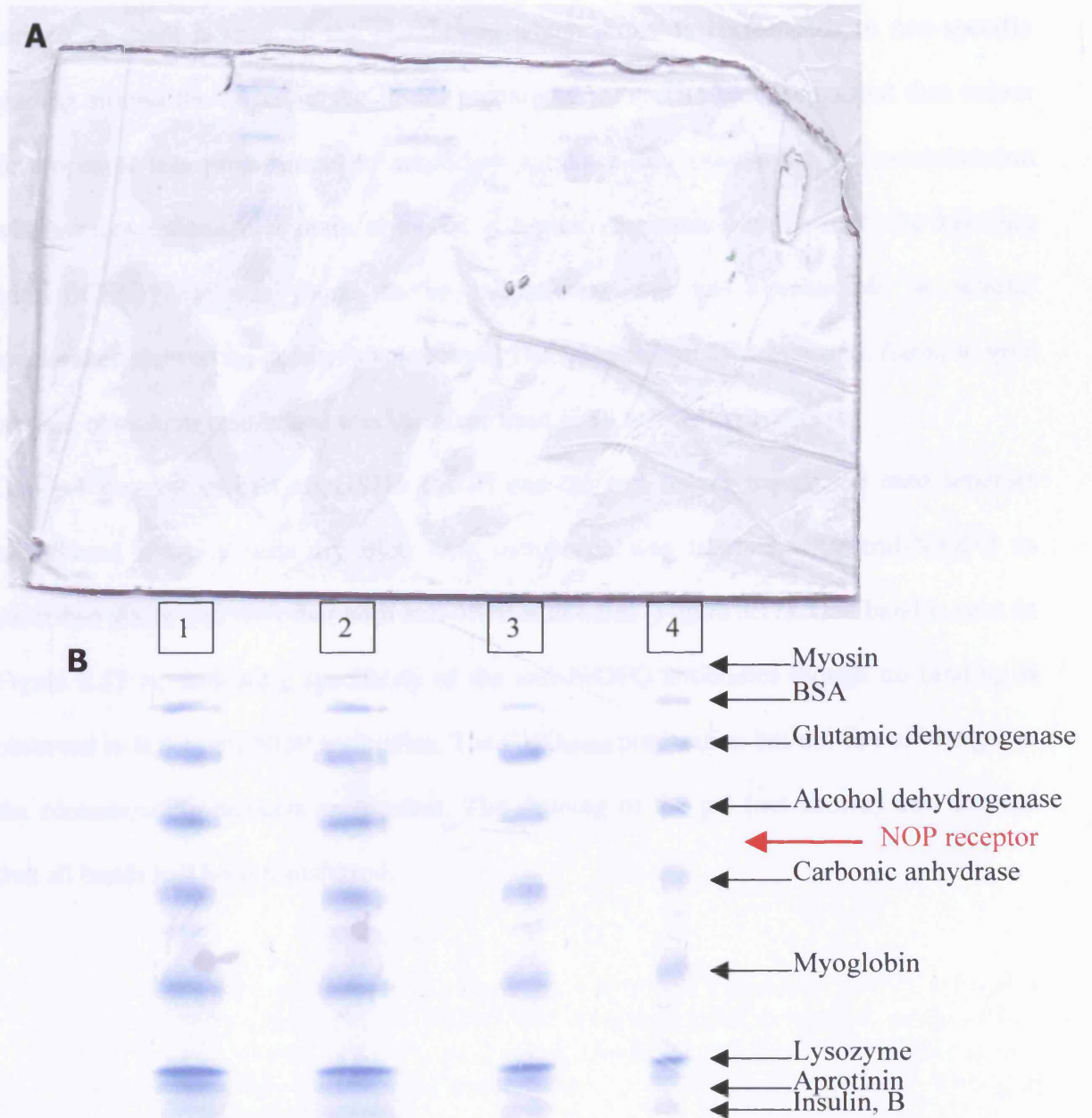


FIGURE 8.15 Picture of 15% gel (A) loaded with markers in four lanes and membrane (B) illustrating transfer of proteins. Lanes 1 – 4 contain 20, 15, 10 and 5 μ l of markers, respectively

Dot blots confirmed the specificity (Figure 8.16) of the antibody-antigen interactions; anti-N/OFQ for N/OFQ (15 μ g) and anti-NOP for cysNOP epitope (7.5 μ g). However, the anti-NOP antibodies did not show any binding to CHO_{hNOP} preparation even with 40.5 μ g antigen. A mark is seen on the membrane, which probably corresponds to non-specific binding around the edges of the initial preparation blot. The blots suggested that colour development was proportional to secondary antibody dilution and antigen concentration with a more intense blue stain observed at higher concentrations. Overall, the labelling with BCIP/TNBT was found to be inconsistent and non-reproducible as several membranes showed no colour development. The SuperSignal kit was tested, found to give precise, consistent results and was therefore used in all further experiments.

One gel was cut in half after SDS PAGE and the two halves transferred onto separate membranes using a semi-dry blot. One membrane was labelled with anti-N/OFQ as described above and the other with anti-NOP antibodies (Figure 8.17). One band is seen in Figure 8.17 A, indicating specificity of the anti-N/OFQ antibodies though no binding is observed in B for anti-NOP antibodies. The CHO_{hNOP} preparation has not run off the gel as the corresponding markers are present. The staining of the gel (not shown) also showed that all bands had been transferred.

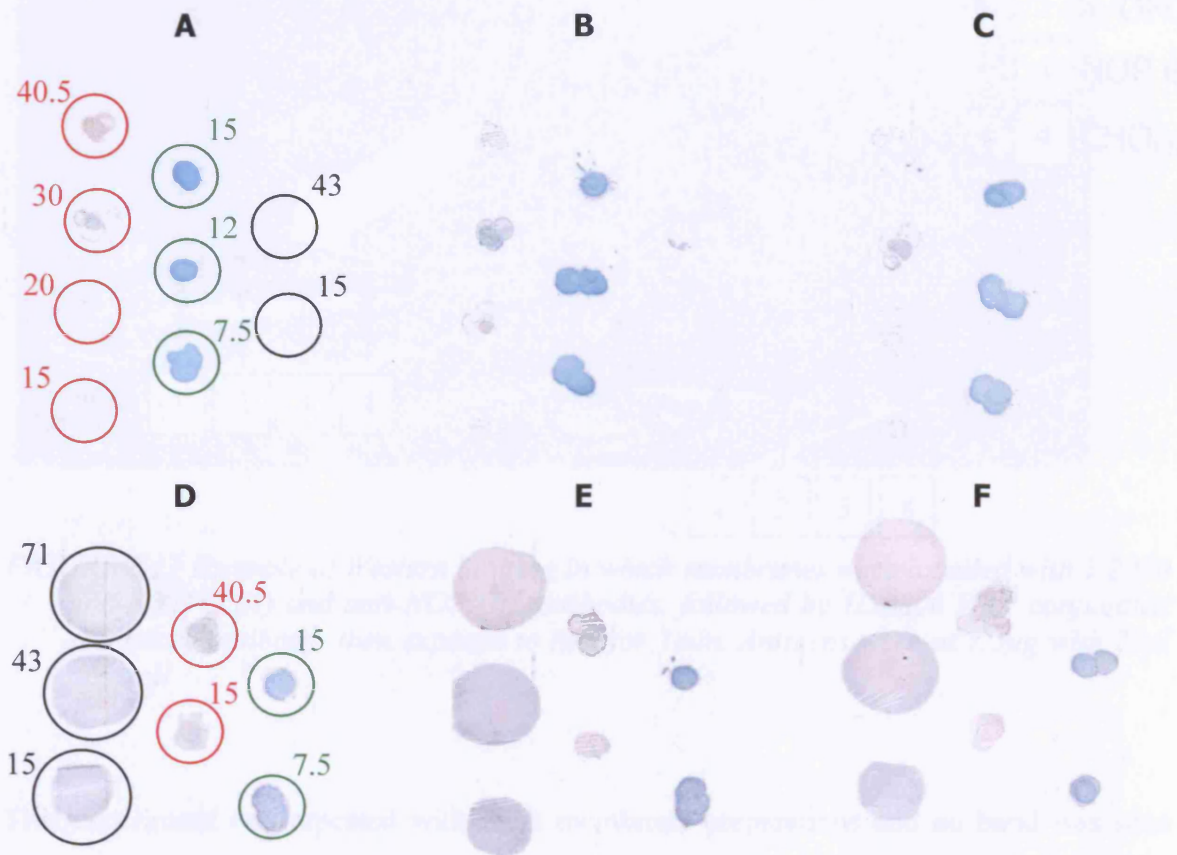


FIGURE 8.16 Dot blotting showing binding of anti-NOP (A-C) and anti-N/OFQ antibodies (D-F). Primary antibody was 1/2000 and AP-conjugated secondary antibody was varied from 1/10000, 1/20000 and 1/50000 (from left to right). Red circles denote CHO_{hNOP} membrane preparation, green denotes cysNOP epitope and black N/OFQ at the concentrations (μg) noted

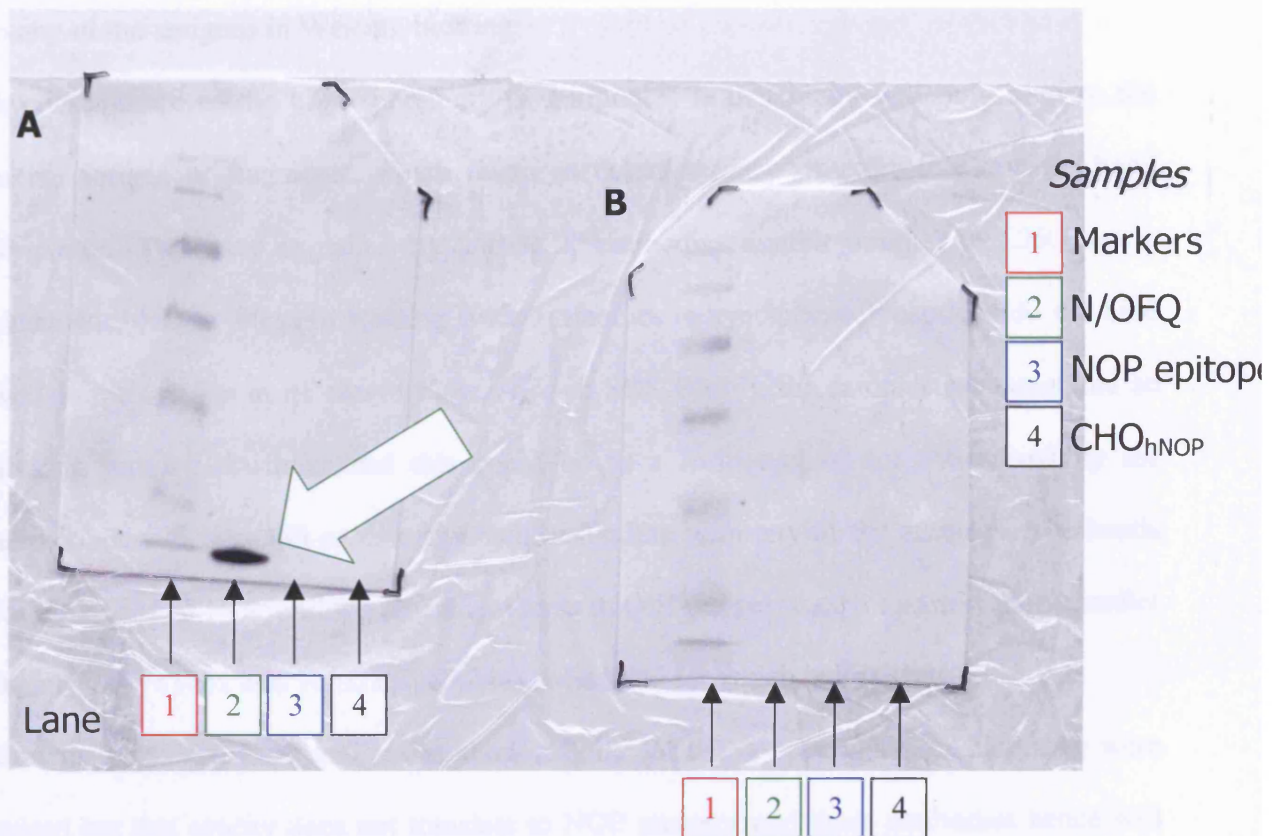


FIGURE 8.17 Example of Western blotting in which membranes were labelled with 1/2000 anti-N/OFQ (A) and anti-NOP (B) antibodies, followed by 1/50000 HRP conjugated secondary antibody, then exposed to film for 1min. Antigens were at 7.5 μ g with 20 μ l per well

This experiment was repeated with fresh membrane preparations and no band was seen corresponding to anti-NOP binding to the NOP epitope or CHO_{hNOP} though positive results were consistent for anti-N/OFQ antibodies. Hence anti-N/OFQ antibodies were used to investigate N/OFQ distribution *in situ* in a series of IHC studies on whole dog brain sections.

No explanation is obvious regarding the lack of binding of anti-NOP antibodies. Further Western blots were carried out, also including a sample of cysNOP and still no bands were observed for anti-NOP antibodies. The antiserum obviously contains various paratopes and

these bind to the NOP epitope and cysNOP in ELISAs and dot blots, respectively, but not to any of the antigens in Western blotting.

A consequence of the high specificity of antibodies is that many will only bind to the native antigen or fragments, which retain sufficient tertiary structure to allow for bond formation. This may explain why anti-NOP antibodies exhibit binding to CHO_{hNOP} in either dot blots or Western blotting since antibodies to synthetic polypeptides do not bind well to the antigen in its native form. Also in SDS PAGE, the samples are denatured so altering tertiary structure, and this could be to a form that is not recognised by the antibodies, which would explain the lack of binding with any of the antigens. The bands for cysNOP and NOP epitope also might have run off the gel since they are slightly smaller than N/OFQ (1752 and 1631, respectively), the band for which is just seen.

Conclusively, anti-NOP antibodies show affinity for the epitope against which they were raised but this avidity does not translate to NOP receptor and these antibodies hence will not recognise native recombinant NOP receptors in any of the described techniques. Anti-NOP antibodies are not investigated further in this thesis.

8.5 Immunohistochemistry

This technique is similar in principle to an ELISA though captures target antigen in whole tissue sections. The method described here uses anti-N/OFQ antibodies to label N/OFQ in whole dog brain sections and is a modification of that described in the booklet for the DAKO EnvisionTM+ System, Peroxidase (DAB) kit for rabbit polyclonals. This system uses a two-step indirect staining technique based on a HRP labelled polymer, which is conjugated to the secondary anti-rabbit antibody.

Whole dog brain sections were cut as described in section 6.6 and stored at -20°C overnight. These were then air-dried for 2h at room temperature. Using a hydrophobic pen,

a reservoir was created around each section as required and the sections then fixed in acetone for 10min. To each section, 7 drops (only 1 or 2 drops required for rat and control sections) of Peroxidase Block (bottle 1 from Dako kit) were added and the slide tilted gently to ensure all tissue was covered. This was incubated for 5min before rinsing in dH₂O and then IHC buffer (section 2.2). The primary antibody solution (in antibody buffer (section 2.2), with or without N/OFQ) was added to each section (1ml for dog brain, 200µl for rat or 100µl for controls) for 30min before rinsing in IHC buffer. 7 drops (1 or 2 drops for rat/control) of the Labelled Polymer (bottle 2) were then applied to the dog sections for 30min. The sections were rinsed with IHC buffer before adding 650µl of the DAB+ Substrate-chromogen (ratio of 1ml bottle 3a + 1 drop or ~20µl bottle 3b) for 5min. Further rinsing with dH₂O followed before counterstaining in haematoxylin for ~45s. Excess stain was removed with copious dH₂O and the sections allowed to dry. Sections were dehydrated and mounted as in section 6.7.1. Pictures were then taken using a Nikon D1x camera. Images were cropped and unsharpened using Adobe Photoshop version 7.

8.5.1 Results

The positive labelling of N/OFQ appears as a brown stain within the tissue sections. Initial experiments compared various dilutions of primary antibody, and also incubation times of DAB and haematoxylin. Initially, random dog brain sections were labelled with primary antibody dilutions of 1/500, 1/1000 and 1/2000 (Figure 8.18). Panels C and D of this figure show that both anti-N/OFQ and Abcam antibodies labelled the sections at the low dilution of 1/2000, with a similar distribution of positive stain. The positive stain appears more apparent in the sections labelled with anti-N/OFQ antibody though this is not indicative of higher specificity as the protein concentrations of the two solutions may differ.

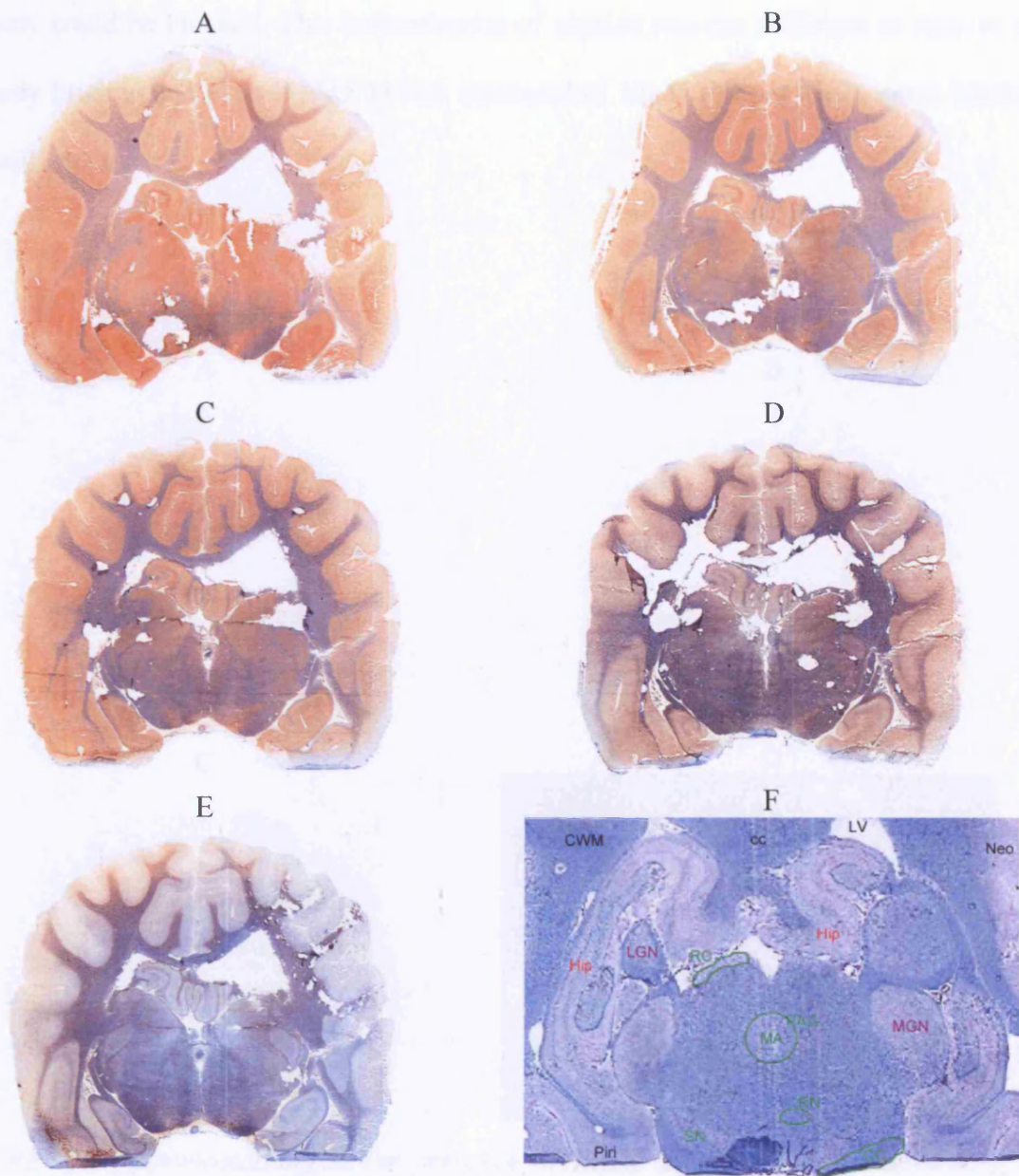


FIGURE 8.18 Various dilutions of primary anti-N/OFQ and Abcam antibodies exhibit staining in IHC corresponding to N/OFQ. A - C anti-N/OFQ at dilutions of 1/500, 1/1000 and 1/2000, respectively; D, Abcam at 1/2000; E, control (no primary antibody) and F, brain atlas on a haematoxylin/eosin stained section showing main areas of interest

cc, corpus callosum; CC, crus cerebri; CWM, cerebral white matter; Hip, hippocampus; LGN, lateral geniculate nucleus; LV, lateral ventricles; MA, mesencephalic aqueduct; MGN, medial geniculate nucleus; Neo, neocortex; PAG, periaqueductal grey; Piri, piriform cortex; RC, rostral colliculus; RN, red nucleus; SN, substantia nigra

Further immunolabelling in the presence of $1\mu\text{M}$ N/OFQ showed that the binding of the antibody could be blocked. This concentration of peptide was not sufficient to remove all antibody binding and even if N/OFQ was increased to $10\mu\text{M}$ (Figure 8.19), some binding was still apparent.

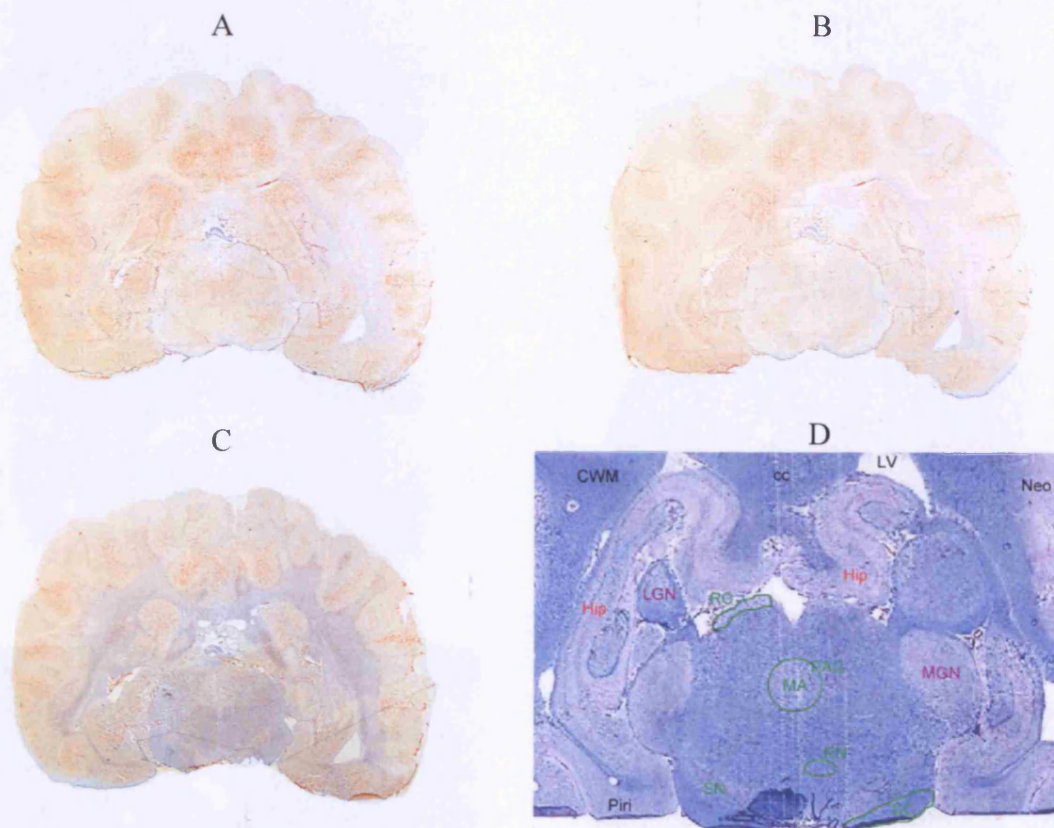


FIGURE 8.19 Immunostaining in the presence of $10\mu\text{M}$ N/OFQ (B) reduces binding of anti-N/OFQ antibodies at $1/10000$ (A). C is control (no primary antibody) and D, brain atlas on a haematoxylin/eosin stained section showing main areas of interest
 cc, corpus callosum; CC, crus cerebri; CWM, cerebral white matter; Hip, hippocampus; LGN, lateral geniculate nucleus; LV, lateral ventricles; MA, mesencephalic aqueduct; MGN, medial geniculate nucleus; neo, Neocortex; PAG, periaqueductal grey; Piri, piriform cortex; RC, rostral colliculus; RN, red nucleus; SN, substantia nigra

The incubation time for the DAB substrate was investigated. All incubation times produced positive DAB staining however brown precipitate was also observed with the longer period (9min). An incubation time of 5min was therefore the optimum length

(Figure 8.20). Therefore in all future IHC experiments, the following were used: a primary antibody dilution of 1/2000 and 5min incubation for DAB substrate.

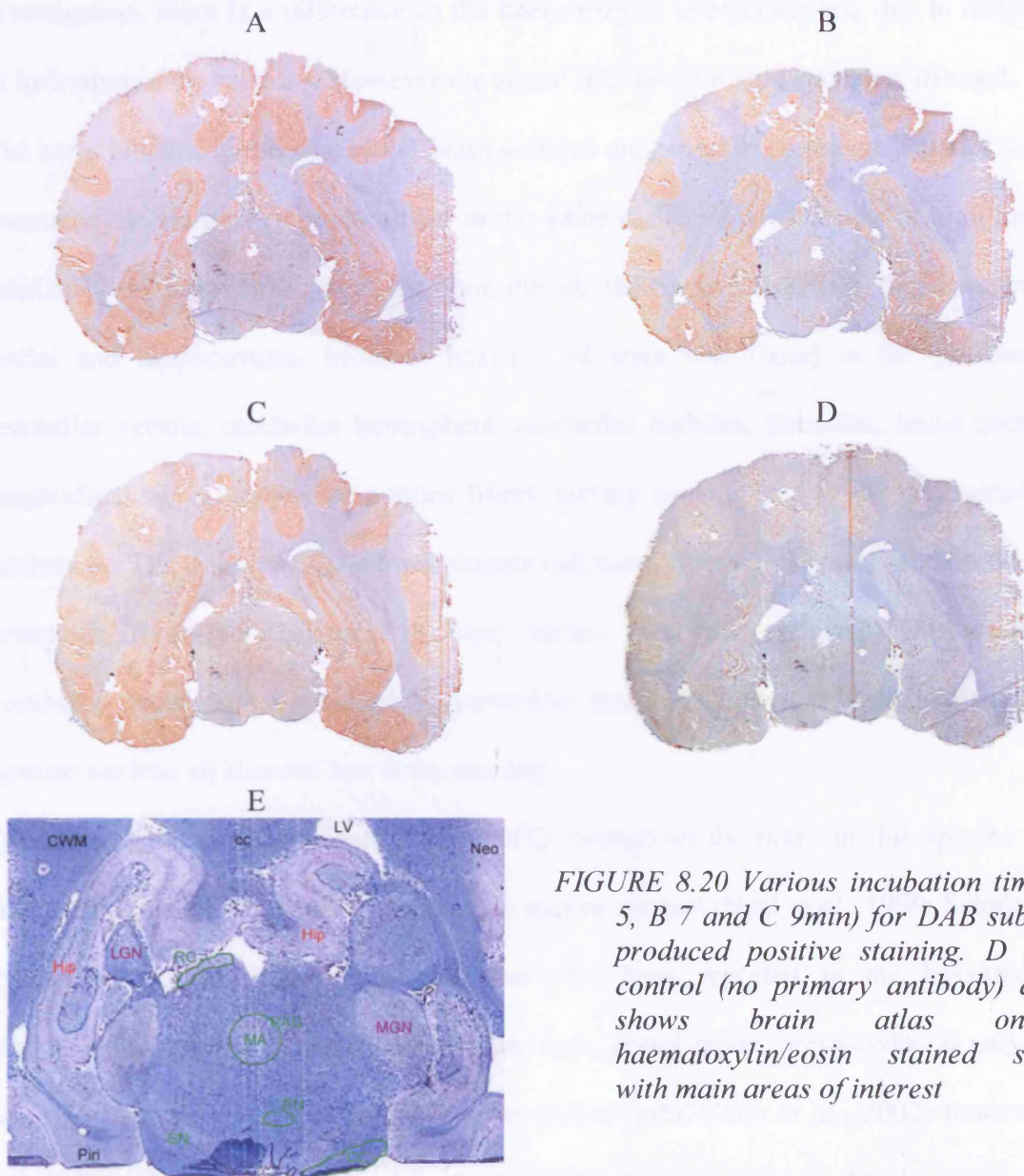


FIGURE 8.20 Various incubation times (A 5, B 7 and C 9min) for DAB substrate produced positive staining. D shows control (no primary antibody) and E shows brain atlas on a haematoxylin/eosin stained section with main areas of interest

cc, corpus callosum; CC, crus cerebri; CWM, cerebral white matter; Hip, hippocampus; LGN, lateral geniculate nucleus; LV, lateral ventricles; MA, mesencephalic aqueduct; MGN, medial geniculate nucleus; neo, Neocortex; PAG, periaqueductal grey; Piri, piriform cortex; RC, rostral colliculus; RN, red nucleus; SN, substantia nigra

IHC with anti-N/OFQ antibodies of whole dog brain sections throughout the brain can be found in Figure 8.21. The brown stain due to antibody labelling indicates the presence of N/OFQ and illustrates its distribution throughout the brain. The stain varies in intensity

according to the amount of primary and hence secondary antibody bound. This is not considered further as these studies aimed to determine relative peptide distribution rather than quantify actual amount. Unfortunately as the slides were split into two batches for investigation, there is a difference in the haematoxylin counterstaining due to differences in hydration of the sections. However the actual IHC labelling has not been affected.

The areas labelled in the whole dog brain sections are generally in the grey matter with the haematoxylin stain more predominant in the white matter regions. Areas of high intensity labelled consistently throughout the brain include the cortex, amygdala, thalamus, caudate nuclei and hippocampus. Medium intensity of stain was found in the putamen, the cerebellar vermis, cerebellar hemisphere, cerebellar nodulus, flocculus, locus coeruleus, longitudinal fibres, transverse pontine fibres, olivary nucleus, and in the parasympathetic nucleus X. The pallidum, claustrum, corpus callosum, internal capsule, caudal colliculus, ventricles, fornix, epithalamus, cochlear nuclei, cerebellar peduncle, choroid plexus, vestibular nuclei, spinal tract of V, pyramidal tract, reticular formation and the lateral cuneate nucleus all showed low or no staining.

This indicates a wide distribution of N/OFQ throughout the brain in this species and is consistent for immunoreactivity reported in murine species (Neal *et al.*, 1999; Schulz *et al.*, 1996). N/OFQ-like immunoreactivity has also been reported in the hypothalamus, hippocampus, cerebral peduncle, substantia nigra, dorsal raphe, periaqueductal grey, locus coeruleus and trapezoid nucleus of the Mongolian gerbil (Kim *et al.*, 2002) however this group did administer colchicine into the lateral ventricle to intensify levels observed, and N/OFQ has even been localized in the cerebral ganglia of snails (Leon-Olea *et al.*, 2001).

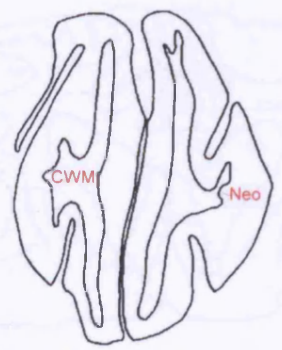
18



44



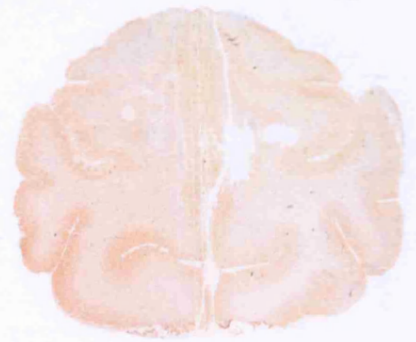
64



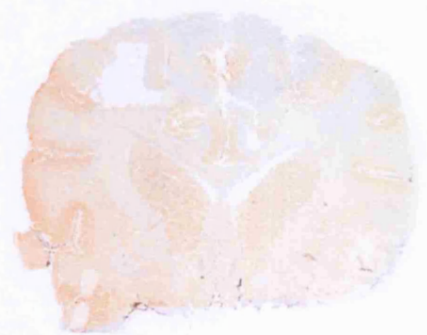
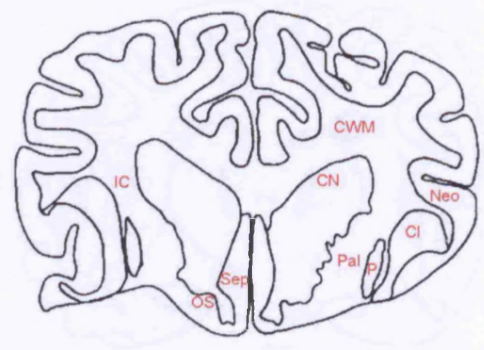
69



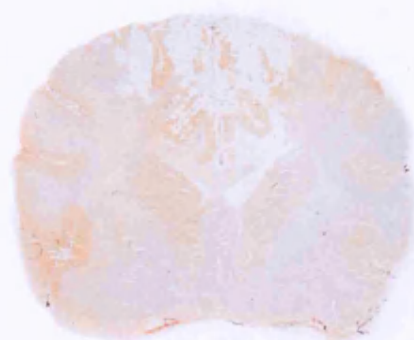
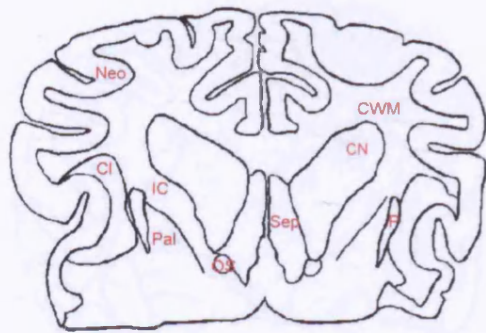
79



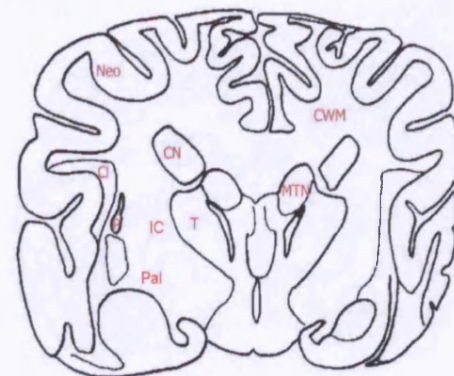
110



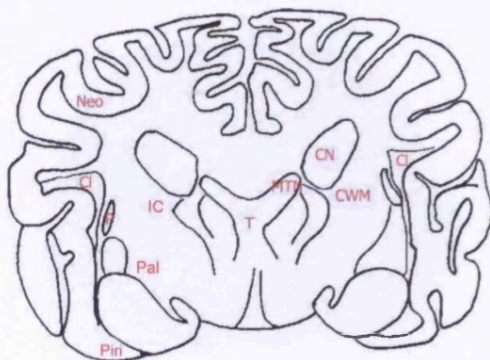
120



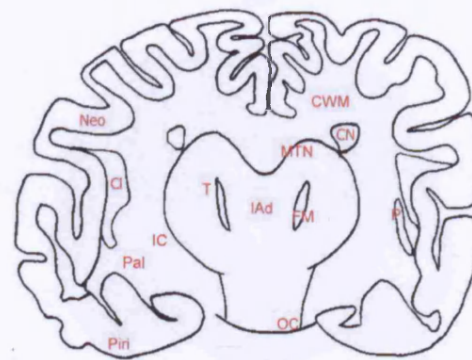
123



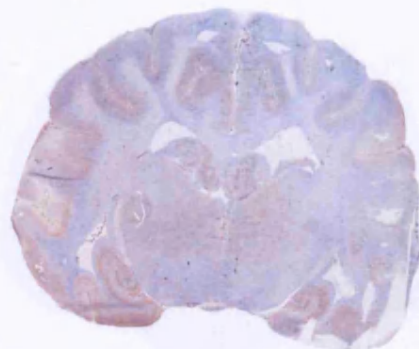
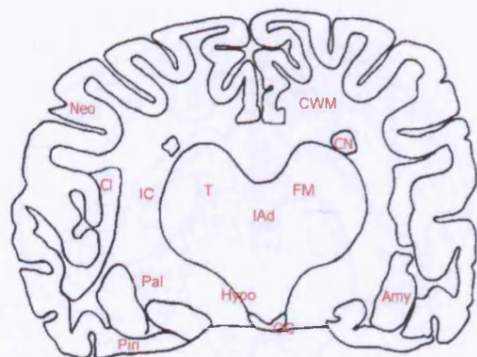
140



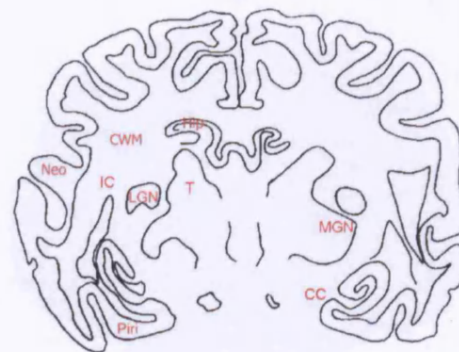
145



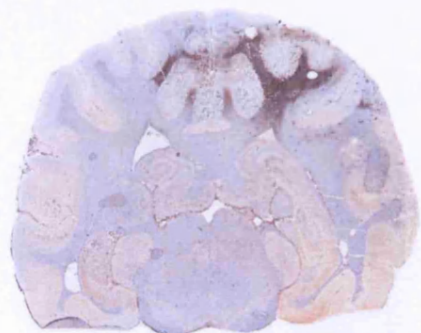
163



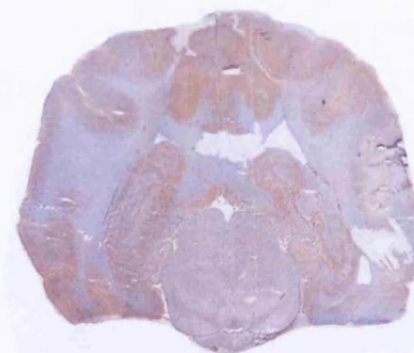
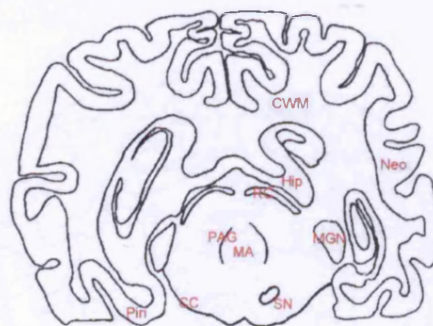
180



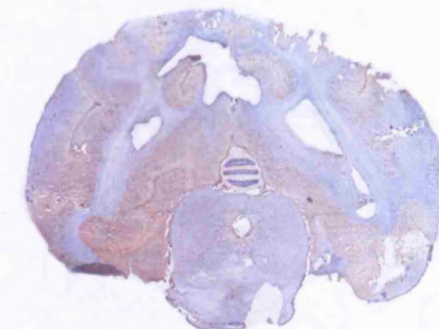
187



200

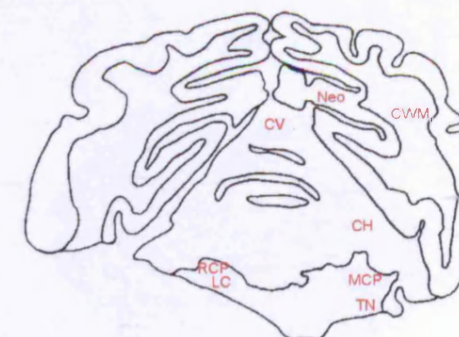
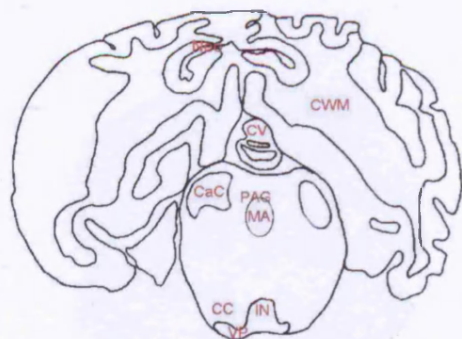


203



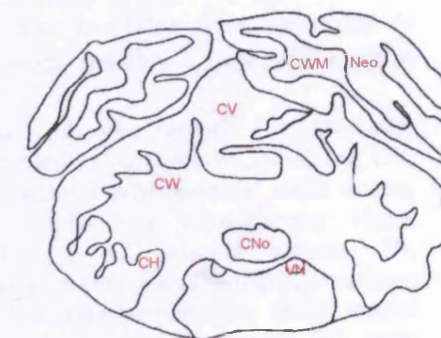
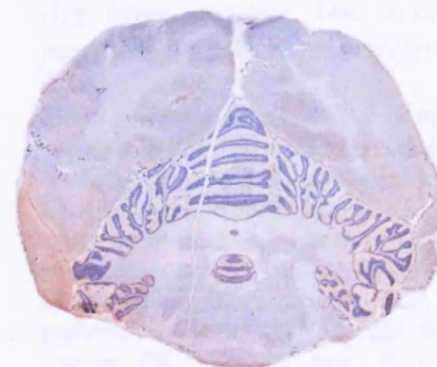
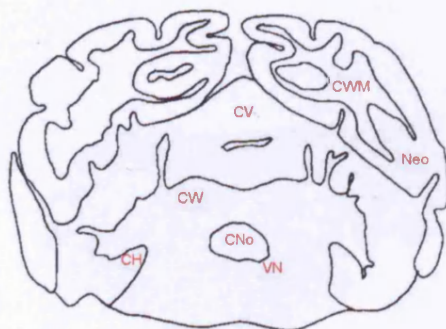
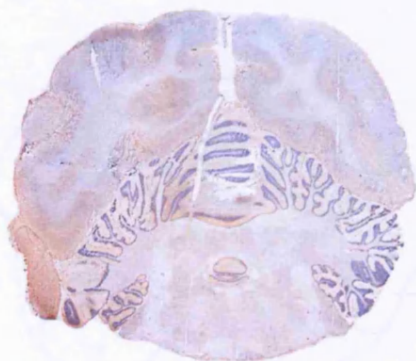
218

221



243

253



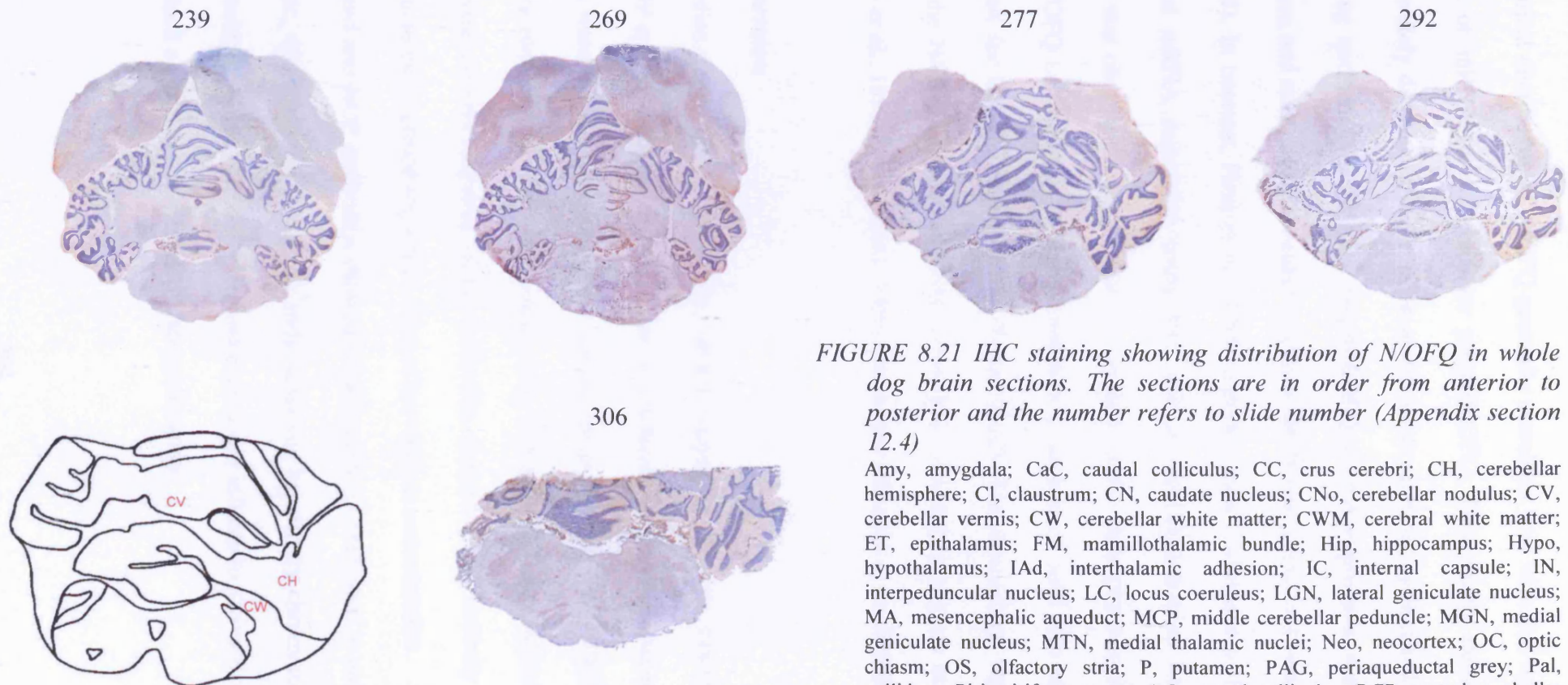


FIGURE 8.21 IHC staining showing distribution of N/OFQ in whole dog brain sections. The sections are in order from anterior to posterior and the number refers to slide number (Appendix section 12.4)

Amy, amygdala; CaC, caudal colliculus; CC, crus cerebri; CH, cerebellar hemisphere; Cl, claustrum; CN, caudate nucleus; CNo, cerebellar nodulus; CV, cerebellar vermis; CW, cerebellar white matter; CWM, cerebral white matter; ET, epithalamus; FM, mamillothalamic bundle; Hip, hippocampus; Hypo, hypothalamus; IAd, interthalamic adhesion; IC, internal capsule; IN, interpeduncular nucleus; LC, locus coeruleus; LGN, lateral geniculate nucleus; MA, mesencephalic aqueduct; MCP, middle cerebellar peduncle; MGN, medial geniculate nucleus; MTN, medial thalamic nuclei; Neo, neocortex; OC, optic chiasm; OS, olfactory stria; P, putamen; PAG, periaqueductal grey; Pal, pallidum; Piri, piriform cortex; RC, rostral colliculus; RCP, rostral cerebellar peduncle; RN, red nucleus; Sep, septum; SN, substantia nigra; T, thalamus; TN, trigeminal nerve; VN, vestibular nucleus; VP, ventral pons

This anatomical distribution of N/OFQ generally correlates well with that reported for the localisation of mRNA for its precursor preproN/OFQ. This clearly demonstrates that N/OFQ is widely distributed in the brain and is most probably synthesised at the site of action. Using northern blot analysis, preproN/OFQ mRNA expression was abundant in hypothalamus and striatum with weaker signals in the hippocampus and cortex (Mollereau *et al.*, 1996). In contrast, Neal *et al.* (1999) reported some difference in localisation of N/OFQ and mRNA expression using IHC and *in situ* hybridisation though a close correlation was observed in brain areas responsible for the main physiological functional roles of N/OFQ i.e. thalamus and mid brain regions associated with pain modulation and hippocampus for learning and memory (Figure 8.22). The distribution reported here is similar to the N/OFQ immunoreactivity within pain modulating regions documented for the rat (Lai *et al.*, 1997; Schulz *et al.*, 1996) and mouse (Houtani *et al.*, 2000).

8.6 Discussion

The antibodies raised here against three distinct continuous epitopes, cysN/OFQ, cysNoc and cysNOP epitope were for use in IHC for *in situ* localisation of their particular epitopes. Antibodies were initially investigated for specificity and avidity using ELISAs, dot blots and Western blotting. All titres did increase with subsequent booster injections compared to pre-immune antisera and none of the antibodies showed cross reactivity with peptides homologous to their epitope sequences, even at low antigen concentration.

Anti-Noc and anti-NOP antibodies showed weaker avidities compared to anti-N/OFQ and, for anti-Noc, this could not be significantly improved by affinity chromatography with a Protein G column. These antibodies showed even lower affinity to native Noc compared to cysNoc, which again was not increased after purification.

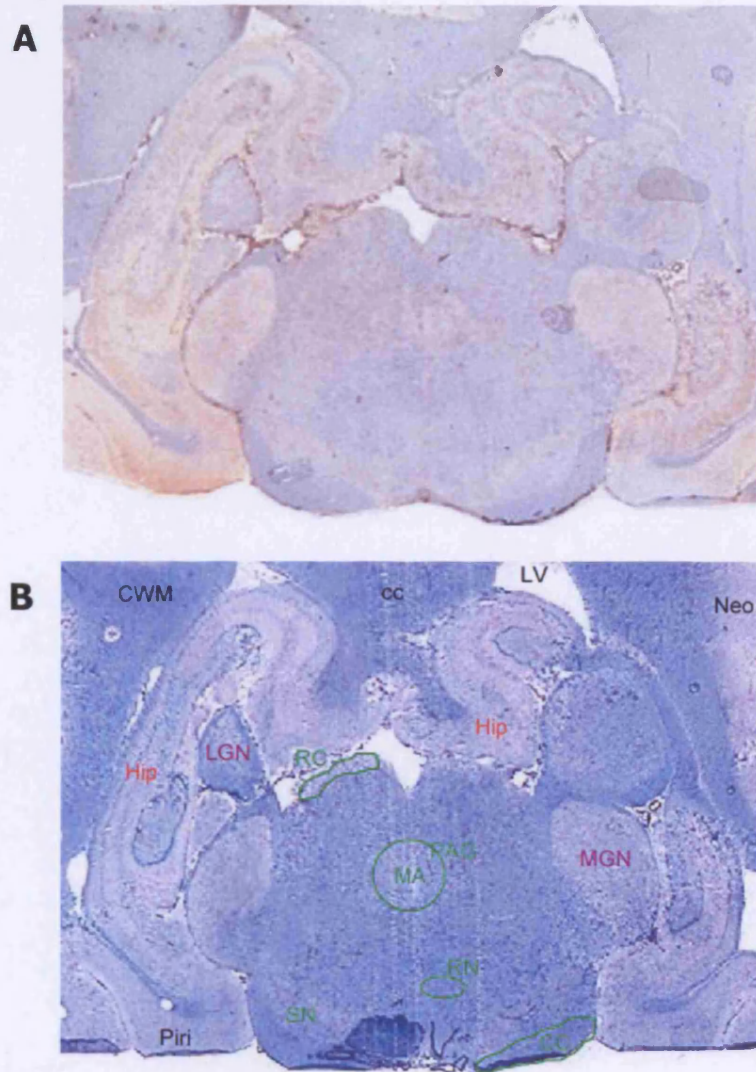


FIGURE 8.22 Slide 187 (A) depict N/OFQ (brown stain) localisation in dog brain sections and atlas B (slide 185) shows haematoxylin and eosin staining. N/OFQ is therefore distributed in brain areas associated with *pain perception, cardiovascular function and learning and memory*

cc, corpus callosum; CC, crus cerebri; CWM, cerebral white matter; Hip, hippocampus; LGN, lateral geniculate nucleus; LV, lateral ventricles; MA, mesencephalic aqueduct; MGN, medial geniculate nucleus; neo, Neocortex; PAG, periaqueductal grey; Piri, piriform cortex; RC, rostral colliculus; RN, red nucleus; SN, substantia nigra

Antibodies have been generated to NOP previously (Monteillet-Agius *et al.*, 1998). These were monoclonals to the N terminal sequence of the receptor, which were used successfully in IHC to localise NOP in rat brain. Those generated here showed affinity for cysNOP and the NOP epitope but would not bind at all to native recombinant NOP receptors. Anti-NOP antibodies therefore were not suitable for use in further experiments. The chosen epitope may not actually be available for antibody binding in the native receptor form or could be structurally different to the conformation adopted by the primary sequence of the immunogen. Affinity chromatography with the Protein G column (section 8.3) separates all classes of IgG, irrespective of their specificity so does not concentrate particular paratopes. Hence an affinity column of particular epitopes i.e. NOP epitope or Noc would be better for purification of both anti-NOP and anti-Noc antisera. This probably would not greatly improve the specificity and avidity of the antibodies since the paratopes of interest are not in abundance in either antisera.

Anti-N/OFQ antibodies showed the highest titre (1/3600) and were comparable in avidity to Abcam, a purchased anti-N/OFQ antibody. These were used to label their antigen *in situ*. N/OFQ was localised in whole dog brain sections using IHC. This peptide was found to be widely distributed throughout the brain particularly in grey matter areas in a manner consistent for that reported for other species. Highest intensity was localised in the cortex, amygdala, caudate nuclei and hippocampus. This anatomical distribution of N/OFQ correlates well with that reported for the localisation of mRNA for its precursor preproN/OFQ and illustrates the presence of N/OFQ in brain areas responsible for; learning and memory (hippocampus), areas involved in pain perception, (thalamus and mid brain regions), and in areas with cardiovascular modulatory functions (pons and hypothalamus). These findings reiterate previous studies (Mollereau *et al.*, 1996; Neal *et al.*, 1999) showing N/OFQ immunoreactivity in these functionally important areas.

9 General discussion

N/OFQ was discovered (Meunier *et al.*, 1995; Reinscheid *et al.*, 1995) after the identification of its orphan receptor, NOP and has since been implicated in various physiological roles. This important system is G protein coupled and on activation the net effect is generally inhibition of neuronal transmission. There is considerable homology between this and the opioid system at the genomic, peptidic and localisation level despite major differences in the central effects of these neuropeptides.

This thesis characterised NOP in Beagle dog brain as much evidence is documented for murine species and recombinant systems but nothing for dog. Furthermore N/OFQ has a central role in pain modulation, a condition associated with debilitating diseases, common in geriatric dogs.

9.1 Summary of findings

NOP receptor expression in the dog and rat membrane preparations was assessed using two radioligands, [*leucyl*-³H]N/OFQ and [³H]N/OFQ13, both of which confirmed lower levels in the dog (B_{\max} values of 29 (dog) and 137fmol mg⁻¹ protein (rat), respectively with [*leucyl*-³H]N/OFQ). Competition studies indicated a significant positive correlation between the species in terms of pK_i though the value for [F/G] showed some variation with 6 fold higher affinity in rat NOP. Selective opioid agonists displaced with very low affinity.

Similar classical opioid receptor (DOP/KOP/MOP) population in dog and rat brain membranes were observed (~78fmol mg⁻¹ protein) so compared to NOP, dog brain membranes contain ~3 fold higher density of classical opioid receptors. The relative density of the subtypes differed between the species with the rank order being KOP > DOP > MOP for dog compared to DOP > MOP > KOP in rat.

Despite low NOP expression in dog brain, functional activity was detectable using “GTP-shift” studies and GTP γ ³⁵S binding assays. Native dog NOP receptors were able to couple G α_{i1-3} protein and this coupling was stimulated by various NOP agonists. These effects were antagonised by selective NOP antagonists, [Nphe¹] and J-113397.

The pharmacological profile of CJ-X determined in classical binding and functional assays, fitted that of a high affinity, potent agonist with selectivity for hNOP over classical rMOP, mDOP and rKOP opioid subtypes. This ligand is hence a useful research tool for characterising NOP.

Antibodies raised against N/OFQ were utilised in IHC to determine distribution of this peptide in whole dog brain sections. Peptide distribution was widespread throughout the brain and was similar to that determined for NOP in [*leucyl*-³H]N/OFQ autoradiography. Distribution of both peptide and receptor correlated well with brain areas involved in the functional effects documented for N/OFQ.

9.2 Low expression of NOP

There is no evidence to suggest that because of such low level expression that NOP is less important in dog. There have been several studies examining receptor expression of NOP in various species. Some of these data are summarised in Table 9.1. As is clearly illustrated, most studies show significantly higher NOP density in a range of species compared with that reported here for dog. However, in a recent study using [³H]acRYYRWKNH₂, Thomsen *et al.* (2000b) reported a very low density (22fmol mg⁻¹ protein) of high affinity NOP receptors in the rat. It is difficult to directly compare all these studies as each uses different assay conditions and radioligands to determine NOP density. Also the integrity of [³H] radioligands is questionable depending on source of radioligand and assay conditions (Quigley *et al.*, 2000).

TABLE 9.1 Comparison of NOP receptor expression in brain membrane preparations from various species with different radioligands

SPECIES	RADIOLIGAND	B _{max} /pK _d	REFERENCE
Rat	[¹²⁵ I]N/OFQOH	180/10.26	Okawa <i>et al.</i> (1998)
	[³ H]N/OFQOH	291/10.67	Albrecht <i>et al.</i> (1998)
	[¹²⁵ I]N/OFQOH	52/10.01	Makman <i>et al.</i> (1997a)
	[³ H]N/OFQOH	254/9.91	Nicholson <i>et al.</i> (1998)
	[³ H]N/OFQOH	420/9.14	Werthwein <i>et al.</i> (1999)
	[³ H]acRYRWKNH ₂	22/10.15	Thomsen <i>et al.</i> (2000b)
Mouse	[³ H]N/OFQNH ₂	94/9.23	Varani <i>et al.</i> (1998)
	[³ H]N/OFQOH	520/8.87	Werthwein <i>et al.</i> (1999)
Guinea pig	[³ H]N/OFQOH	166/10.31	Nicholson <i>et al.</i> (1998)
Rabbit	[³ H]N/OFQOH	143/10.05	Nicholson <i>et al.</i> (1998)
Dog	[³ H]N/OFQOH	36/10.44	<i>This study</i>
Rat	[³ H]N/OFQOH	121/10.53	<i>This study</i>

NQ, not quoted

The relatively low density of NOP receptors in dog has a number of experimental and functional consequences. Firstly, a glance at the numerical data presented in this thesis shows greater variability for dog compared with the rat. Also functional consequences may become important when examining pharmacology of partial agonists. Indeed, [F/G], a NOP partial agonist, whilst being inactive *per se*, antagonised N/OFQ stimulated GTPγ³⁵S binding to dog brain membranes indicating that ligand efficacy is dependent on receptor expression.

Low MOP density observed in dog may be of particular analgesic relevance since MOP agonists are the most commonly administered analgesics. However receptor expression does not necessarily correlate with the likelihood that a particular species will become excited (in terms of locomotor activity) on administration of opioids (Hellyer *et al.*, 2003)

since debilitated dogs experiencing pain generally are sedated in response to opioids. High classical opioid receptor expression in dog compared to NOP levels could be of clinical relevance though the significance of this is not yet understood.

9.3 Ligand affinity for NOP

The binding affinity of the two radioligands for NOP did not differ in dog. However the pK_d of truncated [3H]N/OFQ13 was significantly ($p < 0.005$) lower in rat compared to that for full sequence [*leucyl*- 3H]N/OFQ. The data from these two species can be directly compared since the assay conditions and tissue preparations are identical to those used here hence no explanation for this discrepancy is obvious. The pK_d for [*leucyl*- 3H]N/OFQ in rat was consistent with that reported by other groups, 10.67 (Albrecht *et al.*, 1998), 10.56 (Mason *et al.*, 2001) and 10.35 (Yamada *et al.*, 2003). Affinity data for dog were in agreement with values reported previously by our laboratory for [*leucyl*- 3H]N/OFQ and [3H]N/OFQ13 in CHO_{hNOP} membranes of 10.06 ± 0.04 and 10.35 ± 0.03 , respectively (Hashiba *et al.*, 2002a).

[*leucyl*- 3H]N/OFQ was displaced by various unlabelled ligands with similar pK_i values in both species. Data reported for rat membranes is similar to that observed for other ligands in this species - Mason *et al.* (2001) indicated pK_i values of 10.38 and 10.44 for the agonist N/OFQ and partial agonist CTD in rat, respectively and Ichikawa *et al.* (2001) showed a pK_i of 8.96 for J-113397 with [^{125}I](Tyr¹⁴)N/OFQ. Some differences were observed when comparing rat data with other studies since Yamada *et al.* (2003) reported pK_i values of 9.57, 8.99 and 8.15 for N/OFQ, [F/G] and J-113397, respectively though this variation is probably due to dissimilar assay conditions.

Further comment is required regarding the discrepancy in the affinity values reported in this thesis for [F/G]. It is tempting to suggest that there may be differences in the structures

of the receptors in these species but based on such limited data, this conclusion cannot be supported. There is no explanation to date for these differences but they remain the same for different batches of the synthetic peptide and membrane preparations.

9.4 Functional NOP

N/OFQ at 1 μ M produced a small stimulation of GTP γ ³⁵S binding in dog brain membranes with a pEC₅₀ in the nanomolar range. No previous functional data for comparison is available for binding in dog. However when considering interspecies variation, this value indicates a higher potency for N/OFQ in dog compared with that reported in mouse (7.09, (Ichikawa *et al.*, 2001)) and rat (7.75, (Berger *et al.*, 2000b); 8.26, (Mason *et al.*, (2001); 8.17, (Berger *et al.*, (2000a); 8.04, (Albrecht *et al.*, (1998)). Interestingly, the potency value (pK_B) for the NOP antagonist J-113397 is also higher than that published for rat (7.79, Yamada *et al.*, 2003).

9.5 Antibody production

The response to immunisation was variable hence the antibodies produced showed varying specificity and avidity. Anti-NOP and anti-Noc antibodies were unsuitable for use in IHC as they did not bind native NOP or Noc despite showing specificity for the peptide sequence against which they were raised.

For anti-Noc antibodies, this specificity could not be improved by affinity chromatography. If there had been particularly high concentration of Noc within the antiserum, this could have produced a masking effect in ELISAs. This would have been eliminated after affinity chromatography since this technique produces a concentrated polyclonal antibody solution. However no significant improvement was noted after purification and hence these ELISA results correspond to low titre, low avidity antibodies

with specificity only towards their immunogenic antigen.

Antibodies to synthetic polypeptides do not bind well to the antigen in its native form. It is easier to synthesise short polypeptide antigens than purify native protein from tissue extracts in sufficient amounts for immunisation. Better results would most probably be achieved for anti-Noc antibodies if the native peptides were used for immunisation, as the antibodies produced would be specific for the antigen in its native 3D conformation.

Interestingly the rabbit immunised against cysN/OFQ, which showed an adverse reaction to the immunogen, also produced the better antibodies, in terms of titre and avidity. However there is no evidence to suggest that the other antibodies would have been better if a more potent immune response was induced.

9.6 Localisation of NOP and its ligand N/OFQ

The most important findings regarding peptide and receptor distribution presented in this thesis reiterate previous findings that the peptide system investigated is localised in functionally important areas. Figure 9.1 illustrates the close correlation between the expression of N/OFQ with its receptor NOP. Images 110 and 111 of peptide and receptor distribution (from IHC and autoradiography, respectively) show localisation of this system within the caudate nuclei, a brain area important in locomotor activity. N/OFQ has been documented to have a dose dependent effect on locomotor activity in mice with inhibition at higher doses, which can be abolished with selective NOP antagonist, [Nphe¹] (Rizzi *et al.*, 2001).

Images 187 and 181 show localisation within the hippocampus of dog brain, an area associated with learning and memory. Mice lacking NOP possess greater learning ability and better memory than those expressing NOP (Goda *et al.*, 1998).

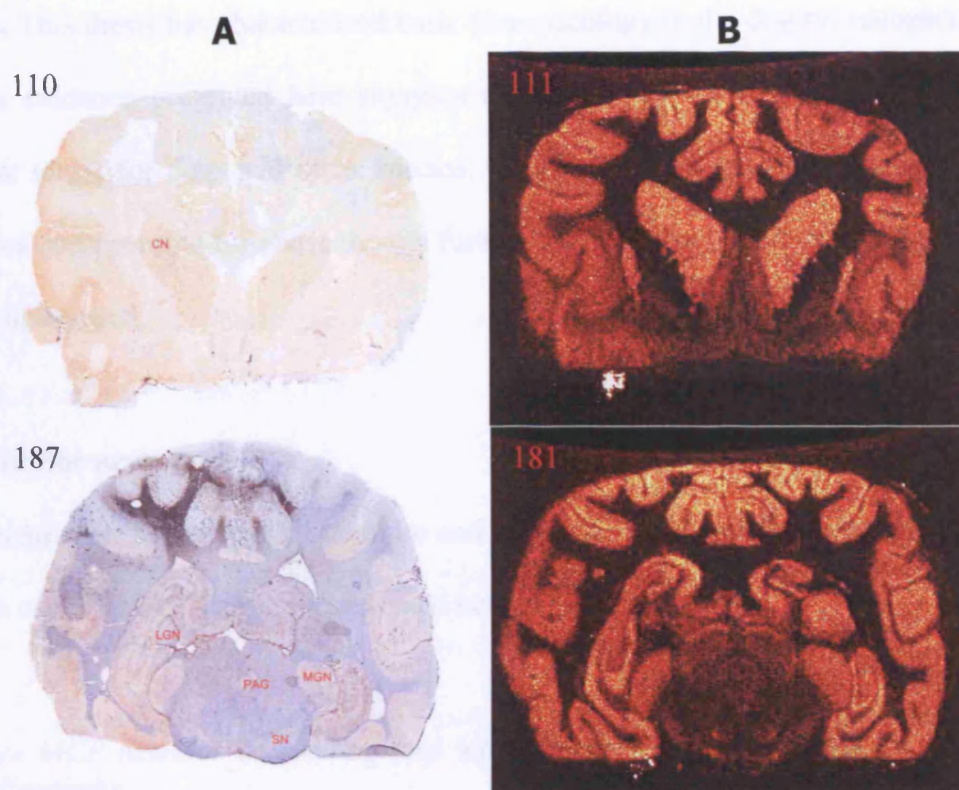


FIGURE 9.1 N/OFQ (A) and NOP (B) are localised in situ in dog brain in functionally important area
(CN, caudate nucleus; Hip, hippocampus; LGN, lateral geniculate nucleus; MGN, medial geniculate nucleus; PAG, periaqueductal grey; SN, substantia nigra)

There is much controversy regarding the role of the N/OFQ-NOP system in pain modulation since N/OFQ can produce analgesia similarly to opioids or hyperalgesia (Pan *et al.*, 2000). Images 187 and 181 also show that this peptide and its receptor are indeed found in mid brain regions involved in pain perception. Thereby it is reasonable to suggest that N/OFQ will also modulate physiological parameters such as those documented in small laboratory animals in dog.

Radioligand binding showed a higher density of NOP receptors in rat compared with dog and this was also confirmed in [*leucyl*-³H]N/OFQ autoradiography. MCID analysis showed ~5 fold higher expression of NOP in rat piriform cortex compared with dog. NOP receptors were also localised in dog vas deferens but not in dog skeletal muscle.

The role of NOP and N/OFQ is clearly widespread and important in a variety of central

systems. This thesis has characterised basic pharmacology in the dog for comparison with rat. The evidence presented here suggests that this system may well be a therapeutic analgesic target for dogs and other species, particularly in view of the lack of addictive properties and potential for abuse though further research into N/OFQ's central role in this species is required.

9.7 Further work

The potential for further work is infinite and particular areas have been highlighted by the findings of this thesis. These are presented here in order of priority:

Compare MCP detector autoradiograms with more traditional methods for quantitative autoradiography

[leucyl-³H]N/OFQ autoradiography should be repeated on whole dog brain sections imaging some sections with the MCP detector and developing the others traditionally using film. Localisation should be similar but more importantly the accuracy of the quantitative analysis can be compared.

Compare [leucyl-³H]N/OFQ binding with [³H]N/OFQ13 binding in autoradiography

This thesis showed that there was a difference albeit not significant in dog NOP receptor expression using these two NOP selective radioligands. It would be interesting to repeat the autoradiography of whole dog brain sections with [³H]N/OFQ13 to localise binding and compare this with that for the full sequence radioligand. Other groups have reported slight discrepancies in binding between full sequence and truncated [¹²⁵I] radioligands (Letchworth *et al.*, 2000).

GTP γ ³⁵S binding in situ

It would be useful to repeat GTP γ ³⁵S binding *in situ* in whole dog brain sections for

comparison with NOP localisation, shown here in the [*leucyl*-³H]N/OFQ autoradiograms. Any binding observed would probably correlate with NOP distribution and further confirm that NOP is a functional receptor in this species. This has been carried out in mouse spinal cord (Narita *et al.*, 1999) in which GTP γ ³⁵S binding was co-localised with distribution of NOP mRNA, and in rat brain (Sim *et al.*, 1996). In practice, carrying out this assay *in situ* could be very difficult because of low NOP expression in dog and hence low counts bound.

Functional effects of CJ-X

CJ-X was here characterised as a potent full agonist and needs to be further characterised in terms of behavioural effects. It could be tested *in vitro* and *in vivo*, for example, in tail flick assay, vas deferens preparation and paw lick test to see how it compares to N/OFQ.

Modulate binding with antibodies

Antibodies are useful tools for visualising their particular antigen. Moreover they can be used as a biological agent to block specific functions since an antibody-peptide complex is not likely to be recognised by the peptide's receptor. This has been investigated in rats by Tian *et al.* (2000) who describes increased electropuncture analgesia after intracerebroventricular injection with anti-N/OFQ antibodies. The anti-N/OFQ antibodies could be used to interfere with the binding of N/OFQ with NOP and hence determine further functional effects after activation of NOP in dog.

Quantitative ELISA

Since N/OFQ has a role in many conditions it would be useful to be able to measure its serum concentration. The antibodies raised here against N/OFQ could be used to develop a quantitative ELISA for use as a diagnostic test. N/OFQ could be labelled with biotin and unlabelled N/OFQ measured based on competition of the two peptides with the anti-N/OFQ antibodies.

10 References

- ABDULLA, F.A. & SMITH, P.A. (1997). Nociceptin inhibits T-type Ca^{2+} channel current in rat sensory neurons by a G protein-independent mechanism. *J Neurosci*, **17**, 8721-8.
- ALBRECHT, E., SAMOVILOVA, N.N., OSWALD, S., BAEGER, I. & BERGER, H. (1998). Nociceptin (orphanin FQ): high-affinity and high-capacity binding site coupled to low-potency stimulation of guanylyl-5'-O-(γ -thio)-triphosphate binding in rat brain membranes. *J Pharmacol Exp Ther*, **286**, 896-902.
- ANDERSEN, A.C. (1970). *The Beagle as an experimental dog*. Ames: The Iowa State University Press.
- ARJOMAND, J., COLE, S. & EVANS, C.J. (2002). Novel orphanin FQ/nociceptin transcripts are expressed in human immune cells. *J Neuroimmunol*, **130**, 100-8.
- BEAR, M.F., CONNORS, B.W. & PARADISO, M.A. (2001). *Neuroscience: exploring the brain*. Philadelphia: Lippincott Williams & Wilkins.
- BECKER, J.A., WALLACE, A., GARZON, A., INGALLINELLA, P., BIANCHI, E., CORTESE, R., SIMONIN, F., KIEFFER, B.L. & PESSI, A. (1999). Ligands for κ -opioid and ORL1 receptors identified from a conformationally constrained peptide combinatorial library. *J Biol Chem*, **274**, 27513-22.
- BENNETT, B., CHECK, I.J., OLSEN, M.R. & HUNTER, R.L. (1992). A comparison of commercially available adjuvants for use in research. *J Immunol Methods*, **153**, 31-40.
- BERGER, H., BIGONI, R., ALBRECHT, E., RICHTER, R.M., KRAUSE, E., BIENERT, M. & CALO, G. (2000a). The nociceptin/orphanin FQ receptor ligand acetyl-RYYRIK-amide exhibits antagonistic and agonistic properties. *Peptides*, **21**, 1131-9.
- BERGER, H., CALO, G., ALBRECHT, E., GUERRINI, R. & BIENERT, M. (2000b). [Nphe¹]NC(1-13)NH₂ selectively antagonizes nociceptin/orphanin FQ-stimulated G-protein activation in rat brain. *J Pharmacol Exp Ther*, **294**, 428-33.
- BERTHELE, A., PLATZER, S., DWORZAK, D., SCHADRACK, J., MAHAL, B., BUTTNER, A., ASSMUS, H.P., WURSTER, K., ZIEGLGANSBERGER, W., CONRAD, B. & TOLLE, T.R. (2003). [³H]-nociceptin ligand-binding and nociceptin opioid receptor mRNA expression in the human brain. *Neuroscience*, **121**, 629-40.
- BIGONI, R., CALO, G., RIZZI, A., GUERRINI, R., DE RISI, C., HASHIMOTO, Y., HASHIBA, E., LAMBERT, D.G. & REGOLI, D. (2000a). *In vitro* characterization of J-113397, a non-peptide nociceptin/orphanin FQ receptor antagonist. *Naunyn Schmiedeberg's Arch Pharmacol*, **361**, 565-8.
- BIGONI, R., CALO, G., RIZZI, A., OKAWA, H., REGOLI, D., SMART, D. & LAMBERT, D.G. (2002a). Effects of naloxone benzoylhydrazone on native and recombinant nociceptin/orphanin FQ receptors. *Can J Physiol Pharmacol*, **80**, 407-12.
- BIGONI, R., RIZZI, A., RIZZI, D., BECKER, J.A., KIEFFER, B.L., SIMONIN, F., REGOLI, D. & CALO, G. (2000b). *In vitro* pharmacological profile of peptide III-BTD: a novel ligand for nociceptin/orphanin FQ and opioid receptors. *Life Sci*, **68**, 233-9.
- BIGONI, R., RIZZI, D., RIZZI, A., CAMARDA, V., GUERRINI, R., LAMBERT, D.G., HASHIBA, E., BERGER, H., SALVADORI, S., REGOLI, D. & CALO, G. (2002b). Pharmacological characterisation of [(pX)Phe⁴]nociceptin(1-13)amide analogues 1. *In vitro* studies. *Naunyn Schmiedeberg's Arch Pharmacol*, **365**, 442-9.
- BLOMS-FUNKE, P., GILLEN, C., SCHUETTLER, A.J. & WNENDT, S. (2000). Agonistic effects of the opioid buprenorphine on the nociceptin/OFQ receptor. *Peptides*, **21**, 1141-6.

- BRIDGE, K.E., WAINWRIGHT, A., REILLY, K. & OLIVER, K.R. (2003). Autoradiographic localization of $^{125}\text{I}[\text{Tyr}^{14}]$ nociceptin/orphanin FQ binding sites in macaque primate CNS. *Neuroscience*, **118**, 513-23.
- BROWN, B.L., ALBANO, J.D., EKINS, R.P. & SGHERZI, A.M. (1971). A simple and sensitive saturation assay method for the measurement of adenosine 3':5'-cyclic monophosphate. *Biochem J*, **121**, 561-2.
- BUNZOW, J.R., SAEZ, C., MORTRUD, M., BOUVIER, C., WILLIAMS, J.T., LOW, M. & GRANDY, D.K. (1994). Molecular cloning and tissue distribution of a putative member of the rat opioid receptor gene family that is not a μ , δ or κ opioid receptor type. *FEBS Lett*, **347**, 284-8.
- BUTOUR, J.L., MOISAND, C., MAZARGUIL, H., MOLLEREAU, C. & MEUNIER, J.C. (1997). Recognition and activation of the opioid receptor-like ORL 1 receptor by nociceptin, nociceptin analogs and opioids. *Eur J Pharmacol*, **321**, 97-103.
- BUTOUR, J.L., MOISAND, C., MOLLEREAU, C. & MEUNIER, J.C. (1998). $[\text{Phe}^1\psi(\text{CH}_2\text{-NH})\text{Gly}^2]$ nociceptin(1-13) NH_2 is an agonist of the nociceptin (ORL1) receptor. *Eur J Pharmacol*, **349**, R5-6.
- CALO, G., BIGONI, R., RIZZI, A., GUERRINI, R., SALVADORI, S. & REGOLI, D. (2000a). Nociceptin/orphanin FQ receptor ligands. *Peptides*, **21**, 935-47.
- CALO, G., GUERRINI, R., BIGONI, R., RIZZI, A., BIANCHI, C., REGOLI, D. & SALVADORI, S. (1998). Structure-activity study of the nociceptin(1-13) NH_2 N-terminal tetrapeptide and discovery of a nociceptin receptor antagonist. *J Med Chem*, **41**, 3360-6.
- CALO, G., GUERRINI, R., BIGONI, R., RIZZI, A., MARZOLA, G., OKAWA, H., BIANCHI, C., LAMBERT, D.G., SALVADORI, S. & REGOLI, D. (2000b). Characterization of $[\text{Nphe}^1]$ nociceptin(1-13) NH_2 , a new selective nociceptin receptor antagonist. *Br J Pharmacol*, **129**, 1183-93.
- CALO, G., GUERRINI, R., RIZZI, A., SALVADORI, S. & REGOLI, D. (2000c). Pharmacology of nociceptin and its receptor: a novel therapeutic target. *Br J Pharmacol*, **129**, 1261-83.
- CALO, G., RIZZI, A., BODIN, M., NEUGEBAUER, W., SALVADORI, S., GUERRINI, R., BIANCHI, C. & REGOLI, D. (1997). Pharmacological characterization of nociceptin receptor: an *in vitro* study. *Can J Physiol Pharmacol*, **75**, 713-8.
- CALO, G., RIZZI, A., BOGONI, G., NEUGEBAUER, V., SALVADORI, S., GUERRINI, R., BIANCHI, C. & REGOLI, D. (1996). The mouse vas deferens: a pharmacological preparation sensitive to nociceptin. *Eur J Pharmacol*, **311**, R3-5.
- CALO, G., RIZZI, A., RIZZI, D., BIGONI, R., GUERRINI, R., MARZOLA, G., MARTI, M., McDONALD, J., MORARI, M., LAMBERT, D.G., SALVADORI, S. & REGOLI, D. (2002). $[\text{Nphe}^1, \text{Arg}^{14}, \text{Lys}^{15}]$ Nociceptin- NH_2 , a novel potent and selective antagonist of the nociceptin/orphanin FQ receptor. *Br J Pharmacol*, **136**, 303-311.
- CARLSSON, J., DREVIN, H. & AXEN, R. (1978). Protein thiolation and reversible protein-protein conjugation. N-Succinimidyl 3-(2-pyridyldithio)propionate, a new heterobifunctional reagent. *Biochem J*, **173**, 723-37.
- CATERINA, M.J. & JULIUS, D. (1999). Sense and specificity: a molecular identity for nociceptors. *Curr Opin Neurobiol*, **9**, 525-30.
- CATERINA, M.J., SCHUMACHER, M.A., TOMINAGA, M., ROSEN, T.A., LEVINE, J.D. & JULIUS, D. (1997). The capsaicin receptor: a heat-activated ion channel in the pain pathway. *Nature*, **389**, 816-24.
- CHAVKIN, C., JAMES, I.F. & GOLDSTEIN, A. (1982). Dynorphin is a specific endogenous ligand of the κ opioid receptor. *Science*, **215**, 413-5.

- CHEN, Y., FAN, Y., LIU, J., MESTEK, A., TIAN, M., KOZAK, C.A. & YU, L. (1994). Molecular cloning, tissue distribution and chromosomal localization of a novel member of the opioid receptor gene family. *FEBS Lett*, **347**, 279-83.
- CHENG, Y. & PRUSOFF, W.H. (1973). Relationship between the inhibition constant (K_i) and the concentration of inhibitor which causes 50 per cent inhibition (IC_{50}) of an enzymatic reaction. *Biochem Pharmacol*, **22**, 3099-108.
- COLPAERT, F.C. (2002). Mechanisms of opioid-induced pain and antinociceptive tolerance: signal transduction. *Pain*, **95**, 287-8.
- CORDEAUX, Y., BRIDDON, S.J., MEGSON, A.E., McDONNELL, J., DICKENSON, J.M. & HILL, S.J. (2000). Influence of receptor number on functional responses elicited by agonists acting at the human adenosine A_1 receptor: evidence for signaling pathway-dependent changes in agonist potency and relative intrinsic activity. *Mol Pharmacol*, **58**, 1075-84.
- COSTENTIN, J., FLORIN, S., SUAUDEAU, C. & MEUNIER, J.C. (1998). Cloning of prepronociceptin has led to the discovery of other biologically active peptides. *C R Seances Soc Biol Fil*, **192**, 1099-109.
- COX, B.M., CHAVKIN, C., CHRISTIE, M.J., CIVELLI, O., EVANS, C., HAMON, M.D., HOELLT, V., KIEFFER, B., KITCHEN, I., MCKNIGHT, A.T., MEUNIER, J.C. & PORTOGHESE, P.S. (2000). Opioid receptors. In *The IUPHAR Compendium of Receptor Characterization*. ed Girdlestone, D. pp. 321-333. London: IUPHAR Media Ltd.
- DAUTZENBERG, F.M., WICHMANN, J., HIGELIN, J., PY-LANG, G., KRATZEISEN, C., MALHERBE, P., KILPATRICK, G.J. & JENCK, F. (2001). Pharmacological characterization of the novel nonpeptide orphanin FQ/nociceptin receptor agonist Ro 64-6198: rapid and reversible desensitization of the ORL1 receptor *in vitro* and lack of tolerance *in vivo*. *J Pharmacol Exp Ther*, **298**, 812-9.
- DENNIS, T., FOURNIER, A., GUARD, S., ST PIERRE, S. & QUIRION, R. (1991). Calcitonin gene-related peptide (hCGRP α) binding sites in the nucleus accumbens. Atypical structural requirements and marked phylogenetic differences. *Brain Res*, **539**, 59-66.
- DESPOPOULOS, A. & SILBERNAGL, S. (1986). *Colour Atlas of Physiology*. New York: Thieme Inc.,
- DHAWAN, B.N., CESSSELIN, F., RAGHUBIR, R., REISINE, T., BRADLEY, P.B., PORTOGHESE, P.S. & HAMON, M. (1996). International Union of Pharmacology. XII. Classification of opioid receptors. *Pharmacol Rev*, **48**, 567-92.
- DICKENSON, A.H., MATTHEWS, E.A. & SUZUKI, R. (2002). Neurobiology of neuropathic pain: mode of action of anticonvulsants. *Eur J Pain*, **6**, 51-60.
- DOOLEY, C.T. & HOUGHTEN, R.A. (2000). Orphanin FQ/nociceptin receptor binding studies. *Peptides*, **21**, 949-60.
- DOOLEY, C.T., SPAETH, C.G., BERZETEI-GURSKE, I.P., CRAYMER, K., ADAPA, I.D., BRANDT, S.R., HOUGHTEN, R.A. & TOLL, L. (1997). Binding and *in vitro* activities of peptides with high affinity for the nociceptin/orphanin FQ receptor, ORL1. *J Pharmacol Exp Ther*, **283**, 735-41.
- EILBERT, J.L., GALLISTEL, C.R. & MCEACHRON, D.L. (1990). The variation in user drawn outlines on digital images: effects on quantitative autoradiography. *Comput Med Imaging Graph*, **14**, 331-9.
- EL KOUHEN, R., BURD, A.L., ERICKSON-HERBRANDSON, L.J., CHANG, C.Y., LAW, P.Y. & LOH, H.H. (2001). Phosphorylation of Ser³⁶³, Thr³⁷⁰, and Ser³⁷⁵ residues within the carboxyl tail differentially regulates μ -opioid receptor internalization. *J Biol Chem*, **276**, 12774-80.

- EVANS, C.J., KEITH, D.E., JR., MORRISON, H., MAGENDZO, K. & EDWARDS, R.H. (1992). Cloning of a δ opioid receptor by functional expression. *Science*, **258**, 1952-5.
- EVANS, H.E. (1993). *Miller's Anatomy of the Dog*. Philadelphia: W B Saunders.
- FISCHER, H.S., ZERNIG, G., HAUSER, K.F., GERARD, C., HERSH, L.B. & SARIA, A. (2002). Neutral endopeptidase knockout induces hyperalgesia in a model of visceral pain, an effect related to bradykinin and nitric oxide. *J Mol Neurosci*, **18**, 129-34.
- FLORIN, S., LEROUX-NICOLLET, I., MEUNIER, J.C. & COSTENTIN, J. (1997). Autoradiographic localization of [³H]nociceptin binding sites from telencephalic to mesencephalic regions of the mouse brain. *Neurosci Lett*, **230**, 33-6.
- FLORIN, S., MEUNIER, J. & COSTENTIN, J. (2000). Autoradiographic localization of [³H]nociceptin binding sites in the rat brain. *Brain Res*, **880**, 11-6.
- FOX, M.W. (1970). Central Nervous System. In *The Beagle as an experimental dog*. ed Andersen, A.C. pp. 350-373. Ames: The Iowa State University Press.
- FUKUDA, K., KATO, S. & MORI, K. (1995). Location of regions of the opioid receptor involved in selective agonist binding. *J Biol Chem*, **270**, 6702-9.
- FUKUDA, K., KATO, S., MORI, K., NISHI, M., TAKESHIMA, H., IWABE, N., MIYATA, T., HOUTANI, T. & SUGIMOTO, T. (1994). cDNA cloning and regional distribution of a novel member of the opioid receptor family. *FEBS Lett*, **343**, 42-6.
- GILLBERG, P.G., JOSSAN, S.S., ASKMARK, H. & AQUILONIUS, S.M. (1986). Large-section cryomicrotomy for *in vitro* receptor autoradiography. *J Pharmacol Methods*, **15**, 169-80.
- GIULIANI, S., LECCI, A. & MAGGI, C.A. (2000). Nociceptin and neurotransmitter release in the periphery. *Peptides*, **21**, 977-84.
- GODA, Y. & MUTNEJA, M. (1998). Memory mechanisms: the nociceptin connection. *Curr Biol*, **8**, R889-91.
- GREAVES, P. (2000). Patterns of cardiovascular pathology induced by diverse cardioactive drugs. *Toxicol Lett*, **112-113**, 547-52.
- GREAVES, P. (1998). Patterns of drug-induced cardiovascular pathology in the beagle dog: relevance for humans. *Exp Toxicol Pathol*, **50**, 283-93.
- GREENSTEIN, B. & GREENSTEIN, A. (2000). *Colour Atlas of Neuroscience*. New York: Thieme.
- GUERRINI, R., CALO, G., BIGONI, R., RIZZI, A., VARANI, K., TOTH, G., GESSI, S., HASHIBA, E., HASHIMOTO, Y., LAMBERT, D.G., BOREA, P.A., TOMATIS, R., SALVADORI, S. & REGOLI, D. (2000). Further studies on nociceptin-related peptides: discovery of a new chemical template with antagonist activity on the nociceptin receptor. *J Med Chem*, **43**, 2805-13.
- GUERRINI, R., CALO, G., BIGONI, R., RIZZI, D., REGOLI, D. & SALVADORI, S. (2001a). Structure-activity relationship of [Nphe¹]-NC-(1-13)-NH₂, a pure and selective nociceptin/orphanin FQ receptor antagonist. *J Pept Res*, **57**, 215-22.
- GUERRINI, R., CALO, G., BIGONI, R., RIZZI, D., RIZZI, A., ZUCCHINI, M., VARANI, K., HASHIBA, E., LAMBERT, D.G., TOTH, G., BOREA, P.A., SALVADORI, S. & REGOLI, D. (2001b). Structure-activity studies of the Phe⁴ residue of nociceptin(1-13)NH₂: identification of highly potent agonists of the nociceptin/orphanin FQ receptor. *J Med Chem*, **44**, 3956-64.
- GUERRINI, R., CALO, G., RIZZI, A., BIANCHI, C., LAZARUS, L.H., SALVADORI, S., TEMUSSI, P.A. & REGOLI, D. (1997). Address and message sequences for the nociceptin receptor: a structure-activity study of nociceptin-(1-13)-peptide amide. *J Med Chem*, **40**, 1789-93.

- GUERRINI, R., CALO, G., RIZZI, A., BIGONI, R., BIANCHI, C., SALVADORI, S. & REGOLI, D. (1998). A new selective antagonist of the nociceptin receptor. *Br J Pharmacol*, **123**, 163-5.
- GUNTHORPE, M.J., BENHAM, C.D., RANDALL, A. & DAVIS, J.B. (2002). The diversity in the vanilloid (TRPV) receptor family of ion channels. *Trends Pharmacol Sci*, **23**, 183-91.
- HARRISON, C. & LAMBERT, D.G. (2000). Opioid Pharmacology. In *Anaesthesia, Pain and Intensive Care Medicine*. ed Gullo, A. pp. 387-394: Springer.
- HARRISON, C., McNULTY, S., SMART, D., ROWBOTHAM, D.J., GRANDY, D.K., DEVI, L.A. & LAMBERT, D.G. (1999). The effects of endomorphin-1 and endomorphin-2 in CHO cells expressing recombinant μ -opioid receptors and SH-SY5Y cells. *Br J Pharmacol*, **128**, 472-8.
- HASHIBA, E., HARRISON, C., CALO, G., GUERRINI, R., ROWBOTHAM, D.J., SMITH, G. & LAMBERT, D.G. (2001). Characterisation and comparison of novel ligands for the nociceptin/orphanin FQ receptor. *Naunyn Schmiedebergs Arch Pharmacol*, **363**, 28-33.
- HASHIBA, E., LAMBERT, D.G., FARKAS, J., TOTH, G. & SMITH, G. (2002a). Comparison of the binding of [³H]nociceptin/orphaninFQ(1-13)NH₂, [³H]nociceptin/orphaninFQ(1-17)OH and [¹²⁵I]Tyr¹⁴nociceptin/orphaninFQ(1-17)OH to recombinant human and native rat cerebrocortical nociceptin/orphanin FQ receptors. *Neurosci Lett*, **328**, 5-8.
- HASHIBA, E., LAMBERT, D.G., JENCK, F., WICHMANN, J. & SMITH, G. (2002b). Characterisation of the non-peptide nociceptin receptor agonist, Ro64-6198 in Chinese hamster ovary cells expressing recombinant human nociceptin receptors. *Life Sci*, **70**, 1719-25.
- HASHIMOTO, Y., CALO, G., GUERRINI, R., SMITH, G. & LAMBERT, D.G. (2002). Effects of chronic nociceptin/orphanin FQ exposure on cAMP accumulation and receptor density in Chinese hamster ovary cells expressing human nociceptin/orphanin FQ receptors. *Eur J Pharmacol*, **449**, 17-22.
- HAWES, B.E., GRAZIANO, M.P. & LAMBERT, D.G. (2000). Cellular actions of nociceptin: transduction mechanisms. *Peptides*, **21**, 961-7.
- HELLYER, P.W., BAI, L., SUPON, J., QUAIL, C., WAGNER, A.E., MAMA, K.R. & MAGNUSSON, K.R. (2003). Comparison of opioid and alpha-2 adrenergic receptor binding in horse and dog brain using radioligand autoradiography. *Vet Anaesth Analg*, **30**, 172-82.
- HELYES, Z., NEMETH, J., PINTER, E. & SZOLCSANYI, J. (1997). Inhibition by nociceptin of neurogenic inflammation and the release of SP and CGRP from sensory nerve terminals. *Br J Pharmacol*, **121**, 613-5.
- HENDERSON, G. & MCKNIGHT, A.T. (1997). The orphan opioid receptor and its endogenous ligand nociceptin/orphanin FQ. *Trends Pharmacol Sci*, **18**, 293-300.
- HIROTA, K., HASHIMOTO, Y., SATO, T., YOSHIOKA, H., KUDO, T., MATSUKI, A. & LAMBERT, D.G. (2001). Bronchoconstrictive and relaxant effects of lidocaine on the airway in dogs. *Crit Care Med*, **29**, 1040-4.
- HOUTANI, T., NISHI, M., TAKESHIMA, H., SATO, K., SAKUMA, S., KAKIMOTO, S., UHEYAMA, T., NODA, T. & SUGIMOTO, T. (2000). Distribution of nociceptin/orphanin FQ precursor protein and receptor in brain and spinal cord: a study using *in situ* hybridization and X-gal histochemistry in receptor-deficient mice. *J Comp Neurol*, **424**, 489-508.

- HUNTER, R., STRICKLAND, F. & KEZDY, F. (1981). The adjuvant activity of nonionic block polymer surfactants. I. The role of hydrophile-lipophile balance. *J Immunol*, **127**, 1244-50.
- ICHIKAWA, D., OZAKI, S., AZUMA, T., NAMBU, H., KAWAMOTO, H., IWASAWA, Y., TAKESHIMA, H. & OHTA, H. (2001). *In vitro* inhibitory effects of J-113397 on nociceptin/orphanin FQ-stimulated [³⁵S]GTPγS binding to mouse brain. *Neuroreport*, **12**, 1757-61.
- JENCK, F., WICHMANN, J., DAUTZENBERG, F.M., MOREAU, J.L., OUAGAZZAL, A.M., MARTIN, J.R., LUNDSTROM, K., CESURA, A.M., POLI, S.M., ROEVER, S., KOLCZEWSKI, S., ADAM, G. & KILPATRICK, G. (2000). A synthetic agonist at the orphanin FQ/nociceptin receptor ORL1: anxiolytic profile in the rat. *Proc Natl Acad Sci U S A*, **97**, 4938-43.
- JORDAN, B.A. & DEVI, L.A. (1999). G protein-coupled receptor heterodimerization modulates receptor function. *Nature*, **399**, 697-700.
- KAMERLING, S., WOOD, T., DEQUICK, D., WECKMAN, T.J., TAI, C., BLAKE, J.W. & TOBIN, T. (1989). Narcotic analgesics, their detection and pain measurement in the horse: a review. *Equine Vet J*, **21**, 4-12.
- KAPUSTA, D.R., DAYAN, L.A. & KENIGS, V.A. (2002). Nociceptin/orphanin FQ modulates the cardiovascular, but not renal, responses to stress in spontaneously hypertensive rats. *Clin Exp Pharmacol Physiol*, **29**, 254-9.
- KAWAMOTO, H., OZAKI, S., ITOH, Y., MIYAJI, M., ARAI, S., NAKASHIMA, H., KATO, T., OHTA, H. & IWASAWA, Y. (1999). Discovery of the first potent and selective small molecule opioid receptor-like (ORL1) antagonist: 1-[(3R,4R)-1-cyclooctylmethyl-3-hydroxymethyl-4-piperidyl]-3-ethyl-1, 3-dihydro-2H-benzimidazol-2-one (J-113397). *J Med Chem*, **42**, 5061-3.
- KENAKIN, T. (2002). Efficacy at G-protein-coupled receptors. *Nat Rev Drug Discov*, **1**, 103-10.
- KENAKIN, T. (1997). *Pharmacologic Analysis of Drug-Receptor Interaction*. New York: Lippincott-Raven.
- KIEFFER, B.L., BEFORT, K., GAVERIAUX-RUFF, C. & HIRTH, C.G. (1992). The δ-opioid receptor: isolation of a cDNA by expression cloning and pharmacological characterization. *Proc Natl Acad Sci U S A*, **89**, 12048-52.
- KIM, H.W., KWON, Y.B., HAM, T.W., ROH, D.H., YOON, S.Y., HAN, H.J., KIM, K.W., LEE, W.S., KIM, J.K., YOON, O.B. & LEE, J.H. (2002). Distribution of nociceptin-like immunoreactivity in the central nervous system of the Mongolian gerbil: an immunohistochemical study. *Anat Histol Embryol*, **31**, 187-92.
- KITCHEN, I., SLOWE, S.J., MATTHES, H.W. & KIEFFER, B. (1997). Quantitative autoradiographic mapping of μ-, δ- and κ-opioid receptors in knockout mice lacking the μ-opioid receptor gene. *Brain Res*, **778**, 73-88.
- KOLCZEWSKI, S., ADAM, G., CESURA, A.M., JENCK, F., HENNIG, M., OBERHAUSER, T., POLI, S.M., ROSSLER, F., ROVER, S., WICHMANN, J. & DAUTZENBERG, F.M. (2003). Novel hexahydrospiro[piperidine-4,1'-pyrrolo[3,4-c]pyrroles]: highly selective small-molecule nociceptin/orphanin FQ receptor agonists. *J Med Chem*, **46**, 255-64.
- KUMMER, W. & FISCHER, A. (1997). Nociceptin and its receptor in guinea-pig sympathetic ganglia. *Neurosci Lett*, **234**, 35-8.
- LACHOWICZ, J.E., SHEN, Y., MONSMA, F.J., JR. & SIBLEY, D.R. (1995). Molecular cloning of a novel G protein-coupled receptor related to the opiate receptor family. *J Neurochem*, **64**, 34-40.

- LAI, C.C., WU, S.Y., DUN, S.L. & DUN, N.J. (1997). Nociceptin-like immunoreactivity in the rat dorsal horn and inhibition of substantia gelatinosa neurons. *Neuroscience*, **81**, 887-91.
- LANGLOIS, X., TE RIELE, P., WINTMOLDERS, C., LEYSEN, J.E. & JURZAK, M. (2001). Use of the beta-imager for rapid *ex vivo* autoradiography exemplified with central nervous system penetrating neurokinin 3 antagonists. *J Pharmacol Exp Ther*, **299**, 712-7.
- LAPIN, G.D. & GROOTHUIS, D.R. (1991). Potential errors due to aliasing in digital video analysis of quantitative autoradiography. *J Neurosci Methods*, **38**, 71-80.
- LEES, J.E. & HALES, J.M. (2001). Imaging and quantitative analysis of tritium-labelled cells in lymphocyte proliferation assays using microchannel plate detectors originally developed for X-ray astronomy. *J Immunol Methods*, **247**, 95-102.
- LEES, J.E. & RICHARDS, P.G. (1999). Rapid, high-sensitivity imaging of radiolabeled gels with microchannel plate detectors. *Electrophoresis*, **20**, 2139-43.
- LEHNER, A.F., ALMEIDA, P., JACOBS, J., HARKINS, J.D., KARPIESIUK, W., WOODS, W.E., DIRIKOLU, L., BOSKEN, J.M., CARTER, W.G., BOYLES, J., HOLTZ, C., HELLER, T., NATTRASS, C., FISHER, M. & TOBIN, T. (2000). Remifentanyl in the horse: identification and detection of its major urinary metabolite. *J Anal Toxicol*, **24**, 309-15.
- LEON-OLEA, M., MILLER-PEREZ, C., CRUZ, R., ANTON, B., VEGA, R. & SOTO, E. (2001). Immunohistochemical localization and electrophysiological action of nociceptin/orphanin-FQ in the snail (*Helix aspersa*) neurons. *Neurosci Lett*, **316**, 141-4.
- LETCHWORTH, S.R., MATHIS, J.P., ROSSI, G.C., BODNAR, R.J. & PASTERNAK, G.W. (2000). Autoradiographic localization of [¹²⁵I]Tyr¹⁴orphanin FQ/nociceptin and [¹²⁵I]Tyr¹⁰orphanin FQ/nociceptin(1-11) binding sites in rat brain. *J Comp Neurol*, **423**, 319-29.
- LI, N., LUNDEBERG, T. & YU, L.C. (2001). Involvement of CGRP and CGRP1 receptor in nociception in the nucleus accumbens of rats. *Brain Res*, **901**, 161-6.
- LOWRY, O.H., ROSEBROUGH, N.J., LEWIS FARR, A. & RANDALL, R.J. (1951). Protein measurement with the Folin phenol reagent. *J Biol Chem*, **193**, 265-275.
- MAKMAN, M.H. & DVORKIN, B. (1997a). Presence of nociceptin (orphanin FQ) receptors in rat retina: comparison with receptors in striatum. *Eur J Pharmacol*, **338**, 171-6.
- MAKMAN, M.H., LYMAN, W.D. & DVORKIN, B. (1997b). Presence and characterization of nociceptin (orphanin FQ) receptor binding in adult rat and human fetal hypothalamus. *Brain Res*, **762**, 247-50.
- MARTI, M., GUERRINI, R., BEANI, L., BIANCHI, C. & MORARI, M. (2002). Nociceptin/orphanin FQ receptors modulate glutamate extracellular levels in the substantia nigra pars reticulata. A microdialysis study in the awake freely moving rat. *Neuroscience*, **112**, 153-160.
- MARTI, M., STOCCHI, S., PAGANINI, F., MELA, F., DE RISI, C., CALO, G., GUERRINI, R., BARNES, T.A., LAMBERT, D.G., BEANI, L., BIANCHI, C. & MORARI, M. (2003). Pharmacological profiles of presynaptic nociceptin/orphanin FQ receptors modulating 5-hydroxytryptamine and noradrenaline release in the rat neocortex. *Br J Pharmacol*, **138**, 91-8.
- MARTIN, E.A. (2002). *Oxford Concise Medical Dictionary*. Oxford: Oxford University Press.
- MARTIN, F.J. & PAPAHDJOPOULOS, D. (1982). Irreversible coupling of immunoglobulin fragments to preformed vesicles. An improved method for liposome targeting. *J Biol Chem*, **257**, 286-8.

- MASON, S.L., HO, M., NICHOLSON, J. & MCKNIGHT, A.T. (2001). *In vitro* characterization of Ac-RYYRWK-NH₂, Ac-RYYRIK-NH₂ and [Phe¹ψ(CH₂-NH)Gly²] nociceptin(1-13)NH₂ at rat native and recombinant ORL1 receptors. *Neuropeptides*, **35**, 244-56.
- MCDONALD, J., BARNES, T.A., CALO, G., GUERRINI, R., ROWBOTHAM, D.J. & LAMBERT, D.G. (2002). Effects of [(pF)Phe⁴]nociceptin/orphanin FQ(1-13)NH₂ on GTPγ³⁵S binding and cAMP formation in Chinese hamster ovary cells expressing the human nociceptin/orphanin FQ receptor. *Eur J Pharmacol*, **443**, 7-12.
- MCDONALD, J., BARNES, T.A., OKAWA, H., WILLIAMS, J., CALO, G., ROWBOTHAM, D.J. & LAMBERT, D.G. (2003). Partial agonist behaviour depends upon the level of nociceptin/orphanin FQ receptor expression: studies using the ecdysone-inducible mammalian expression system. *Br J Pharmacol*, **140**, 61-70.
- MCQUAY, H. (1999). Opioids in pain management. *Lancet*, **353**, 2229-32.
- MCQUEEN, D.S. (1983). Opioid peptide interactions with respiratory and circulatory systems. *Br Med Bull*, **39**, 77-82.
- MEIS, S. & PAPE, H.C. (2001). Control of glutamate and GABA release by nociceptin/orphanin FQ in the rat lateral amygdala. *J Physiol*, **532**, 701-12.
- MERRIFIELD, R.B. (1963). Solid Phase Peptide Synthesis I. The synthesis of a tetrapeptide. *J Am Chem Soc*, **85**, 2149.
- MESSLINGER, K. (1997). What is a nociceptor?. *Anaesthetist*, **46**, 142-53.
- MEUNIER, J.C. (1997). Nociceptin/orphanin FQ and the opioid receptor-like ORL1 receptor. *Eur J Pharmacol*, **340**, 1-15.
- MEUNIER, J.C., MOLLEREAU, C., TOLL, L., SUAUDEAU, C., MOISAND, C., ALVINERIE, P., BUTOUR, J.L., GUILLEMOT, J.C., FERRARA, P., MONSARRAT, B. & AL., E. (1995). Isolation and structure of the endogenous agonist of opioid receptor-like ORL1 receptor. *Nature*, **377**, 532-5.
- MEUNIER, J.C., MOULEDOUS, L. & TOPHAM, C.M. (2000). The nociceptin (ORL1) receptor: molecular cloning and functional architecture. *Peptides*, **21**, 893-900.
- MEYER, H. (1993). The Brain. In *Miller's Anatomy of the Dog*. ed Evans, H.E. pp. 842-902. Philadelphia: W B Saunders.
- MIKA, J., LI, Y., WEIHE, E. & SCHAFER, M.K. (2003). Relationship of pronociceptin/orphanin FQ and the nociceptin receptor ORL1 with substance P and calcitonin gene-related peptide expression in dorsal root ganglion of the rat. *Neurosci Lett*, **348**, 190-4.
- MOGIL, J.S. & PASTERNAK, G.W. (2001). The molecular and behavioral pharmacology of the orphanin FQ/nociceptin peptide and receptor family. *Pharmacol Rev*, **53**, 381-415.
- MOLLEREAU, C. & MOULEDOUS, L. (2000). Tissue distribution of the opioid receptor-like (ORL1) receptor. *Peptides*, **21**, 907-17.
- MOLLEREAU, C., PARMENTIER, M., MAILLEUX, P., BUTOUR, J.L., MOISAND, C., CHALON, P., CAPUT, D., VASSART, G. & MEUNIER, J.C. (1994). ORL1, a novel member of the opioid receptor family. Cloning, functional expression and localization. *FEBS Lett*, **341**, 33-8.
- MOLLEREAU, C., SIMONS, M.J., SOULARUE, P., LINERS, F., VASSART, G., MEUNIER, J.C. & PARMENTIER, M. (1996). Structure, tissue distribution, and chromosomal localization of the prepronociceptin gene. *Proc Natl Acad Sci USA*, **93**, 8666-70.
- MONTEILLET-AGIUS, G., FEIN, J., ANTON, B. & EVANS, C.J. (1998). ORL-1 and μ opioid receptor antisera label different fibers in areas involved in pain processing. *J Comp Neurol*, **399**, 373-83.

- MONTELL, C., BIRNBAUMER, L. & FLOCKERZI, V. (2002). The TRP channels, a remarkably functional family. *Cell*, **108**, 595-8.
- NARITA, M., MIZOGUCHI, H., OJI, D.E., DUN, N.J., HWANG, B.H., NAGASE, H. & TSENG, L.F. (1999). Identification of the G-protein-coupled ORL1 receptor in the mouse spinal cord by [³⁵S]-GTPγS binding and immunohistochemistry. *Br J Pharmacol*, **128**, 1300-6.
- NEAL, C.R., JR., MANSOUR, A., REINSCHIED, R., NOTHACKER, H.P., CIVELLI, O. & WATSON, S.J., JR. (1999). Localization of orphanin FQ (nociceptin) peptide and mRNA in the central nervous system of the rat. *J Comp Neurol*, **406**, 503-47.
- NELSON, R.M., CALO, G., GUERRINI, R., HAINSWORTH, A.H., GREEN, A.R. & LAMBERT, D.G. (2000). Nociceptin/orphanin FQ inhibits ischaemia-induced glutamate efflux from rat cerebrotical slices. *Neuroreport*, **11**, 3689-92.
- NICHOLSON, J.R., PATERSON, S.J., MENZIES, J.R., CORBETT, A.D. & MCKNIGHT, A.T. (1998). Pharmacological studies on the "orphan" opioid receptor in central and peripheral sites. *Can J Physiol Pharmacol*, **76**, 304-13.
- NICOL, B., LAMBERT, D.G., ROWBOTHAM, D.J., OKUDA-ASHITAKA, E., ITO, S., SMART, D. & MCKNIGHT, A.T. (1998). Nocistatin reverses nociceptin inhibition of glutamate release from rat brain slices. *Eur J Pharmacol*, **356**, R1-3.
- NICOL, B., ROWBOTHAM, D.J. & LAMBERT, D.G. (2002). Nociceptin/orphanin FQ inhibits glutamate release from rat cerebellar and brain stem slices. *Neurosci Lett*, **326**, 85-88.
- NISHI, M., TAKESHIMA, H., MORI, M., NAKAGAWARA, K. & TAKEUCHI, T. (1994). Structure and chromosomal mapping of genes for the mouse κ-opioid receptor and an opioid receptor homologue (MOR-C). *Biochem Biophys Res Commun*, **205**, 1353-7.
- OKADA, K., SUJAKU, T., CHUMAN, Y., NAKASHIMA, R., NOSE, T., COSTA, T., YAMADA, Y., YOKOYAMA, M., NAGAHISA, A. & SHIMOHIGASHI, Y. (2000). Highly potent nociceptin analog containing the Arg-Lys triple repeat. *Biochem Biophys Res Commun*, **278**, 493-8.
- OKAMOTO, K., IMBE, H., MORIKAWA, Y., ITOH, M., SEKIMOTO, M., NEMOTO, K. & SENBA, E. (2002). 5-HT_{2A} receptor subtype in the peripheral branch of sensory fibers is involved in the potentiation of inflammatory pain in rats. *Pain*, **99**, 133.
- OKAWA, H., HIRST, R.A., SMART, D., MCKNIGHT, A.T. & LAMBERT, D.G. (1998). Rat central ORL-1 receptor uncouples from adenylyl cyclase during membrane preparation. *Neurosci Lett*, **246**, 49-52.
- OKAWA, H., NICOL, B., BIGONI, R., HIRST, R.A., CALO, G., GUERRINI, R., ROWBOTHAM, D.J., SMART, D., MCKNIGHT, A.T. & LAMBERT, D.G. (1999). Comparison of the effects of [Phe¹ψ(CH₂-NH)Gly²]nociceptin(1-13)NH₂ in rat brain, rat vas deferens and CHO cells expressing recombinant human nociceptin receptors. *Br J Pharmacol*, **127**, 123-30.
- OKUDA-ASHITAKA, E. & ITO, S. (2000). Nocistatin: a novel neuropeptide encoded by the gene for the nociceptin/orphanin FQ precursor. *Peptides*, **21**, 1101-9.
- OKUDA-ASHITAKA, E., MINAMI, T., TACHIBANA, S., YOSHIHARA, Y., NISHIUCHI, Y., KIMURA, T. & ITO, S. (1998). Nocistatin, a peptide that blocks nociceptin action in pain transmission. *Nature*, **392**, 286-9.
- OZAKI, S., KAWAMOTO, H., ITOH, Y., MIYAJI, M., IWASAWA, Y. & OHTA, H. (2000). A potent and highly selective nonpeptidyl nociceptin/orphanin FQ receptor (ORL1) antagonist: J-113397. *Eur J Pharmacol*, **387**, R17-8.
- PAN, Y.X., CHENG, J., XU, J., ROSSI, G., JACOBSON, E., RYAN-MORO, J., BROOKS, A.I., DEAN, G.E., STANDIFER, K.M. & PASTERNAK, G.W. (1995). Cloning and

- functional characterization through antisense mapping of a κ 3-related opioid receptor. *Mol Pharmacol*, **47**, 1180-8.
- PAN, Y.X., XU, J., MAHURTER, L., BOLAN, E., XU, M. & PASTERNAK, G.W. (2001). Generation of the μ opioid receptor (MOR-1) protein by three new splice variants of the Oprm gene. *Proc Natl Acad Sci U S A*, **98**, 14084-9.
- PAN, Z., HIRAKAWA, N. & FIELDS, H.L. (2000). A cellular mechanism for the bidirectional pain-modulating actions of orphanin FQ/nociceptin. *Neuron*, **26**, 515-22.
- PERT, C.B., PASTERNAK, G. & SNYDER, S.H. (1973). Opiate agonists and antagonists discriminated by receptor binding in brain. *Science*, **182**, 1359-61.
- PERTWEE, R.G. (2001). Cannabinoid receptors and pain. *Prog Neurobiol*, **63**, 569-611.
- PETTERSSON, L.M., SUNDLER, F. & DANIELSEN, N. (2002). Expression of orphanin FQ/nociceptin and its receptor in rat peripheral ganglia and spinal cord. *Brain Res*, **945**, 266-75.
- POONYACHOTI, S., KULKARNI-NARLA, A. & BROWN, D.R. (2002). Chemical coding of neurons expressing δ - and κ -opioid receptor and type I vanilloid receptor immunoreactivities in the porcine ileum. *Cell Tissue Res*, **307**, 23-33.
- QUIGLEY, D.I., ARTTAMANGKUL, S., ALLEN, R.G. & GRANDY, D.K. (2000). Integrity of tritiated orphanin FQ/nociceptin: implications for establishing a reliable binding assay. *Peptides*, **21**, 1111-8.
- RAO, S.P., CONLEY, A. & DUNBAR, J.C. (2003). Cardiovascular responses to central administration of μ and κ opioid receptor agonist and antagonist in normal rats. *Peptides*, **24**, 745-54.
- REINSCHIED, R.K., NOTHACKER, H.P., BOURSON, A., ARDATI, A., HENNINGSEN, R.A., BUNZOW, J.R., GRANDY, D.K., LANGEN, H., MONSMA, F.J., JR. & CIVELLI, O. (1995). Orphanin FQ: a neuropeptide that activates an opioidlike G protein-coupled receptor. *Science*, **270**, 792-4.
- RIZZI, A., BIGONI, R., MARZOLA, G., GUERRINI, R., SALVADORI, S., REGOLI, D. & CALO, G. (2001). Characterization of the locomotor activity-inhibiting effect of nociceptin/orphanin FQ in mice. *Naunyn Schmiedebergs Arch Pharmacol*, **363**, 161-5.
- ROGERS, H., HAYES, A.G., BIRCH, P.J., TRAYNOR, J.R. & LAWRENCE, A.J. (1990). The selectivity of the opioid antagonist, naltrindole, for δ -opioid receptors. *J Pharm Pharmacol*, **42**, 358-9.
- ROITT, I., BROSTOFF, J. & MALE, D. (1998). *Immunology*. London: Mosby International Ltd.
- SADEE, W., PERRY, D.C., ROSENBAUM, J.S. & HERZ, A. (1982). [3 H]diprenorphine receptor binding *in vivo* and *in vitro*. *Eur J Pharmacol*, **81**, 431-40.
- SALIS, M.B., EMANUELI, C., MILIA, A.F., GUERRINI, R. & MADEDDU, P. (2000). Studies of the cardiovascular effects of nociceptin and related peptides. *Peptides*, **21**, 985-93.
- SANDIN, J., GEORGIEVA, J., SCHOTT, P.A., OGREN, S.O. & TERENIUS, L. (1997). Nociceptin/orphanin FQ microinjected into hippocampus impairs spatial learning in rats. *Eur J Neurosci*, **9**, 194-7.
- SATO, K., SEKI, S. & MURRAY, P.A. (2002). Effects of halothane and enflurane anesthesia on sympathetic beta-adrenoreceptor-mediated pulmonary vasodilation in chronically instrumented dogs. *Anesthesiology*, **97**, 478-87.
- SBRENNNA, S., MARTI, M., MORARI, M., CALO, G., GUERRINI, R., BEANI, L. & BIANCHI, C. (2000). Modulation of 5-hydroxytryptamine efflux from rat cortical synaptosomes by opioids and nociceptin. *Br J Pharmacol*, **130**, 425-33.
- SCHLICKER, E. & MORARI, M. (2000). Nociceptin/orphanin FQ and neurotransmitter release in the central nervous system. *Peptides*, **21**, 1023-9.

- SCHMIDHAMMER, H., BURKARD, W.P., EGGSTEIN-AEPPLI, L. & SMITH, C.F. (1989). Synthesis and biological evaluation of 14-alkoxymorphinans. 2. (-)-N-(cyclopropylmethyl)-4,14-dimethoxymorphinan-6-one, a selective μ opioid receptor antagonist. *J Med Chem*, **32**, 418-21.
- SCHULZ, S., SCHREFF, M., NUSS, D., GRAMSCH, C. & HOLLT, V. (1996). Nociceptin/orphanin FQ and opioid peptides show overlapping distribution but not co-localization in pain-modulatory brain regions. *Neuroreport*, **7**, 3021-5.
- SHARIF, N.A., DURIE, E., MICHEL, A.D. & WHITING, R.L. (1990). Dog cerebral cortex contains μ -, δ - and κ -opioid receptors at different densities: apparent lack of evidence for subtypes of the κ -receptor using selective radioligands. *Brain Res*, **510**, 108-14.
- SIM, L.J., XIAO, R. & CHILDERS, S.R. (1996). Identification of opioid receptor-like (ORL1) peptide-stimulated [35 S]GTP γ S binding in rat brain. *Neuroreport*, **7**, 729-33.
- SMART, D., HIRST, R.A., HIROTA, K., GRANDY, D.K. & LAMBERT, D.G. (1997). The effects of recombinant rat μ -opioid receptor activation in CHO cells on phospholipase C, [Ca^{2+}] $_i$ and adenylyl cyclase. *Br J Pharmacol*, **120**, 1165-71.
- STEIN, C., MILLAN, M.J., SHIPPENBERG, T.S., PETER, K. & HERZ, A. (1989). Peripheral opioid receptors mediating antinociception in inflammation. Evidence for involvement of μ , δ and κ receptors. *J Pharmacol Exp Ther*, **248**, 1269-75.
- STRANGE, P.G. (1996). *Brain Biochemistry and Brain Disorders*. Oxford: Oxford University Press.
- SZETO, H.H., SOONG, Y., WU, D., OLARIU, N., KETT, A., KIM, H. & CLAPP, J.F. (1999). Respiratory depression after intravenous administration of δ -selective opioid peptide analogs. *Peptides*, **20**, 101-5.
- TAKITA, K., MORIMOTO, Y. & KEMMOTSU, O. (2003). Roles of nociceptin/orphanin FQ and nociceptin/orphanin FQ peptide receptor in respiratory rhythm generation in the medulla oblongata: an *in vitro* study. *Br J Anaesth*, **91**, 385-9.
- TAO, P.L., CHANG, L.R., LAW, P.Y. & LOH, H.H. (1988). Decrease in δ -opioid receptor density in rat brain after chronic [D-Ala 2 ,D-Leu 5]enkephalin treatment. *Brain Res*, **462**, 313-20.
- TERENIUS, L., SANDIN, J. & SAKURADA, T. (2000). Nociceptin/orphanin FQ metabolism and bioactive metabolites. *Peptides*, **21**, 919-22.
- THOMPSON, R.C., MANSOUR, A., AKIL, H. & WATSON, S.J. (1993). Cloning and pharmacological characterization of a rat μ opioid receptor. *Neuron*, **11**, 903-13.
- THOMSEN, C. & HOHLWEG, R. (2000a). (8-Naphthalen-1-ylmethyl-4-oxo-1-phenyl-1,3,8-triaza-spiro[4.5]dec-3-yl)-acetic acid methyl ester (NNC 63-0532) is a novel potent nociceptin receptor agonist. *Br J Pharmacol*, **131**, 903-8.
- THOMSEN, C., VALSBORG, J.S., PLATOU, J., MARTIN, J., FOGED, C., JOHANSEN, N.L., OLSEN, U.B. & MADSEN, K. (2000b). [^3H]ac-RYYRWK-NH $_2$, a novel specific radioligand for the nociceptin/orphanin FQ receptor. *Naunyn Schmiedebergs Arch Pharmacol*, **362**, 538-45.
- TIAN, J.H. & HAN, J.S. (2000). Functional studies using antibodies against orphanin FQ/nociceptin. *Peptides*, **21**, 1047-50.
- TORTORA, G.J. & ANAGNOSTAKOS, N.P. (1990). *Principles of Anatomy and Physiology*. London: Harper Collins.
- TOTH, G., LOVAS, S. & OTVOS, F. (1997). Tritium labeling of neuropeptides. *Methods Mol Biol*, **73**, 219-30.
- TOWBIN, H., STAHELIN, T. & GORDON, J. (1979). Electrophoretic transfer of proteins from polyacrylamide gels to nitrocellulose sheets: procedure and some applications. *Proc Natl Acad Sci U S A*, **76**, 4350-4.

- UEDA, H. (1999). *In vivo* molecular signal transduction of peripheral mechanisms of pain. *Jpn J Pharmacol*, **79**, 263-8.
- VARANI, K., CALO, G., RIZZI, A., MERIGHI, S., TOTH, G., GUERRINI, R., SALVADORI, S., BOREA, P.A. & REGOLI, D. (1998). Nociceptin receptor binding in mouse forebrain membranes: thermodynamic characteristics and structure activity relationships. *Br J Pharmacol*, **125**, 1485-90.
- VARANI, K., RIZZI, A., CALO, G., BIGONI, R., TOTH, G., GUERRINI, R., GESSI, S., SALVADORI, S., BOREA, P.A. & REGOLI, D. (1999). Pharmacology of [Tyr¹]nociceptin analogs: receptor binding and bioassay studies. *Naunyn Schmiedebergs Arch Pharmacol*, **360**, 270-7.
- WALKER, G.R., FEATHER, K.D., DAVIS, P.D. & HINES, K.K. (1995). Supersignal™ CL-HRP: A new enhanced chemiluminescent substrate for the development of the horseradish peroxidase label in Western blotting applications. *J NIH Res*, **7**, 76.
- WANG, J.B., JOHNSON, P.S., IMAI, Y., PERSICO, A.M., OZENBERGER, B.A., EPPLER, C.M. & UHL, G.R. (1994). cDNA cloning of an orphan opiate receptor gene family member and its splice variant. *FEBS Lett*, **348**, 75-9.
- WATANABE, M., SHIMADA, M. & KURIMOTO, K. (1975). Staining method for whole-body autoradiography. *Stain Technol*, **50**, 239-43.
- WEI, L.N. & LOH, H.H. (2002). Regulation of opioid receptor expression. *Curr Opin Pharmacol*, **2**, 69-75.
- WERTHWEIN, S., BAUER, U., NAKAZI, M., KATHMANN, M. & SCHLICKER, E. (1999). Further characterization of the ORL1 receptor-mediated inhibition of noradrenaline release in the mouse brain *in vitro*. *Br J Pharmacol*, **127**, 300-8.
- XIE, G.X., MEUSER, T., PIETRUCK, C., SHARMA, M. & PALMER, P.P. (1999). Presence of opioid receptor-like (ORL1) receptor mRNA splice variants in peripheral sensory and sympathetic neuronal ganglia. *Life Sci*, **64**, 2029-37.
- YAMADA, H., NAKAMOTO, H., SUZUKI, Y., ITO, T. & AISAKA, K. (2002). Pharmacological profiles of a novel opioid receptor-like1 (ORL1) receptor antagonist, JTC-801. *Br J Pharmacol*, **135**, 323-32.
- YAMADA, S., KUSAKA, T., URAYAMA, A., KIMURA, R. & WATANABE, Y. (2003). *In vitro* and *ex vivo* effects of a selective nociceptin/orphanin FQ (N/OFQ) peptide receptor antagonist, CompB, on specific binding of [³H]N/OFQ and [³⁵S]GTPγS in rat brain and spinal cord. *Br J Pharmacol*, **139**, 1462-8.
- YANG, D. & GEREAU, R.W.T. (2002). Peripheral group II metabotropic glutamate receptors (mGluR2/3) regulate prostaglandin E₂-mediated sensitization of capsaicin responses and thermal nociception. *J Neurosci*, **22**, 6388-93.
- YASUDA, K., RAYNOR, K., KONG, H., BREDER, C.D., TAKEDA, J., REISINE, T. & BELL, G.I. (1993). Cloning and functional comparison of κ and δ opioid receptors from mouse brain. *Proc Natl Acad Sci U S A*, **90**, 6736-40.
- ZHANG, S., TONG, Y., TIAN, M., DEHAVEN, R.N., CORTESBURGOS, L., MANSSON, E., SIMONIN, F., KIEFFER, B. & YU, L. (1998). Dynorphin A as a potential endogenous ligand for four members of the opioid receptor gene family. *J Pharmacol Exp Ther*, **286**, 136-41.
- ZILLES, K. (1985). *The cortex of the rat: a stereotaxic atlas*. Berlin: Springer-Verlag.
- ZUBRZYCKA, M. & JANECKA, A. (2000). Substance P: transmitter of nociception (Minireview). *Endocr Regul*, **34**, 195-201.

11 Publications arising from this thesis

Papers

- JOHNSON, E.E., McDONALD, J., BARNES, T.A., WILLIAMS, J., NICOL, B., ZANZINGER, J., ROWBOTHAM, D. & LAMBERT, D.G. *In vitro* characterisation of CJ-X. *Pfizer Ltd.*, legal clearing, IP issue.
- JOHNSON, E.E., McDONALD, J., NICOL, B., GUERRINI, R. & LAMBERT, D.G. Functional coupling of the nociceptin receptor natively expressed in dog brain membranes, *Brain Res*, 1003(1-2):18-25.
- JOHNSON, E.E., GIBSON, H., NICOL, B., ZANZINGER, J., WIDDOWSON, P., HAWTHORN, M., TOTH, G., FARKAS, J., GUERRINI, R. & LAMBERT, D.G. (2003). Characterization of nociceptin/orphanin FQ binding sites in dog brain membranes. *Anaesth Analg*, 97, 741-7.

Reviews, Book chapters

- JOHNSON, E.E. & LAMBERT, D.G. Receptor Mechanisms. Book chapter, Eds: Dr Anita Holdcroft & Dr Sian Jaggar, in press.
- JOHNSON, E.E. & LAMBERT, D.G. (2002) Molecular Pharmacology of the Opioid/Nociceptin System. *Current Anaesthesia and Critical Care*, 13 (6) 305-312.

Abstracts

- JOHNSON, E.E., NICOL, B. & LAMBERT, D.G. (2003) Functional coupling of the nociceptin receptor natively expressed in dog brain membranes. *British Journal of Pharmacology*, 138, 221P
- JOHNSON, E.E. & LAMBERT, D.G. (2002) Characterisation of the nociceptin receptor in dog brain membranes. *British Journal of Pharmacology*, 135, 257P

Oral Presentations

- Characterisation of the nociceptin receptor in dog brain. Seminar at the University of Ferrara (20/06/03)
- Characterisation of the nociceptin receptor in dog brain membranes. Pfizer Veterinary Medicine Student Symposium (05/07/02)
- Characterisation of the nociceptin receptor in dog brain membranes. Pfizer Veterinary Medicine Senior Biologists Meeting (24/10/01)

12 Appendix

12.1 Single letter amino acid code

A	Ala	Alanine	M	Met	Methionine
C	Cys	Cysteine	N	Asn	Asparagine
D	Asp	Aspartic acid	P	Pro	Proline
E	Glu	Glutamic acid	Q	Gln	Glutamine
F	Phe	Phenylalanine	R	Arg	Arginine
G	Gly	Glycine	S	Ser	Serine
H	His	Histidine	T	Thr	Threonine
I	Ile	Isoleucine	V	Val	Valine
K	Lys	Lysine	W	Trp	Tryptophan
L	Leu	Leucine	Y	Tyr	Tyrosine

12.2 Example Protocol for Preparation of an Immunogen

The following was scanned from Pierce instructions for NHS-Esters-Maleimide Crosslinkers.

Example Protocol for Preparation of an Immunogen

The protocol below is for the conjugation of a sulfhydryl-containing peptide to the carrier protein, KLH, to prepare an immunogen. A sulfhydryl-containing protein may be substituted for the peptide, another carrier protein may be substituted for KLH, and another NHS-ester-maleimide heterobifunctional crosslinker may be substituted for sulfo-MBS.

Materials

- Imject® Keyhole Limpet Hemocyanin (Prod. No. 77100).
- Sulfo-MBS (Prod. No. 22312).
- Conjugation buffer: 0.083 M sodium phosphate, 0.9 M NaCl, 0.1 M EDTA, pH 7.2.
- D-Salt™ Dextran Desalting Column (Prod. No. 43230), 5 ml.
- BupH™ Phosphate Buffered Saline (Prod. No. 28372).

Method

- Reconstitute KLH with 2 ml of distilled water. This results in a 10 mg/ml concentration. If using your own KLH, dissolve in conjugation buffer.
- Add 200 µl of KLH to a test tube.
- Dissolve 2 mg of Sulfo-MBS in 1 ml of conjugation buffer. Immediately transfer 100 µl of Sulfo-MBS solution into test tube containing the KLH.
- React for 1 hour at room temperature.
- Equilibrate the desalting column with 15 ml of conjugation buffer. Apply the 300 µl of reaction volume onto the column. Elute with 0.5 ml aliquots of conjugation buffer. Monitor the protein elution by absorbance at 280 nm. The maleimide-activated KLH should elute in fractions 4-6.
- Dissolve 2 mg of sulfhydryl-containing peptide in 500 µl of conjugation buffer.
- Add peptide solution to pooled fractions containing maleimide-activated KLH.
- Incubate for 2 hours at room temperature.
- Dialyze against PBS to remove EDTA prior to injection.

12.3 Preparation of Emulsion from TiterMax[®] 'Research Adjuvants' instructions

The following was scanned from TiterMax[®] 'Research Adjuvants' instructions.

Method 3: Two-Syringe, 3-Way Stopcock

This method is suitable for emulsion volumes between 1 ml and 10 mls. Available 3-way stopcocks have larger bores than the 18 gauge double hub needles (Method 1) so that emulsification takes longer and the syringes connected to 3-way stopcocks are often more difficult to hold. Recovery of emulsion is approximately 70 to 80%.

Materials:

1. TiterMax[®] Classic or TiterMax[®] Gold Research Adjuvant
2. Two 3.0 ml all-plastic or siliconized glass syringes (preferably lock tip)
3. One 18 gauge needle for withdrawing TiterMax[®] from the vial, or syringe without needle or positive displacement precision pipette if you open entire vial
4. One 3-way plastic disposable or stainless steel reusable stopcock (see Page 8)
5. Antigen in saline or other suitable fluid (typical dose range in mice is 15 to 125 $\mu\text{g}/\text{mouse}$)

Procedure:

NOTE: Prior to preparation of a TiterMax[®] water-in-oil emulsion, warm the TiterMax[®] to room temperature and vortex for 30 seconds. Make sure the TiterMax[®] is a homogeneous suspension of copolymer-coated microparticles before proceeding to emulsify by any method.

For 1 ml of a 50:50 water-in-oil emulsion you will need 0.5 ml of the aqueous antigen and 0.5 ml of TiterMax[®].

1. After TiterMax[®] has been vortexed, load a syringe with 0.5 ml TiterMax[®]. Load the second syringe with 0.25 ml of antigen in aqueous medium. Set aside the other 0.25 ml of antigen. **NOTE:** It is important to add the aqueous antigen phase to the TiterMax[®] in at least 2 small volumes.
2. Connect the two syringes via a 3-way stopcock (Figure 3). Mix the TiterMax[®] with the antigen by forcing the materials back and forth through the stopcock for approximately 1 minute. **NOTE:** It is important to push the antigen into the TiterMax[®] syringe first, so that the aqueous phase enters the oil phase rather than vice versa. Hold the syringes carefully so that they do not come apart from the 3-way stopcock during emulsification. **NOTE:** After approximately 1 minute a whipped-cream-like water-in-oil emulsion forms. Push all of the emulsion into one syringe and disconnect the empty syringe.
3. Load the empty syringe with the remaining 0.25 ml aqueous antigen solution. Reconnect the syringes and emulsify for another 30 to 60 seconds. **NOTE:** Again, first push the antigen into the water-in-oil emulsion. Care must be taken in holding the syringes together since the oil may lubricate and loosen the connection. It is preferable to use a lock tip syringe. Push all of the emulsion into one syringe. Disconnect the empty syringe and connect the syringe you have chosen for injecting for filling. Alternatively, simply disconnect the full syringe and add the appropriate needle for injecting animals.
4. To test stability, place a drop of emulsion on water (see details on Page 7).

Precautions:

The syringes should be siliconized glass or all-plastic. Plastic syringes with rubber pistons contain a lubricant which fails in the presence of TiterMax[®] and causes the syringes to stick. Use extreme caution during emulsification so that you do not loosen the syringes from the 3-way stopcock. This will cause you to lose the emulsion.

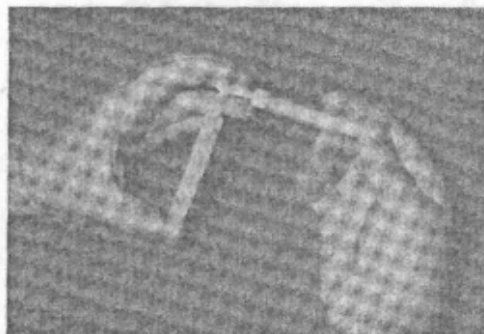


Figure 3: 1 ml of a 50:50 water-in-oil emulsion being prepared using the 3-way stopcock and two all-plastic syringes.

12.4 Usage of dog whole brain sections

The following table indicates how the slides were used in this thesis where ^3H is [*leucyl*- ^3H]N/OFQ autoradiography, ^{125}I , [^{125}I](Tyr 14)N/OFQ autoradiography, Res slides included in appropriate results section, H/E, haematoxylin and eosin stain and CresV, Cresyl Fast Violet stain.

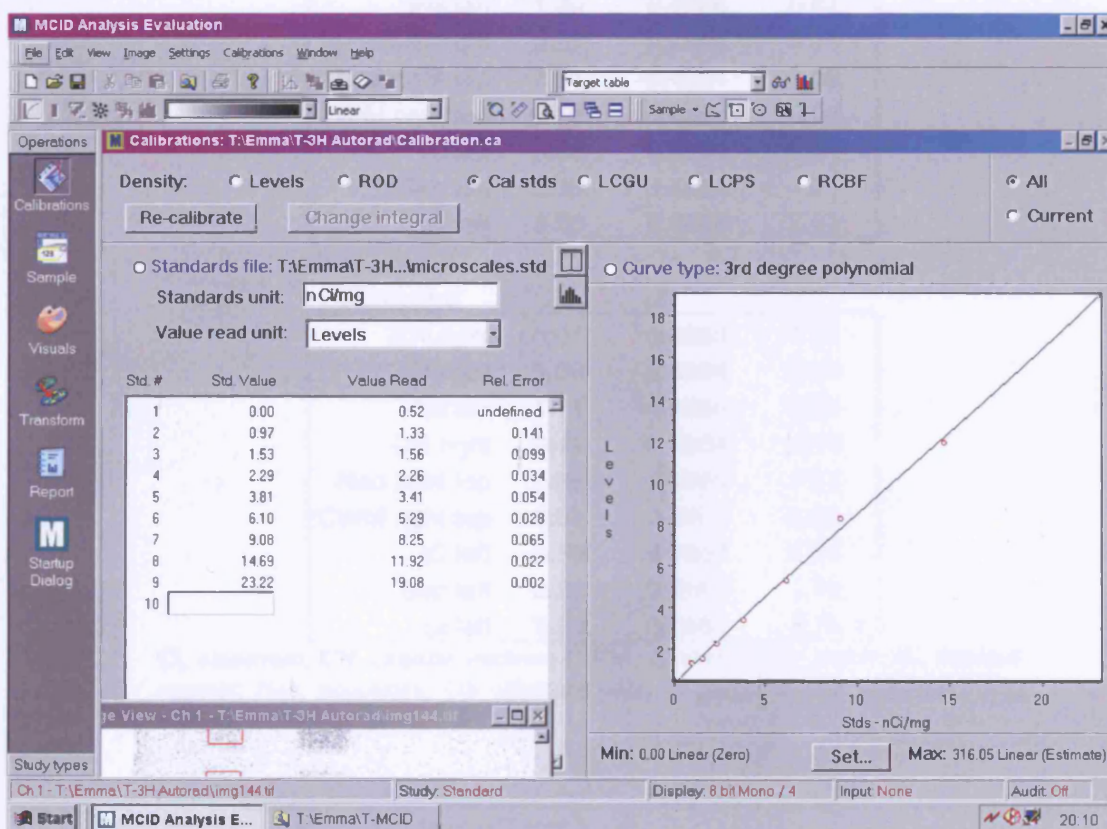
Section	Slide	Slice	Use
S1 S1/4	1	28-112	^3H
	2	86-114;37	IHC
	3	88-117;40	H/E
	4	90-119;44	CresV
	5	92-121;47	
	6	94-124;49	
S4-1	7	39,38	^3H
	8	41	
	9	42	
	10	46	
	11	48	H/E
	12	51	CresV
S4-2	13	86,82	
	14	89,87	
	15	91,90	^3H Res
	16	94,93	
	17	100,99	
	18	104,102	IHC
S5-1	19	46,45	
	20	49,48	
	21	56,55	^3H
	22	58,57	
	23	63,62	IHC
	24	65,64	
S5-2	25	90	^3H
	26	91	^3H
	27	92	H/E
	28	93	CresV
	29	94	
	30	97	
	31	98	
	32	99	
	33	100	
	34	101	
	35	127	
	36	131	
	37	133	
	38	134	
	39	139	
	40	140	
	41	141	
	42	142	
	43	143	
	44	144	IHC
S6-1	45	37	IHC
	46	39	H/E
	47	40	CresV
	48	42	
	49	47	^3H
	50	48	^3H
	51	49	
	52	51	
	53	52	
	54	53	
S6-2	55	98	
	56	100	^3H
	57	101	^3H
	58	106	
	59	108	
	60	109	
	61	110	
	62	111	
	63	112	
	64	113	IHC
S7-1	65	46	^3H
	66	47	^3H
	67	52	H/E
	68	53	CresV
	69	54	IHC
	70	55	
	71	56	
	72	57	
	73	58	
	74	59	
S7-2	75	87	^3H
	76	88	^3H
	77	89	
	78	90	

S8-1	79	91	IHC	S10-2	131	134	³ H Res
	80	93			132	135	³ H
	81	94			133	136	Stain test
	82	95			134	137	Stain test
	83	96			135	138	CresV test
	84	100			136	139	
	85	43	IHC		137	140	
	86	44			138	141	¹²⁵ I test
	87	46,45			139	142	¹²⁵ I test
	88	48,47			140	143	IHC
S8-2	89	49	³ H	S11-1	141	62	¹²⁵ I test
	90	50	³ H		142	63	¹²⁵ I test
	91	52,51			143	64	³ H Res
	92	79	H/E		144	65	³ H
	93	82	IHC		145	66	IHC
	94	84	³ H		146	67	¹²⁵ I Res
	95	85	³ H		147	68	
	96	87	CresV		148	69	destroyed
	97	89,88			149	70	H/E
	98	91			150	71	CresV
S9-1	99	92		S11-2	151	112	³ H Res
	100	93			152	113	³ H
	101	92	³ H Res		153	114	¹²⁵ I Res
	102	93	³ H		154	115	
	103	94			155	118	IHC
	104	95			156	121	
	105	106			157	122	
	106	107			158	123	H/E test
	107	109			159	125	Stain test
	108	110	H/E		160	126	Stain test
S9-2	109	111	CresV	S12-1	161	76	³ H Res
	110	112	IHC		162	77	³ H
	111	154	³ H Res		163	78	IHC
	112	155	³ H Res		164	79	H/E
	113	156			165	80	CresV
	114	160			166	81	¹²⁵ I Res
	115	161			167	82	¹²⁵ I Res
	116	162			168	83	
	117	163			169	84	¹²⁵ I test
	118	164			170	85	¹²⁵ I test
S10-1	119	165		S12-2	171	126	³ H Res
	120	166	IHC		172	127	³ H
	121	63	³ H Res		173	128	
	122	64	³ H Res		174	129	
	123	65	IHC		175	130	
	124	68	Stain		176	131	
	125	73	CresV		177	132	
	126	75			178	133	
	127	76			179	134	
	128	77			180	135	IHC
129	89		S13-1	181	26	³ H Res	
130	91			182	27	³ H	

S13-2	183	29	¹²⁵ I test									
	184	28	¹²⁵ I test									
	185	30	H/E									
	186	31	CresV									
	187	33	IHC									
	188	34										
	189	35										
	190	36										
	191	79	¹²⁵ I Res									
	192	80	¹²⁵ I Res									
	193	81										
	194	82	³ H Res									
	195	83	³ H									
	196	84										
	197	86										
	198	87	¹²⁵ I test									
	199	88	¹²⁵ I test									
	200	89	IHC									
S14-1	201	72	³ H									
	202	73	³ H									
	203	74	IHC									
	204	75										
	205	76										
	206	77										
	207	78	H/E									
	208	80	CresV									
	209	81	³ H Res									
	210	82	³ H									
S14-2	211	145	¹²⁵ I Res									
	212	146	¹²⁵ I Res									
	213	147										
	214	148										
	215	149										
	216	150										
	217	151										
	218	152	IHC									
	219	153	³ H									
	220	154	³ H									
S15-1	221	102	IHC									
	222	108										
	223	139										
	224	151	¹²⁵ I Res									
	225	156	³ H Res									
	226	157	³ H									
	227	158										
	228	166										
	229	167	H/E									
	230	168	CresV									
S15-2	231	201										
	232	202										
	233	203	IHC									
	234	204										
	235	205										
	236	206										
	S16-1	241	56					³ H				
		242	57					³ H				
		243	58					IHC				
244		59	¹²⁵ I Res									
245		60	H/E									
246		63	CresV									
247		64										
248		65										
249		66										
250		67										
S16-2	251	103	³ H Res									
	252	104	³ H									
	253	105	IHC									
	254	106										
	255	122										
	256	123										
	257	124										
	258	125										
	259	126										
	260	127										
S17-1	237	27	³ H									
	238	28	³ H									
	239	29	IHC									
	240	32	H/E									
	261	33	CresV									
	262	34										
	263	35										
	264	36										
	265	37										
	266	38										
S17-2	267	69	³ H Res									
	268	70	³ H									
	269	71	IHC									
	270	72										
	271	73										
	272	74										
	273	75										
	274	76										
	275	77										
	276	78	CresV									
S18	277	41	IHC									
	278	43	³ H									
	279	44	³ H									
	280	45										
	281	46										
	282	47										
	283	48										
	284	56	H/E									

	285	57	destroyed		296	73,74	IHC
	286	58	Stain		297	75,76	H/E
	287	64	³ H		298	77,78	CresV
	288	65	³ H		299	149,150	
	289	66	destroyed		300	151,152	³ H Res
	290	67			301	153,154	
	291	68			302	155,156	
	292	69	IHC		303	157,158	
S19	293	65,64,63,62			304	159,160	
	294	66,67,68,69			305	162,161	
	295	71,72	³ H		306	164,163	IHC

12.5 MCID calibration curve for [*leucyl*-³H]N/OFQ autoradiography



12.6 Example of MCID data analysis for slide 111 after [*leucyl*-³H]N/OFQ autoradiography

Slide 111 was sampled for total binding using the square tool, the NSB (determined from the four NSB sections) then was subtracted and the values for specific intensity averaged.

<i>Analysis1</i>	Total	NSB	Specific
	nCi/mg	nCi/mg	nCi/mg
CN right	8.27	0.4864	7.78
P right	5.96	0.4864	5.47
Pal left	1.17	0.4864	0.69
OS right	0.58	0.4864	0.10
Neo right top	7.38	0.4864	6.90
CWM right top	0.51	0.4864	0.02
IC left	0.55	0.4864	0.07
Sep left	2.13	0.4864	1.65
Cl left	3.32	0.4864	2.84

<i>Analysis2</i>			
CN right	8.25	0.4864	7.76
P right	6.05	0.4864	5.56
Pal left	1.30	0.4864	0.82
OS right	0.53	0.4864	0.05
Neo right top	7.51	0.4864	7.02
CWM right top	0.52	0.4864	0.03
IC left	0.53	0.4864	0.04
Sep left	2.30	0.4864	1.81
Cl left	3.30	0.4864	2.81

<i>Analysis3</i>			
CN right	8.01	0.4864	7.52
P right	5.89	0.4864	5.40
Pal left	1.11	0.4864	0.63
OS right	0.44	0.4864	-0.05
Neo right top	7.62	0.4864	7.13
CWM right top	0.51	0.4864	0.02
IC left	0.53	0.4864	0.04
Sep left	2.22	0.4864	1.73
Cl left	3.28	0.4864	2.79

Cl, claustrum; CN, caudate nucleus; CWM, cerebral white matter; IC, internal capsule; Neo, neocortex; OS olfactory stria; P, putamen; Pal, pallidum; Sep, septum

	Specific binding (nCi mg ⁻¹)			Average	Stdev	n	s.e.m
	1	2	3				
CN right	7.78	7.76	7.52	7.69	0.15	3	0.08
P right	5.47	5.56	5.40	5.48	0.08	3	0.05
Pal left	0.69	0.82	0.63	0.71	0.10	3	0.06
OS right	0.10	0.05	-0.05	0.03	0.07	3	0.04
Neo right top	6.90	7.02	7.13	7.02	0.12	3	0.07
CWM right top	0.02	0.03	0.02	0.03	0.01	3	0.00
IC left	0.07	0.04	0.04	0.05	0.01	3	0.01
Sep left	1.65	1.81	1.73	1.73	0.08	3	0.05
Cl left	2.84	2.81	2.79	2.81	0.02	3	0.01